DEPOSITIONAL CONTROLS AND SEQUENCE STRATIGRAPHY OF LACUSTRINE TO MARINE TRANSGRESSIVE DEPOSITS IN A RIFT BASIN, LOWER CRETACEOUS BLUFF MESA, INDIO MOUNTAINS, WEST TEXAS

ANDREW ANDERSON

Master's Program in Geology

APPROVED:

Katherine Giles, Ph.D., Chair

Richard Langford, Ph.D.

Vanessa Lougheed, Ph.D.

Charles Ambler, Ph.D.
Dean of the Graduate School

Copyright ©

by

Andrew Anderson

2017

DEDICATION

To my parents for teaching me to be better than I was the day before.

DEPOSITIONAL CONTROLS AND SEQUENCE STRATIGRAPHY OF LACUSTRINE TO MARINE TRANSGRESSIVE DEPOSITS IN A RIFT BASIN, LOWER CRETACEOUS BLUFF MESA, INDIO MOUNTAINS, WEST TEXAS

by

ANDREW ANDERSON, B.S.

THESIS

Presented to the Faculty of the Graduate School of
The University of Texas at El Paso
in Partial Fulfillment
of the Requirements
for the Degree of

MASTER OF SCIENCE

Department of Geological Sciences
THE UNIVERSITY OF TEXAS AT EL PASO
December 2017

ProQuest Number: 10689125

All rights reserved

INFORMATION TO ALL USERS
The quality of this reproduction is dependent upon the quality of the copy submitted.

In the unlikely event that the author did not send a complete manuscript
and there are missing pages, these will be noted. Also, if material had to be removed,
a note will indicate the deletion.

ProQuest 10689125

Published by ProQuest LLC (2018). Copyright of the Dissertation is held by the Author.

All rights reserved.
This work is protected against unauthorized copying under Title 17, United States Code
Microform Edition © ProQuest LLC.

ProQuest LLC.
789 East Eisenhower Parkway
P.O. Box 1346
Ann Arbor, MI 48106 – 1346

ACKNOWLEDGEMENTS

In the Fall of 2014, Dr. Kate Giles agreed to take a chance on a geologist from Chicago with limited fieldwork and no exploration experience. I am incredibly grateful for the opportunity to be part of Institute of Tectonic Studies and especially for the patience and guidance provided by Kate. It has made all the difference in transforming myself from a student into a scientist. A mountain of additional thanks goes to Dr. Rip Langford for introducing me to the Indio Mountains and providing me with incredible support during fieldwork. I thank members of the UTEP Biology Department, Dr. Vanessa Lougheed for serving as committee member and Dr. Jerry Johnson for support with coordination in the study area. I also thank Dr. Benjamin Brunner and Dr. Gail Arnold for guidance on geochemical problems, as well as for allowing me liberal access to a backyard rocksaw. I also owe a great debt to a number of my Professors from the University of Illinois at Chicago for sparking my interest in geology, specifically Dr. Roy Plotnick and Dr. Steve Guggenheim.

I am extremely grateful to Nila Matsler for technical support as well as her good old fashioned Midwest attitude that went a long way to helping me feel at home in ITS.

I'm reminded of the old proverb "If you want to go fast, go alone, but if you want to go far, go together". This certainly applies to my colleagues that have worked tirelessly along side me in the field. I am extraordinarily grateful to Matthew Fox, Andre Llanos, Alan Vennemann, Marc Lucero, Myra Guerrero, Samantha Ramirez, Guillermo Vargas, Jose Cervantes, and Ryan Jimenez for various contributions towards fieldwork. I am honored that I was able to work alongside with everyone.

I would also like to thank Irish, my parents, and my friends, for supporting me throughout this incredible journey.

ABSTRACT

Successful hydrocarbon exploration in former rift basins of the South Atlantic pre-salt has generated interest in understanding depositional, diagenetic, and stratigraphic controls on pre-salt deposits. However, most studies to date have focused on attributes and controls on pre-salt lacustrine carbonate reservoir systems and little work has been done on the overlying marine sealing facies. Currently our standard sequence stratigraphic model of marine transgression of rift systems involves a single pulse of marine flooding over fluvially-incised valleys resulting in backstepping of fluvial and estuarine siliciclastic facies within the erosionally confined zone of an incised valley. However, the pre-salt systems of the South Atlantic involve deep and broad alkaline lakes containing microbial carbonate facies that were deposited on rift structurally generated geomorphic surfaces. Using an outcrop analogue from the Indio Mountains of West Texas, this study aims to provide a depositional and stratigraphic model for marine transgression of lacustrine rift basin sediments that are similar in age, tectonic regime, and climatic setting to the pre-salt sealing facies of the South Atlantic.

The Lower Cretaceous Bluff Mesa Formation was deposited on the eastern margin of the Chihuahuan Trough failed rift and is exposed within multiple Laramide-age thrust panels in the Indio Mountains of West Texas. The mixed carbonate-siliciclastic system thins from 360 to 220 meters across the study area and contains five non-marine lithofacies and seven marine lithofacies. The depositional facies stack into five fourth-order sequences that record the transition from fluvio-lacustrine to shallow marine deposition. Sequences 1-2 are characterized by fluvio-lacustrine sandstones during lowstand systems tracts (LST) and lacustrine siltstones or thin marine wackestones during highstand systems tracts (HST). Sequences 3-5 are composed of exclusively marine facies characterized by shoreface to shelfal sandstones during transgressive

systems tracts (TST) and thick ooid grainstones and fossiliferous packstones deposited during HST. Sequence 2 records a significant rise in base level and the onset of marine deposition with LST fluvial sandstones overlain by thick marine carbonates during HST. The presence of thin marine limestones in sequences 1and 2 suggest that periodic marine incursion occurred during HST, but the basin was still primarily an enclosed rift lake. This idea is supported by analysis of carbonate associated sulfate from septarian nodules of lacustrine and marine origin. The observed succession of mixed terrestrial-marine sequences suggests transgression of rift basins involves multiple pulses of marine incursion.

TABLE OF CONTENTS

ACKNOWLEDGEMENTS v

ABSTRACT vi

TABLE OF CONTENTS viii

LIST OF FIGURES AND TABLES x

1. INTRODUCTION 1

2. GEOLOGICAL SETTING 9

2.1 THE CHIHUAHUA TROUGH 9
2.2 THE INDIO MOUNTAINS 17
2.3 THE BLUFF MESA AS AN ANALOG TO THE SOUTH ATLANTIC RIFT BASIN 22

3. METHODS 25

4. FACIES ASSOCIATIONS 27

4.1 FLUVIAL FACIES ASSOCIATION (FA-1) 27
4.1.1 Matrix-Supported Pebble Conglomerate (Fc) 35
4.1.2 Trough Cross-Bedded Quartz Arenite (Fs) 37
4.1.3 Horizontal Laminated Quartz Arenite (Fsl) 37
4.1.4 Depositional Environment of FA-1 39
4.2 LACUSTRINE FACIES ASSOCIATION (FA-2) 44
4.2.1 Burrowed Fine-Grained Quartz Arenite (Ls) 46
4.2.2 Massive Nodule-Bearing Mudstone (Lm) 46
4.2.3 Depositional Environment of FA-2 48
4.3 SHALLOW MARINE CARBONATE FACIES ASSOCIATION (FA-3) 52
4.3.1 Ooid Grainstone (Cg) 53
4.3.2 Fossiliferous Wackestone-Packstone (Cf) 56
4.3.3 Sandy Packstone-Grainstone (Cs) 58
4.3.4 Marl (Cm) 59
4.3.5 Depositional Environment of FA-3 59
4.4 SHALLOW MARINE SILICICLASTIC (FA-4) 63
4.4.1 Hummocky/Swaley Cross-Stratified Quartz Arenite (Ss) 65
4.4.2 Matrix-Supported Carbonate Clast Conglomerate (Sc) 69
4.4.3 Depositional Environment of FA-4 69
4.5 MIDDLE SHELF SILICICLASTIC FACIES ASSOCIATION (FA-5) 73
4.5.1 Olive Green Shale, Siltstone, and Fine-Grained Quartz Arenite (Mss) 74

4.5.2 Depositional Environment of FA-5 76
5. STRATAL ARCHITECTURE AND FACIES DISTRIBUTION 80

5.1 SEQUENCE #1 84
5.3 SEQUENCE #2 88
5.3 SEQUENCE #3 92
5.4 SEQUENCE #4 93
5.5 SEQUENCE #5 94
6. DISCUSSION 96

6.1 GEOCHEMISTRY OF SEPTARIAN NODULES 96
6.1.1 Carbonate Associated Sulfate (CAS) 96
6.1.2 Carbon and Oxygen Isotope Composition 100
6.2 STRATIGRAPHIC ARCHITECTURE AND THE PALEOENVIRONMENT 102
6.2.1 Syn-Depositional Faulting and Paleotopography 104
6.2.2 Paleoshoreline and Sediment Dispersal 106
6.3 REGIONAL CORRELATIONS 108
6.3.1 Correlations with the Bluff Mesa Type Section, Devil's Ridge 108
6.3.2 Correlations with the Campagrande Formation, Finlay Mountains 115
6.3.3 Correlations with the Quitman Formation, Southern Quitman Mountains 120
6.4 APPLICATIONS AS AN ANALOG 124
6.4.1 The Evaporite Problem 125
6.4.2 South Atlantic Basins Lacking Evaporites 126
6.4.3 Marine vs Lacustrine Carbonates 127
6.4.4 Stratigraphic Models 129
7. SUMMARY AND CONCLUSIONS 131

8. REFERENCES 135

9. APPENDIX 144

VITA 181

LIST OF TABLES

Table 1.1 Summary of depositional controls and comparison of their predicted expression in both passive margins and rift basins.. 4
Table 4.1: Lithofacies descriptions of fluvial facies association (FA-1). 28
Table 4.2: Lithofacies descriptions of lacustrine littoral facies association (FA-2) 29
Table 4.3: Lithofacies descriptions of shallow marine carbonate shelf facies association (FA-3)30
Table 4.4: Lithofacies descriptions of shallow marine siliciclastic shelf facies association (FA-4) 31
Table 4.5: Lithofacies descriptions of middle shelf siliciclastic facies association (FA-5)..... 32
Table 4.6: Isotope composition of carbonate and carbonate associated sulfate results from various septarian concretions. 79

LIST OF FIGURES AND TABLES

Figure 1.1: World map of giant oil and gas fields in rift and passive margin systems. 2
Figure 1.2: Cross-section of typical rift. 3
Figure 1.3: Schematic facies and depositional environment of estuaries. 6
Figure 1.4: Stratigraphic architecture of an ideal rift sequence. 7
Figure 2.1: The border rift system. 11
Figure 2.2: Schematic basin to margin transect of the Chihuahua Trough. 12
Figure 2.3: Geologic features and evaporite distribution of the Chihuahua Trough. 13
Figure 2.4: Regional stratigraphy of the Chihuahua Trough. 15
Figure 2.5: Local mountain belts near the US-Mexico border and simplified geologic map of the Indio Mountains (inset). 18
Figure 2.6: Simplified stratigraphic column and unit descriptions exposed in the Indio Mountains. 21
Figure 2.7: Early Cretaceous (120 ma) global reconstruction and regional reconstruction (inset). 23
Figure 4.1: Aerial photograph of the Indio Mountains southern thrust panel showing locations of measured sections, major faults and important sequence stratigraphic surfaces. 33
Figure 4.2: Stratigraphic correlation and facies distribution of uppermost Yucca and Bluff Mesa formations between Echo and Squaw Canyons, Indio Mountains, TX. 34
Figure 4.3: Idealized vertical succession of fluvial facies FA-1 and field photos showing transitions. 36
Figure 4.4: Outcrop photos of Fluvial Facies Association (FA-1). 38
Figure 4.5: Photomicrographs of Fluvial Facies Association (FA-1). 40
Figure 4.6: Idealized depositional environments of the Chihuahua Trough during fluvio-lacustrine deposition. 43
Figure 4.7: Outcrop and hand sample photos of Lacustrine Facies Association (FA-2). 45
Figure 4.8: Photomicrographs of Lacustrine Facies Association (FA-2). 47
Figure 4.9: Hand samples and morphologies of septarian concretions (Lm) in the Bluff Mesa and Upper Yucca formations. 51
Figure 4.10: Outcrop photos of Shallow Marine Carbonate Facies Association (FA-3) 54
Figure 4.11: Photomicrographs of Shallow Marine Carbonate Facies Association (FA-3). 55
Figure 4.12: Outcrop photos and photomicrographs of the banded mound structure. 57
Figure 4.13: Idealized depositional environments during marine deposition. 64
Figure 4.14: Idealized shallowing-upward facies succession in Shallow Marine Siliciclastic Facies Association (FA-4). 65
Figure 4.15: Outcrop photos of Shallow Marine Siliciclastic Facies Association of (FA-4) 67
Figure 4.16: Photomicrographs of shallow marine siliciclastics (FA-4). 68
Figure 4.17: Burrow extending from Cg into Cs (FA-3). 72
Figure 4.18: Outcrop photos and photomicrographs of Middle Shelf Siliciclastic Facies Association (FA-5) 75
Figure 4.19: Marine sulfur isotope curve through geologic time. 78
Figure 5.1: Outcrop photos of a variety of sequence boundaries. 82
Figure 5.2: Outcrop photos of sequence boundary #3 83
Figure 5.3: Outcrop photo of TST-1 and HST-1 85
Figure 5.4: Cross-section of measured sections recording the Echo Canyon horst block. 87

Figure 5.5: Outcrop photo of sequences #1 and #2 89
Figure 5.6: Outcrop photos of Sequence #2..... 91
Figure 6.1: Sulfate concentration and fractionation trends (not to scale). 101
Figure 6.2: Map of regional mountain belts with type section locations. 103
Figure 6.3: Correlation with the Bluff Mesa type section. 109
Figure 6.4: Correlation with the Campagrande Formation. 110
Figure 6.5: Correlation with the Quitman Formation. 111
Figure 6.6: Inferred shoreline trends and paleogeographic setting during deposition of various sequence tracts. 116

1. INTRODUCTION

A significant amount of the world's hydrocarbons are located in former rift basins, currently the most prolific being those on the South Atlantic Margin, which formed during the breakup of Gondwana in the Mesozoic Era (Figure 1.1; Mann, 2003). Hydrocarbon occurrence and distribution in rift basins is largely a product of the stratigraphic succession in the syn-rift and post-rift phases of basin evolution (Lambiase and Morley, 1999). Rift basins containing marine fill are more conducive to hydrocarbon accumulation than rift basins containing only non-marine fill and passive margins due to the higher occurrence of adequate sealing facies such as thick offshore mudstones and evaporites (Lambiase and Morley, 1999). Thick and extensive evaporite deposition can occur when tectonism and eustatic sea level falls isolate the basin from the open ocean after initial marine transgression has inundated the former rift lake (Figure 1.2; Bryant et al., 2012). Fine-grained marine transgressive deposits, including the thick evaporites, form the seal rocks that make marine fill rift systems such prolific hydrocarbon hosts.

Increased successful exploration in the South Atlantic has revealed the importance of pre-salt traps developed during continental rifting (Mohriak et al., 1990; Carminatti et al., 2008). Reservoir facies of the pre-salt petroleum plays of the Santos and Campos basins are composed of lacustrine microbialites or coquinas (Beasley et al., 2010; Bryant et al., 2012; Gomes et al., 2012; Thompson et al., 2015). These facies were deposited during the syn-rift stage in a series of interconnected rift lakes preceding cycles of desiccation and marine incursion, which resulted in deposition of the evaporite seal facies (Figure 1.2; Mohriak, 1990; Beasley et al., 2010; Beglinger et al., 2012; Bryant et al., 2012).

The trap seals in the South Atlantic systems are extensive marine shales or laterally extensive autochthonous salt horizons, which make seismic imaging of the pre-salt section

difficult (Beasley et al., 2010). Difficulties in interpretation due to poor seismic imaging are compounded by the long distances between wells in publicly available datasets throughout the South Atlantic Santos and Campos basins. Depositional and diagenetic models derived from detailed outcrop analogs have proven useful in predicting the geometry and characteristics of play elements in the absence of sufficient subsurface datasets (Bahniuk et al., 2015; Thompson et al., 2015).

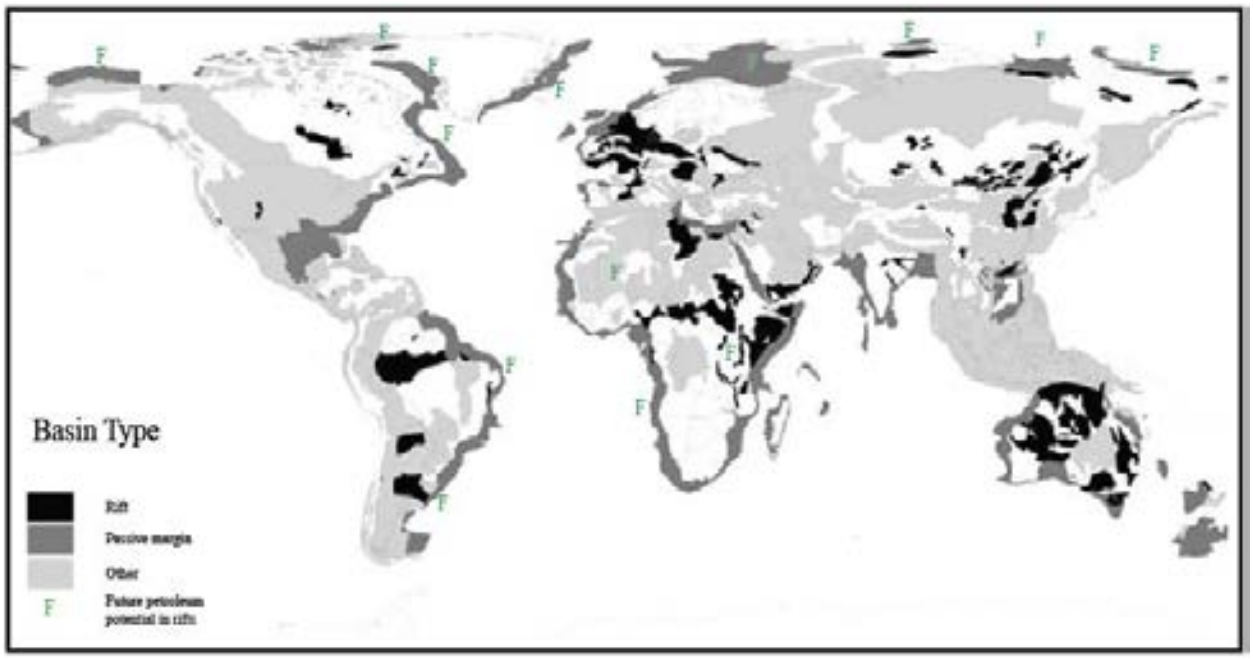

Figure 1.1: World map of giant oil and gas fields in rift and passive margin systems.
Global distribution of petroleum provinces and areas with potential for hydrocarbon exploration in former extensional basins. Davison and Underhill (2012) courtesy of M.K. Taylor and P.V. Baptista (2010).

Most previous studies utilizing outcrop analogs have focused on syn-rift lacustrine reservoir facies while largely ignoring the overlying marine transgressive deposits of the system, which are an integral part of the trap seal (Thompson, 2013; Li, 2014; Bahniuk et al., 2015). Most models of syn-post rift marine transgression are based on marine transgressions over fluvial and alluvial sandbodies deposited within incised paleovalleys along coastlines that were

shaped during previous transgressive-regressive cycles (Catuneanu, 2006). However, the transgressive seal facies in the South Atlantic rift systems were deposited over carbonate rift lakes during the syn-post rift transition (Bryant et al., 2012). The controls on deposition during marine transgression of lacustrine rift basins should be expected to differ from current passive margin models with regards to tectonic influence on creation of accommodation space, differences in water chemistry, sediment input, antecedent topography and basin physiography between a previously lacustrine rift basin and an incised paleovalley (Table 1.1; Ravnas and Steel, 1998). Outcrop analogs that were deposited under similar conditions to syn-rift strata of the South Atlantic should account for these differences, thereby refining both reservoir and trap models.

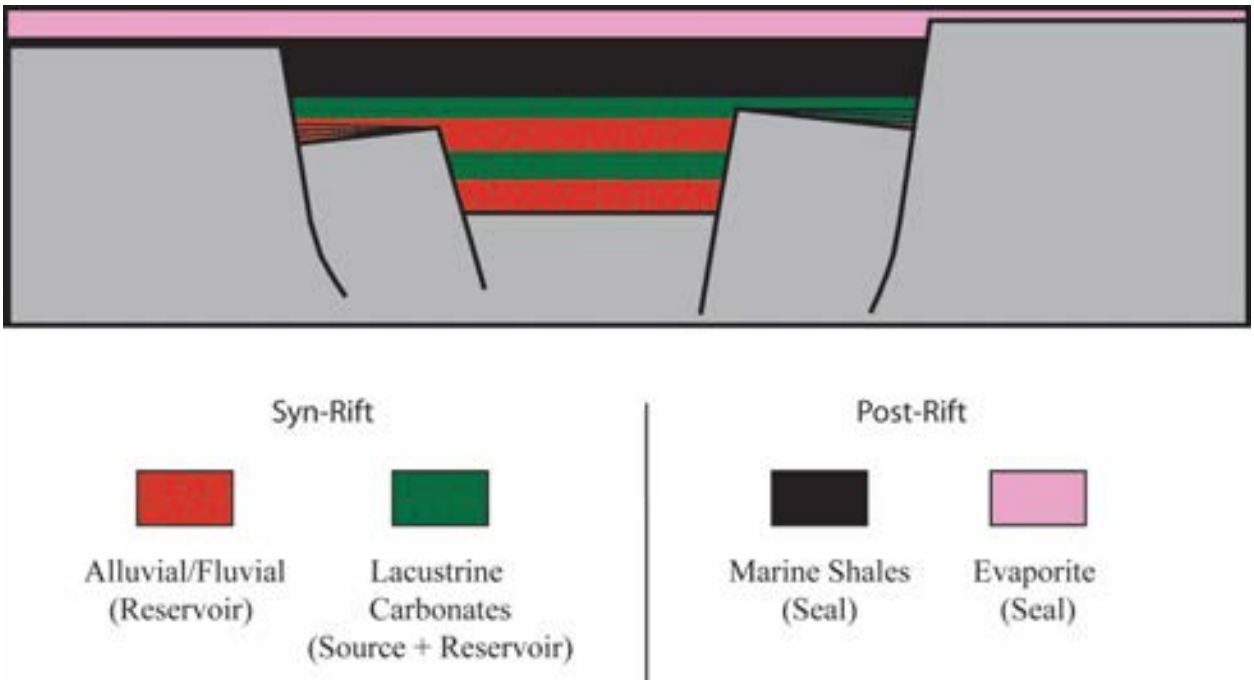

Figure 1.2: Cross-section of typical rift.
Schematic rift-fill sequence deposited over half graben geometries. Basal alluvial and fluvial deposits interbedded with lacustrine carbonates constitute the source and reservoir facies of the pre-salt petroleum system. Rift-related subsidence leads to repeated marine transgressions and regressions, resulting in deposition of thick evaporites that form an effective seal facies

Table 1.1 Summary of depositional controls and comparison of their predicted expression in both passive margins and rift basins.

Depositional Control	Passive Margin	Rift Basin
Tectonism	• Eustasy creates accommodation • Relatively steady	• Tectonism creates accommodation • Pulses of extension followed by periods of standstill
Antecedent Topography	• Incised channels • Coastline shaped by previous T-R cycles	• Horst and graben structures, half-grabens • Former rift lake beds
Sedimentary Input	• Steady	• Highly variable in space and time
Water Chemistry	• Fresh-brackish-marine gradient	• High alkalinity
Basin Physiography	• Open circulation with Ocean	• Vulnerable to circulation restriction

Currently the standard sequence stratigraphic model of marine transgression on passive margins involves marine flooding of fluvially incised valleys (Figure 1.3; Catuneanu, 2006). This results in deposition of back-stepping fluvial facies and flooding of the former incised valley forming an estuary, which are often capped by a regionally extensive shoreface erosional transgressive surface (Catuneanu, 2006). The transgressive systems tract is characterized by a regionally extensive retrogradational stacking pattern of fining upward sequences (Catuneanu, 2006). Typically backstepping estuarine facies are deposited within an incised valley as the fluvial system struggles to fill the newly created accommodation space. A bayhead delta will replace the estuary if transgression of the shoreline occurs at a higher rate than the river mouth can supply sediment, but the geomorphology of the incised valley remains. Alternatively, transgression of a rift basin is not confined to an incised valley but is instead subject to the antecedent geomorphology of the rift basin, typically a series of grabens or half grabens with axial drainage (Lambiase and Bosworth, 1995; Bosence, 1998; Ravnas and Steel, 1998). The pre-salt systems of the South Atlantic involve transgression over deep alkaline rift lakes containing microbial carbonate reservoir facies that were deposited on rift basin geomorphologic surfaces (Beasley et al., 2010; Bryant et al., 2012). Additionally, Martins-Neto and Catuneanu

(2010) recognized that sequence stratigraphy was developed for use on passive margins and developed a model for application in rift basins that accounts for creation of accommodation space through tectonic subsidence.

The model proposed by Martins-Neto and Catuneanu (2010) is based on depositional sequences observed in the South Atlantic, backed by an understanding of the controls on accommodation and the resulting stratigraphic architecture (Figure 1.4). A depositional environment where accommodation is primarily created through tectonic subsidence will exhibit several unique stratigraphic patterns. The model assumes that accommodation is created in short bursts in response to tectonic subsidence through extension, followed by longer stages of tectonic quiescence. Sediment is delivered to the basin during this period of relative standstill, resulting in a progradational coarsening-up sequence. This coarsening-up sequence may be split into underfilled, filled, and overfilled phases that describe the relationship between sediment supply and accommodation space generation (Figure 1.4). Eventually another relatively short period of tectonic subsidence occurs, creating accommodation and returning the basin to the underfilled phase.

As the majority of the stratigraphic architecture is progradational, authors have found that the most useful stratigraphic surface for defining individual sequences is the marine flooding surface. This flooding surface is the direct result of the tectonic subsidence stage and defines a sequence boundary. Therefore the sequence boundary in the rift model is characterized by distal facies abruptly overlying more proximal facies, which differs from sequence boundaries on passive margins which are described as erosive surfaces with proximal facies abruptly overlying distal facies (Catuneanu, 2006).

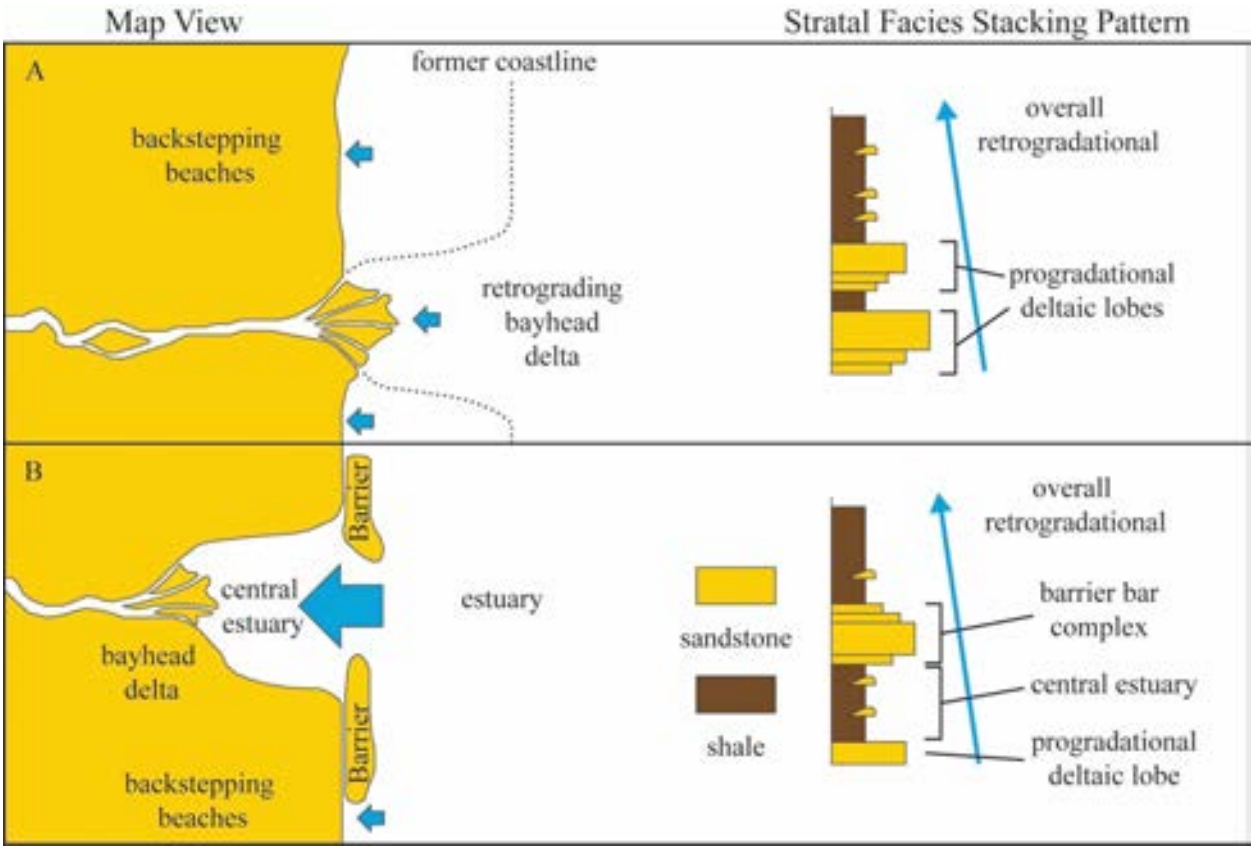

Figure 1.3: Schematic facies and depositional environment of estuaries.
Characteristics of depositional environments and typical stacking patterns during transgression of an incised valley on a passive margin. A) Retrograding bayhead delta flanked by backstepping beaches. B) Estuary complex that includes a bayhead delta, a low energy central estuary, and barrier bars.

The Martins-Neto and Catuneanu (2010) model predicts that a typical rift sequence consists of a thin transgressive systems tract overlain by a maximum flooding surface and a relatively thick highstand systems tract (HST). The transgressive systems tract (TST), consisting of retrogradational facies, is expected to be relatively thin within a rift basin as accommodation is generated instantaneously on geologic time scales. If the period of tectonic subsidence is sufficiently short, retrogradational stacking patterns will not be observed and the (TST) is absent. This also implies that the sequence boundary, the transgressive surface, and the maximum flooding surface are all superimposed on the sequence boundary. The LST is characterized by

progradational and aggradational stacking patterns above the sequence boundary and below the transgressive surface (Catuneanu, 2006).

The HST consists of the progradational facies deposited during the prolonged standstill following extension (tectonic quiescence). The LST is deposited when accommodation is increasing but has not yet outpaced sediment supply. Due to the high relative speed that accommodation is created in rift basins, the LST is typically absent. The thin or absent TST and the lack of a LST should easily differentiate rift sequences from passive margin sequences.

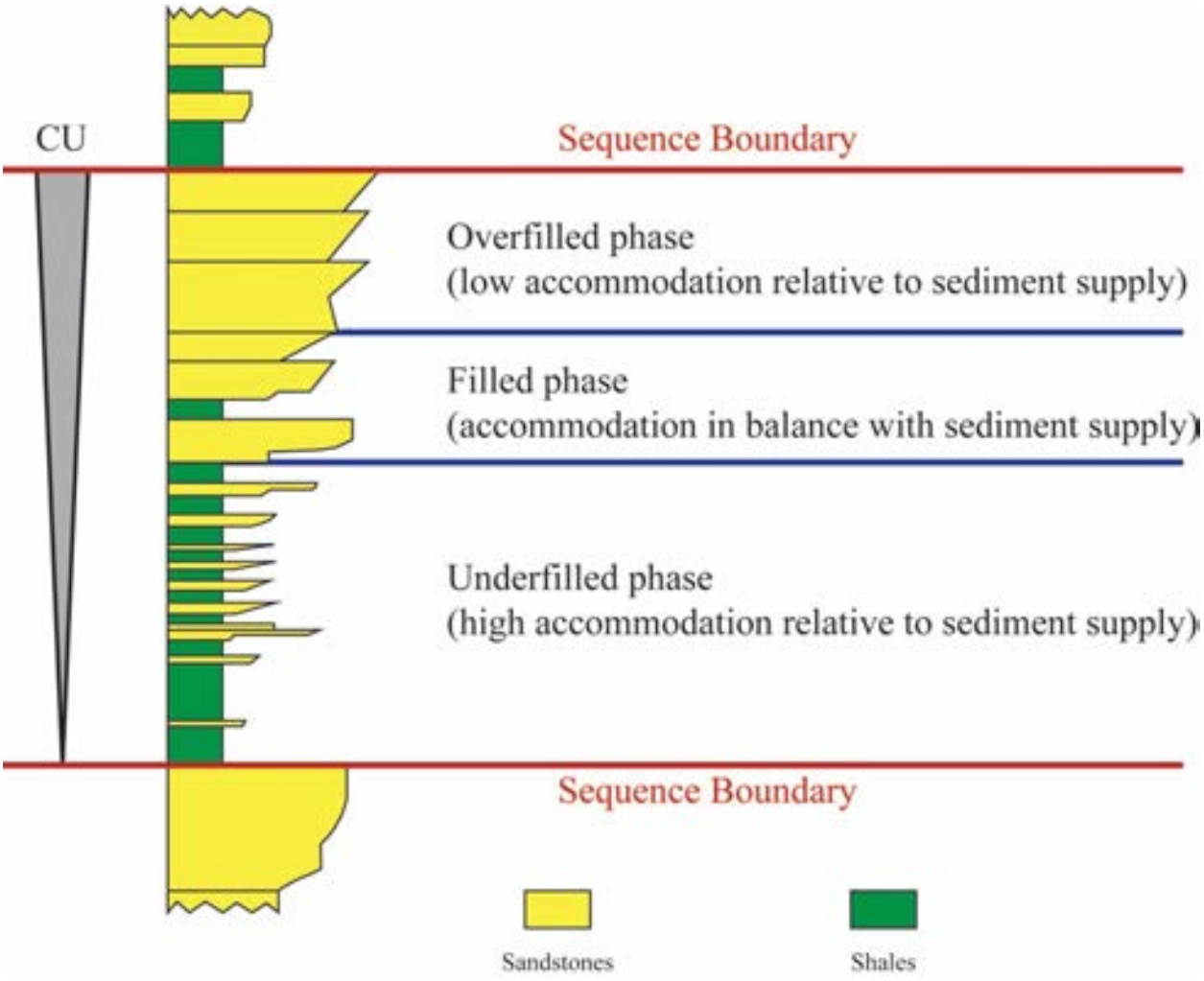

Figure 1.4: Stratigraphic architecture of an ideal rift sequence.
An ideal sequence shows a progression from an underfilled to overfilled relationship between accommodation and sediment supply. Modified from Martins-Neto and Catuneanu (2010).

Although the conclusions of the Martins-Neto and Catuneanu (2010) rift model are intriguing, the model is limited to siliciclastic systems consisting of fluvial and lacustrine cycles and has yet to be tested on a carbonate dominated system containing lacustrine and marine carbonates. It has been established that carbonates respond to accommodation differently than siliciclastics, rendering the siliciclastic rift model incomplete (Bosence, 1998). Additionally, the model assumes that tectonism is the only depositional control while ignoring eustasy, antecedent basin geomorphology, sediment input, and water chemistry. In order to refine the existing Martins-Neto and Catuneanu (2010) depositional model for transgression in rift settings, examples of both lacustrine and carbonate depositional response need to be documented in detail.

This study focuses on the characterization of the Cretaceous Bluff Mesa Formation exposed in the Indio Mountains of west Texas in order to provide an outcrop analog for the seal facies of the pre-salt petroleum plays of the South Atlantic. The goals of this study include: 1) documentation of facies distributions, depositional geometries, and cyclicity of the Bluff Mesa Formation: 2) generation of a depositional model for the Bluff Mesa: 3) comparison of the generated model to the standard sequence stratigraphic model and the rift sequence stratigraphic model proposed by Martins-Neto and Catuneanu (2010): 4) refining the internal stratigraphy and age of the Bluff Mesa Formation.

Documentation of trends in spatial and temporal distribution of depositional and diagenetic facies of the Bluff Mesa were used to develop a depositional and stratigraphic model for marine carbonate transgression over lacustrine carbonate facies in rift basins, which has not been developed previously. Results from this study are intended to improve our understanding of trap seal facies distribution and integrity in South Atlantic petroleum systems and similar extensional basins worldwide.

2. GEOLOGICAL SETTING

The Indio Mountains study area is located in western Texas near the US/Mexico border where Cretaceous strata record deposition on the eastern margin of the Chihuahua Trough Mesozoic rift system (Figure 2.1). Primarily east dipping Paleozoic through lower Cenozoic strata are exposed in west Texas by Neogene, roughly north-south trending extensional faults associated with the Rio Grande Rift and the Basin and Range province (Rohrbaugh, 2001).

2.1 THE CHIHUAHUA TROUGH

The Chihuahua Trough is a Mesozoic depositional basin that was part of a series of rift basins, separated by uplifts across northeastern Chihuahua, Trans-Pecos Texas, southern New Mexico and northeastern Sonora (Haenggi, 2002). The trough was connected to the Sabinas Basin to the southeast and the Bisbee Basin to the northwest, it is bounded by uplifts of the Diablo platform to the northeast and the Aldama platform to the southwest (Figure 2.1).

Multiple tectonic regimes were intermittently active throughout the Paleozoic causing significant faulting in the southwest margin of the North American craton. This resulted in a zone of relatively weak crust susceptible to northwest trending fault formation when stress was applied during the Jurassic (Brown and Dyer, 1987; Tucholke and Schouten, 1988; Haenggi, 2002). This zone of weakness was likely responsible for the formation of a number of Paleozoic features including the Pennsylvanian Pedrogosa Basin, which encompassed the northern and eastern parts of the Chihuahua Trough with a northeast boundary at the Diablo platform margin forming a sort of proto-Chihuahua Trough (Haenggi, 2001). Although the exact tectonic processes involved in the formation of the Pedregosa Basin are unknown, it is assumed that they were a product of a stress regime that took advantage of the same weak northwest trending fabric that set the stage for the formation of a number of extensional basins in the Jurassic. These basins comprise the

Cretaceous Border Rift System, which includes the Chihuahua Trough, Ariveche-Cucurpe Trough, Sabinas Basin, Altar-Cucurpe Basin, Bisbee Basin, and the McCoy Basin (Figure 2.1).

Formation of the Chihuahua Trough and other coeval basins of the border rift system have been attributed to 3 possible, but not exclusive processes: 1) extension or dextral transtension related to counter-clockwise rotation of the North American plate associated with the formation of the Gulf of Mexico (Haenggi, 2001): 2) extension related to back-arc rifting associated with slab rollback and asthenospheric upwelling (Dickinson and Lawton, 2001a; Dickinson and Lawton, 2001b; Peryam et al., 2012): 3) sinistral transtension associated with the Mojave-Sonoran Megashear (Silver and Anderson, 1974; Anderson and Nourse, 2005; Anderson and Silver, 2005). Although there is not a consensus, workers generally invoke transtension in scenario 1 or extension in scenario 2 as the primary mechanism for trough formation in the Jurassic (Haenggi and Muehlberger, 2005). The existence of a megashear in scenario 3 has been controversial since its inception but may also have played a role in formation of pull-apart basins in the Jurassic (Anderson and Silver, 2005; Molina-Garza and Iriondo, 2007).

Geoscientists generally agree that the Jurassic represents a period of change in North America between tectonic regimes highlighted by the initiation of continental rifting (168 Ma), trenchward migration of a magmatic arc (157-149 Ma), and the rapid increase of northward movement of the North American plate (160-125 Ma) (Mauel et al., 2011). The earliest marine transgression of the Chihuahua Trough is recorded in the Upper Jurassic (Kimmeridgian-Tithonian) La Casita Formation, which consists of fluvial sandstone grading up into shallow marine facies, capped by extensive evaporite deposition in the trough center (Figure 2.2; Figure 2.3; Cantu-Chapa et al., 1985; Araujo-Mendieta and Casar-Gonzalez, 1987). Oxfordian and/or Kimmeridgian ammonites are present in the Bisbee Basin and the Ariveche-Cucurpe Basin,

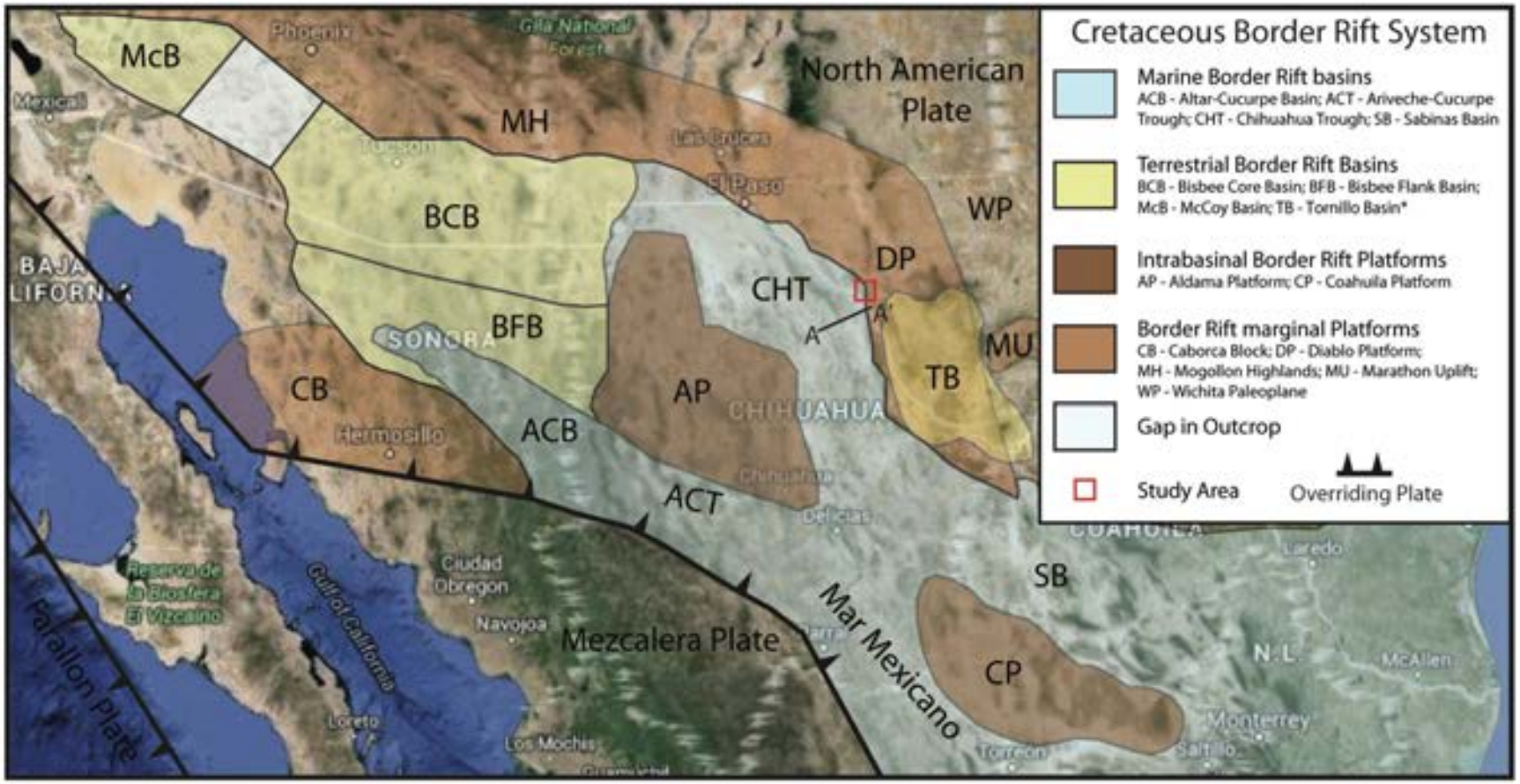

Figure 2.1: The border rift system.
Configuration of the Border Rift System at the time of maximum transgression in the Jurassic (Oxfordian-Kimmeridgian 160-151 Ma) with the exception of the Tornillo Basin. The Laramide Tornillo foreland basin represents the path of sea level retreat and therefore the youngest strata of the border rift system. The Bisbee Flank Basin, seperated from the Bisbee Core Basin by the Cananea high, is sometimes referred to as the Sonora-Bisbee Basin. The Altar-Cucurpe Basin is referred to as a distinct basin in the Jurassic but its Cretaceous deposits are sometimes grouped with either the Bisbee Flank Basin or the Lampazos Shelf. Compiled from Lehman (1991), Dickinson and Lawton (2001b), Haenggi (2002), Stern and Dickinson (2010), and Mauel et al. (2011).

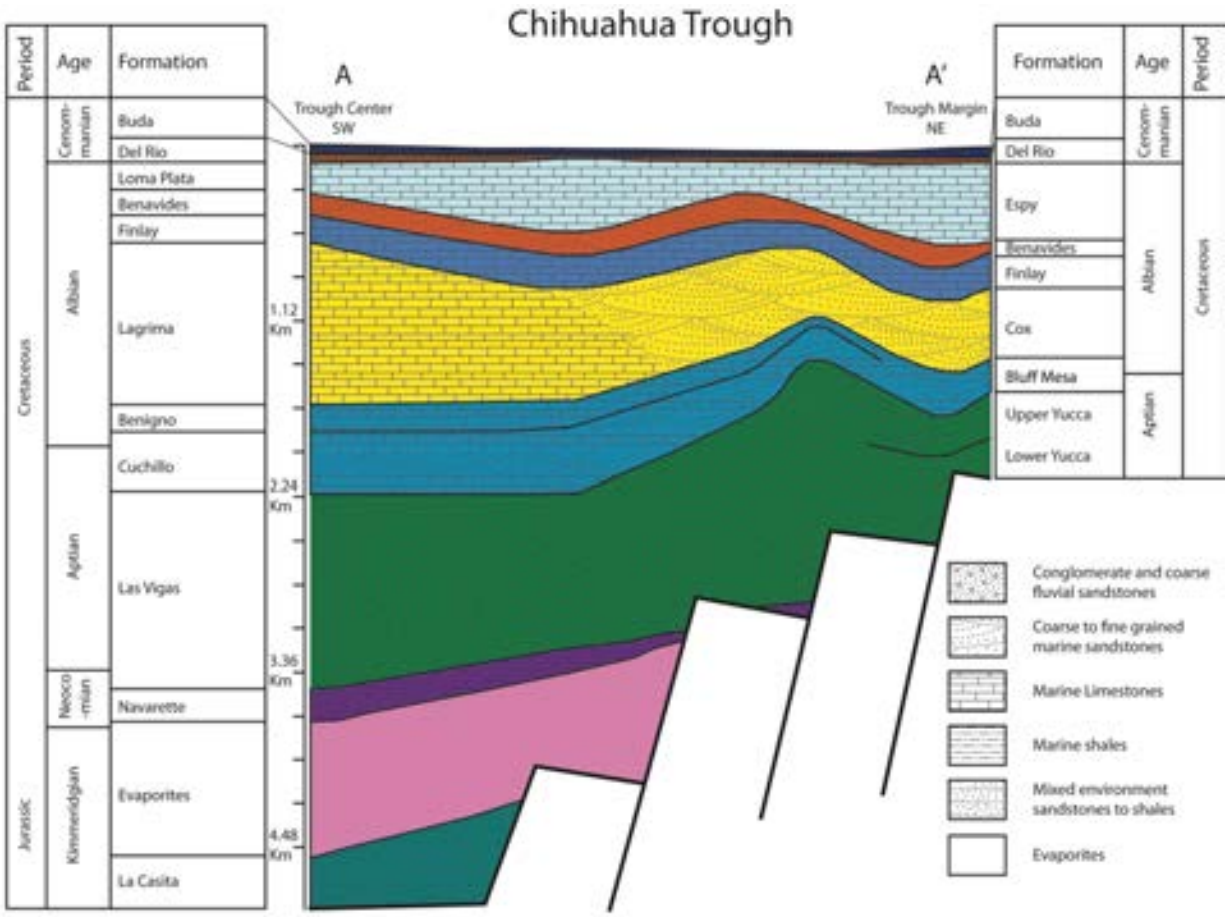

Figure 2.2: Schematic basin to margin transect of the Chihuahua Trough.
Cross section showing typical formation names and thicknesses from the trough margin to center (see figure 2.1 for transect location). Compiled from Haenggi (1970), Haenggi (2002), and Budhathoki (2013).

indicating that the Chihuahua Trough was already inundated by marine conditions at this time (Olmstead and Young, 2000; Villasenor et al., 2005). This is confirmed by observations of the dominant depositional trends in the Bisbee Basin suggesting that it was transgressed through the Chihuahua Trough rather than from the south through the Ariveche-Cucurpe Basin (Dickinson and Lawton, 2001b).

Sedimentation eventually outpaced subsidence in the trough leading to regression during Tithonian-Neocomian time. Periodic influx of marine waters served as a recharge for restricted

lagoons resulting in evaporite deposition in the eastern portion of the trough (Haenggi, 2002). Evaporite deposition is recorded only in the eastern margin of the Chihuahua Trough and the Sabinas Basin as these areas were proximal to the open ocean, which facilitated recharge.

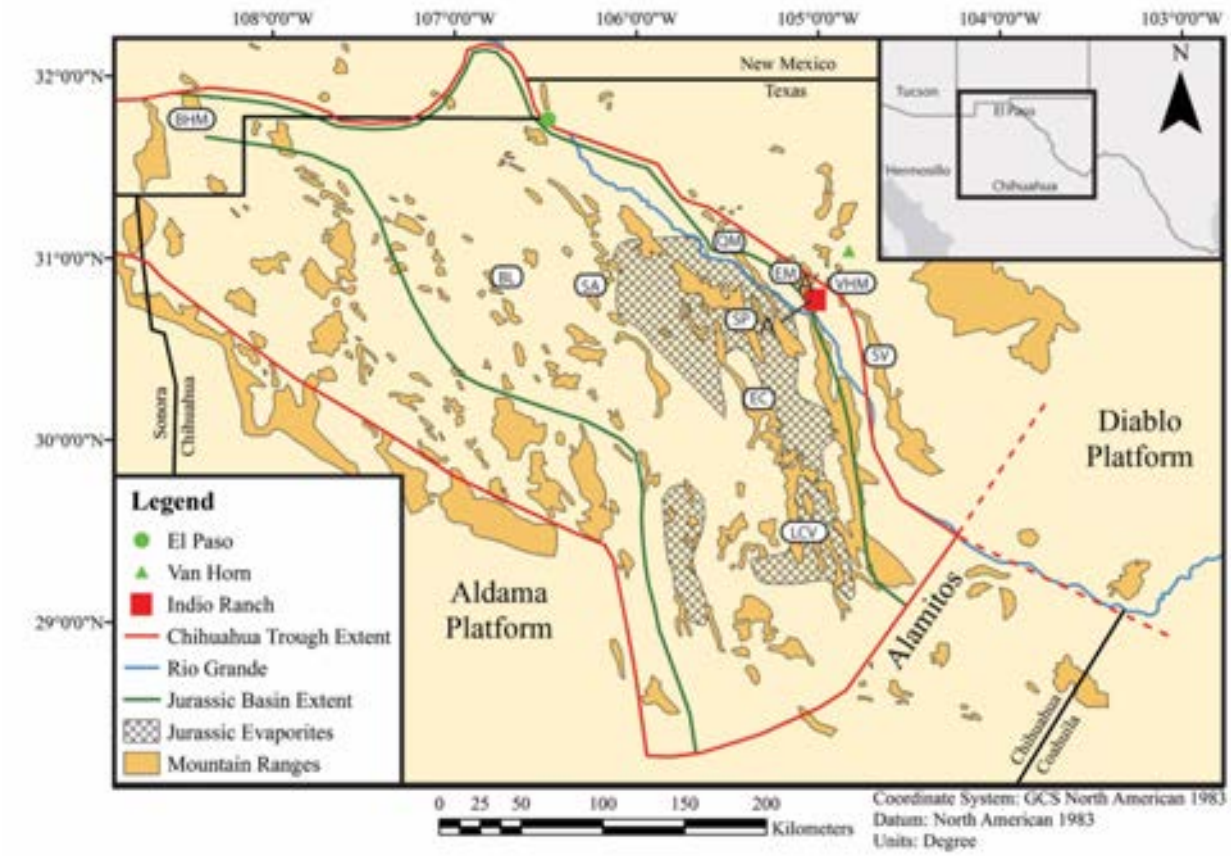

Figure 2.3: Geologic features and evaporite distribution of the Chihuahua Trough.
Evaporite deposition was confined to the Jurassic extent of the trough, which was separated from the Sabinas Basin by the Alamitos lineament. BHM = Big Hatchet Mountains, BL = Banco Lucero, EC = El Cuervo, EM = Eagle Mountains, LCV = Lower Conchos Valley, QM = Quitman Mountains, SA = Sierra De Alcaparra, SP = Sierra Del Pinos, SV = Sierra Vieja, VHM = Van Horn Mountains. Modified from Carciumaru and Ortega (2008).

An extended period of relative balance between sedimentation and subsidence occurred following another regressive event in the early Neocomian. Deposition in the Chihuahua Trough during this time is represented by the Las Vigas Formation, the largest stratigraphic unit in the trough by volume (Haenggi, 1966; Haenggi, 2002). The Las Vigas consists of alluvial, fluvial,

lacustrine, lagoonal and bay environments that are dominantly siliciclastic. The Las Vigas is generally grouped with the Yucca, Hell-to-Finish, and Mountain formations as they all represent siliciclastic deposition on the trough margin during this time (Monreal and Longoria, 1999; Haenggi, 2002).

The asymmetry of the Las Vigas within the trough, which thickens towards the northeast, suggests that the majority of sediment was sourced from the Diablo platform, rather than the Aldama platform (Haenggi, 2002). The thick chert-rich conglomerates of the Yucca Formation are unique within the Las Vigas lithosome and were likely sourced from exposed rocks of the Marathon orogenic belt, however these chert conglomerates are not widespread so their contribution to the overall basin fill is considered minimal (Underwood, 1962; Haenggi, 2002). Despite the presence of other unique locally sourced conglomerates throughout the trough, a much larger source must be invoked to fill accommodation space in the basin at this time. The likely candidate is the Wichita paleoplane, a degradational feature built during the early Mesozoic by erosion of the Ouachita fold belt and the Ancestral Rocky Mountains (Haenggi, 2002). This terrigenous sediment was delivered to the Chihuahua Trough from the northeast over the Diablo platform where it was deposited in the range of environments typical of the Las Vigas lithosome.

The Aptian is characterized by transgression throughout the Chihuahua Trough and the neighboring basins of the border rift system. Deposition within the trough is recorded by the Cuchillo Formation, which is time equivalent to a number of formations including the Bluff Mesa, U-bar, Quitman, Mosqueteros, Mural, Lucero, Travis Peak, La Pena, and the Glen Rose (Figure 2.4; Haenggi, 2002). These formations may be included in the “Chihuahuan Group”, which has been used in some publications to describe all formations from the Cuchillo through

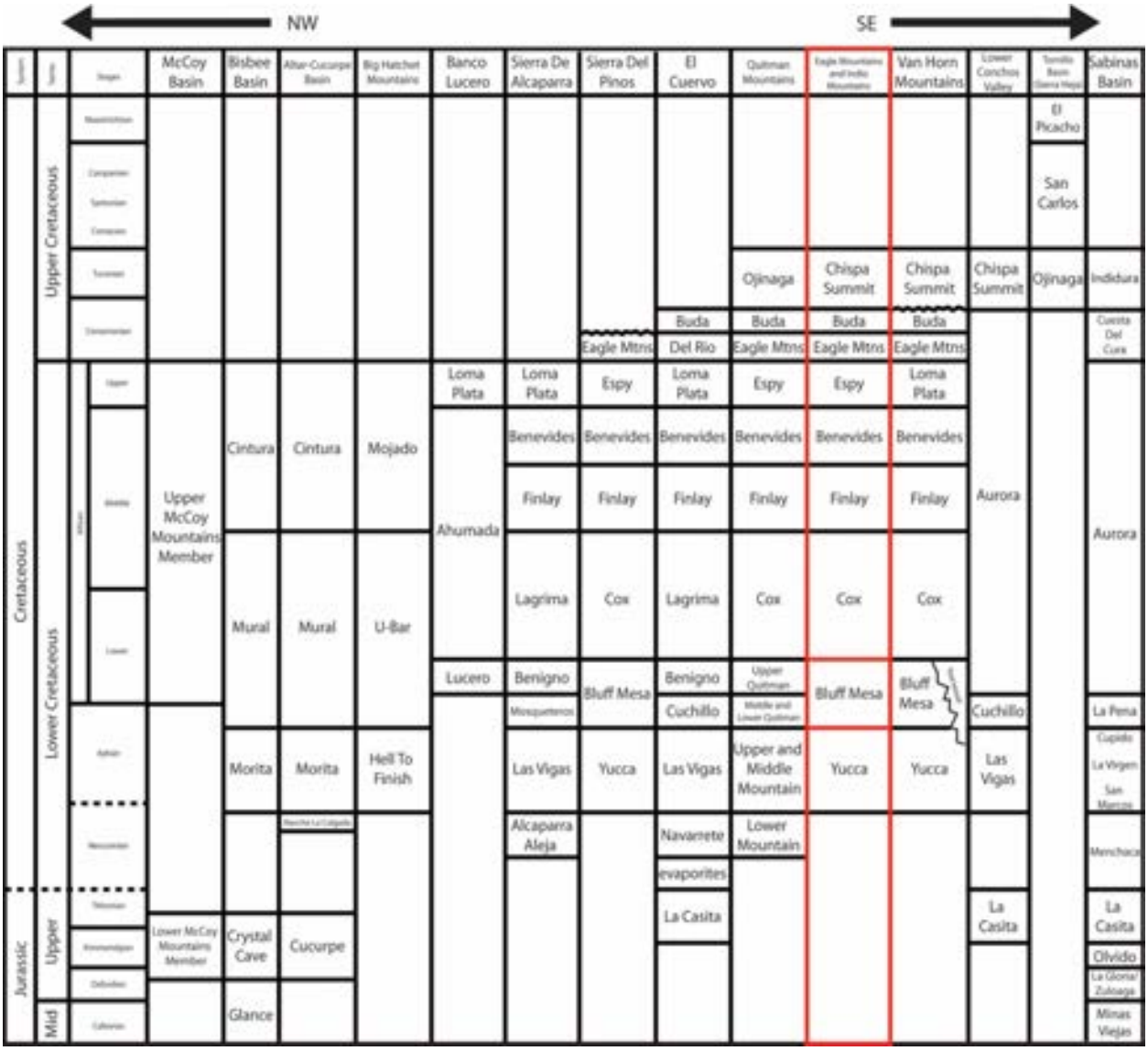

Figure 2.4: Regional stratigraphy of the Chihuahua Trough.
Stratigraphy of the Chihuahuan Trough from NW to SE. Locations are shown in Figure 2.3, with the exceptions of McCoy, Bisbee, Altar-Cucurpe, and the Sabinas Basins, which can be located in Figure 2.1. Compiled from King and Adkins (1946), Ramirez and Acevedo (1957), Haenggi (1966), Cordoba (1969), Rodriguez-Torres (1969), DeFord and Haenggi (1970), Jones and Reaser (1970), Zeller (1970), Underwood (1980), Peterson (1985), Monreal and Longoria (1999), Dickinson and Lawton (2001b), Haenggi (2002), Duque-Botero (2006), Gonzalez-Leon (2008), Mauel et al. (2011), Spencer et al. (2011), Dietzel (2013), and Li (2014).

the late Albian Loma Plata (Monreal and Longoria, 1999). These formations consist of a wide range of lithologies but limestone is prominent throughout as most deposition occurred on

shallow marine platforms and shoreface environments (Haenggi, 2002). Deposition was confined to the trough until the late Aptian when rising sea levels established marine conditions on the Diablo platform and completely submerged the Aldama platform.

Seas had inundated large swaths of the North American continent by middle Albian time resulting in the deposition of the Cox Sandstone on the Diablo platform and into the eastern margins of the trough where it thickens from 60 m to over 300 m (Figure 2.2; Albritton and Smith, 1965; Budhathoki, 2013). Carbonate platform environments were typical of the western margin and keel of the Chihuahua Trough with deposition of the Lagrima Formation, which grades laterally into the Cox Sandstone (Figure 2.2; Cordoba, 1969). Carbonate lithologies continued to dominate the trough from late Albian to early Cenomanian time with units such as the Finlay, Loma Plata, Buda, and Espy formations with occasional periods of clastic deposition represented by the Benevides and the Del Rio formations (Haenggi, 2002).

A sudden influx of clastic material into the Chihuahua Trough occurred in the Cenomanian with deposition of the Ojinaga, a thick predominantly marine shale with some sand and limestone interbeds. The Ojinaga is coeval with a number of clastic wedges deposited in the Western Interior Cretaceous Seaway (Figure 2.4; Haenggi, 2002). These deposits are most likely related to a stage of increased uplift in the Cordillera, which supplied large amounts of clastics to the basins of western North America (Muehlberger, 1992). The Ojinaga grades upward into the marginal marine San Carlos Formation and then the terrestrial El Picacho Formation, both of which are rarely preserved. The El Picacho Formation is a claystone-sandstone, which marks the return of the trough to a terrestrial environment and the end of Cretaceous deposition (Haenggi, 2002).

Inversion of the Chihuahua Trough during the Laramide orogeny (84-43 Ma) resulted in exposure of previously buried Cretaceous basin fill in thrust panels across Trans-Pecos Texas, New Mexico, and Chihuahua (DeFord, 1958; Haenggi, 2002). Laramide shortening was driven by the movement of the North American plate over the Farallon plate resulting in progressively younger deformation from west to east across the American southwest (Coney, 1976). Although exact timing of Laramide shortening is unclear, the Chihuahua Trough had ceased to exist as a major depocenter by 83 Ma as the ocean retreated to the Tornillo foreland basin (Figure 2.1; Stevens and Stevens, 1990; Lehman, 1991). A discussion of the deformation style is beyond the scope of this project but it should be noted that faulting was heavily controlled by characteristics of the basin fill such as evaporite décollement and a high density of pre-existing faults at the trough-platform margin (Haenggi, 2002). Although tectonism, volcanism, and evaporite withdrawal have continued to modify the inverted basin fill Post-Laramide, the effects have been comparatively minor in comparison to the Laramide Orogeny.

2.2 THE INDIO MOUNTAINS

Approximately 200 km southwest of El Paso the Indio Mountains contain an exceptionally well exposed Lower Cretaceous rift-fill sequence, which was first described by Underwood in 1962 (Figure 2.5; Figure 2.6). The Indio Mountains are a north-northwest trending range that extend from the Eagle Mountains to the Rio Grande (Figure 2.5). Previous authors have described the Indio Mountains as an arcuate, convex-eastward shaped range that can be divided into two general domains divided by the Indio normal fault (Underwood, 1962; Rohrbaugh, 2001; Carciumaru, 2005; Page, 2011). The eastern domain is characterized by a fold and thrust imbricate stack transported marginward of the old rift system from the southwest. The western domain is composed of complexly deformed strata of the Yucca and Bluff Mesa

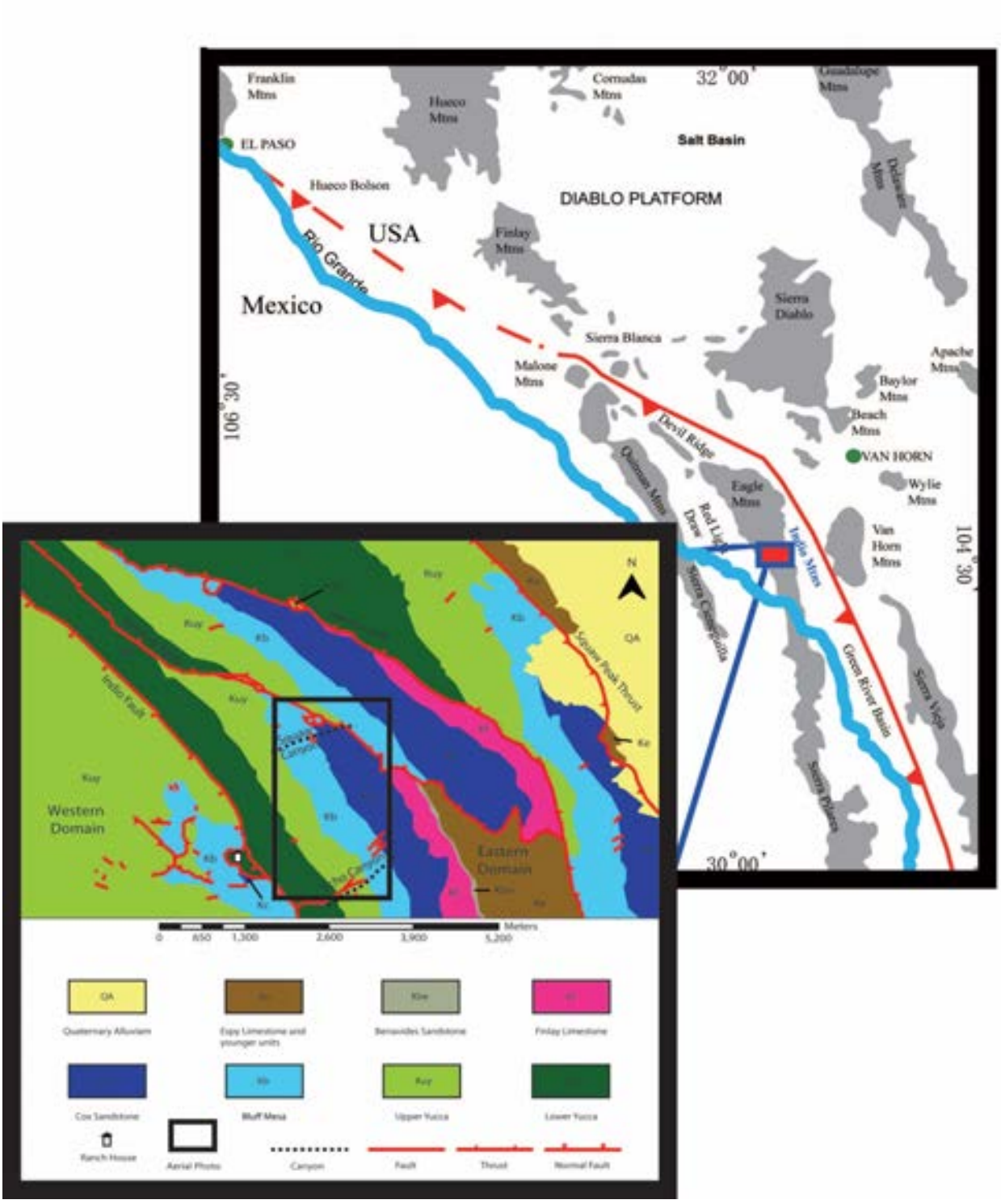

Figure 2.5: Local mountain belts near the US-Mexico border and simplified geologic map of the Indio Mountains (inset).
Aerial photo on inset map refers to Figure 4.1. Modified from Rohrbaugh (2001), Page (2011), and Li (2014).

formations (Page, 2011). Exposures in the eastern domain are controlled by two major thrust faults that divide the domain into three thrust panels. The Squaw fault separates the northern and central thrust panels with a minimum displacement of 17-18 km (Page, 2011). The Bennet fault parallels the Squaw fault and separates the central and southern thrust panels with a displacement of approximately 7 km (Page, 2011). The resulting exposures are characterized by older and more distal deposits in hanging walls and younger, proximal deposits in footwalls. This study focuses on the southern thrust panel, which represents proximal deposits of lower Yucca through Espy formations that were originally deposited 7 kilometers southwest of the present location (Figure 2.5; Figure 2.6).

The southern thrust panel is cut by numerous northeast trending small-scale normal faults with an average offset of 5 meters. Previous studies have identified growth strata and facies changes in the upper Yucca and Cox formations across the normal faults indicating active faulting during deposition on the Chihuahua Trough eastern margin (Page, 2011; Budhathoki, 2013; Li, 2014; Fox, 2016). These syndepositional faults are distributed across the southern thrust panel in lower Yucca through Cox strata with notably higher density in the Echo Canyon area (Figure 2.5).

The Cretaceous (Aptian to Turonian) rift-fill sequence exposed on the southern thrust panel contains basal alluvial and fluvial strata of the lower member of the Yucca Formation transitioning upward to cyclic lacustrine and fluvial facies of the upper Yucca Formation (Figure 2.6; Underwood, 1962; Li, 2014; Fox, 2016). The Yucca is overlain by a transitional zone of mixed marine and non-marine strata, which progress upwards to the open marine facies of the Bluff Mesa Formation (Li, 2014). Underwood designated the 1st appearance of the foraminifera *Orbitalina* as the base of the Bluff Mesa Formation representing the onset of open marine

conditions. Li (2014) reported the presence of a sandy oyster-rich packstone interpreted as a transitional estuarine deposit in what was formerly classified as a part of the underlying upper Yucca Formation. Although it was not laterally continuous across the study area, its presence signifies that marine transgression began earlier than previously thought and this oyster bed is currently interpreted as the initial marine transgression (Li, 2014).

The majority of the Bluff Mesa Formation consists of interbedded fossiliferous ooid grainstones and fine-grained siliciclastics indicative of fluctuating depositional controls on the open marine environment until the demise of the carbonate ramp marking the base of the overlying Cox Sandstone. Previous studies have divided the Bluff Mesa Formation into 3 unofficial units (Underwood, 1962; Page, 2011). The 3 unofficial units are described in stratigraphic order: 1) a lower unit of massive fossiliferous limestone beds; 2) a middle unit of interbedded limestone and quartz sandstone; 3) an upper unit of blue-gray fossiliferous limestone marl. This study does not formally utilize these subdivisions, however some units can be helpful as marker beds in aerial photos. Correlative formations of Aptian-Albian age in West Texas, New Mexico, and Chihuahua record regional marine transgression across the Chihuahua Trough margin in several localities (Figure 2.3; Figure 2.4; Jones and Reaser, 1970; Underwood, 1980; Monreal and Longoria, 1999; Haenggi, 2002).

The Cox Sandstone overlies the Bluff Mesa Formation within the Chihuahua Trough separated by a regionally extensive sequence boundary (Budhathoki, 2013). The Cox grades laterally into the Lagrima Formation to the southwest away from the margin (Figure 2.2; Figure 2.4; Haenggi, 1966). While the Bluff Mesa Formation is confined to the trough, the Cox extends onto the Diablo platform where it unconformably overlies Permian limestones (Albritton and

Smith, 1965). The Cox thins from >750 m in the El Cuervo area to 60 m outside of the trough

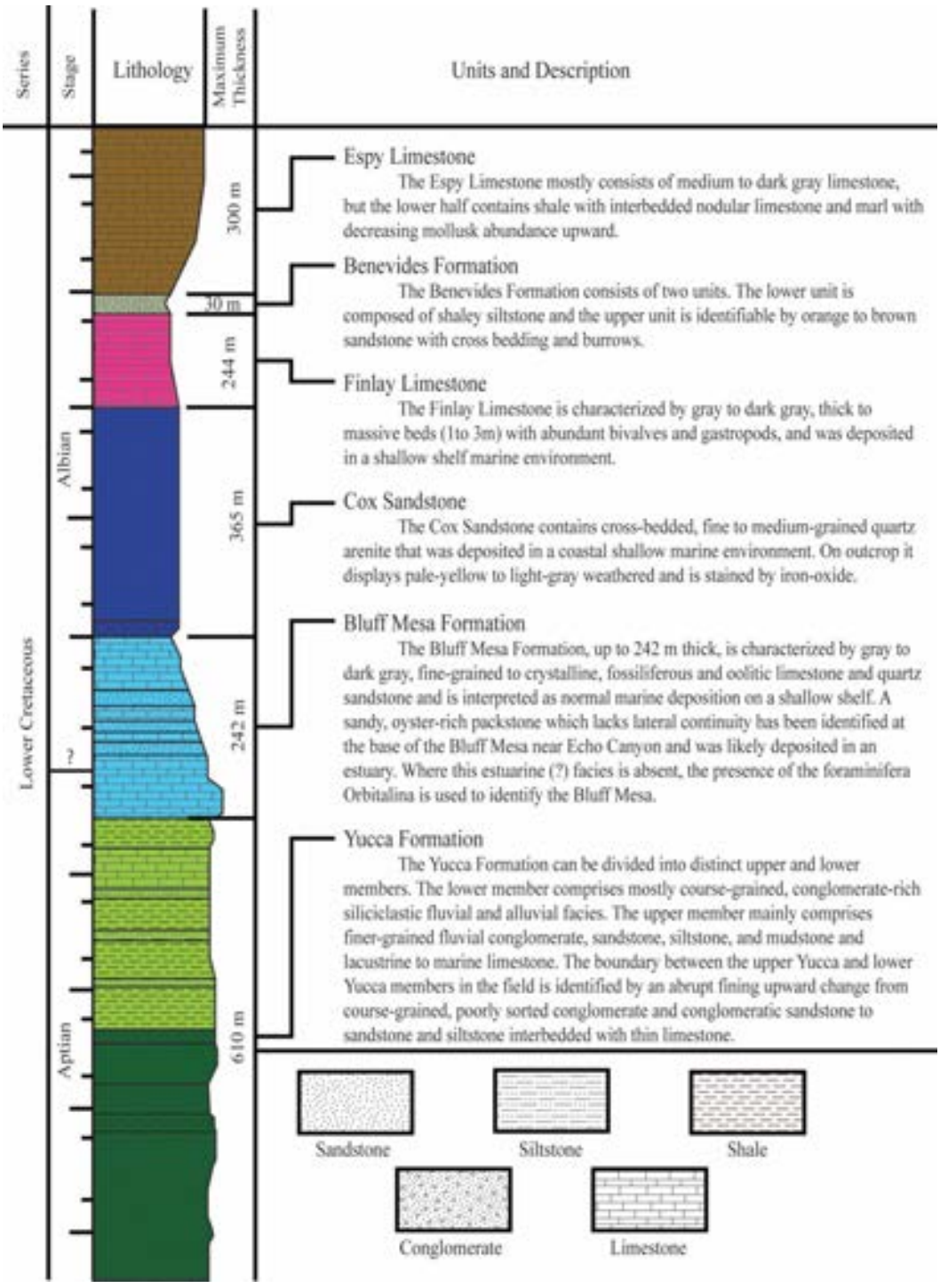

Figure 2.6: Simplified stratigraphic column and unit descriptions exposed in the Indio Mountains.
Modified from Underwood (1962), Page (2011), and Li (2014).

with a thickness of 365 m in the study area consistent with its location on the trough margin (Figure 2.2; Underwood, 1962; Albritton and Smith, 1965; Haenggi, 1966; Budhathoki, 2013).

The lower and upper Yucca, Bluff Mesa, and Cox formations are inherently different from the overlying Finlay, Benavides, and Espy formations in that they record syndepositional faulting and are either confined to the Chihuahua Trough or significantly thin over the Diablo platform. The Finlay Formation conformably overlies the Cox Sandstone and was deposited during widespread transgression over the Diablo platform. The Finley Formation is 244 m thick in the study area and composed of fossiliferous limestone with local Rudistid reefs (Underwood, 1962). The Benavides Formation is a 30 meter thick sandstone that conformably overlies the Finlay representing a short lived regression (Underwood, 1962). Conditions conducive to carbonate deposition on the platform returned with deposition of the Espy Formation (Underwood, 1962). The Espy is composed of 300 m of fossiliferous limestones, marls and shales. The Buda, Ojinaga and Chispa Summit formations overly the Espy Formation in the vicinity of the study area (Eagle Mountains, Quitman Mountains, and Van Horn Mountains respectively) but are not exposed in the southern thrust panel (Figure 2.4; Underwood, 1962; Jones and Reaser, 1970; Monreal and Longoria, 1999; Dietzel, 2013).

2.3 THE BLUFF MESA AS AN ANALOG TO THE SOUTH ATLANTIC RIFT BASIN

The Bluff Mesa is interpreted to have been deposited under similar conditions to the marine sealing facies of the South Atlantic Margin pre-salt reservoirs, because it is equivalent in age, tectonic regime, and climatic setting (Figure 2.7; Li, 2014). The Bluff Mesa was deposited during marine transgression onto a former lacustrine rift basin on the eastern margin of the Mesozoic Chihuahua Trough, a NW-SE trending rift basin bounded by the Diablo Platform to

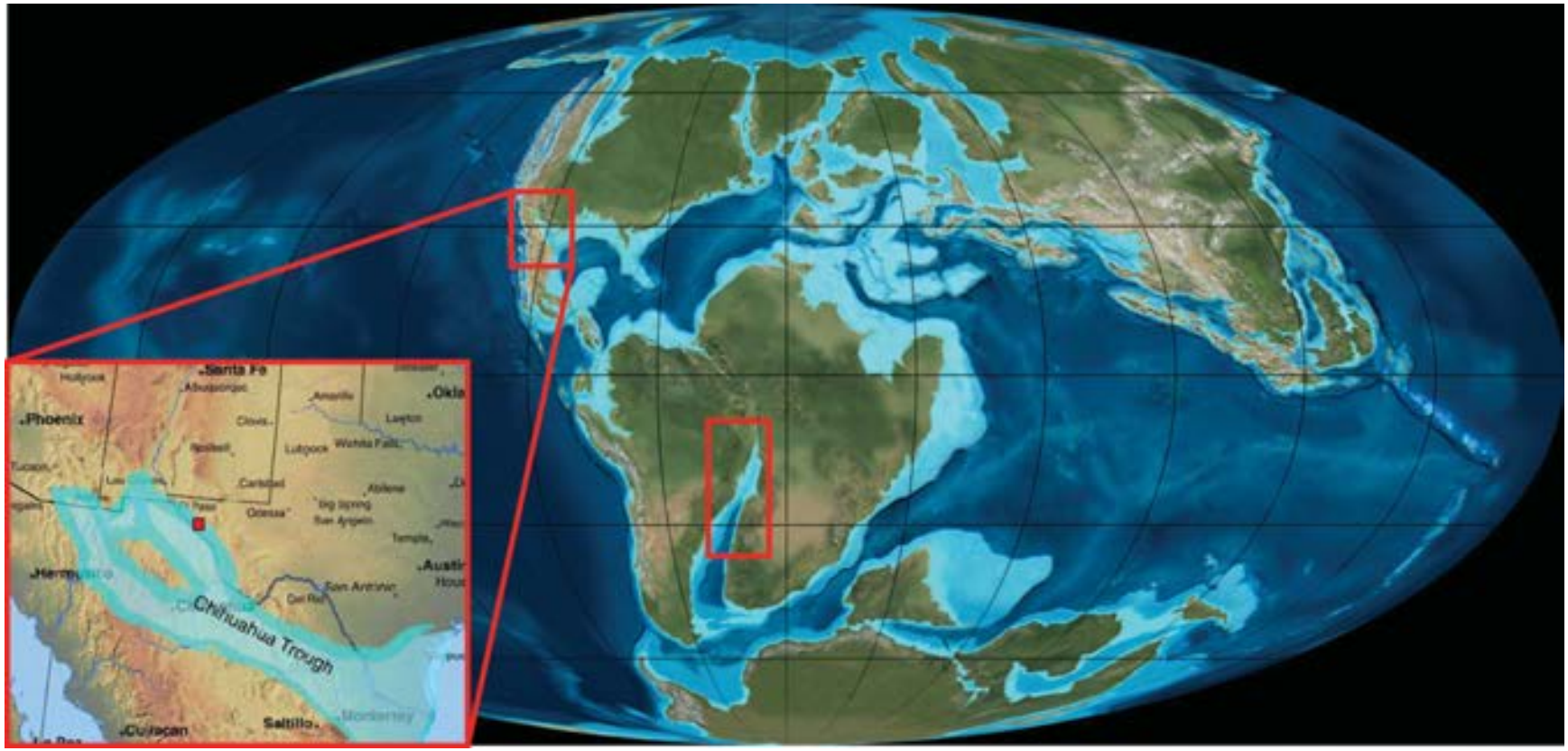

Figure 2.7: Early Cretaceous (120 ma) global reconstruction and regional reconstruction (inset).
Red boxes denote the South Atlantic Rift and the Chihuahuan Trough while the red rectangle within the inset represents the study area. Modified from Blakey (2010) and Budhathoki et al. (2010)

the NE and the Aldama Platform to the SW (Figure 2.1; Figure 2.2; Underwood, 1962; Haenggi, 2002). The Chihuahua Trough was likely influenced by the same tectonic processes controlling deposition of syn-rift fill in the South Atlantic during the breakup of Gondwana. Marine transgression occurred in both areas during a shift from a cool, dry climate to warmer and wetter conditions (Li, 2014; Wang et al., 2014). Additionally, the Bluff Mesa and the reservoirs of the South Atlantic were both deposited in the Upper Mesozoic, which minimizes the temporal possibility of largely different faunal assemblages and global ocean chemistry as both generally fall within the Albian-Upper Aptian Carbonate Analogs Through Time (CATT) timeslice (94-118 Ma) (Markello et al., 2008).

The two rift-fill sequences differ in that the initial marine transgressive deposits of the South Atlantic are capped by thick evaporites, whereas no evaporites have been observed above the Bluff Mesa in the study area. However, gypsum beds have been documented in the Chihuahua Trough center within lower sections of the correlative Cuchillo Formation and the Jurassic La Casita Formation, which is associated with a regressive event in the late Tithonian-Neocomian (Figure 2.2; Figure 2.3; Figure 2.4; Haenggi, 2002). Thick evaporites were also deposited in the Sabinas Basin during the Jurassic (Minas Viejas Formation) and the Neocomian-Aptian (La Virgen Formation) (Figure 2.4; Peterson, 1985). It is important to note that the lack of thick evaporite deposits does not preclude the Bluff Mesa as a useful depositional and stratigraphic model for extensional basins as evaporite deposition occurs post-transgression (Figure 1.2; Carminatti et al., 2008; Bryant, 2012; Quirk et al, 2012; Arai, 2014).

3. METHODS

Detailed facies and stratigraphic analysis of the Bluff Mesa Formation was based on the results from 6 measured sections within the southern thrust panel. Sections were measured from the base of the uppermost fluvial unit in the Upper Yucca Formation to the base of the Cox Sandstone identified by Budhathoki (2013). Full sections range in thickness from 250.2 to 362.1 meters with a maximum distance of 850 meters between sections. An additional partial section was measured on a horst block near Echo Canyon (EH) in order to accurately document facies changes across the horst and both adjacent grabens that record syn-depositional faulting.

Stratigraphic sections and geobody geometries were measured using GPS, Brunton and Jacob's staff. Sections were located using QGIS and high resolution satellite imagery in order to produce accurate figures in map view. Depositional geometries and contacts were recorded in the field and within satellite imagery with special attention being paid to the transitional zone near the top of the upper Yucca Formation above the lacustrine-marine contact and below the thick marine carbonate interval. Aerial photography utilizing a drone fitted with a GoPro camera was used to carry out initial reconnaissance, but no figures were constructed using this data. Important stratigraphic contacts were walked between sections with the aid of consenting field assistants. Lithofacies were tentatively categorized in the field and then refined after detailed examinations of both polished hand samples and thin sections. Lithofacies were then grouped into five facies associations, which were used to construct the sequence stratigraphic architecture of the Bluff Mesa Formation.

Hand samples were cut and polished at The University of Texas at El Paso Rock Lab with a water-based saw. Billets were cut from hand samples and sent to Texas Petrographic Inc. for thin section production. 25 x 46 mm thin sections were stained with alizarin red and

potassium ferricyanide to detect calcite and iron carbonate minerals. Petrographic analysis was performed on 52 thin sections, 12 of which underwent systematic 350 count point counts. Petrographic analysis of samples focused on descriptions of lithology, sedimentary structures, faunal assemblages, and diagenetic fabrics in order to identify and interpret depositional environments.

Sulfate, carbon, and oxygen isotope data was analyzed from septarian concretions of the Bluff Mesa and Upper Yucca formations. Samples were crushed and powdered using a hand mortar and then sieved through a 150 micron Standard USA Test Sieve. Samples were sent to the University of Washington's IsoLab for carbon and oxygen isotope analysis with results being reported in standard delta notation relative to the Vienna Pee Dee Belemnite (VPBD) standard. Sulfate was extracted at UTEP with a sequential leaching procedure using the carbonate associated sulfate extraction method detailed by Wotte et al. (2012) and Bergersen (2016). Sulfur isotope compositions are reported in delta notation relative to the Vienna Canyon Diablo Troilite (VCDT) standard.

4. FACIES ASSOCIATIONS

Twelve lithofacies were identified within the Bluff Mesa Formation exposed within the southern thrust panel of the Indio Mountains. Lithofacies were determined through outcrop and polished hand sample analysis, as well as observations obtained through petrographic analysis of 52 thin sections. Outcrop analysis focused on lithology, depositional geometry, bedding type and contacts, color (weathered and fresh), sedimentary structures and fossil content. These observations were aided by hand sample and thin section analysis focused on identification of faunal assemblages, sedimentary structures, and mineralogy. Eight siliciclastic and four carbonate lithofacies were subsequently partitioned into five depositional facies associations: 1) fluvial, 2) lacustrine littoral, 3) shallow marine carbonate shelf, 4) shallow marine siliciclastic shelf, and 5) siliciclastic mid-shelf, (Tables 4.1-5). The detailed measured stratigraphic sections used to document the lithofacies stratal distributions are compiled in Appendix A. The stratigraphic distribution of these depositional facies associations and important sequence boundaries are summarized in figures 4.1 and 4.2 and discussed in chapter five.

4.1 FLUVIAL FACIES ASSOCIATION (FA-1)

FA-1 comprises siliciclastic deposits with lenticular channel-shaped geobodies with erosive bases indicative of fluvial deposition that are common within the lower sequences of the Bluff Mesa. These deposits are composed of matrix-supported pebble conglomerate (Fc), fine to coarse-grained trough cross-bedded quartz arenite (Fs), and fine-grained laminated quartz arenite (Fsl) (Table 4.1). An ideal channel-fill sequence, grades upward from: 1) a matrix-supported pebble conglomerate with an erosional base grading into 2) trough cross-bedded sandstone overlain by 3) horizontally laminated sandstone (Figure 4.3). The ideal sequence is often incomplete in measured sections, typically due to an absence of basal conglomerates of FC.

Table 4.1: Lithofacies descriptions of fluvial facies association (FA-1).

Name	Lithology	Code	Color and Weathering Profile	Clast/Grain Type	Bedding	Sedimentary Structures	Depositional Interpretation
Matrix-Supported Pebble Conglome-rate	Chert and limestone pebble conglomerat e	Fc	Light to dark tan, gray, maroon; well-exposed	Generally matrix-supported, medium to coarse-grained detrital quartz matrix, subordinate detrital feldspar, chert and limestone pebbles, rare plant material, zircons, and chalcedony	Medium to massive, lenticular	Trough cross bedded, inclined cross strata	Fluvial channel
Trough-Cross Bedded Quartz Arenite	Fine to coarse-grained quartz arenite	Fs	Light tan, light beige, light gray, pinkish; well-exposed/ledge former	Fine to coarse-grained detrital quartz, rare chert pebbles, mudstone clasts and limestone clasts	Thin to thick, lenticular	Channelized, trough crossbedding, horizontal laminae, inclined laminae, soft-sediment deformation, burrows, ripple cross laminae, overturned troughs	Fluvial channel and point bar
Horizontal Laminated Quartz Arenite	Fine-grained quartz arenite	Fsl	Light to dark brown, pinkish to reddish tints; general well-exposed	Fine-grained detrital quartz, petrified wood	Thin to medium, lenticular or tabular	Horizontal laminae, faint ripple cross laminae, burrows, soft-sediment deformation	Overbank

Table 4.2: Lithofacies descriptions of lacustrine littoral facies association (FA-2).

Name	Lithology	Code	Color and Weathering Profile	Clast/Grain Type	Bedding	Sedimentary Structures	Depositional Interpretation
Burrowed Fine-Grained Quartz Arenite	Silt – fine grained quartz arenite	Ls	Sandstone: medium to dark brown; siltstone: tan to dark green, dark brown, poorly exposed	Silt – fine detrital quartz, chert, rare limestone clasts	Thin – thick tabular or lenticular	Burrowed/mottled, horizontal laminae, ripple cross laminae, and rare lenses of limestone pebbles	Lacustrine littoral
Massive Nodule-Bearing Mudstone	Massive nodule-bearing mudstone	Lm	Light red to maroon, very poorly exposed	Fine detrital quartz and micritic septarian nodules	Thick – massive tabular	Structureless	Lacustrine littoral

Table 4.3: Lithofacies descriptions of shallow marine carbonate shelf facies association (FA-3).

Name	Lithology	Code	Color and Weathering Profile	Clast/Grain Type	Bedding	Sedimentary Structures	Depositional Interpretation
Ooid Grainstone	Ooid grainstone	Cg	Dark gray, rusty orange striping, grayish green; well exposed/ledge former, blocky weathering pattern	Ooids, peloids, echinoids, crinoids, brachiopods, bivalves, gastropods, forams, micrite rip up clasts; 5-10% detrital quartz by volume	Medium – massive lenticular	Trough cross stratified, chickenwire fabrics, burrows, barforms can have erosive bases	Shallow open marine
Fossiliferous Wackestone-Packstone	Fossiliferous wackestone - packstone	Cf	Blue, dark blue, gray; well exposed/ledge former, nodular weathering pattern	Larger intact fossils than Cg, peloids, echinoids, crinoids, brachiopods, bivalves, gastropods, forams, and ostracods in a micritic matrix; 5-10% detrital quartz by volume	Thin – massive lenticular, can be wavy	Chickenwire fabrics and shell-rich bands	Shallow open marine; basinward from Cg
Sandy Packstone-Grainstone	Sandy packstone - grainstone	Cs	Light to dark gray, dark tan; moderate weathering and exposures	Ooids, peloids, echinoids, crinoids, brachiopods, bivalves, gastropods, forams, micrite rip up clasts; 20-60% detrital quartz by volume	Medium – thick, lenticular	Burrows, chickenwire fabrics, shell-rich bands ripple cross laminae, possible ray feeding trace	Shallow open marine; landward from Cg
Marl	Marl	Cm	Gray, tan with black splotches; poorly exposed	Very fine detrital quartz and lime mud, rare micritic limestone nodules or clasts	Thin - massive	Structureless	Shallow open marine; basinward from Cg, Cf, and Cs

Table 4.4: Lithofacies descriptions of shallow marine siliciclastic shelf facies association (FA-4).

Name	Lithology	Code	Color and Weathering Profile	Clast/Grain Type	Bedding	Sedimentary Structures	Depositional Interpretation
Hummocky /Swaley Cross-Stratified Quartz Arenite	Fine – Coarse Quartz Arenite	Ss	Sandstones: light gray, off-white, black and white speckles, can be tan to orange in thin bedded exposures; moderately weathered; Siltstones: Tan, khaki, olive green, dark green approaching black, dark brown, reddish brown; generally friable and poorly exposed	Fine – coarse detrital quartz; phosphate, rare brachiopod and gastropod fragments	Thin – massive lenticular or tabular	Trough cross stratified, inclined laminae, planar laminae, ripple laminae, overturned troughs, channelized, hummocks and swales, burrows	Middle shoreface, upper shoreface, and foreshore
Matrix-Supported Carbonate Clast Conglomer-ate	Conglom-erate	Sc	Light to dark brown, dark gray	Limestone pebbles and rip up clasts, chert pebbles, bivalve and brachiopod fragments in a coarse detrital quartz matrix	Thick – massive lenticular	Channel scours, inclined laminae	Shallow marine channel

Table 4.5: Lithofacies descriptions of middle shelf siliciclastic facies association (FA-5).

Name	Lithology	Code	Color and Weathering Profile	Clast/Grain Type	Bedding	Sedimentary Structures	Depositional Interpretation
Olive Green Shale, Siltstone, and Fine-Grained Quartz Arenite	Shale – Fine Grained Sandstone	Mss	Tan or khaki with green undertones, faded olive green, dark olive green; poorly exposed	Fine detrital quartz, rare gastropods, chert, and shale clasts	Thin – medium lenticular or tabular	Horizontal laminae, inclined laminae, symmetrical ripples, mud drapes, can be burrowed/mottled	Open marine mid-shelf

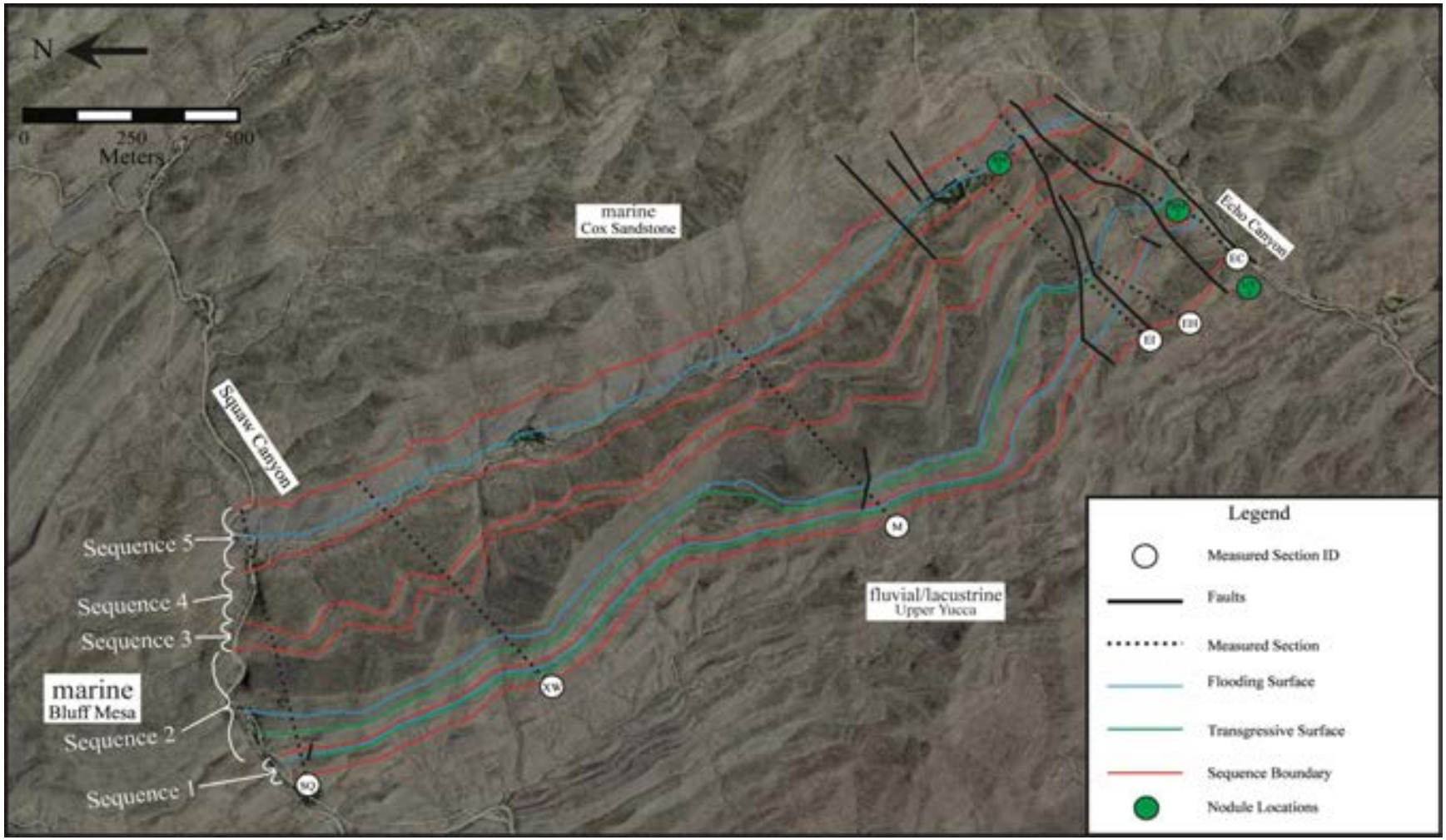

Figure 4.1: Aerial photograph of the Indio Mountains southern thrust panel showing locations of measured sections, major faults and important sequence stratigraphic surfaces.

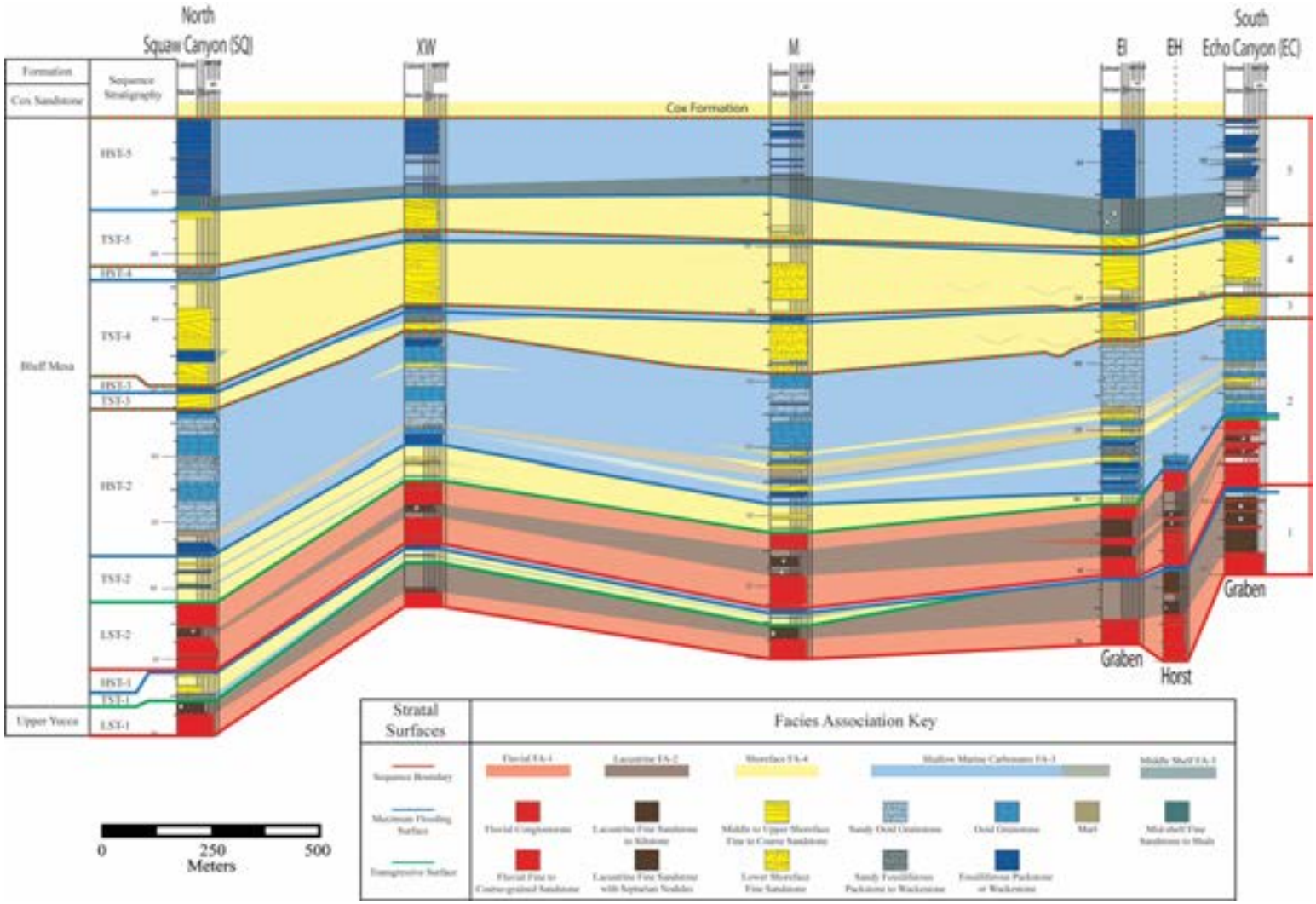

Figure 4.2: Stratigraphic correlation and facies distribution of uppermost Yucca and Bluff Mesa formations between Echo and Squaw Canyons, Indio Mountains, TX.

Individual channels are 4 m wide on average with some extending over 100 meters laterally. Channels average 0.5 meters in thickness, resulting in width to depth ratios clustering around 9:1. Channels can occur as isolated single-story bodies or stacked into amalgamated multistory channel complexes. Individual channels are not continuous across the thrust panel but two sand-rich intervals are reliably traceable between Echo and Squaw canyons (Figure 4.2). The presence of amalgamated channel complexes helps differentiate FA-1 from channels of marine origin (Sc), which only occur as isolated channels.

4.1.1 Matrix-Supported Pebble Conglomerate (Fc)

Conglomerates are characterized by 25-35 cm thick discontinuous (<15 meters laterally) lenticular beds with sharp erosive concave-up bases (Figures 4.3B, 4.4A, and B). Fc is composed of an upper medium to coarse-grained detrital quartz sand matrix containing abundant sub-angular to sub-rounded chert and limestone pebbles (Figure 4.5A and B). Outcrops are dark gray or maroon on weathered surfaces with light to dark gray or red matrix exposed on fresh surfaces. The detrital quartz matrix is poorly to moderately sorted with grain sizes ranging from 0.8 to 0.05 millimeters (.35 mm average). Quartz grains have high to moderate sphericity and are sub-rounded to sub-angular.

Fc may be clast or matrix-supported with a measurable size change from .3 mm average quartz grains in matrix-supported conglomerates to a .45 mm average in clast-supported conglomerates (Figure 4.5A and B). Matrix-supported conglomerates are much more common than their clast-supported counterparts, which are only observed in substantial thickness (> 2-3 cm) in a single measured section (see appendix).

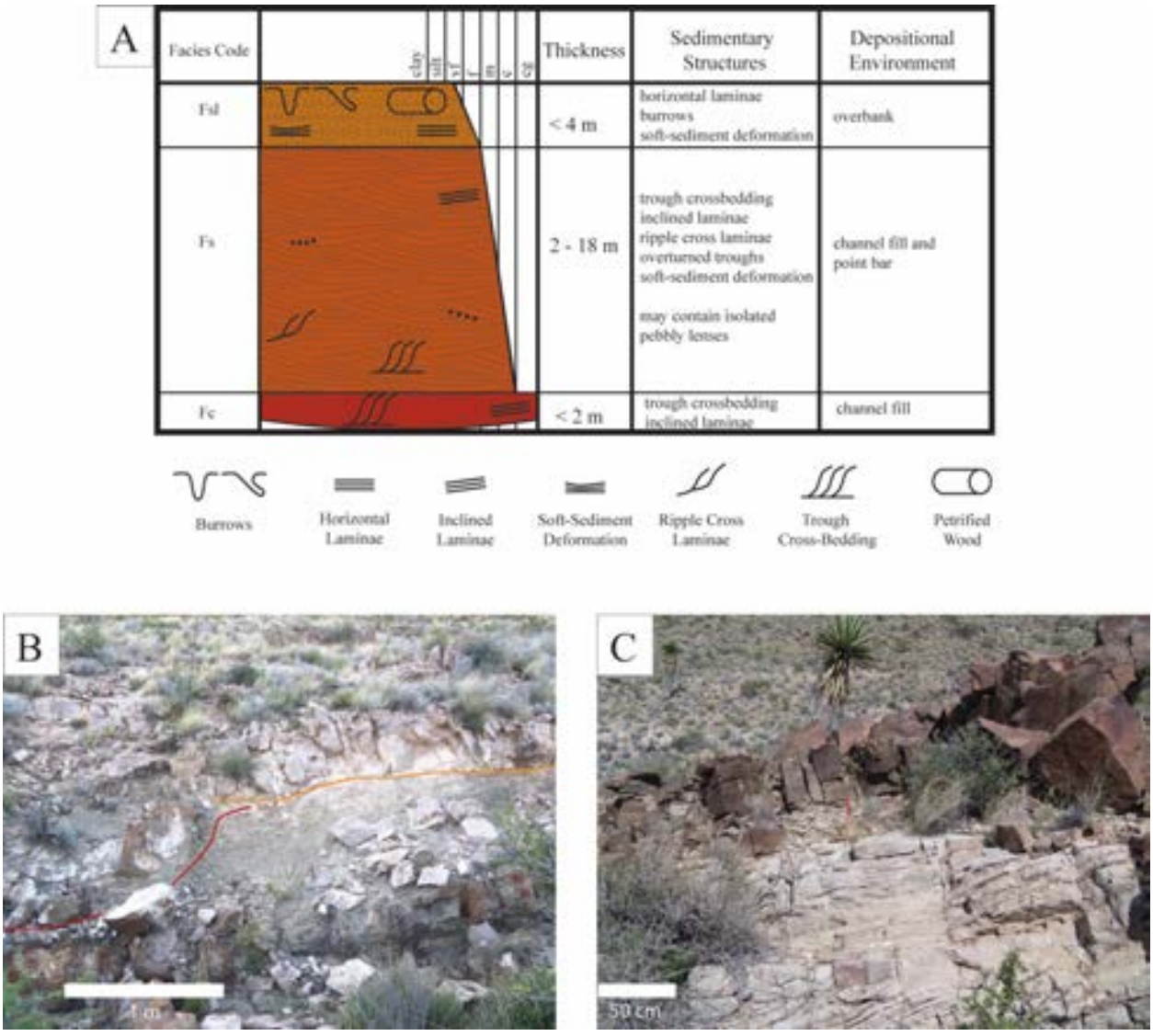

Figure 4.3: Idealized vertical succession of fluvial facies FA-1 and field photos showing transitions.
(A) Idealized vertical succession of FA-1; (B) Conglomerate lense (red) (Fc) grading upwards into a channel-fill sandstone of Fs (orange). Note the concave-up erosive base of the channel is cut into underlying lacustrine facies; (C) Trough cross-bedded sands of Fs that grade upwards into finer-grained horizontally laminated sandstone of Fsl

Chert pebbles are orange to red (2-8 mm) and trend towards sub-rounded while limestone pebbles are dull gray to black and trend towards sub-angular (4 mm - 3 cm). Limestone clasts are primarily micrite but also contain a sizeable percentage of quartz grains and rare unidentified

shell fragments (Figure 4.5B). Rare examples include clasts of septarian nodular origin (Li, 2014) where channels directly cut into lacustrine facies.

4.1.2 Trough Cross-Bedded Quartz Arenite (Fs)

Basal conglomerates (Fc) are overlain by low angle (10 -20 degree) trough cross-bedded sandstones (Fs) (Figure 4.4A). These sandstones are colored light tan to dark brown, light gray, and pink in weathered samples with varying percentages of off-white and red grains in fresh samples. Fs is composed of 90-95% detrital quartz with a subordinate amount of detrital feldspar, chert and carbonate rip-up clasts (Figure 4.5D). Quartz grains are sub-angular to sub-rounded, moderately sorted, and range from upper fine (0.25 mm) to lower coarse grains (0.55 mm).

Fs exhibits a variety of sedimentary structures including trough cross-bedding, overturned troughs, planar tabular cross-bedding, inclined laminae, ripple laminae, and soft-sediment deformation structures (Figure 4.4C, D and E). Lenticular beds of Fs are 15-40 cm thick and typically have concave-up erosive bases (Figure 4.4E). Trough cross-bedded sandstones can contain rare localized chert and limestone pebble intervals but they are generally less than 5 cm thick and are laterally discontinuous (<40 cm).

4.1.3 Horizontal Laminated Quartz Arenite (Fsl)

Trough cross-bedded sandstones are often overlain by horizontally laminated sandstones of similar lithology (Fsl) (Figure 4.4C). Laminae are typically cm scale within 10-30 cm beds, which tend to be more laterally continuous and tabular than their trough cross-bedded counterparts. Laminated sandstones can be finer-grained, redder, and more thinly bedded than trough cross-bedded sandstones of Fs, however successions with little to no change in lithology

were also observed (Figure 4.4C). Detrital quartz grains are typically sub-rounded with moderate

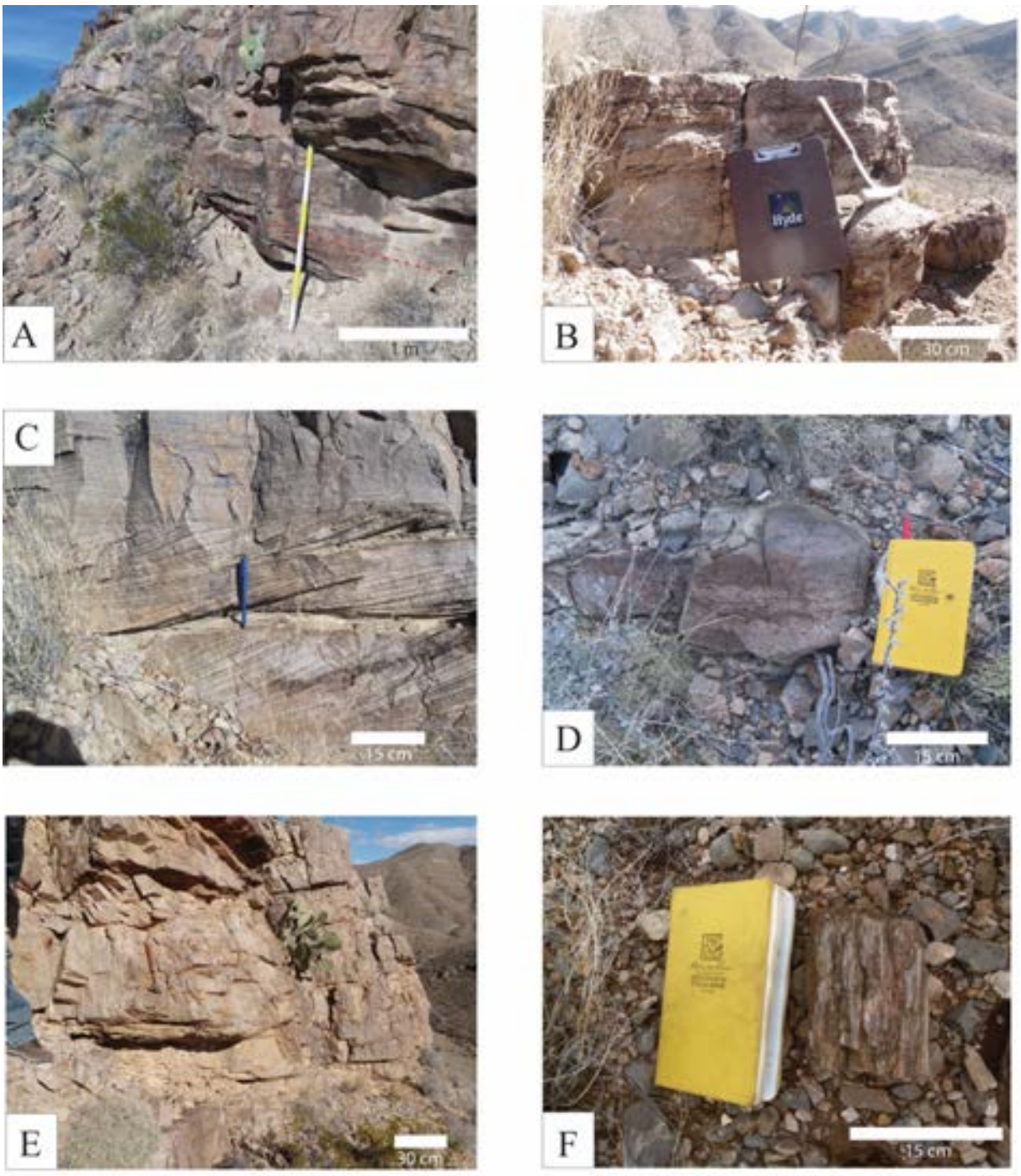

Figure 4.4: Outcrop photos of Fluvial Facies Association (FA-1).
(A) Channel fill with erosive concave-up conglomerate (Fc) overlain by lenticular beds of trough cross-stratified sandstone (Fs) (separated by red line); (B) Trough cross-bedding in Fc; (C) Trough cross-bedding overlain by horizontal laminae in Fs; (D) Soft sediment deformation in Fs;

(E) Channelized lenticular beds of medium-grained sandstone (Fs) cutting into one another, resulting in a stacked channel complex; (F) Petrified wood float in a recessive interval of Fsl.

to high sphericity, ranging from 0.1 to 0.07 millimeters. Laminae may be destroyed in the upper 5-10 cm by burrowing near bed tops. Poorly-exposed intervals of Fsl occasionally produce petrified wood as float but it is not common enough to be a reliable diagnostic characteristic (Figure 4.4F). Although horizontally laminated sandstones cap the ideal sequence, they are often observed interbedded with lenticular trough cross-bedded sandstones throughout the fluvial channel fill deposits.

4.1.4 Depositional Environment of FA-1

Fluvial deposits are widespread throughout the rift-fill sequence of the Indio Mountains (Underwood, 1962). Some are located in the Upper Yucca Formation where they are interpreted to represent the top of a series of coarsening-upwards cycles (Underwood, 1962; Li, 2014; Fox, 2016). Fluvial deposits are also identified as interbedded with alluvial fan deposits in the Lower Yucca Formation and as lowstand deposits in the predominantly shallow marine Cox Sandstone (Underwood, 1962; Budhathoki, 2013). No fluvial deposits had previously been identified in the Bluff Mesa Formation, however this study finds a significant fluvial component in the lower depositional sequences of the Bluff Mesa.

Criteria commonly used to identify fluvial facies includes channel geomorphologies with erosional bases, immature sediment textures and compositions, evidence of subaerial exposure, unidirectional paleocurrents, and a lack of marine fossils (Miall, 1985; Collinson, 1996). Channelized beds are recognized throughout the lower Bluff Mesa in both Fc and Fs with unimodal paleocurrents indicating sediment transport from south to north. The lack of marine fossils and presence of conglomerate deposits were instrumental in confirming a fluvial origin

for FA-1 and separating it from shallow marine deposits of FA-4. However, no obvious evidence for subaerial exposure such as desiccation cracks or paleosols were identified. Stratigraphic evidence also supports a fluvial interpretation of FA-1 as it is always positioned directly below or above lacustrine deposits of FA-2.

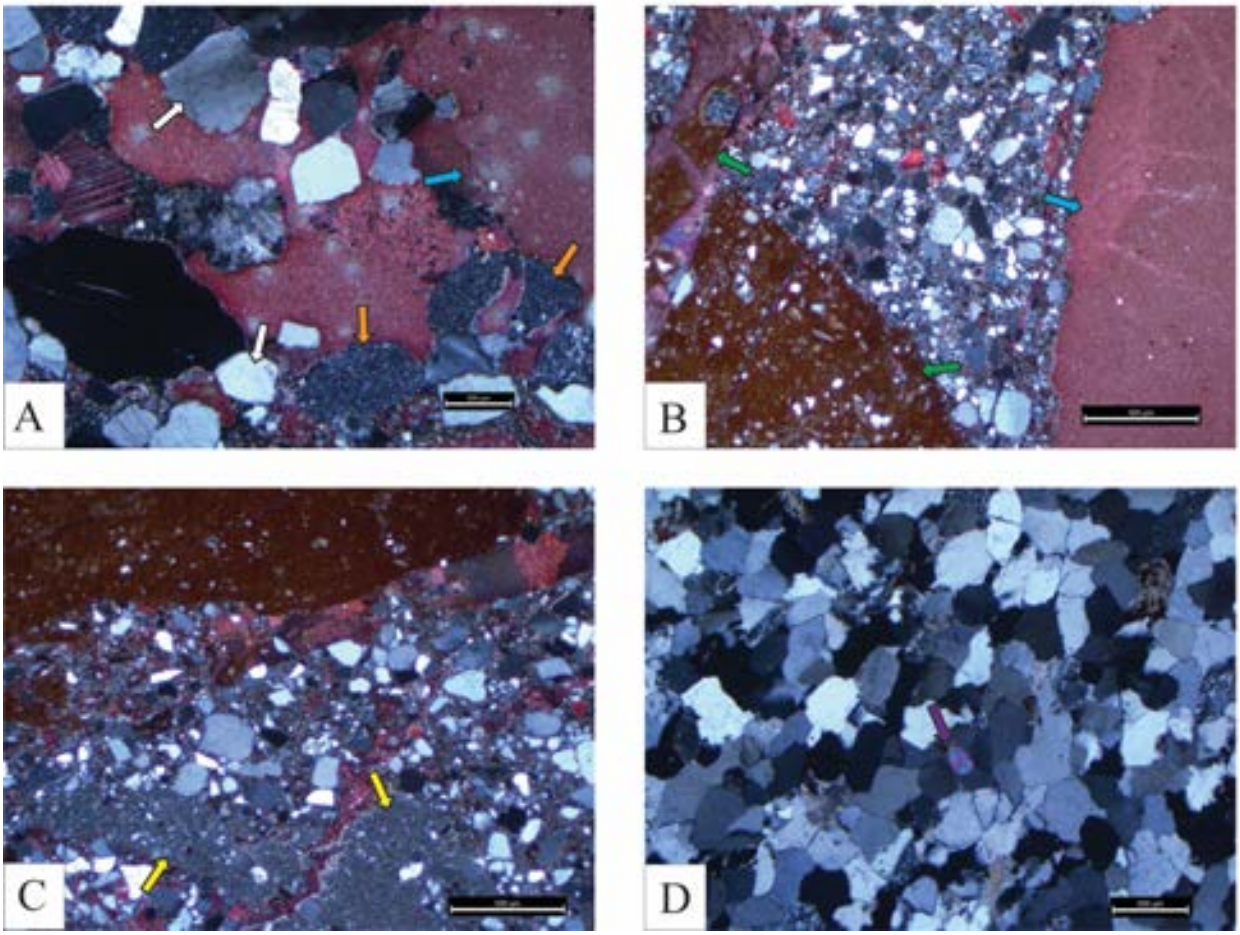

Figure 4.5: Photomicrographs of Fluvial Facies Association (FA-1).
(A) Coarse grained detrital quartz (white arrow), chert pebbles (orange arrow), and limestone clasts (blue arrow) typical of clast-supported Fc, cross polarized light, scale bar = 200 μm; (B) Large angular limestone clasts composed of micrite (blue arrow) and quartz-rich microcrystalline quartz (green arrow), note the finer quartz matrix associated with matrix supported Fc, cross polarized light, scale bare = 500 μm; (C) Poorly sorted detrital quartz matrix with 2 fine grained siliciclastic clasts (yellow arrow), cross polarized light, scale bar = 500 μm; (D) Medium grained sandstone (Cs) with a moderately well rounded zircon (purple arrow). Cs is highly compacted throughout the study area as indicated by concavo-convex boundaries between quartz grains, cross polarized light, scale bar = 200 μm.

Li (2014) identified fluvial deposits throughout the Upper Yucca associated with thick ledge-forming conglomerates that reached up to 52 meters in thickness. No conglomerate facies of comparable thicknesses and distributions were identified in the Bluff Mesa, indicating the style of fluvial deposition had changed. Matrix-supported conglomerates of Fc differ from conglomerates of the Lower and Upper Yucca in that they are found only within discontinuous lenticular beds with thicknesses of < 2 meters.

The discontinuous nature and erosive bases of Fc suggests it was deposited in a confined turbulent flow regime at the channel base of a braided or meandering river (Figure 4.6). Gravel sheets deposited during periods of unconfined turbulent flow are more closely associated with braided rivers and are notably absent in the Bluff Mesa (Collinson, 1996). The distal reaches of braided systems are sand-dominated and contain < 10% gravel by volume (Miall, 1985). Channel belts in the lower Bluff Mesa are approximately 2% gravel by volume, falling well below the 10% threshold for distal braided systems. The presence of a braided river system during Bluff Mesa time cannot be ruled out but the lack of thick conglomerates favors a meandering interpretation. Deposition in a meandering river system is further supported by the presence of lateral accretion sets associated with point bars in Fs (Miall, 2010).

The size and rounding difference between chert and limestone pebbles suggests that clasts originated from two distinct source areas as limestones should be smaller and more rounded due to higher clast chemical weathering rates and ease of mechanical weathering (Bathurst, 1975; Rimstidt, 1997; Gunnarsson and Arnórsson, 2000; Fox, 2016). Although limestone pebbles contain rare fossils, they predominantly resemble micrite-rich nodules found

in the lacustrine intervals of the Bluff Mesa and Upper Yucca (Li, 2014; Fox, 2016). Therefore we can assume that well-rounded chert pebbles were transported a significant distance from the source area, while more angular limestone pebbles were sourced from underlying lacustrine sediments near the study area.

Paleocurrents gathered from channelized Fs deposits cluster in a northwards direction semi-parallel to the rift axis (see Appendix B). The lack of chert-rich conglomerates in the basinward Las Vigas Formation suggests that the study area received sediment from a unique chert-bearing source area to the southeast (Haenggi, 2002). Fluvial deposits in the Bluff Mesa Formation show north-trending paleocurrents and similar pebble assemblages to conglomerates of the Upper Yucca Formation suggesting the dominant southeast-northwest axial drainage pattern was still active at this time.

Fine to coarse-grained quartz arenites of Fs exhibit a variety of sedimentary structures that indicate high (trough crossbedding) to low (planar tabular cross-bedding) energy deposition. The succession of coarse to fine-grained higher energy deposits grading upwards into fine-grained lower energy deposits is typical of fluvial deposition (Collinson, 1996). Trough cross-bedding in Fs represents migrating subaqueous 3-D dunes while planar tabular cross-bedding is a result of 2-D dunes deposited in a lower energy flow regime (Ashley, 1990; Miall, 2010). Both 3-D and 2-D dunes represent deposition within channels and the point bar environment (Collinson, 1996; Miall, 2010). Lateral accretion sets are recognized sporadically throughout the panel, suggesting point bar deposition within a meandering stream. Medium-grained trough cross-bedded sandstone of Fs represents the majority of fluvial channel belts by volume, indicating that the system was primarily sandy with lower volumes of fine-grained particles carried through suspension (Collinson, 1996).

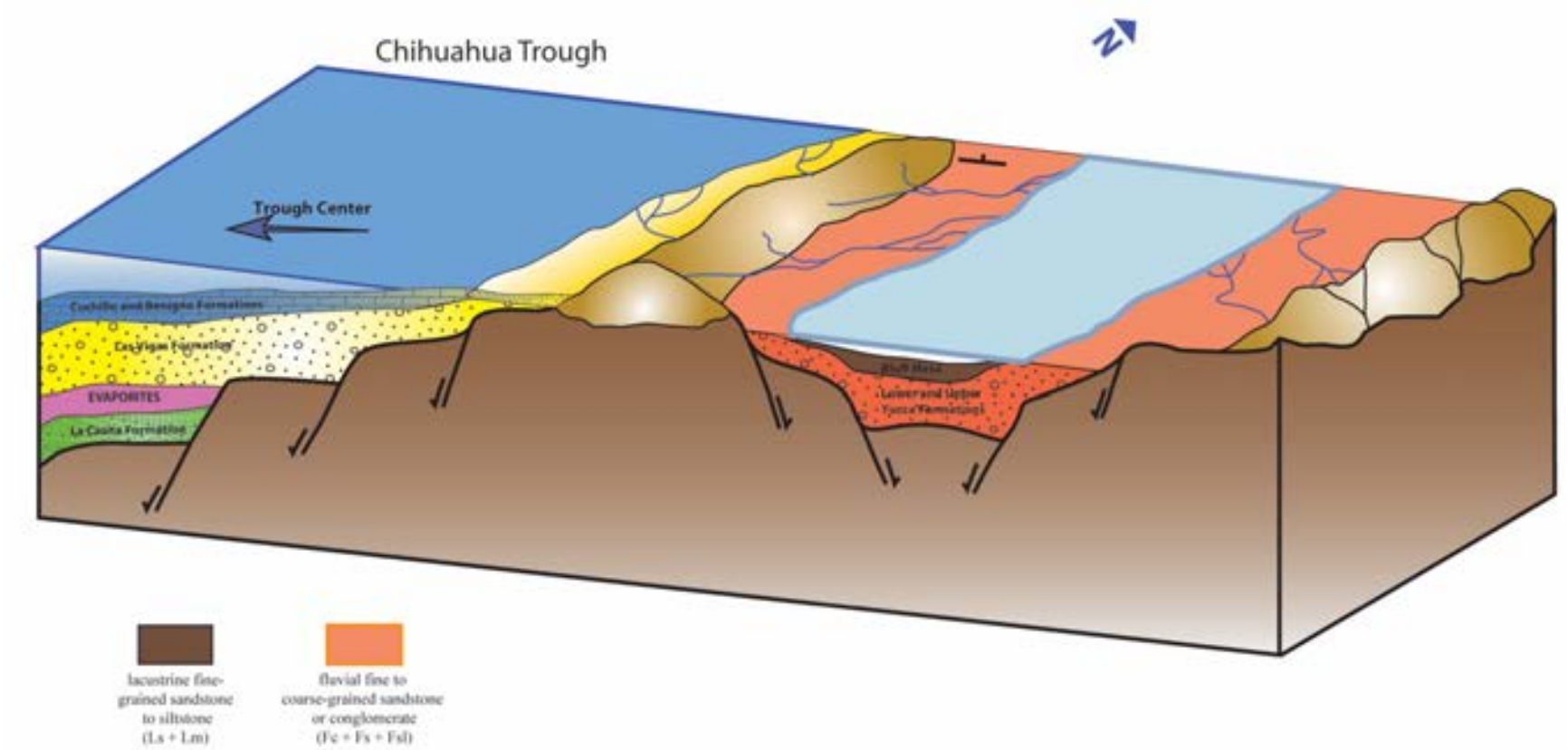

Figure 4.6: Idealized depositional environments of the Chihuahua Trough during fluvio-lacustrine deposition.

Fine-grained horizontally laminated or burrowed sandstones of Fsl are interpreted as well-preserved overbank/floodplain deposits. Planar bedding may occur under high velocity flow regimes that exceed the energy necessary for creation of dunes (Collinson, 1996). If planar laminations of fsl were deposited under a high velocity flow regime we would expect them to occur directly above Fc and generally below cross-bedded fs as energy decreases upwards in the fluvial system. This is not the case as planar laminated beds of fsl are found interbedded or overlying fs. The presence of faint ripples in fsl, which form under low velocity flows, indicate deposition was under a low energy regime (Collinson, 1996). Desiccation cracks and paleosol development are commonly observed in overbank deposits associated with periods of subaerial exposure (Miall, 1978; Collinson, 1996; Miall, 2010). However, no desiccation cracks or paleosols were identified in the Bluff Mesa Formation. The highly burrowed nature of many bed tops indicate periods of slow depositional rates typical of the overbank environment. The absence of subaerial exposures is puzzling but this may be explained by destruction of desiccation cracks through extensive burrowing or insufficient periods of subaerial exposure and non-deposition permitting paleosol development.

4.2 LACUSTRINE FACIES ASSOCIATION (FA-2)

Lacustrine deposits in the study area are composed of silt to fine-grained sandstones (Ls) and nodule-bearing mudstones (Lm) (Figure 4.7; Table 4.2). Fine-grained sandstones and siltstones generally overlie nodule-bearing mudstones and contacts may be gradational or sharp. Both lithologies are often highly weathered and recessive so their presence was inferred in covered sections when diagnostic float is present in the absence of sufficient outcrop exposure.

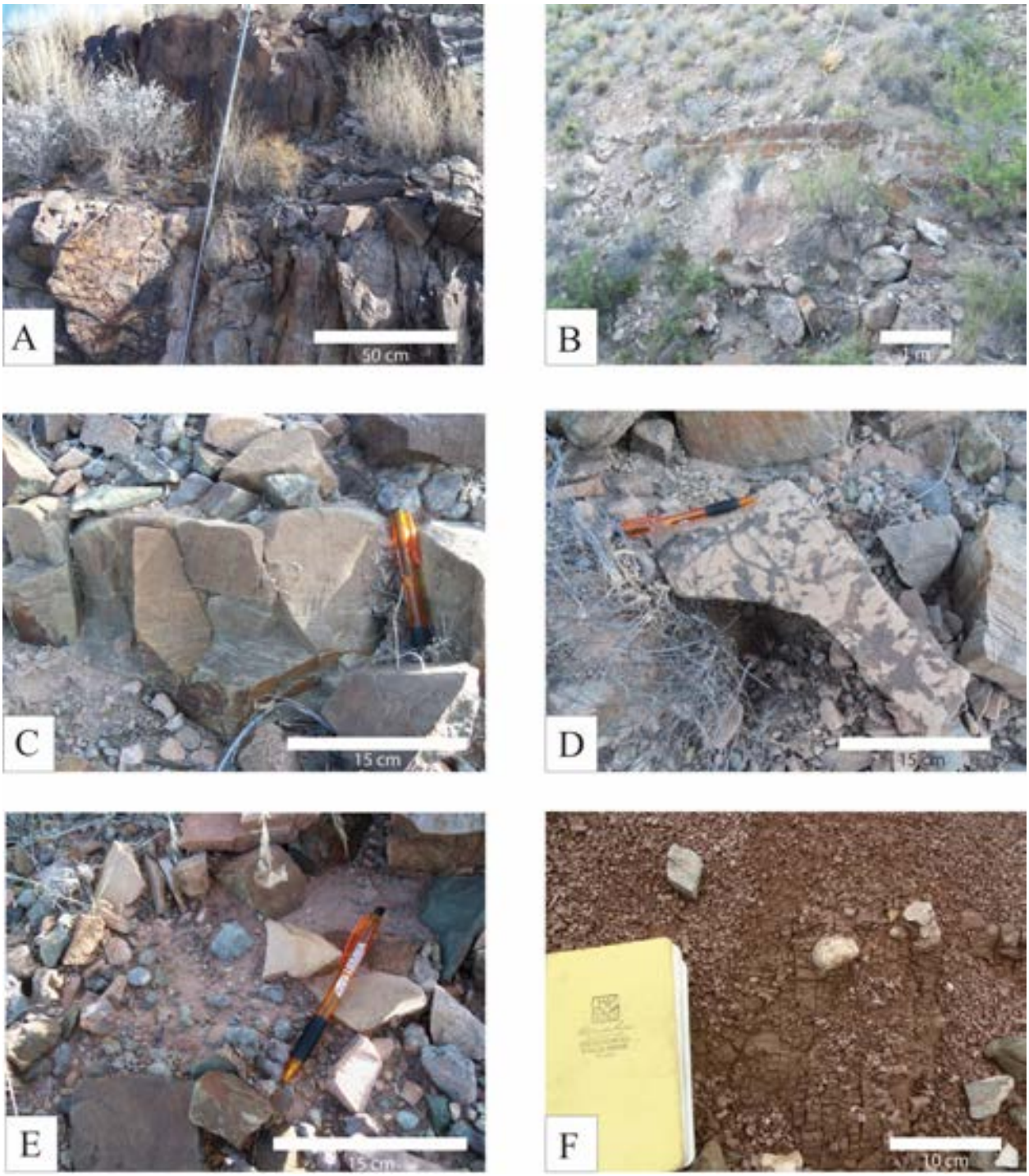

Figure 4.7: Outcrop and hand sample photos of Lacustrine Facies Association (FA-2).
(A) Fine grained mottled sandstone (Ls) overlying fine grained sandstone (Fs); (B) Well exposed tabular siltstone (Ls) overlying massive fine grained sandstone (Ln); (C) Ripple laminated fine grained sandstone grading up into mottled sandstone indicative of heavy burrowing (Ls); (D) Ichnofacies in fine grained sandstone in plan view (Ls); (E) Nodules are the dominant float indicator for Lm; (F) Nodule weathering directly out of the massive fine-grained sandstone.

4.2.1 Burrowed Fine-Grained Quartz Arenite (Ls)

Interbedded burrowed siltstones and fine-grained sandstones (Ls) are characterized by 10-30 cm lenticular and tabular beds (Figure 4.7A and B). Fine-grained sandstones are buff to dark brown, greenish-brown, light gray, or light red to maroon in weathered outcrops with off-white to khaki, green, or light red grains on fresh surfaces. Siltstones can be tan to brown or green in weathered outcrops and are dark green on fresh surfaces. Ls is composed of moderately to well-sorted sub-rounded detrital quartz (0.25 mm) and silt (0.05 mm) with rare chert and carbonate clasts (Figure 4.8A and B).

Common sedimentary structures include horizontal laminae, inclined laminae, and ripple cross-stratification or mottled textures associated with intense burrowing (Figure 4.7C; Figure 4.8B). Burrowed textures are concentrated in upper bedding surfaces and are best viewed in plan view (Figure 4.7D). Burrows crosscut and destroy laminae, which suggests bioturbation can be inferred in mottled structureless beds in the absence of preserved burrows.

4.2.2 Massive Nodule-Bearing Mudstone (Lm)

Nodule-bearing mudstones (Lm) are characterized by poorly exposed tabular beds that can extend laterally for hundreds of meters (Figure 4.7E). The groundmass is composed of silt to mud-sized detrital quartz grains that appear buff, tan, or pink to maroon in weathered outcrop. In rare cases the highly recessive Lm outcrops as massive beds (>1 m) (Figure 4.7F). Lm is typically identified by the presence of carbonate concretions and septarian nodules as float.

Nodules are either reddish gray or yellowish/orange to tan, spherical to oval, and range from 2 to 10 cm in diameter (Figure 4.9A). Micrite makes up over 95% of nodules by volume but scattered pyrite crystals and bitumen can be observed floating in the micritic groundmass

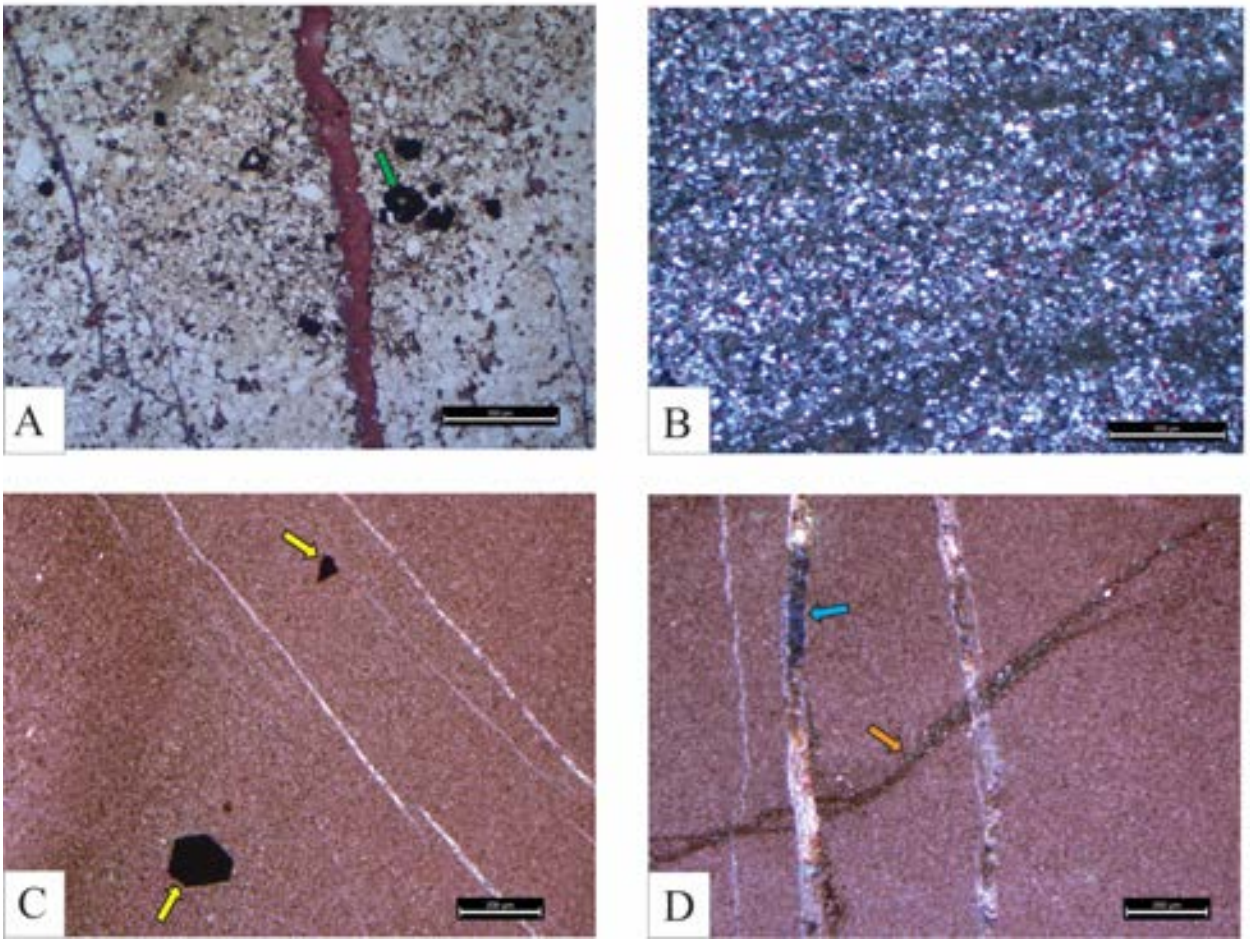

Figure 4.8: Photomicrographs of Lacustrine Facies Association (FA-2).
(A) Fine-grained sandstone (Ls) with significant unidentified organic material (green arrow), note the abundance of iron-rich calcite (blue-purple pore filling cement), plane light, scale bar = 500 μm; (B) Fine ripple laminae typical of Ls, cross polarized light, scale bar = 500 μm; (C) Pyrite crystals or unidentified organic material (yellow arrow) floats in a ground mass of micrite with subordinate fine quartz and silt, cross polarized light, scale bar = 200 μm; (D) Immature septarian crack filled with microcrystaline quartz (orange arrow) is cross-cut by crystalline calcite filled veins (blue arrow), scale bar = 200 μm.

(Figure 4.8C). Septarian cracks are filled with microcrystalline calcite and dolomite, which are crosscut by veins filled with coarse-crystalline calcite (Figure 4.8D). Compound nodules up to 50 centimeters across were observed in certain intervals. Unfortunately, it is difficult to tell whether compound nodule presence is controlled by higher nodule densities within a given

interval or simply a lack of weathering that would preferentially separate compound concretions. Nodules are generally distributed evenly throughout the beds. Outcrops exposed in the roadcut in Echo Canyon have undergone less weathering and may show a slight increase in nodule density near bed tops. Lm is differentiated from a marine nodule bearing bed Mss by nodule morphology and stratigraphic position between fluvial sandstone successions (Figure 4.9).

4.2.3 Depositional Environment of FA-2

Lacustrine deposits represent a significant component of the Upper Yucca rift-fill sequence in the Indio Mountains (Underwood, 1962; Li, 2014). Li (2014) identified five different types of lacustrine deposits based on lithology, sedimentary structures, and the presence of septarian concretions. Using similar criteria, lacustrine strata have been identified in the lower sequences of the Bluff Mesa where previous interpretations had assigned to the shallow marine environment (Underwood, 1962).

Lacustrine deposits are typically characterized by a lack of marine fauna, reduced wave activity, subaerial exposure surfaces, and perturbations in geochemical proxies such as oxygen isotopes (Leng et al., 2006; Renaut and Gierlowski-Kordesch, 2010). Of the 5 lacustrine subfacies that Li (2014) identified in the Upper Yucca Formation, only one (Lm) is present in the Bluff Mesa Formation. Diagnostic features of Lm described by Li (2014) include highly burrowed textures, septarian nodules, and dolomite cements, which was used to recognize lacustrine deposits in the Bluff Mesa Formation as part of the study. Other diagnostic features reported by Li (2014) such as thrombolites, stromatolites, and calcite radial fans were not observed in the Bluff Mesa. It is worth noting that this may simply reflect the volume of available lacustrine deposits (2 cycles in the Bluff Mesa Formation vs 11 cycles in the Upper Yucca Formation), rather than a change in depositional environment or lake water chemistry.

Fine-grained sands and siltstones of Ls are interpreted to have been deposited in a low energy lacustrine environment based on observed faunal assemblages, sedimentary structures and stratigraphic positioning. No evidence for marine fauna were recognized in thin sections, polished hand samples, or outcrops of Ls. An absence of marine fauna is an important diagnostic feature of Ls as marine transgression pre-dates some deposits, meaning stratigraphic position alone is insufficient to separate Ls from superficially similar fine-grained marine facies.

Horizontal laminae, inclined laminae, and ripple cross stratification suggest deposition in low to moderate energy settings in lacustrine environments (Renaut and Gierlowski-Kordesch, 2010). Fine horizontal laminae and ripple cross-laminae are also associated with levee and overbank deposits on floodplains (Collinson, 1996). Floodplain deposits are often highly bioturbated and exhibit subaerial exposure surfaces, although this criteria is insufficient as no subaerial exposure surfaces were observed in the study area and lacustrine facies can be also be heavily burrowed. Fine-grained sandstones of Ls may superficially resemble horizontally laminated sandstones of Fsl, which are interpreted to have been deposited in an overbank setting. However, Fsl is always gradational with trough cross-bedded sandstones of Fs, whereas Ls is clearly separated from Fs or Fsl by a sharp flooding surface. Ls somewhat resembles the fine-grained lacustrine sandstone of Li (2014), with the major caveat that no thrombolites were identified in the Bluff Mesa.

Stratigraphic positioning of Ls also supports a lacustrine interpretation as it is found interbedded with Lm. No evidence for channelization is recorded in these tabular beds, making a fluvial origin unlikely. Additionally, the lacustrine interval that contains multiple Ls deposits is separated from marine deposits by thick fluvial sandstones. This close association of lacustrine and fluvial deposits is to be expected as both represent marginward terrestrial environments.

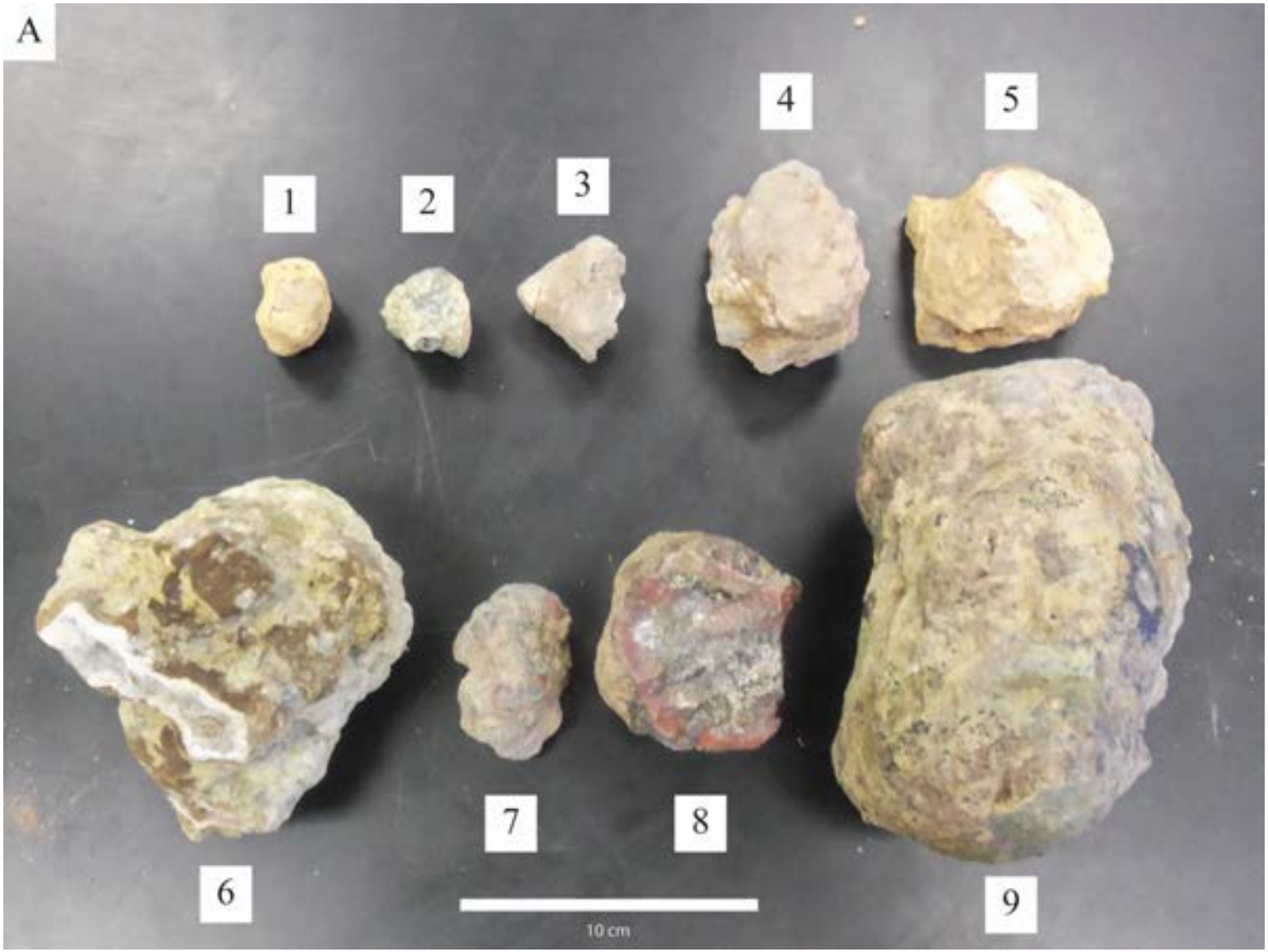
A
1
2
3
4
5
6
7
8
9
10 cm

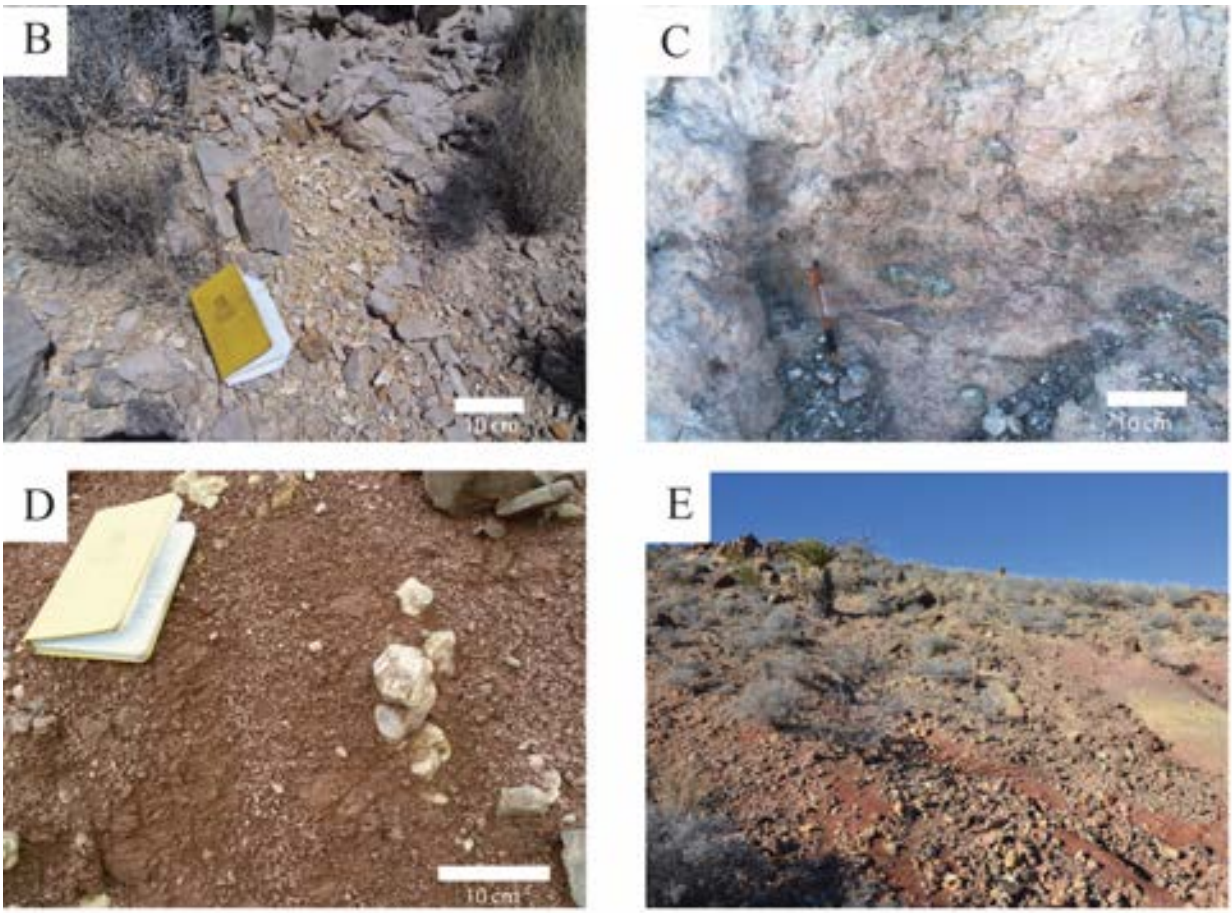

Figure 4.9: Hand samples and morphologies of septarian concretions (Lm) in the Bluff Mesa and Upper Yucca formations.
(A) Variety of carbonate concretions collected from the Bluff Mesa Formation: 1-3) Most common nodule types are small roughly oval to circular; 4-5) Columnar concretions which closely resemble concretions in the Upper Yucca Formation; 6) Compound concretion; 7-9) Nodules collected from the upper Bluff Mesa that formed under marine conditions. These nodules are differentiated from nodules of Lm by size and the bright red staining seen in 7 and 8; (B) Nodules of Lm in the Bluff Mesa Formation present as float; (C) Nodules of Lm in the Bluff Mesa Formation showing similar coloring to marine nodules but are the significantly smaller and represent the minority of nodules in Lm; (D) Compound septarian concretions from the Upper Yucca Formation similar to the compound nodules gathered from the Bluff Mesa Formation in (A6); (E) Isolated septarian concretions weathering out of fine-grained sandstone in the Upper Yucca Formation show similar coloring and sizes to those of Lm (B) (Li, 2014).

Septarian nodules are common in marine settings but have rarely been documented in lacustrine deposits (Dietrich, 1977). Using a combination of nodule mineralogy and stratigraphic

position of nodule-bearing beds, Li (2014) showed deposition occurred in a shallow lacustrine environment. Nodules of Lm from the lower Bluff Mesa closely resemble those of the Upper Yucca in mineralogy, morphology, and surrounding strata (Figure 4.9) (Li, 2014). Nodules were also identified in the upper Bluff Mesa, but are assigned to formation under marine conditions due to markedly different morphology, mineralogy and marine fossil evidence in surrounding strata (Figure 4.9A).

Sulfur isotope values were obtained from nodules of the Upper Yucca (lacustrine), upper Bluff Mesa (marine), and lower Bluff Mesa (Lm) using the carbonate associated sulfate method (CAS) (Table 4.6). Nodules of Lm showed similar sulfur concentrations to marine nodules, both being an order of magnitude more sulfur-rich than lacustrine nodules from the Upper Yucca Formation. However, sulfur values derived from nodules of Lm are isotopically heavier than sulfur from marine nodules (18.7 ‰ vs 13.6 ‰) and closely resemble values obtained from the Upper Yucca Formation (17.1 ‰). Therefore, nodules of Lm carry an intermediate geochemical signature between those deposited in lacustrine and marine environments. This suggests that marine influx likely altered lake water chemistry, as evidenced by the high sulfur content, but deposition occurred in a lacustrine environment due to the lack of marine fossils, morphological similarity to lacustrine nodules of the Upper Yucca, and stratigraphic position between fluvial units.

4.3 SHALLOW MARINE CARBONATE FACIES ASSOCIATION (FA-3)

The shallow marine carbonate facies association is composed of ooid grainstones (Cg), fossiliferous wackestones and packstones (Cf), sandy fossiliferous packstones and grainstones (Cs), and marls (Cm) (Table 4.3). Cg and Cf represent the major cliff forming lithology in the study area and are easily traceable across the thrust panel. Cm often forms the base of

coarsening-upward packages with Cg, Cf, and Cs. Cs is found throughout the Bluff Mesa in a number of different styles and stratigraphic associations.

4.3.1 Ooid Grainstone (Cg)

Ooid grainstones (Cg) are exposed in medium to massively bedded lenticular barforms that prograde to the north (Figure 4.10A). Individual bars are 0.6 to 3 meters thick and can be exposed for up to a km before termination. Cg is dark gray to rusty gray on weathered surfaces and black on fresh surfaces. Small (0.2 - 0.5 mm) ooids are the primary constituent of Cg but peloids and highly abraded (< .5 cm) shell fragments of bivalves, brachiopods, echinoids, crinoids, gastropods, and foraminifers are also present. Ooids typically nucleate on quartz grains, but ooid nucleation on echinoid fragments, gastropods, peloids, recrystallized calcite, and chert grains were also observed (Figure 4.11A, B, and C). Ooids with multiple layered cortices are mixed with single layered cortex ooids and fossils with thin underdeveloped micrite envelopes suggesting ooid formation may have taken place in another environment before transport and mixing in the bar. Detrital quartz accounts for 5-10% of Cg by volume. Cg may appear structureless but many beds contain trough cross stratification and cm thick irregular orange banding (Figure 4.10B). An important component of Cg is that locally ooids may not represent more than 50% of the sample by volume. However, in samples where ooids are not the dominant grain type, they are present with highly fractured and abraded fossil fragments indicative of high energy deposition. Ooid grainstones tend to weather in a diagnostic sharp and blocky pattern, differentiating them from the more rounded weathering of similar-sized fossiliferous packstone (Cf) barforms.

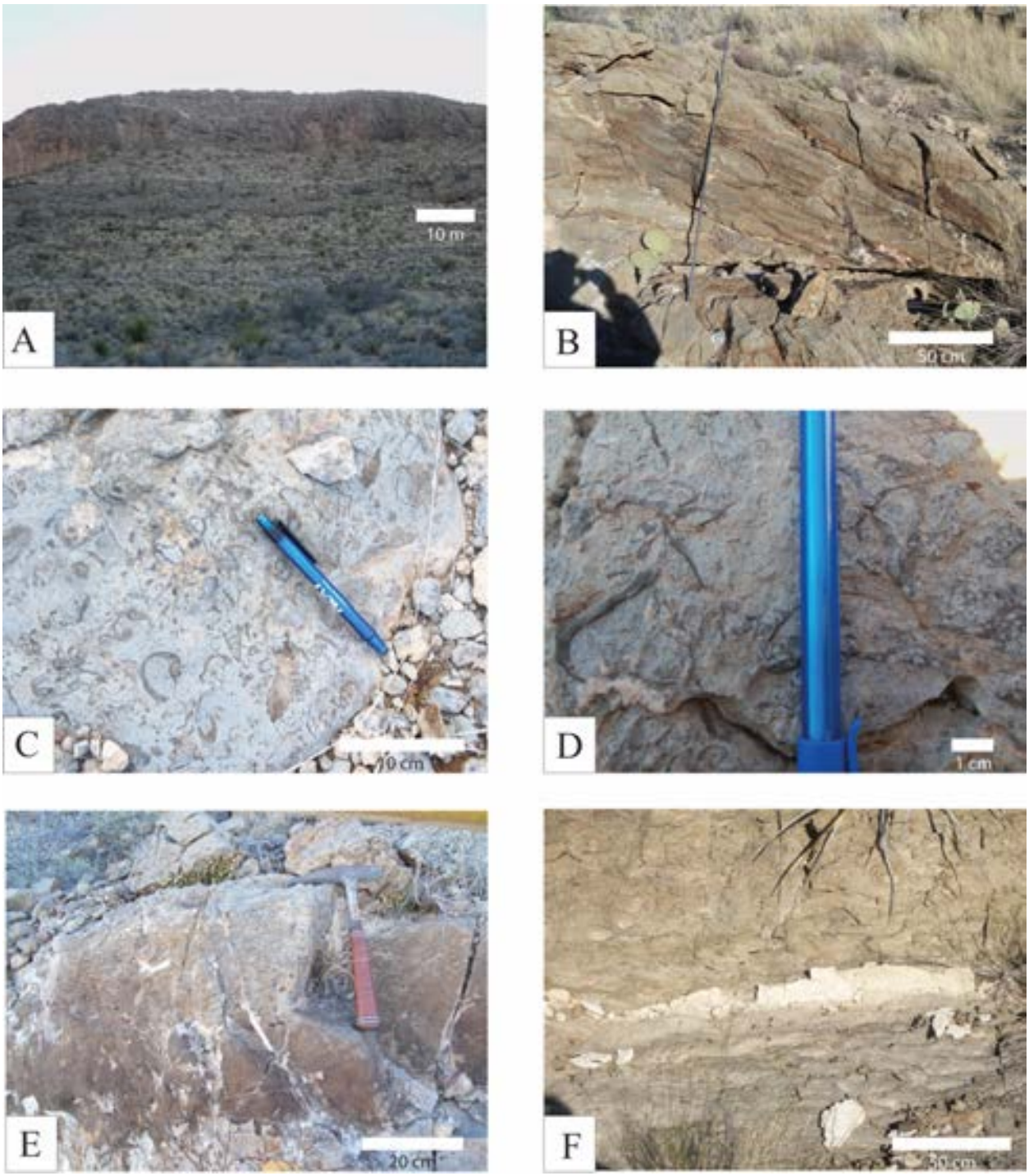

Figure 4.10: Outcrop photos of Shallow Marine Carbonate Facies Association (FA-3).
(A) Prograding barforms of ooid grainstone (Cg) (upper cliff) and fossiliferous packstone (Cf) prograding to the north; (B) Cross-bedding in ooid grainstone (Cg); (C) Diverse intact faunal assemblage of Cf; (D) Intensely bored bivalves in Cf; (E) Erosional contact between a sandy limestone (Cs) and marine sandstone (Ss); (F) Highly weathered marl (Cm) coarsening up into a sandy limestone (Cs).

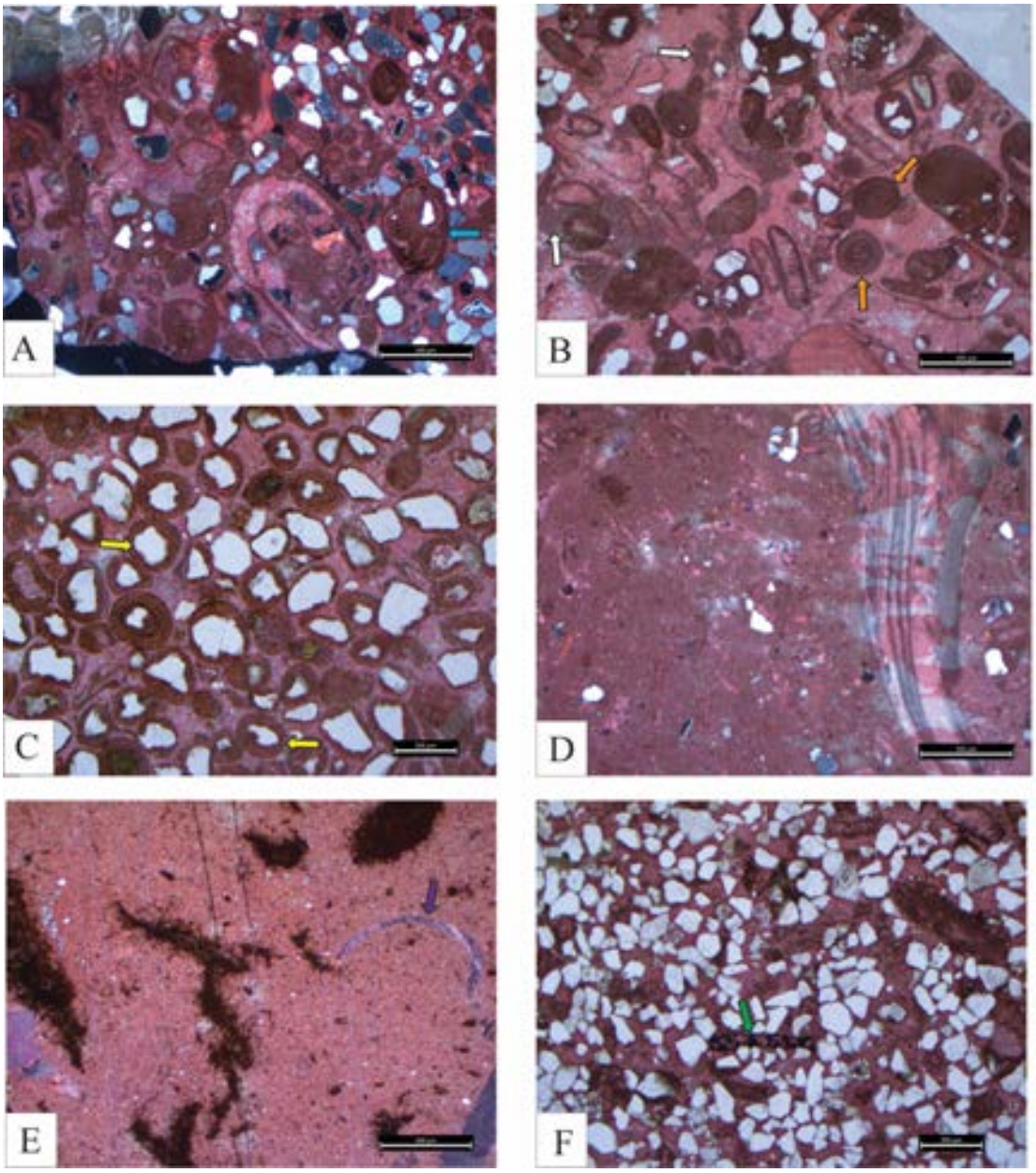

Figure 4.11: Photomicrographs of Shallow Marine Carbonate Facies Association (FA-3).
(A) Cg with varying amounts of micritization and ooid formation, although Cg is known for a lack of intact fossils preservation is aided by oolitic coating (intact gastropod, blue arrow), cross polarized light, scale bar = 500 μm; (B) Cg with a peloidal component (white arrow) and heavily micritized tests (orange arrow) likely caused by endolithic borers, plane light, scale bar = 500 μm; (C) Grainstone dominated by ooids in different stages of formation nucleating predominantly on subangular quartz (yellow arrow), plane light, scale bar = 200 μm; (D) Typical wackestone (Cf) containing large intact fossils (brachiopod), cross polarized light, scale bar = 500 μm; (E) Extensive organic staining appears to be fabric selective as a bivalve composed of replacement crystalline calcite (purple arrow) remains intact, cross polarized light, scale bar = 500 μm; (F) Plant material (green arrow) in a sandy limestone (Cs), plane light, scale bar = 200 μm.

4.3.2 Fossiliferous Wackestone-Packstone (Cf)

Fossiliferous wackestones and packstones (Cf) are exposed in thin to medium bedded tabular benches or medium to massive bedded lenticular barforms that prograde to the north similar to Cg (Figure 4.10A). Thin bedded tabular geometries are typically <60 centimeters thick and trend towards wackestone textures, whereas lenticular barforms of Cf trend towards packstone textures with typical thicknesses of 1.5 to 2.5 meters. Cf is dark gray to light gray or light blueish gray on weathered surfaces and black to dark gray on fresh surfaces. The composition of Cf is characterized by a similar faunal assemblage to Cg with two major differences: 1) a micrite component of 5-80% by volume, and 2) larger and more complete fossils that can are easily identified in hand samples. Bivalves, brachiopods, gastropods, foraminifers, echinoids, crinoids, calcareous sponges and peloids were observed in thin sections (Figure 4.11D and E; Figure 4.12). A number of interesting features are observed in outcrop such as alternating bands of micrite-rich and highly fossiliferous strata, encrusting bivalve colonies, irregular banding, intense micritization by endolithic borers, and heavily bored shells in close proximity to untouched shells of the same species (Figure 4.10C and D). Cf may appear rippled or flaggy, leading to a distinctive nodular weathering pattern, in contrast to the blocky weathering observed in Cg.

A strange black and gray banded mound-like feature is exposed at the base of a wackestone bar in the middle Bluff Mesa (Figure 4.12). The feature is approximately 92 centimeters across, 70 centimeters at maximum height, and extends at least 45 centimeters into the rock face. Alternating bands of black with sporadic white centers and gray calcite share jagged sawtooth-like contacts that grow concentrically away from the center. Banding is fairly regular throughout most of the structure but becomes wavy and disjointed near the structure

edges. The ratio of black band thickness to gray band thickness increases away from the structure center. Black bands are composed of smaller calcite crystals (0.25 mm average) than the white calcite (0.75 mm average) (Figure 4.12). Functional porosity occurs within white calcite bands with the long axis of cavities oriented parallel to banding (Figure 4.12).

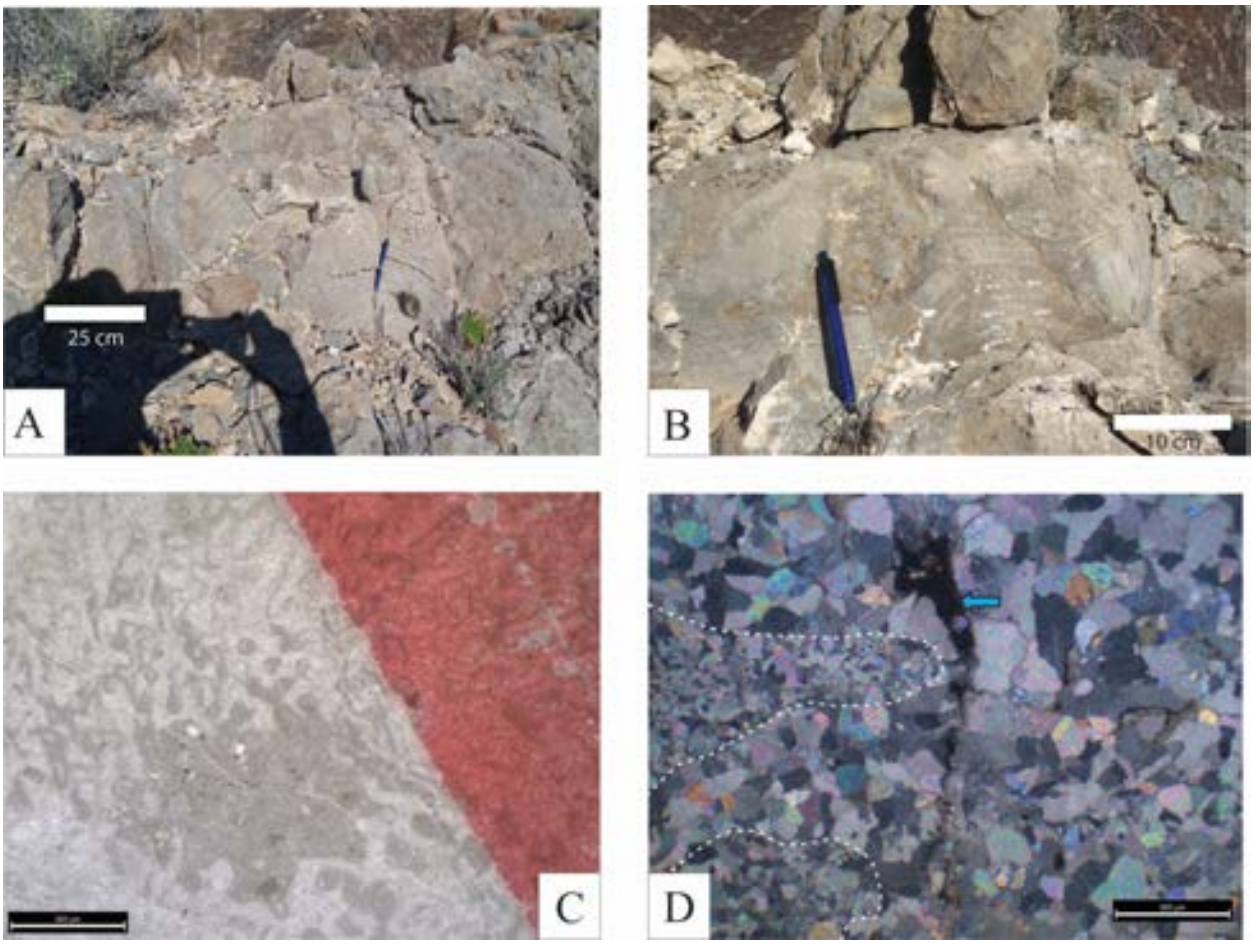

Figure 4.12: Outcrop photos and photomicrographs of the banded mound structure.
(A) Banded structure encased in wackestone (Cf); (B) Banding near the structure peak is no longer hemispherical, possibly due to increased sedimentation rate; (C) Irregular labyrinthine pore structure of the unidentified sponge (*Corynella Mexicana*?), plane light, scale bar = 500 μm; (D) Bands are composed of fine-grained calcite (black in hand sample, inside dotted white lines) with coarser-grained white calcite and functional porosity (blue arrow) in the center. The sawtooth pattern of the coarser-grained calcite results in what appear to be intrusions of fine-grained calcite on the millimeter scale, cross polarized light, scale bar =500 μm.

Interestingly, the only calcareous sponge found in the study area is located in the adjacent wackestone, within five centimeters of the banded structure margin (Figure 4.12). Rigby and Scott (1981) formally described the first two Albian calcareous sponges of North America from outcrops of Mural Limestone in Arizona and Sonora. *Corynella Mexicana* is found encrusting tabular and massive colonies of *Actinastrea* and *Microsolena*-stromatolite communities up to 1 meter in thickness (Scott, 1981; Rigby and Scott, 1981). Although the banded mound is similar in size, nothing about the irregular nature of sponges suggest that the depositional fabric would be susceptible to alternating banded mineralogy during diagenesis. The banded mound may be related to sponge encrusted *Microsolena*-stromatolite corals, but this this cannot definitively be proven without additional samples of corals that did not undergo remineralization.

4.3.3 Sandy Packstone-Grainstone (Cs)

Sandy fossiliferous packstones and grainstones (Cs) are characterized by thin to thick bedded lenticular deposits that generally prograde to the north (similar to Cg and Cf), as isolated thin tabular marine incursions, or as isolated lenses in marine quartz sandstone successions (Figure 4.10E). Cs often forms coarsening-up parasequences composed of finer-grained sandy fossiliferous packstone or marl (Cm) grading up into a coarser-grained fossiliferous sandy packstones or grainstones (Figure 4.10F). Cs is dark to light gray on weathered surfaces and medium gray to black on fresh surfaces. Cs is defined in this study as limestones containing 20-60% detrital quartz by volume (Figure 4.11F). Sandier limestones composed of 40-60% quartz tend to be lighter on both weathered and fresh surfaces and often have burrowed tops. Sandy limestones in the 20-40% quartz range tend to have larger preserved fossils that are visible in hand sample, similar to Cf. The variety of depositional styles exhibited by Cs suggests that it represents quartz-rich variants of different limestone endmembers.

4.3.4 Marl (Cm)

Marls (Cm) represent the finer grained constituent of Cs and are exposed in recessive intervals that grade up into Cg, Cf, and Cs. Cm appears medium gray to black or dark tan in the rare weathered intervals where they are not covered with float (Figure 4.10F). No samples suitable for thin sections were collected but some marls contain nodular micritic mudstone nodules that are more resistant to weathering. Nodules of Cm differ from nodules found in Lm and Mss, as those nodules show both immature and well-developed septarian cracks. These nodule-rich intervals are always located near bed tops that grade into Cf suggesting that clasts represent an unfossiliferous transition to wackestone or packstone deposition.

4.3.5 Depositional Environment of FA-3

The fossiliferous and oolitic carbonates of the Bluff Mesa led Underwood (1962) to an interpretation of deposition on an open marine shelf. Findings of this study suggest that a significant percentage (> 50%) of the formation was deposited on an open marine shelf, although notable deviations are documented (See sections 4.1, 4.2, and 4.5). The Bluff Mesa is ultimately classified as a mixed carbonate – siliciclastic system and is divided into two shallow marine facies associations based on the dominant lithology.

Ooid formation occurs in settings where the following conditions are met: 1) source of nuclei grains, 2) agitation to move grains, 3) supersaturated water, 4) a process of water renewal, and 5) a minimal amount of grain degradational processes (Flugel, 2010). These conditions may be met in both lacustrine and shallow marine depositional environments with modern lacustrine examples from the Great Salt Lake, Utah (Eardley, 1938) and Pyramid Lake, Nevada (Popp and Wilkinson, 1983). The presence of marine fossils is therefore necessary to assign a shallow marine origin to ooid grainstones of the Bluff Mesa. Fossils are difficult to identify in hand

samples of Cg as they have undergone high levels of disarticulation, fragmentation, and abrasion. However, a plethora of marine fossil fragments including echinoids, crinoids, and foraminifera are readily identified in thin section. Stratigraphic evidence also supports a marine interpretation for ooid grainstones of the Bluff Mesa Formation as Cg is commonly interbedded with fossiliferous marine wackestones and packstones (Cf) and shallow marine sandstones (FA-4).

Morphological characteristics of ooids and abraded fossil grains can be extremely useful in determining the energy of the depositional environment, which can then be used to estimate water depth (Flugel, 2010). Major controls on ooid morphology include burial rate, growth rate, agitation, and abrasion (Bathurst, 1975; Sumner and Grotzinger, 1993). Burial rate is intrinsically tied to the supply of available ooid nuclei with higher burial rates resulting in smaller ooids due to shorter periods of agitation before burial. The effects of growth rate and agitation on ooid size are fairly complicated but higher agitation is positively correlated with larger ooids (Bathhurst, 1975; Sumner and Grotzinger, 1993). Numerical modeling by Sumner and Grotzinger (1993) showed that ooid mass loss through abrasion during agitation increases as a cube of the radius, while mass gained through precipitation increases as a square of the radius. This means that eventually mass loss during agitation will exceed mass gained through precipitation and maximum ooid size will be limited. The size distribution and percentage of ooids by volume of Cg offers some insights on the factors discussed above.

Ooids of Cg range from approximately 0.2 to 0.5 mm suggesting that transport was primarily through suspension as ooids above 0.6 mm are typically transported as part of the bed load (Heller et al., 1980). The majority of ooids are nucleated on detrital quartz grains suggesting formation in close proximity to a siliciclastic source. Cg also contains a low percentage of detrital quartz and bioclasts that do not exhibit micrite envelopes. These grains should be

extremely rare in an environment where ooids were actively forming and would require an extremely high deposition rate. It seems more likely that grains lacking micrite envelopes were transported from an environment that did not have the necessary conditions for ooid formation to the shoal environment where deposition occured. The possibility of autochthonous ooid formation cannot be ruled out but given the rounding of detrital quartz nuclei and presence of grains lacking micrite envelopes Cg likely represents deposition of allochthonous ooids and abraded bioclasts in a high energy shoal environment close to the shoreline. Trough cross-bedding indicative of sediment mobility in a high energy regime can also be found throughout Cg.

The diverse faunal assemblage in fossiliferous packstones and wackestones of Cf indicates that deposition occurred under normal marine conditions. High energy environments typically lack fine-grained sediments and micrite due to winnowing. The presence of intergranular micrite matrix in packstones suggest they were deposited under a moderate energy regime that was calmer than Cg. Packstones contain large bioclasts (typically bivalves) that have been heavily bored (Figure 4.10D). Extensive boring by predators occurs when bioclasts are exposed at the substrate surface for extended periods of time. Therefore, it is likely that burial and sedimentation rates in the packstone environment were lower than in the shallower ooid grainstone environment. Additionally, intense micritization of a variety of tests by endolithic borers suggests a fairly slow burial rate in the photic zone (Flugel, 2010). Packstones are interbedded with Cg, Cs, and marine sandstones of FA-4 in the mid-upper Bluff Mesa. This stratigraphic association when combined with the previously discussed textures and features suggests that packstones were deposited in a moderate energy regime located basinward of Cg (Figure 4.13).

Energy in wackestone environments was lower than packstone environments based on the relatively higher percentage of micrite found in wackestones and the higher percentage of fragmented fossils in packstones. Despite these differences the faunal assemblages of Cf wackestones are incredibly similar to those of Cf packstones, which warrants their inclusion in FA-3.

Definitions for sandy limestones may vary in the literature but are typically defined as having a sizeable volume of detrital quartz within their matrix. Sandy grainstones and packstones of the Bluff Mesa Formation are defined as 20-60% detrital quartz by volume and contain similar faunal assemblages to Cg and Cf. It is likely that sandy grainstones and packstones represent variants of Cg and Cf that were deposited closer to a siliciclastic source.

Proximity to a siliciclastic sediment source may be recorded by 1) deposition in a slightly more landward position of the carbonate factory or by 2) encroachment of migrating siliciclastic barforms along strike (Figure 4.13). If only sandy grainstones that resembled Cg (ooids and abraded bioclasts) were present, then it would be safe to assume that Cs was deposited exclusively marginward of the ooid shoal environment. However, due to the fact that sandy variations of Cf are also observed (sandy packstones with large intact bioclasts), Cs likely also represents lateral zones of Cf deposited closer to a siliciclastic point source. The notion that Cs may represent lateral changes is also supported by the presence of sandy limestone lenses appearing within thicker marine sandstone intervals of FA-4.

Marls are defined as a semifriable mixture of 35-65% carbonate and a complimentary clay component (Pettijohn, 1957). This mixture of fine-grained sediments can occur in both marine and lacustrine environments. Marine fossils are difficult to identify in the marls of the Bluff Mesa Formation as the outcrops are either weathered or covered by alluvium. Nodules

collected from marl intervals do not contain marine fossils, but the micritic matrix often superficially resembles the matrix of marine wackestones (Cf). This resemblance is speculative in nature and is therefore not enough to eliminate the possibility of a lacustrine origin.

The stratigraphic distribution of marls suggest that they were deposited in a low energy marine environment. Marls are only found in post-transgression intervals in close association with carbonate facies of FA-3 and FA-5. Marls are often gradational with marine carbonate facies Cg, Cf, and Cs in coarsening-up parasequences. This suggests that they were deposited in a lower energy marine environment basinward from carbonates of FA-3 and that gradational relationships were recorded through progradational processes. No marls were identified in lacustrine intervals of the Bluff Mesa Formation or the Upper Yucca Formation, even in association with nodule-rich layers of Ln. The previously discussed stratigraphic evidence and fine-grained nature of marl deposits in the Bluff Mesa Formation show that they were deposited in a low energy marine environment located basinward of marine carbonates of FA-3 and FA-5 (Figure 4.13).

4.4 SHALLOW MARINE SILICICLASTIC (FA-4)

Normal marine siliciclastics are composed of fine to medium-grained sandstone (Ss) and rare conglomerate (Sc) (Table 4.4). Sandstones are widespread while conglomerates appear as

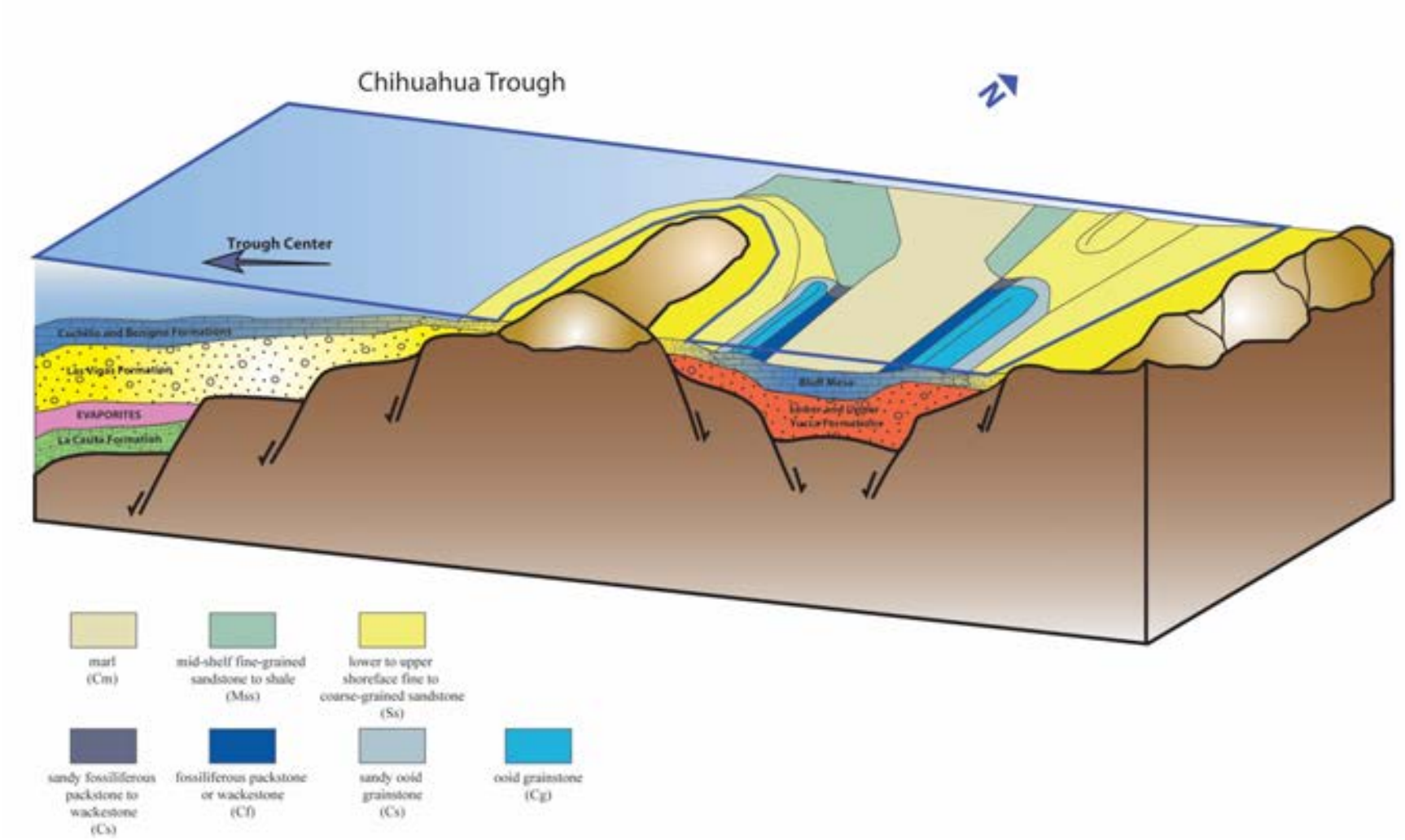

Figure 4.13: Idealized depositional environments during marine deposition.

transgressive lags or in isolated channel fills where they are overlain by massive sands that abruptly grade upward into hummocky cross-stratified sandstones (Figure 4.14).

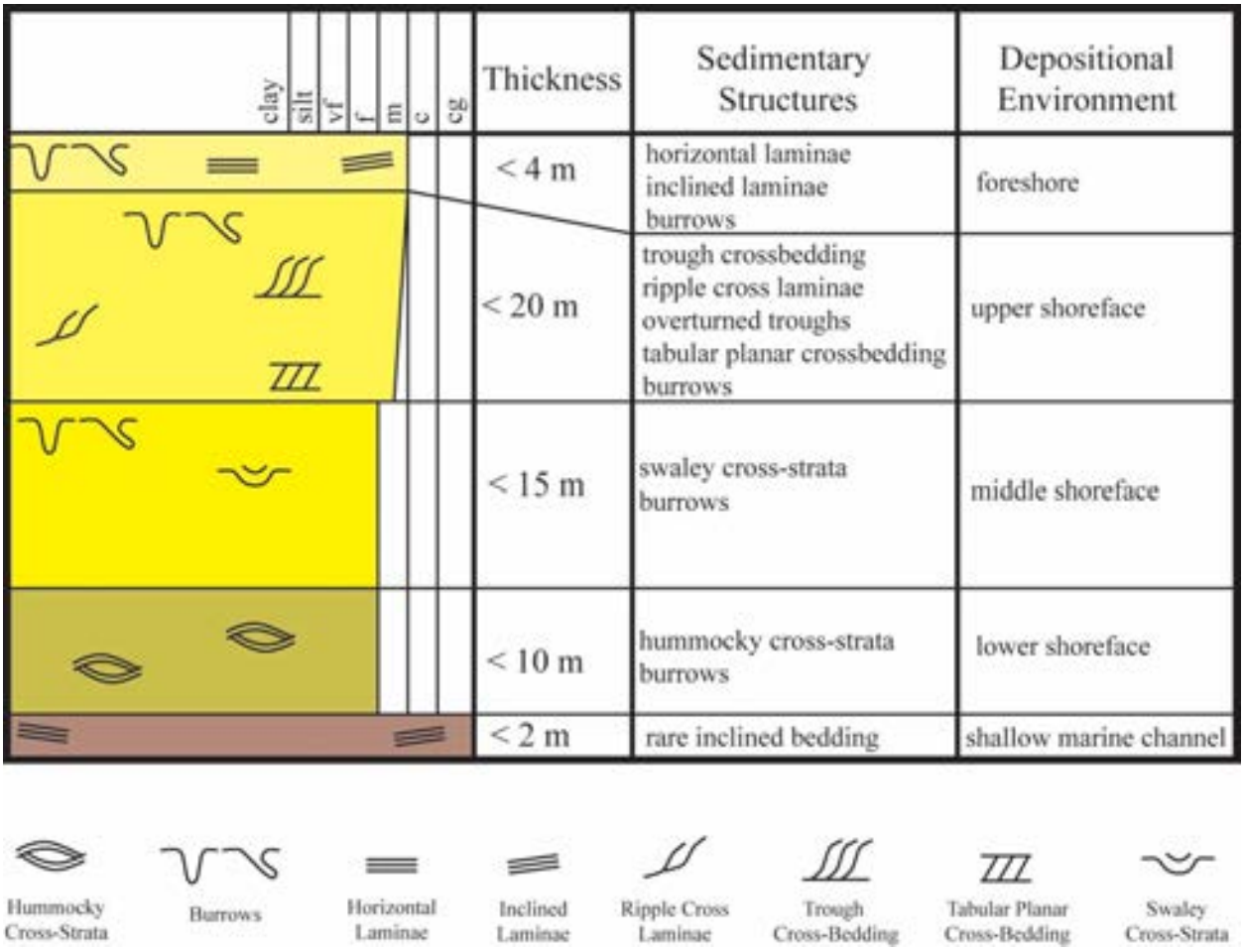

Figure 4.14: Idealized shallowing-upward facies succession in Shallow Marine Siliciclastic Facies Association (FA-4).

4.4.1 Hummocky/Swaley Cross-Stratified Quartz Arenite (Ss)

Fine to medium-grained sandstones (Ss) outcrop primarily in 20-75cm lenticular beds that often pinch and swell along strike (Figure 4.15A). Tabular bedding is less common and is characterized by inclined laminae as the dominant sedimentary structure. Sands are typically light tan, light gray, or off-white with black speckles in weathered outcrops while fresh surfaces

appear off-white with red speckles. Siltstones are dark tan, dark brown, or green on weathered surfaces and dark brown or green on fresh surfaces. Ss is composed of sub-rounded to well-rounded detrital quartz that can range from poorly sorted in hummocky beds to well sorted in laminated deposits. Ss is generally clean with >90% quartz, however phosphatic grains, chert, zircons, plant material, carbonate rip-up clasts, and marine fossils (typically bivalve fragments) are found throughout (Figure 4.16A, B, and C). Common sedimentary structures include hummocky cross-strata, swaley cross-strata, wave ripple laminae, trough crossbedding, tabular planar crossbedding, overturned troughs, low angle inclined laminae and skolithos burrows (Figure 4.15A, B, C, and D; Figure 4.16D). Siltstones and fine-grained sandstones of Ss may superficially resemble Ls, but are separated by the presence of marine fossils (bivalves and brachiopods) in Ss and the stratigraphic proximity between Ls and Ln.

Normal marine silt and sandstones (Ss) are exposed in 2 different styles within the study area. The 1st style is represented by excellent exposures consisting of coarsening-up cycles or thick aggradational stacking in the upper Bluff Mesa (Figure 4.14). These cycles are composed of primarily swaley cross-stratified fine-grained sands that pass upward into tabular planar and trough cross-bedded sandstones. These cycles typically contain a basal channel and the associated conglomerate fill (Sc), which cut down into marine carbonates (Cg, Cf, and Cs) or fine-grained siliciclastics (Ss). These cycles are continuous across the thrust panel with fairly minor fluctuations in thickness. It is worth noting that basal channels of each cycle are confined to a narrow lateral zone, which may have been controlled by basin configuration through time (Figure 4.1; Figure 4.2).

The 2nd style of Ss deposition is represented by thin sandstone lenses that intertongue with ooid grainstones (Cg) and fossiliferous wackestones-packstones (Cf) in the middle and

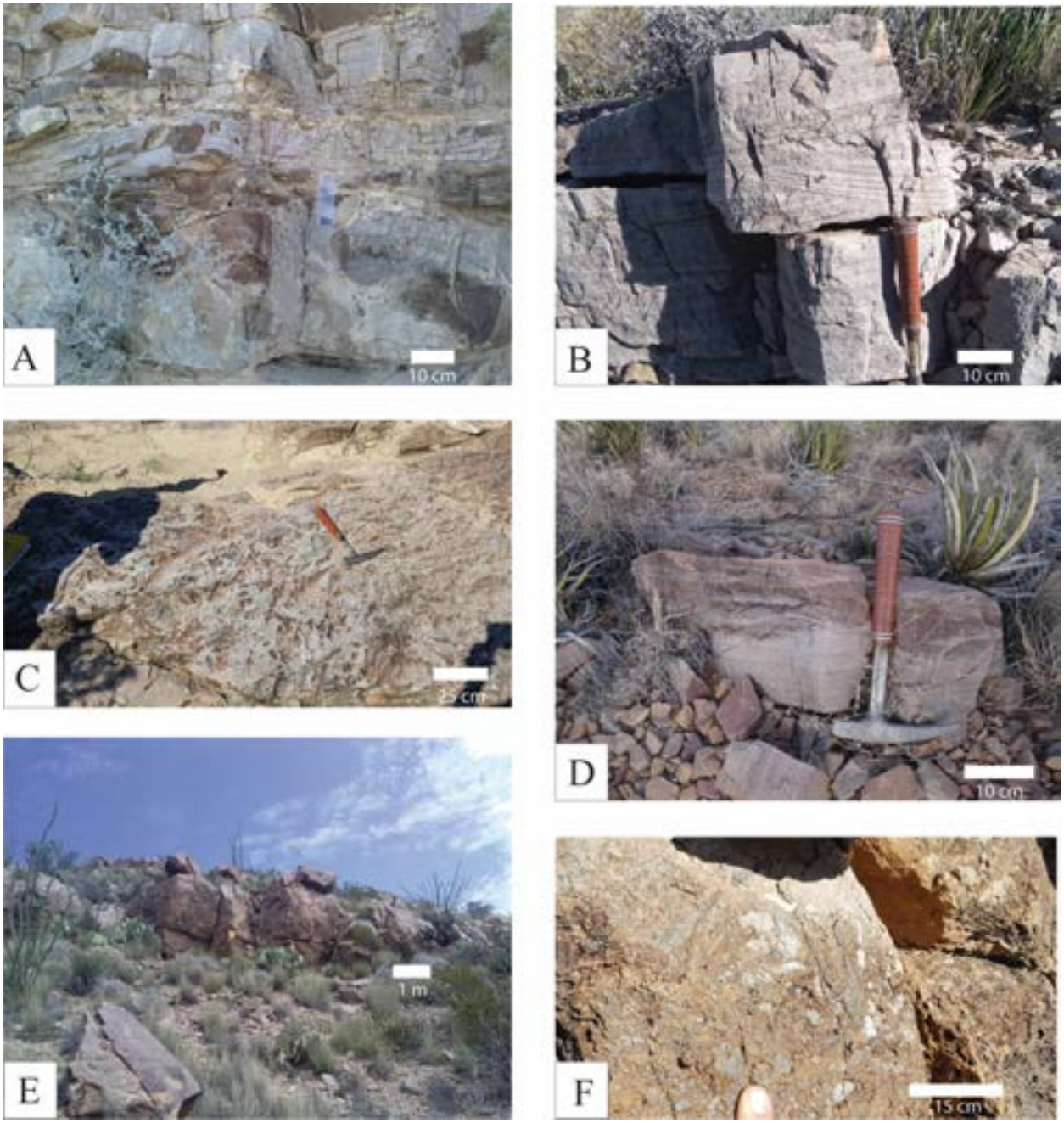

Figure 4.15: Outcrop photos of Shallow Marine Siliciclastic Facies Association of (FA-4)
(A) Swaley bedding in Ss typical of middle shoreface deposition; (B) Trough cross stratified Ss overlain by horizontally laminated sandstone associated with a change from upper shoreface to the foreshore environment; (C) Abundant Skolithos burrows (Ss); (D) Trough cross stratified sandstone cutting into horizontally laminated sandstone (Ss); (E) Slightly asymmetric channel fill with basal lag conglomerate (Sc) overlain by massive sandstone; (F) Marine fossils and limestone clasts within Sc.

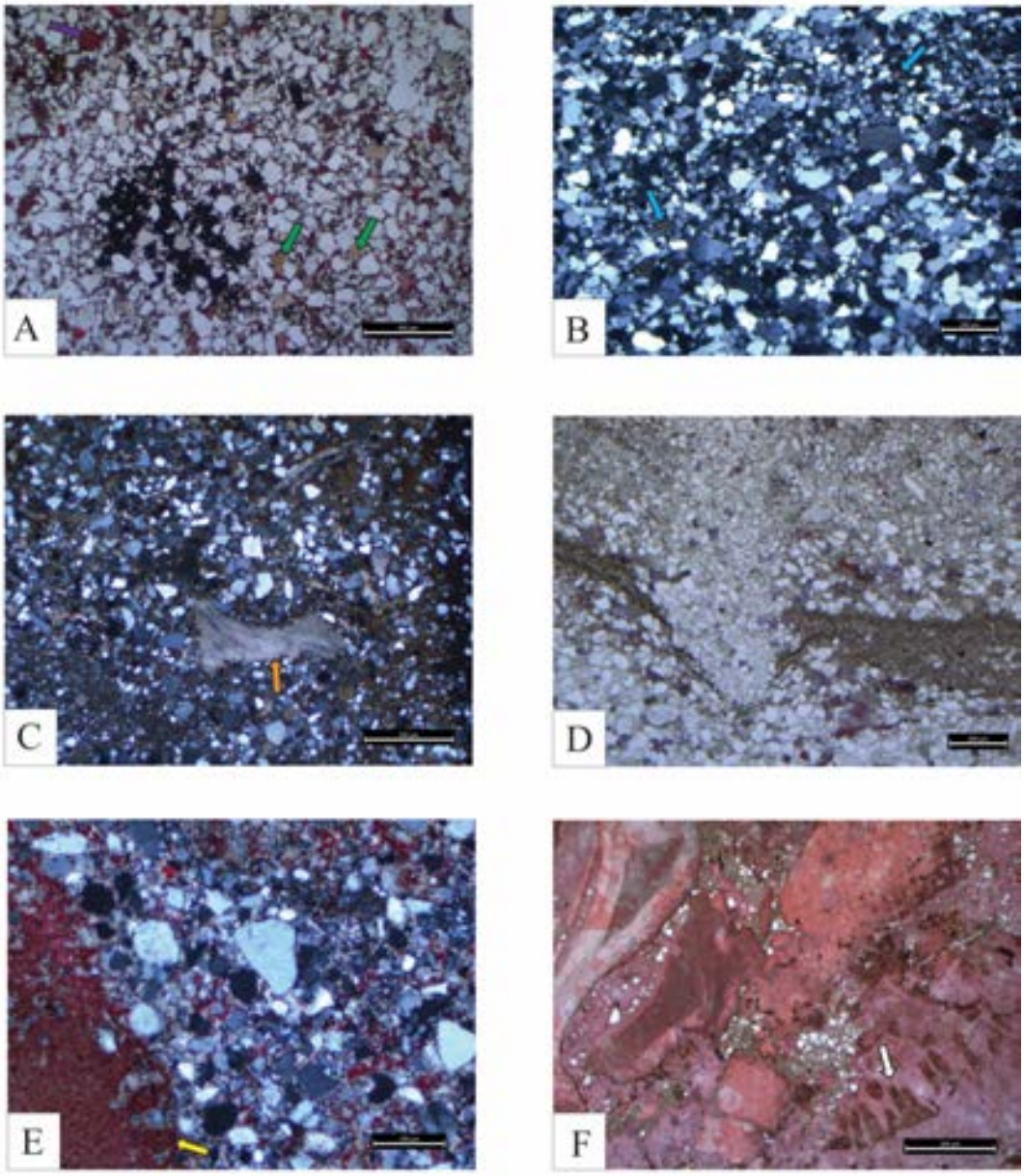

Figure 4.16: Photomicrographs of shallow marine siliciclastics (FA-4).
(A) Variety of common grains in Ss including fine to medium-grained quartz (white), organic material (black), phosphatic grains (tan, green arrow), and calcite grains and cement (red and blue-purple). Iron-rich (blue-purple) calcite can be seen grading into standard calcite (red) at grain centers (purple arrow) suggesting secondary iron enrichment, plane light, scale bar = 500 μm; (B) Sub-rounded detrital quartz with multiple moderately rounded to well-rounded zircons (blue arrow), cross polarized light, scale bar = 200 μm; (C) Bivalve fragment (orange arrow) in a mottled Ss sample, unstained, cross polarized light, scale bar = 500 μm; (D) Soft sediment deformation of laminae separating deposits of different grain sizes, plane light, scale bar = 200 μm; (E) Poorly sorted Sc containing a carbonate clast (yellow arrow), cross polarized light, scale bar = 100 μm; (F) Shell-rich lag deposit containing brachiopods and/or bivalves with borings (white arrow) and subordinate detrital quartz, plane light, scale bar = 500 μm.

lower Bluff Mesa. Sandstones are discontinuous and may pinch out or grade laterally into sandy limestones (Cs). Sandstones may grade vertically into sandy limestones (Cs), but can also have sharp erosive upper and lower contacts (Figure 4.10E). Sands often contain trough crossbedding and can be extensively burrowed, however hummocky cross strata are typically absent. The discontinuous nature of Ss in the middle Bluff Mesa makes lateral correlations of individual beds impossible, but a general zone of interbedded Ss-Cs-Cm can be traced across the thrust panel.

4.4.2 Matrix-Supported Carbonate Clast Conglomerate (Sc)

Conglomerates (Sc) are rare and are confined to 3-12 m wide channels with erosive bases (Figure 4.15E). Sc is composed of coarse-grained sub-angular detrital quartz with abundant angular to subangular carbonate rip-up clasts, pebbles, and shell fragments (Figure 4.15F; Figure 4.16E and F). Deposits are generally thick bedded and structureless, but some inclined strata are visible parallel to channel walls. Sc is differentiated from fluvial conglomerates (Fc) by its carbonate clast and marine fossil content (Fc having significant chert), lateral discontinuity, and stratigraphic position below hummocky cross stratified sandstones.

4.4.3 Depositional Environment of FA-4

Underwood (1962) assigned a marine origin for sandstones throughout the Bluff Mesa Formation. This was a logical decision as the base of the Bluff Mesa clearly contained a normal marine faunal assemblage. Additionally, the presence of a regional clastic source is supported by the thick marine sands of the overlying Cox Sandstone (Budhathoki, 2013). This study concludes that the majority of lower Bluff Mesa siliciclastics, previously identified as marine by Underwood (1962), are fluvio-lacustrine in origin (FA-1 and FA-2), (section 4.1 and 4.2). Examination of faunal assemblages, sedimentary structures, and stratigraphic relationships

indicates that the siliciclastic deposits of the middle and upper Bluff Mesa were correctly assigned to a shallow marine depositional environment.

Shallow marine siliciclastic deposits are characterized by marine faunal assemblages and sedimentary structures indicative of tidal, storm and/or wave action (Plint, 2010) (Figure 4.14). Features such as hummocky cross-strata, swaley cross-strata, and isolated shell lenses were useful proxies when combined with observed stratigraphic relationships between sandstones of FA-4 and normal marine limestones (FA-3). Normal marine siliciclastics often intertongue with sandy limestones and ooid grainstones in the middle Bluff Mesa and overlie them in the upper Bluff Mesa.

Siliciclastic sediments deposited in nearshore environments are subject to flow regimes composed of long-term unidirectional waves and short-term oscillatory currents (Plint, 2010). These processes leave distinct sedimentary structures that help guide interpretations regarding wave energy, water depth, and ultimately, depositional environment. Silts and sandstones of Ss exhibit a variety of sedimentary structures that suggest deposition occurred in the lower to upper shoreface environment on a wave or storm-dominated shelf.

Hummocky cross-stratified sandstones are formed by storm wave processes below fair weather wave base (Dumas and Arnott, 2006). The presence of hummocky cross-stratified sandstones and scattered thin-bedded siltstones suggests deposition occurred in the lower shoreface, where low energy conditions allowed for the accumulation of fine-grained particles, which were intermittently disrupted by storms. Replacement of hummocky cross-stratified sandstones by swaley cross-stratified sandstones signifies deposition under a slightly higher energy regime diagnostic of the middle shoreface. Trough cross bedded, sub-horizontally laminated and tabular planar cross-bedded sandstones are more well-rounded and better sorted

than hummocky cross stratified sands. Sorting and the presence of wave influenced sedimentary structures suggests deposition above wave base in the upper shoreface (Plint, 2010). Trough cross-bedded and tabular planar sandstones generally overlie hummocky cross-stratified and swaley cross-stratified sandstones in coarsening up cycles typical of prograding shoreface deposits (Plint, 2010; Figure 4.14).

Although the previously discussed suite of sedimentary structures is typical of the shoreface environment, it is important to note that structures reflect flow regimes rather than depositional environments. Sedimentary structures such as trough cross-bedding representing subaqueous dune migration are common in fluvial environments while a number of wave related structures can develop in lacustrine littoral environments. The presence of rare marine fossils, both in thin sections and as isolated shells in outcrop, provides more evidence for marine deposition as no evidence for marine fossils were identified in fluvial or lacustrine sandstones of FA-1 and FA-2.

Stratigraphic evidence provides strong support for a shallow marine interpretation of Ss as it is closely associated with marine carbonates of FA-3. Thin sandstone lenses of Ss intertongue with ooid grainstones (Cg), fossiliferous packstones (Cf), and sandy fossiliferous packstones-grainstones (Cs) throughout the middle Bluff Mesa. Sandstones in this interval may be gradational with sandy limestones or have sharp contacts with any of the aforementioned carbonate lithofacies. Burrows piercing both Ss and Cg indicate that both were deposited in close succession and remained unlithified (Figure 4.17). The variety of contacts in close succession suggest multiple lateral facies shifts were occurring as siliciclastic barforms encroached the carbonate factory in the nearshore environment.

Figure 4.17: Burrow extending from Cg into Cs (FA-3).

Separating fluvial conglomeratic facies from marine gravels deposited in shallow water can be difficult. Key attributes in identification include depositional geometries, stratigraphic placement, clast lithology, grading, and imbrication (Reading and Collinson, 1996). No significant patterns in grading and imbrication were observed when comparing Sc to fluvial conglomerates (Fc). Depositional geometries of both Sc and Fc were fairly similar, although a few observed lenticular beds of Fc were significantly more laterally continuous suggesting a lack of a well-defined topographic low. Sc clearly differs from Fc in clast lithology and stratigraphic placement, which were used to assign it to a shallow marine depositional environment.

Sc can be readily identified due to the presence of shelly marine fauna that range from highly fractured and abraded to nearly intact. Sc also contains rare nodular rip-up clasts reaching up to 8 centimeters in diameter, much larger than any clasts observed in Fc. These larger rip-up clasts superficially resemble micrite-rich sections of shallow marine wackestones (Cf). The presence of the large rip-up clasts and especially seemingly intact marine fauna indicates that Sc was deposited in a shallow marine environment.

Comparisons regarding the stratigraphic and lateral distributions of Sc and Fc are also a useful tool. Sc is found in channels that typically cut into marine carbonates of FA-3 or fine-grained sandstones of Ss in mid-upper Bluff Mesa. Sc is always overlain by either hummocky cross-stratified sandstone of Ss or massively-bedded medium-grained sandstone that grades upwards into Ss. Comparatively, Fc is only found in the lower Bluff Mesa, where it is closely associated with other fluvial sandstones of FA-1 or lacustrine deposits of FA-2. Deposits of Fc are discontinuous but can be found reliably along the same stratigraphic surfaces and thicken slightly towards Echo Canyon. However, Sc is extremely discontinuous along stratigraphic surfaces and seems to cluster around a single lateral zone in the thrust panel or in close proximity to syndepositional faults (Figure 4.1; Figure 4.2). This distribution is discussed further in chapter five, but for the purpose of comparing Sc to Fc it is clear that these facies are not genetically related. Due to stratigraphic associations with marine facies associations 3 and 4, presence of marine fauna, and a significantly different lateral distribution from fluvial conglomerates, Sc is assigned to the shallow marine shoreface sandstone facies association.

4.5 MIDDLE SHELF SILICICLASTIC FACIES ASSOCIATION (FA-5)

Fine-grained siliciclastics (Mss) indicative of deposition in a moderate to low energy environment are concentrated in the upper Bluff Mesa Formation. Siliciclastics of FA-5 exhibit a

diagnostic olive green tint in weathered outcrops and float. This was extremely useful in separating covered sections of Mss from recessive siliciclastics of FA-4 in the upper Bluff Mesa. This diagnostic olive green tint is even clearer in aerial photos, making it a practical tool for mapping over long distances and onto different thrust panels with complicated structural histories (Figure 4.1; Budhathoki, 2013).

4.5.1 Olive Green Shale, Siltstone, and Fine-Grained Quartz Arenite (Mss)

Shales, siltstones, and fine-grained sandstones (Mss) outcrop in thin to medium (5-30 cm) tabular beds that consistently coarsen upward. Outcrops generally consist of either shale or silt that coarsens-up into fine-grained sandstone or highly weathered shale that coarsens up into well cemented shale (Figure 4.18A and C). Shales and siltstones are dark to light green weathered with fresh surfaces from dark green to black. Fine-grained sandstones are also dark to light green on weathered surfaces but trend towards lighter green on both weathered and fresh surfaces. Sandstones are composed of subrounded detrital quartz that is moderately to well-sorted. Sandstones and siltstones can be structureless but often contain horizontal laminae or symmetrical ripple marks (Figure 4.18A).

A single unique shale bed containing carbonate nodules was identified near Echo Canyon and is included in the Mss lithofacies. This bed superficially resembles other highly weathered green shales of Mss with the exception of significant red staining at its base (Figure 4.18B). Nodules have a wide size range from 2 to 60 cm in diameter and appear dark green to rare red patches on weathered surfaces. Nodules are spherical to oval and are often observed weathering

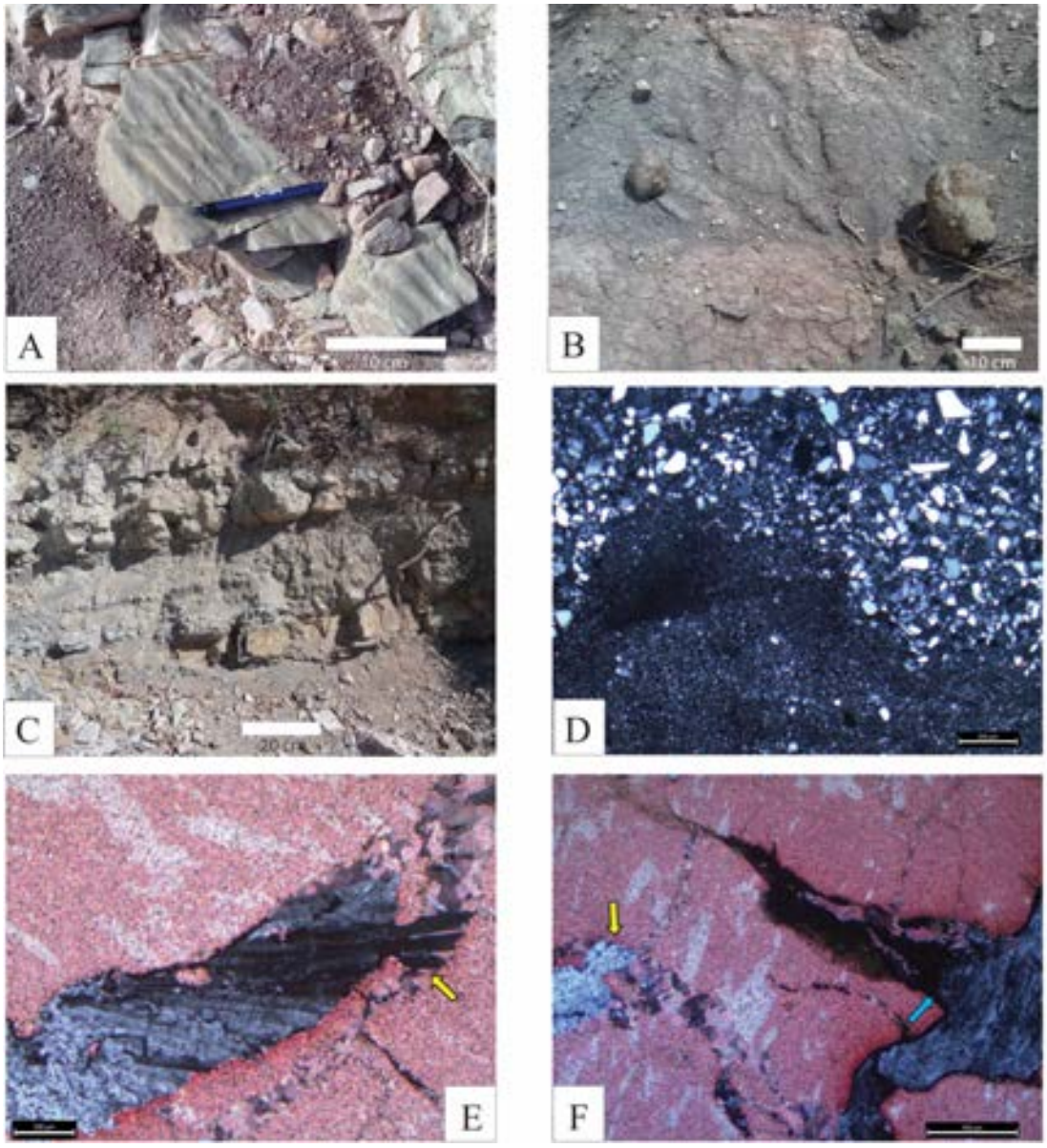

Figure 4.18: Outcrop photos and photomicrographs of Middle Shelf Siliciclastic Facies Association (FA-5).

(A) Symmetrical ripples in fine grained sandstone (Mss); (B) Nodule bearing interval of Mss, note long axis of nodules oriented perpendicular to bedding; (C) Wavy bedded wackestone (Cf) overlying siltstone (Mss) (D) Wavy contact between fine-grained sandstone and siltstone, cross polarized light, scale bar = 200 μm; (E) Bladed silica cement cross cutting calcite vein (yellow arrow), cross polarized light, scale bar = 200 μm; (F) Well developed septarian cracks within the micritic body of a nodule (Mss), silica cement grows inward towards the vug center pushing dead oil into adjacent septarian cracks (blue arrow). Note that calcite veins are cut by silica cement (yellow arrow) associated with septarian cracks suggesting a different diagenetic evolution for marine and lacustrine nodules in the study area, cross polarized light, scale bar = 500 μm.

out of the shale with the longest axis perpendicular to bedding (Figure 4.18B). Nodule lithology is characterized by a micritic groundmass that grades sharply into microcrystalline dolomite or silica cement at the borders of septarian concretion cracks (Figure 4.18E). Cracks and vugs are predominantly filled with silica cement but a significant amount of dead oil is also present (Figure 4.18F). Crystalline calcite is present in veins but instead of cross-cutting septarian cracks, as observed in lacustrine nodules, it appears to have been replaced by younger silica cements (Figure 4.18E and F). The nodule-bearing bed was also identified <10 meters south of Echo Canyon but exposure was poor and nodules were only observed as float.

4.5.2 Depositional Environment of FA-5

Fine-grained siliciclastic material can be found in low energy environments with slow settling rates including open marine shelves, protected lagoons, and lakes. Large volumes of Mss are highly recessive, making it difficult to gather information on sedimentary structures or faunal assemblages. Mss constitutes most of the highly recessive valley-forming interval in the upper Bluff Mesa, signifying a basinwide rise in base level. Fine-grained lacustrine deposits are confined to the lower Bluff Mesa and are closely associated with fluvial deposits rather than marine limestones. This suggests that shale to fine-grained sandstone of Mss was not deposited in a lacustrine environment, despite the presence of a nodule-bearing bed.

Common characteristics of lagoon deposits include fine-grained lithologies that are typically structureless or finely laminated, restricted faunal assemblages, high in organic matter and plant debris, and are often interbedded with sand-rich washover fans (Martin and Dominguez, 1994). Mss is often structureless or finely laminated, although it can contain symmetrical wave ripples, which require an oscillatory flow regime (Plint, 2010). Mss does not exhibit notable levels of plant debris or a restricted faunal assemblage. Significant organic matter

is present within septarian nodules of Mss but this represents a single bed and organic material in other sampled beds was comparable to marine sands of FA-4. Fine-grained sandstones of Mss represent the top of coarsening-upward parasequences and are often gradational with underlying shales and siltstones. Vertical transitions in lagoons are typified by sharp contacts between sandy washover fans and lagoonal muds. Abrupt vertical transitions from shale or silt to sand are rare within Mss deposits and no depositional geometries resembling washover fans were observed. Mss exhibits some characteristics associated with deposition in a lagoon environment but the predominance of coarsening-up parasequences rather than sharp vertical contacts suggests that deposition on an open marine shelf is the most likely scenario (Figure 4.13).

Septarian concretions of lacustrine origin have been extensively studied in the Upper Yucca Formation in the Indio Mountains (Li, 2014; Llanos, 2017). Sulfate isotopes were obtained from Mss septarian concretions and are compared to lacustrine samples from the Upper Yucca Formation and Lm in Table 4.6. Carbonate associated sulfate is a reliable proxy for the sulfur isotope composition ($\delta^{34}S$) values of paleo-seawater sulfate during the deposition of carbonates (Payton and Gray, 2012). Sulfate values obtained from these concretions are lighter than the Aptian/Albian average compiled by Claypool et al. (1980), but still fall within the expected range for the Aptian/Albian (Figure 4.19). The primary fractionation process during burial is sulfate reduction, which preferentially removes light sulfur isotopes resulting in carbonates that are enriched in heavy sulfur isotopes (Barton and Tomei, 1995). The light values produced from these septarian concretions are therefore fairly surprising, possibly indicating deposition under anoxic conditions that are discussed in detail within chapter six.

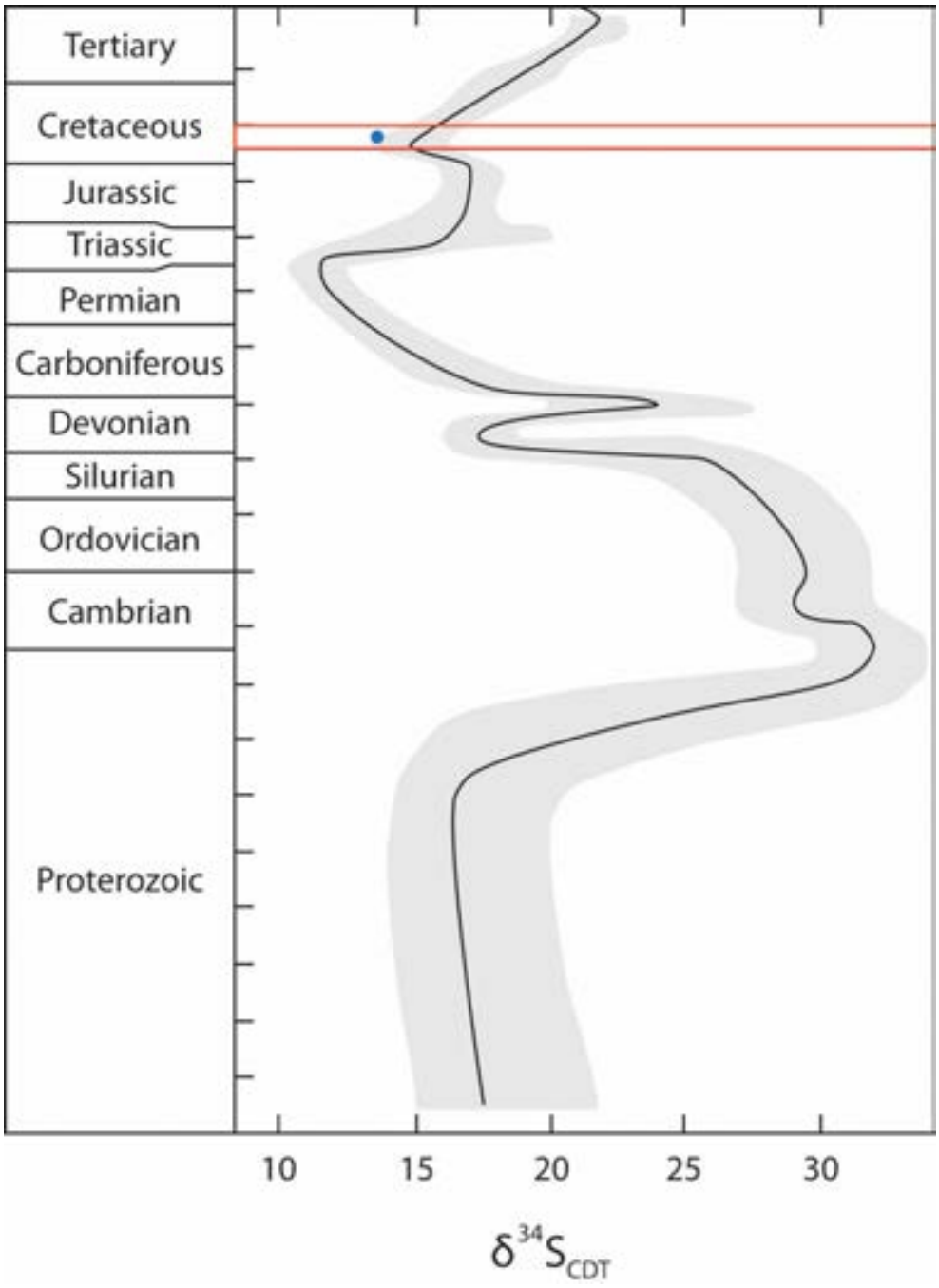

Figure 4.19: Marine sulfur isotope curve through geologic time.
Red box denotes Albian time frame while the blue dot represents the δ34Svalue acquired from marine septarian concretions of Mss. Modified from Claypool et al. (1980).

Table 4.6: Isotope composition of carbonate and carbonate associated sulfate results from various septarian concretions.

Location	Sample ID	$\delta^{13}C$ ‰	$\delta^{18}O$ ‰	CAS ppm	$\delta^{34}S$ ‰	Observations	Interpretation
HST-5	BM-5	-5.91	-6.94	172	13.6	green in hand sample, found in fine-grained marine sandstone/shale	$\delta^{34}S$ is similar to expected values for early Albian seas
LST-2	BM-2	-6.62	-5.75	241	18.7	red to tan but can have green tints in basinward samples, found in fine lacustrine sand above initial marine transgression	significantly higher sulfate content than other lacustrine samples and color change in basinward samples suggests minor marine influence on lacustrine deposition
Upper Yucca Formation	UY-1	-5.14	-5.82	11	17.1	red to tan, found in fine lacustrine sand in the Upper Yucca Formation	extremely low sulfate content suggests a lack of marine influence on lacustrine deposition

5. STRATAL ARCHITECTURE AND FACIES DISTRIBUTION

The southern thrust panel in the Indio Mountains contains a well-exposed 2.5 kilometer long stratal panel of Bluff Mesa Formation, which thickens from 220 meters at Echo Canyon on the southern end to 360 meters at Squaw Canyon on the northern end. Strata typically dip 24-34 degrees to the east and strike 342 degrees. The stratal panel is inferred to trend oblique to the paleoshoreline with the northern end representing deposition in a slightly more basinward position (Figure 4.1). This is supported by: 1) pronounced thickening to the north in multiple marine siliciclastic intervals, 2) greater volume of proximal facies (ooid grainstones vs fossiliferous wackestones and marine siliciclastics vs marine carbonates) in the southern portion of the transect and 3) northward orientation of progradational barforms (Cg, Cf, and Cs), which typically build basinward (Figure 4.2; Figure 4.10A). Syndepositional faults are present throughout the panel but increase in density to the south. Fault systems created a series of horst and graben blocks that extend into the overlying Cox Formation and underlying Upper Yucca Formation. Differences in facies distributions between horsts and grabens near Echo Canyon are typically minimal with notable exceptions discussed in the context of individual sequences. Offset and differences in facies distribution across faults typically decrease upwards suggesting tectonism was waning throughout deposition of the Bluff Mesa.

The utility of different surfaces in construction of a sequence stratigraphic model were discussed in Chapter one. It is readily apparent that the Bluff Mesa Formation in the study area cannot be described sufficiently using the rift model proposed by Martins-Neto and Catuneanu (2010). The rift model merges both the transgressive surface and sequence boundary with the flooding surface, which represents accommodation created by mechanical subsidence. The rift model predicts that the transgressive system tract should be thin or absent, however transgressive

systems tracts are present in every sequence across the southern thrust panel. Another integral key to the rift basin model is that fluvial deposits are interpreted as progradational infill and are placed at the top of the highstand systems tract instead of at the base of the lowstand systems tract. The erosional nature of fluvial facies of FA-1 suggests that they represent a decrease in base level, and therefore a sequence boundary, rather than progradational infilling of the basin.

The following summary of the stratal architecture of the Bluff Mesa utilizes standard sequence stratigraphic terminology (Catuneanu, 2006) to describe five sequences recorded within the study area. The Bluff Mesa Formation represents deposition approximately 113-110 Ma (uppermost Aptian to lower Albian), suggesting that individual cycles represent 600,000 years on average, and are therefore categorized as 4^{th} order sequences (Catuneanu, 2006). Higher order (5^{th}) climatic cycles are superimposed on fluvio-lacustrine lowstand systems of the Bluff Mesa and the transgressive surface of a lower order cycle (3^{rd}) is almost certainly located within the Bluff Mesa Formation.

Sequence boundaries are marked by abrupt non-waltherian facies shifts whereby erosive based fluvial deposits (FA-1) overly marine siliciclastics (FA-4) or marine carbonates (FA-3) (Figure 5.1A). Sequence boundaries often form compound surfaces with transgressive surfaces where marine siliciclastics (FA-4) overly marine carbonates (FA-3) (Figure 5.1B-D; Figure 5.2). Transgressive surfaces are identified at the base of retrogradational packages of marine siliciclastics that overly marine carbonates (FA-3) or terrestrial intervals (FA-1 and FA-2). Lenses of shell hash are commonly found throughout marine siliciclastic intervals (Ss), but have limited lateral distributions and are therefore not considered transgressive surfaces. Erosive surfaces are always considered sequence boundaries or compound sequence boundary/transgressive ravinement surfaces, with the exception of two Sc channel-fill deposits in

the transgressive systems tract of sequence #3. This was due to the lack of a non-waltherian facies shift above the channels and might therefore represent a higher frequency sequence boundary in which the depositional environment remained largely unchanged. Maximum flooding surfaces are represented by marine carbonates with progradational parasequence stacking patterns that conformably overly marine siliciclastics (Ss and Mss) or terrestrial facies (Fs, Fsl, Ls, and Lm).

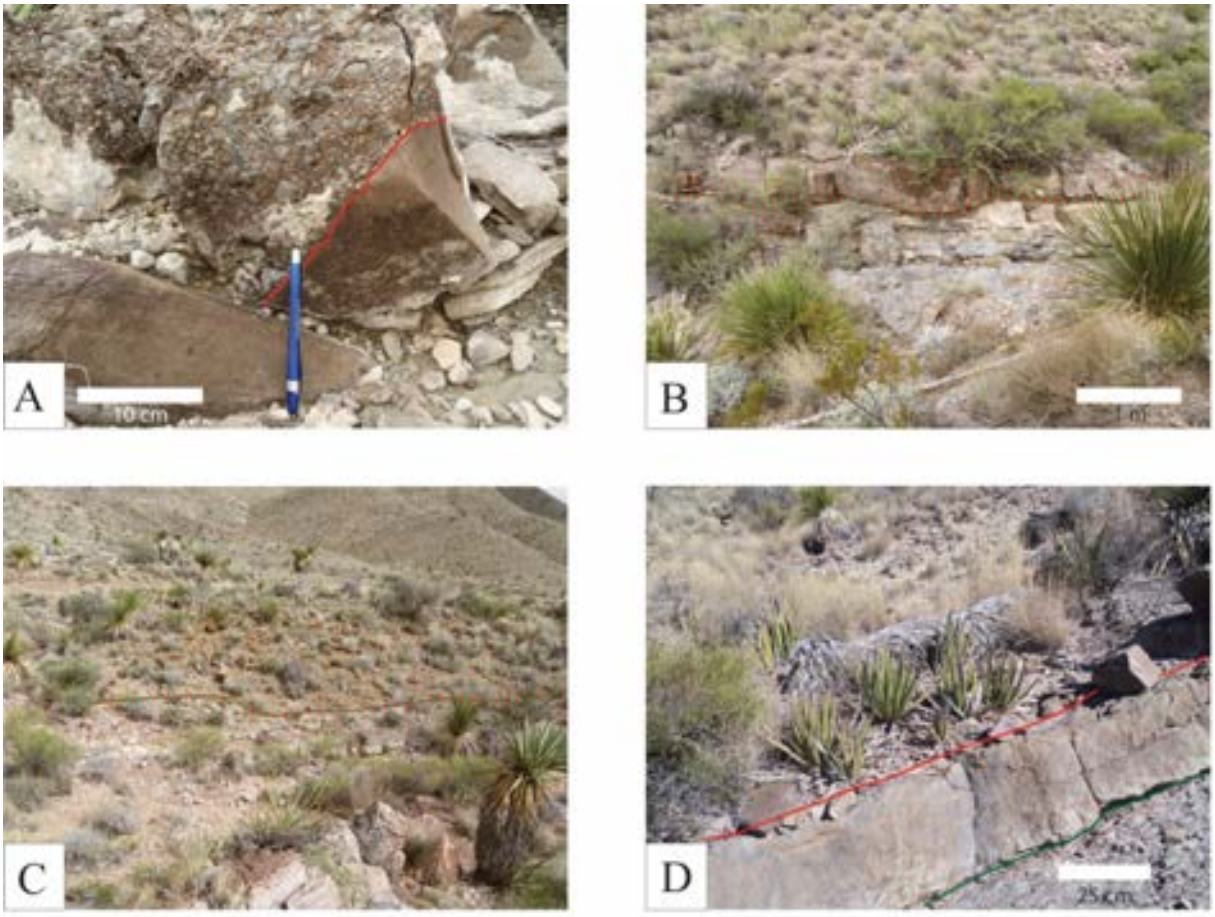

Figure 5.1: Outcrop photos of a variety of sequence boundaries.
(A) Sequence boundary #2 (red) Fc cutting into Cs of HST-1; (B) Compound surface SB-4/TS-4 (red and green) exhibits significantly less erosive power than compound surface SB-3/TS-3 (Figure 5.2); (C) Compound surface SB-5/TS-5 (red and green) is non-erosional and is identified by the vertical change from marine carbonates of HST-4 to marine siliciclastics of LST-5; (D) Sequence boundary #6 (red) separates cross-bedded sandstone of the Cox Formation from the possible transgressive lag (green) which caps the Bluff Mesa Formation.

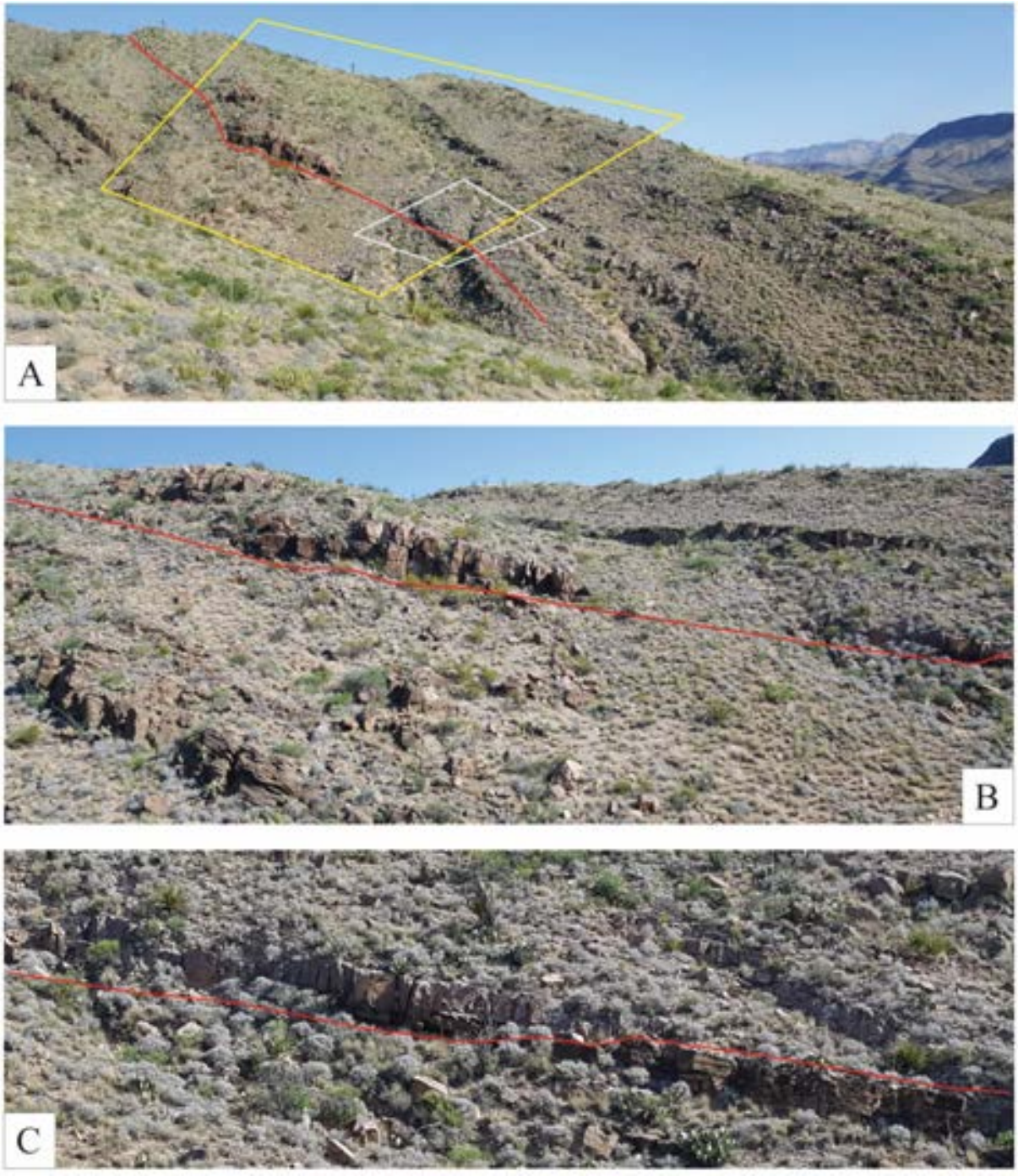

Figure 5.2: Outcrop photos of sequence boundary #3
(A) Channel at base of Sequence #3 cutting into carbonates of HST-2 looking north from measured section EI (red line - sequence boundary; yellow box - 5.2B; white box - 5.2C); (B) Closer view nearly perpendicular to primary channel, coarser parasequence top of HST-2 is absent as the channel cuts down into the lower recessive interval; (C) Closer view of channel margin truncating the well-exposed parasequence top of HST-2 (Cg).

Lowstand systems tracts (LST) occur between the sequence boundary and the transgressive surface when they do not form a compound surface. LSTs are confined to the lower Bluff Mesa Formation where they are composed of fluvial channel belts (FA-1) and recessive lacustrine intervals (FA-2) with rare fluvial tongues. LSTs are absent in the mid-upper Bluff Mesa where sequence boundaries form compound surfaces with transgressive surfaces. Transgressive systems tracts (TST) are found between transgressive surfaces and maximum flooding surfaces. TSTs are thicker in the mid-upper Bluff Mesa where they are composed of marine siliciclastics (FA-4) with sporadic marls (Cm) and sandy limestones (Cs). TSTs exhibit southward thinning in the lower Bluff Mesa where the transgressive surface does not share a compound surface with the sequence boundary. Highstand Systems Tracts, located between maximum flooding surfaces and sequence boundaries, are composed of marine carbonates (FA-3) with interbedded marine siliciclastics (Ss). HST thickness is fairly variable between sequences but is typically consistent across the panel in any given sequence.

5.1 SEQUENCE #1

The base of the Bluff Mesa Formation is contained within Sequence #1, which represents initial marine transgression in the basin. Sequence #1 is typically between 34 and 39 meters thick across the panel, with the significant exception of the horst block near Echo Canyon where it thickens to 52.9 meters. Detailed stratigraphic analysis shows that the marine carbonate identified as the base of the Bluff Mesa Formation by Underwood (1962) actually represents the base of highstand systems tract #1 (HST-1). Li (2012) showed that the first marine influence occurred earlier with the deposition of an oyster-rich packstone exposed intermittently across the panel. The classification scheme used here places this deposit at the base of transgressive systems tract #1 (TST-1) (Figure 5.3). In order to better understand the pre-existing depositional

geometries, the underlying lowstand systems tract (LST-1) of Sequence #1 needs to be included. LST-1 is technically part of the Upper Yucca Formation and coincides with the top of sequence #10 and sequence #11 identified by Li (2014).

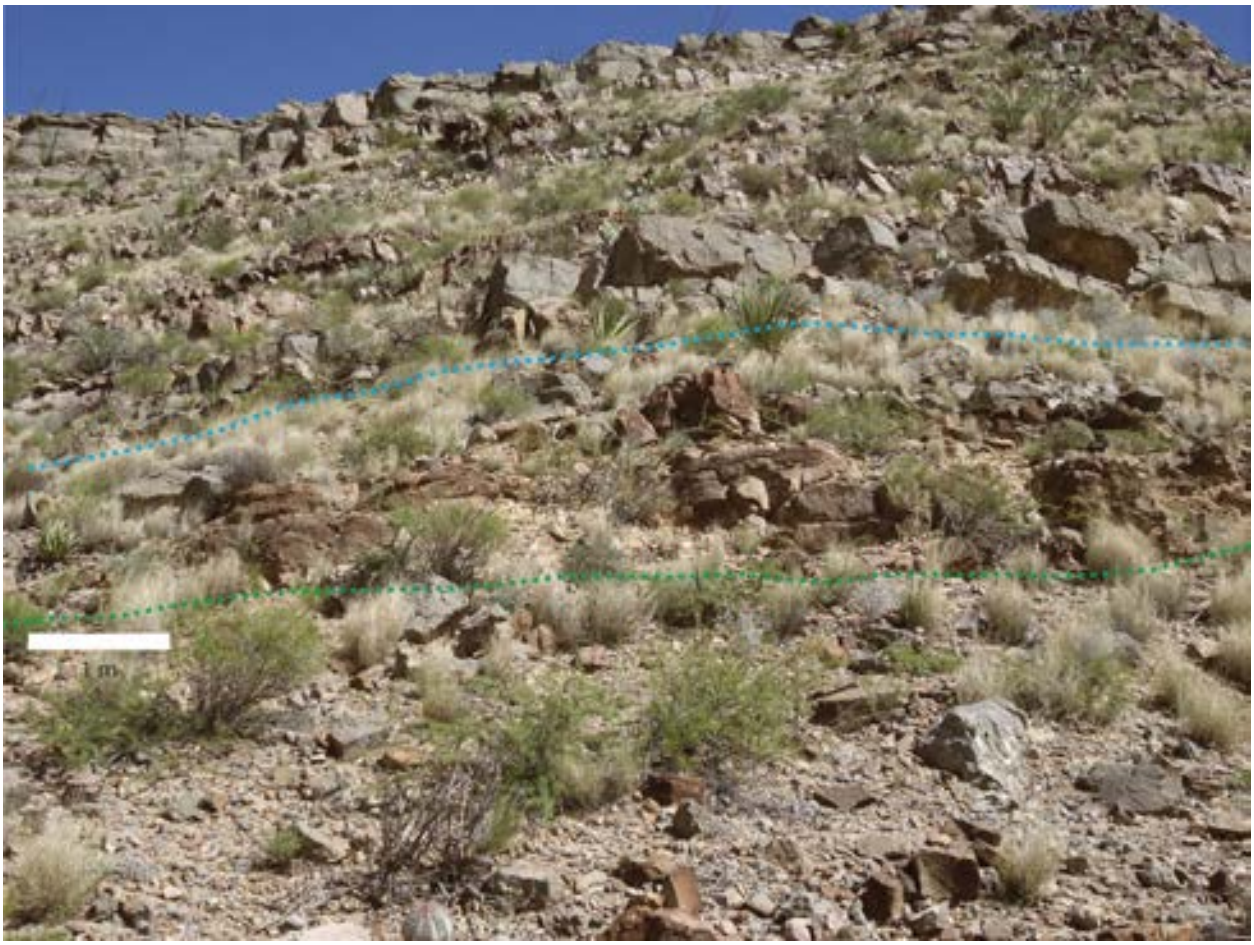

Figure 5.3: Outcrop photo of TST-1 and HST-1
Sandy oyster-rich packstone overlain by fine-grained marine sandstone (Ss) and fossiliferous packstone. TS-1 (green) is placed at the base of the oyster-rich packstone and MFS-1 (blue) is at the base of fossiliferous packstone.

The base of LST-1 is marked by an erosive contact between fluvial facies of FA-1 and the underlying recessive lacustrine facies (FA-2) across the panel. LST-1 thickens significantly from 18.8 meters in Squaw Canyon to 35.3 meters in Echo Canyon. The southward thickening trend of LST-1 is shared with LST-2 and the majority of fluvio-lacustrine cycles in the Upper

Yucca Formation (Li, 2014; Fox, 2016). Sequence #1 appears anomalously thick (52.9 meters) on the horst block near Echo Canyon with the change in thickness attributed mostly to LST-1 (Figure 5.4). The lacustrine interval of LST-1 on the horst is similar in thickness to measured sections in the adjacent grabens. The major difference lies in the thickness of the fluvial interval, which exceeds 26 meters, effectively doubling the measured thickness in the adjacent grabens (13.3m and 12.1m) (Figure 5.4). Fluvial channel density on the horst block decreases upward until a well-defined channel belt is exposed 6.5 meters below the transition to lacustrine deposition. This belt is 2.5-3 meters thick and contains scattered conglomeratic lags (Fc), possibly representing the true base of Sequence #1 on the horst block.

A transgressive surface is exposed locally across the stratal panel with the best exposures located between measured sections XW and M (Figure 4.1). This surface is represented by the generally fossiliferous base of Li's (2014) sandy oyster-rich packstone (Cs) (Figure 5.3). TST-1 is primarily composed of fine-grained marine siliciclastics with shell hash lenses (FA-4) and sporadic exposures of a thin bedded wackestone (Cf), which is less fossiliferous than typical Cf deposits. TST-1 is 14.1 meters thick in Squaw Canyon before thinning to approximately 6-7 meters in the panel center and finally pinching out between measured sections M and EI. Poor exposures make it impossible to document onlap where TST-1 pinches out, but MFS-1 appears to lie directly above lacustrine facies of LST-1 throughout the southern third of the panel.

The base of HST-1 (MFS-1) is marked by a non-waltherian shift from fine-grained marine siliciclastics to overlying shallow marine fossiliferous packstone (Cf) that is continuous across the most of the panel (Figure 5.5; Figure 5.6). These Cf deposits conformably overly lacustrine shales of the Upper Yucca Formation in the southern third of the panel and recessive fine-grained Ss of TST-1 in the north and center. HST-1 is composed of fossiliferous packstone

(Cf) over the southern 95% of the panel, but becomes extremely sand-rich and more thinly bedded (Cs) near Squaw Canyon. HST-1 is approximately 2.5 meters thick over most of the panel but thins to 70 centimeters in Squaw Canyon. The thin-bedded Cs deposit in Squaw Canyon is erosively cut by overlying fluvial units of LST-2 between measured sections SEQ and XW (Figure 5.1A).

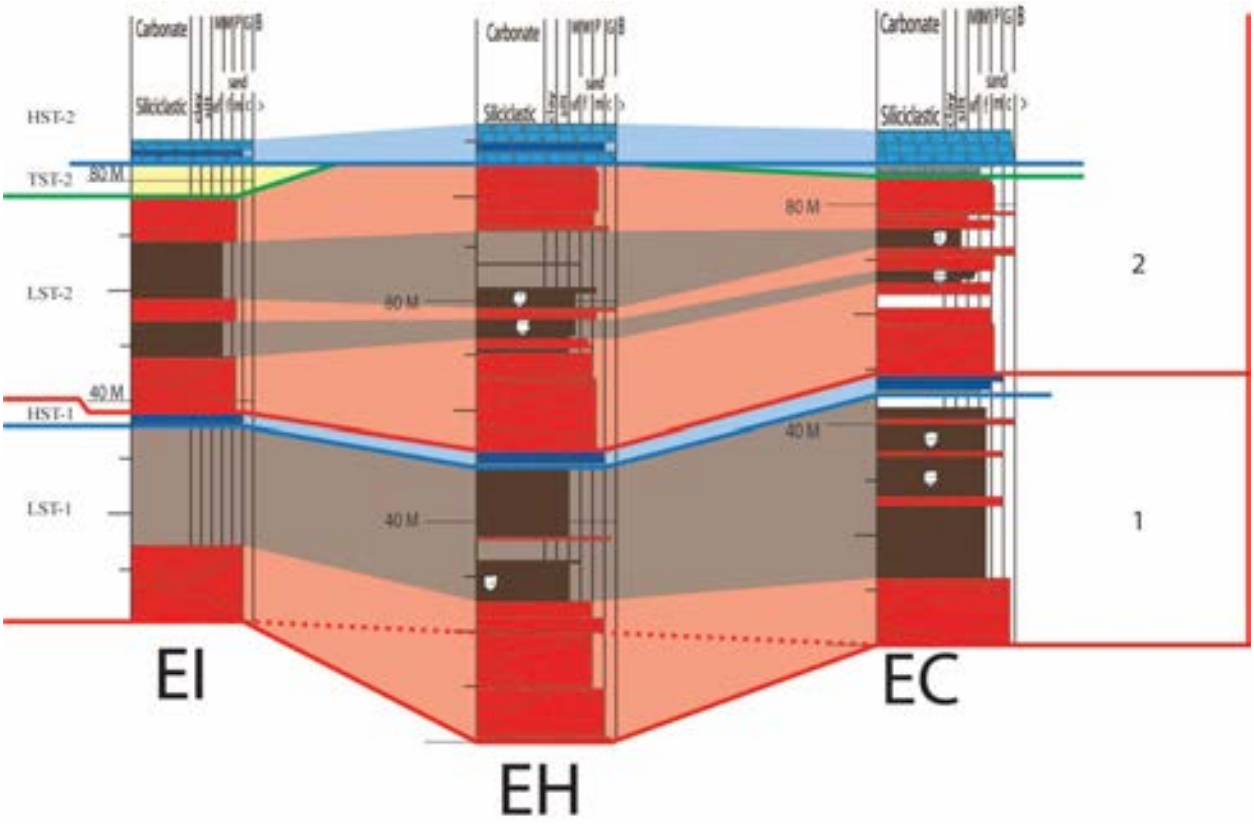

Figure 5.4: Cross-section of measured sections recording the Echo Canyon horst block. Stratigraphic correlation and facies distribution across horst block (center) and adjacent grabens near Echo Canyon. Dotted red line denotes SB-1 across the horst if the fluvial interval at EH is actually two lowstands.

5.3 SEQUENCE #2

Sequence #2 initiates with a non-waltherian return to fluvio-lacustrine deposition, followed by marine transgression marking the onset of continuous marine deposition for the remainder of Bluff Mesa deposition. The sequence thickens progressively from 96.65 meters in Echo Canyon to 153.15 meters in Squaw Canyon. This trend of northward thickening differs from the southward thickening documented in fluvio-lacustrine intervals (LST), suggesting that marine transgression affected basin physiography and changed the nature of accommodation created thereafter.

The base of Sequence #2 is marked by fluvial facies of FA-1, which typically overlie a single bed of fossiliferous packstone (Cf) of HST-1 across all but the northernmost 400 meters of the panel. Near Squaw Canyon the fluvial facies cut into a wedge of fine-grained marine facies of the underlying HST-1 (FA-4). LST-2 is composed of two fluvial belts (Fc, Fs, and Fsl) separated by a continuous lacustrine interval (Ls and Lm). Exposures are generally excellent and covered areas are confidently categorized as recessive intervals of fluvial overbank deposits (Fsl) or lacustrine deposits using differences in float characteristics. Although both fluvial belts maintain similar thicknesses across the panel, the upper fluvial belt is more channelized and contains a higher ratio of Fs:Fsl (Figure 5.5). LST-2 is typically 34 to 40 meters thick, increasing to 50 meters on the horst block near Echo Canyon (measured section EH) and thinning slightly to the north (Figure 4.2). Multiple prograding tongues of fluvial facies (Fs and Fc) are interbedded within the fine-grained lacustrine interval near Echo Canyon and can be traced onto the horst and the graben to the north. One particular tongue extends over 300 meters across the stratal panel from Echo Canyon. This fluvial interval thins from 4.9 meters in the graben to 2.3 meters on the horst block with both facies thinning proportionally. When present,

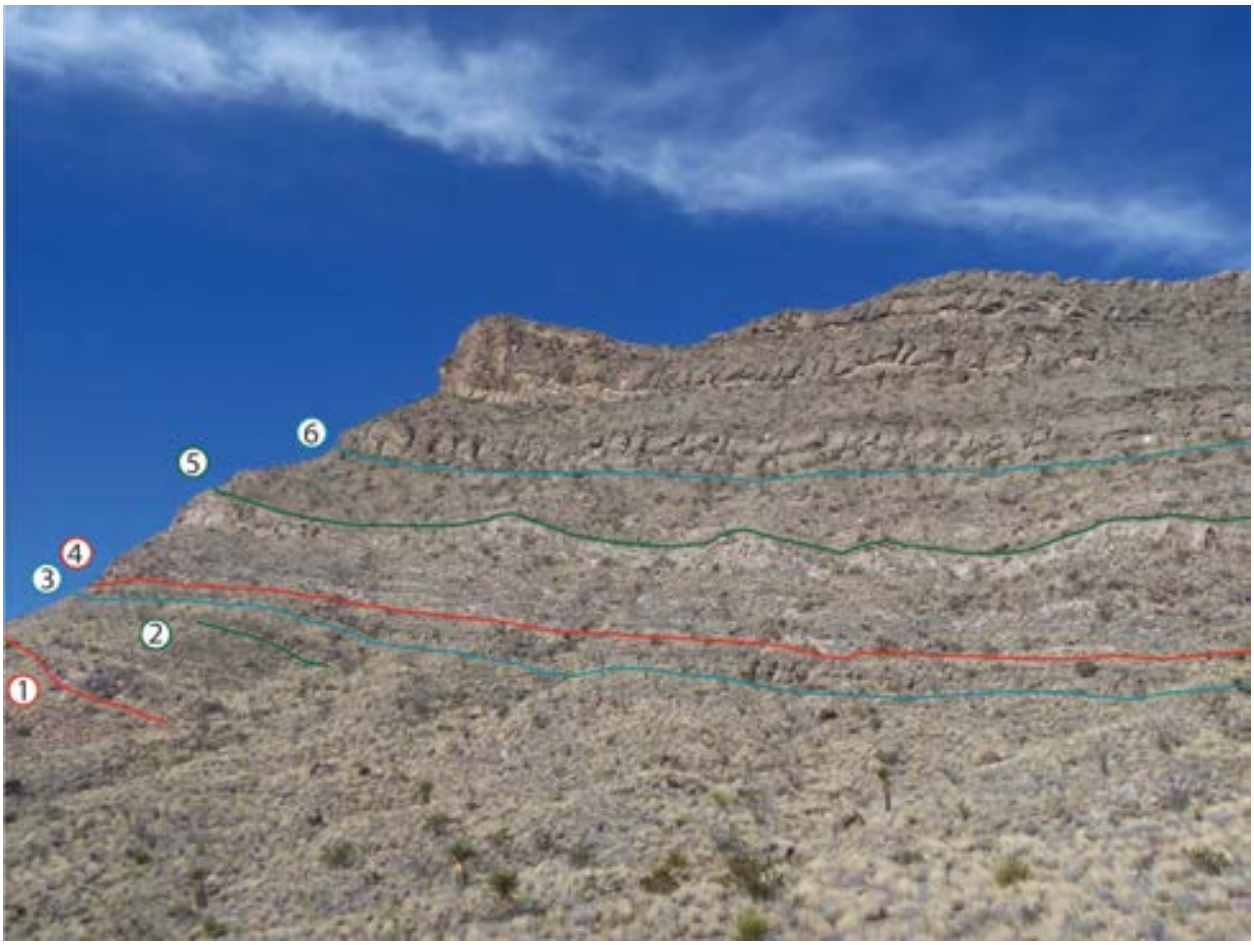

Figure 5.5: Outcrop photo of sequences #1 and #2
Typical exposures of sequences #1 and #2 approximately 200 meters south of measured section XW. (1) SB-1 below a fluvial channel; (2) Rare well-exposed TS-1 below the oyster-rich packstone; (3) MFS-1 below northward prograding barforms of Cf; (4) SB-2, note the presence of thin isolated channels in the overlying recessive lacustrine interval; (5) TS-2; (6) MFS-2 northward prograding bars of Cf, the well-exposed cliff-forming interval is composed of Cg barforms.

the tongue separates two distinct intervals of lacustrine mudstone (Lm), which remain separated and distinguishable from one another across the entire panel.

The base of TST-2 is marked by a compound transgressive/maximum flooding surface on the Echo Canyon horst block and a transgressive surface across the rest of the stratal panel. This transgressive surface is represented by a non-waltherian shift to marine deposition over the

uniform upper fluvial interval of LST-2. TST-2 is composed of a wedge of shallow marine facies (Cf, Cs, and Ss) that downlap the transgressive surface and thin from 28 meters in Squaw Canyon to 16.4 meters in the panel center before nearly pinching out at Echo Canyon where it is absent on the horst block (Figure 5.6A; Figure 5.6C). A thin sandy marine wackestone (Cs) sits directly above the fluvial package in the Echo Canyon graben, which was located marginward of the horst block (Figure 4.2; Figure 5.4; Figure 5.6B). Although this wackestone could be related to the overlying highstand carbonates, it is superficially similar to carbonate facies of the wedge. The wedge is composed primarily of Ss that is more recessive than typical Ss deposits in overlying sequences. These Ss deposits contain rare, scattered shell hash lenses and are occasionally interbedded with more continuous thin-bedded Cf and Cs deposits that trend towards wackestone fabrics.

The maximum flooding surface lies at the base of a continuous interval of well-exposed marine carbonates. This interval is composed almost entirely of fossiliferous packstone (Cf) barforms that prograde to the north. The carbonate interval always contains 2-3 stacked bars with individual bars that are typically exposed for 200-300 meters before downlapping the maximum flooding surface (Figure 5.6D). Near Echo Canyon Cf barforms are interbedded with ooid grainstone bars (Cg) that behave in a similar fashion. The last of these Cg bars pinches out 600 meters from Echo Canyon with the remainder of the interval composed of Cf across the panel. This indicates that ooid generation had already begun in a marginward position of the study area. HST-2 thickens from 57.25 meters in Echo Canyon to 87.3 meters in Squaw Canyon. HST-2 is composed of marine carbonates of FA-3 and marine siliciclastics of FA-4. Distribution of Cf deposits vary vertically and are most common near the base and top of HST-2. Lateral changes are less pronounced but Cf deposits are more common in basinward positions near Squaw

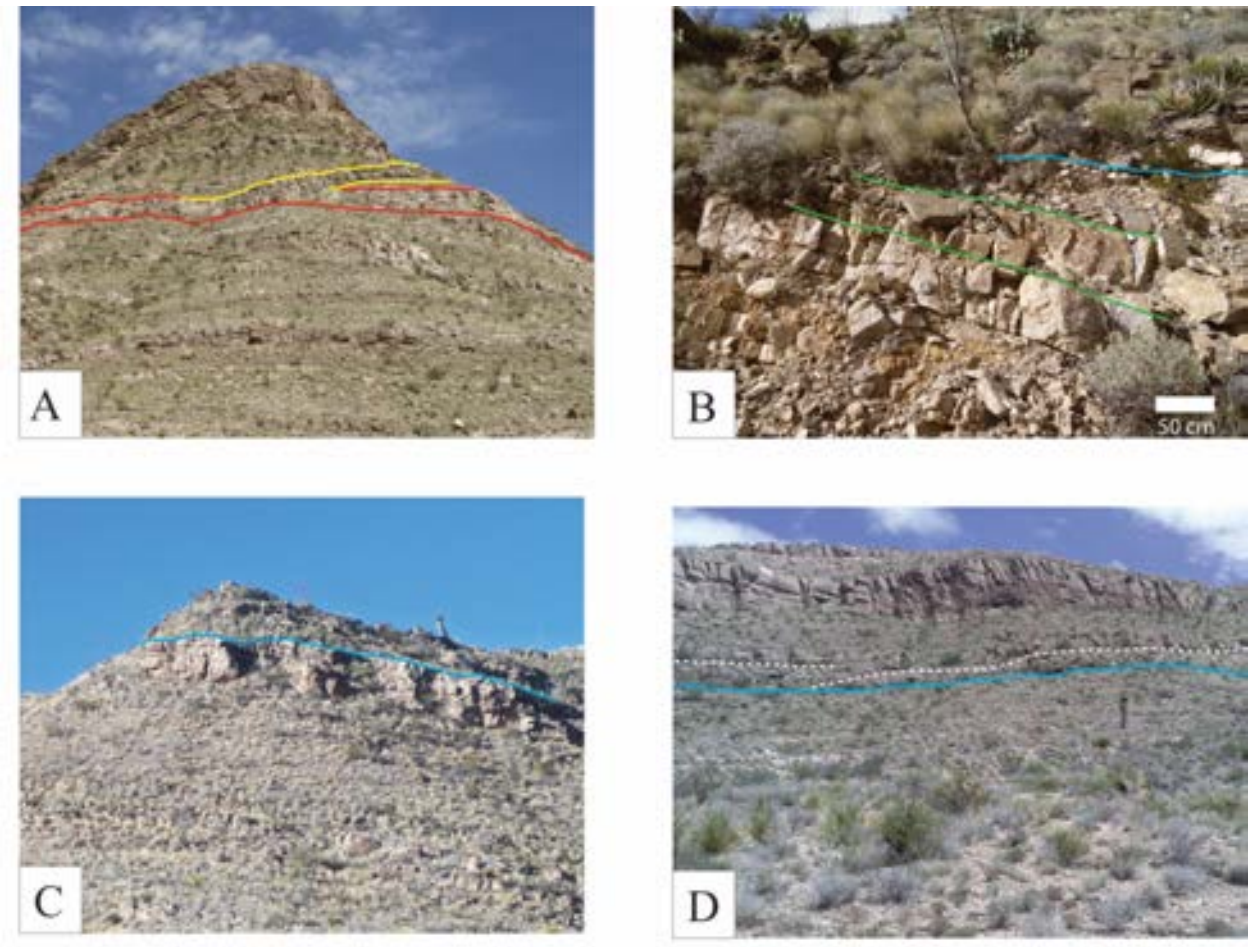

Figure 5.6: Outcrop photos of Sequence #2.
(A) Marine sandstone (Ss) (yellow outline) of TST-2 downlaps fluvial belt of LST-2 (red outline); (B) Sandy fossiliferous packstone (Cs) (green outline) in Echo Canyon graben records marine incursion before drastic base level rise associated with MFS-2 (blue); (C) Ooid grainstones (Cg) and fossiliferous packstones (Cf) sit directly above fluvial channels of LST-2 on the Echo Canyon horst block (MFS-2 - blue); (D) Northward prograding barforms (white) of fossiliferous packstone downlap MFS-2 (blue).

Canyon. Cg deposits are well distributed throughout HST-2 excluding the basal carbonate, which is entirely Cf outside of Echo Canyon. Ss deposits are normally found as isolated lenses in thicker carbonate intervals throughout HST-2 while continuous Ss intervals are only found in lower interval and are confined to the southern half of the panel. Cs deposits are distributed fairly evenly, both vertically throughout HST-2 and laterally across the panel. Widespread distribution

of Cs and the nature of Ss deposits in HST-2 support the conclusion that siliciclastic input can represent either progradation (continuous Ss intervals) or along-strike encroachment of longshore bar complexes (isolated Ss lenses).

5.3 SEQUENCE #3

Sequence #3 represents the lowest entirely marine sequence in the Bluff Mesa Formation and an influx of siliciclastic sediment across the study area (Figure 4.2). Sequence #3 is 34.55 meters thick in the center of the panel and thins to roughly 14 meters in both Echo and Squaw canyons.

The base of Sequence #3 is marked by a compound sequence boundary/transgressive surface where an abrupt change from thick shelf carbonates of HST-2 to siliciclastic deposition of TST-3 occurs. Most of the compound surface is represented by a medium-grained Ss that does not cut into the underlying carbonates of HST-2. However, 100 and 150 meters north of measured section EI, two channelized Sc deposits cut up to 5 meters down into carbonates (Cm and Cs) of HST-2 (Figure 5.2). TST-3 thickens significantly towards the center of the panel reaching a maximum of 34.55 meters and thins towards both canyons, albeit less drastically to the south. Three similar channels are found higher in the section within the same lateral zone. These channels are composed of proportionally more Ss than Sc compared to the two basal channels and cut into fine-grained Ss deposits instead of carbonate facies. This suggests that although the base level may have dropped at this time, the change was not great enough to trigger a non-waltherian facies shift. Therefore, these channels do not represent a sequence boundary and are included within TST-3.

The base of HST-3 is marked by an abrupt change from marine siliciclastics (FA-4) of TST-3 to fossiliferous marine packstone (Cf). HST-3 is fairly thin, ranging from 11.3 meters in

the north at measured section XW to 60 centimeters in Echo Canyon (Figure 4.2). HST-3 is composed of fossiliferous packstone (Cf) which is often poorly exposed in the dip slope, but is inferred to be continuous across the panel. A sandy packstone (Cs) is locally present underlying the Cf bed at measured section XW, but it is gradational with the underlying sandstone, suggesting it belongs to TST-3.

5.4 SEQUENCE #4

Sequence #4 is a marine interval compositionally similar to Sequence #3. Sequence #4 thins to the south from 68.6 meters in Squaw Canyon to a minimum of 29.8 near Echo Canyon. Sediment distribution in Sequence #4 shares characteristics with Sequence #2 in that it generally thickens to the north, however the degree of thinning to the south is less extreme.

The sequence boundary at the base of TST-4 marks an abrupt non-waltherian shift from shallow marine carbonate to shallow marine shoreface siliciclastic deposition across much of the panel. SB-4 forms a compound surface with TS-4, which is poorly-exposed as it is almost entirely confined to the dip slope across the panel. An excellent exposure shows the erosive base of TST-4 cutting into Cf of HST-3 (Figure 5.1B). This channel is located approximately 120 meters north of measured section EI, in the same lateral zone as the basal channel of TST-3 (Figure 4.1). TST-4 differs slightly from TST-3 in that it steadily thickens northward from 29.8 meters near Echo Canyon to 62 meters in Squaw Canyon. TST-4 is composed primarily of marine siliciclastics of FA-4 with the notable exception of a 6m thick fossiliferous packstone (Cf) in Squaw Canyon that is untraceable to the south. At least one more channel fill deposit is exposed higher in the section but in line with the basal channel of TST-3, suggesting this area was a preferred sediment fairway during Sequence #4.

The base of HST-4 is marked by a maximum flooding surface separating shallow marine siliciclastics (FA-4) from overlying shallow marine carbonates (FA-3). HST-4 is often poorly exposed in the dip slope, but is regarded as a high confidence interval as it appears nearly identical across the panel when fully exposed. HST-4 is reliably 6.1-6.4 meters thick across the entire stratal panel. The continuous thickness of HST-4 is maintained on both sides of the fault separating the horst and graben near Echo Canyon, indicating that the fault was inactive at this time. HST-4 is composed of several fossiliferous wackestones (Cf and Cs) interbedded with a single well-cemented marine sandstone bed (Ss). The nature of HST-4 is different in Squaw Canyon where it is represented by multiple coarsening-up parasequences of Cs. These beds are not traceable southward into the panel as they are aligned directly with the road. It should be noted that they might not be related to HST-4 and the thickness of 6 meters is a coincidence.

5.5 SEQUENCE #5

Sequence #5 represents a marked deepening of both siliciclastic and carbonate depositional environments preceding coarser-grained deposition of the Cox Sandstone. Sequence #5 thickens from 62 meters in Echo Canyon to 92 meters in Squaw Canyon. Northward thickening of Sequence #5 is similar to Sequences #2 and #4, suggesting that the paleoshoreline lay somewhere to the southeast of the study area.

The base of TST-5 is represented by a compound surface separating shallow marine carbonates (FA-3) of HST-4 from a fine to medium-grained Ss interval (Figure 5.1C). The SB-5/TS-5 compound surface is the only sequence boundary that does not have an identifiable erosive base, but is instead chosen on its widespread distribution across the panel indicative of an abrupt non-waltherian shift (Figure 5.1C). These Ss deposits form a basinward thickening wedge that thins significantly from 33.8 meters in Squaw Canyon to 3.05 meters in Echo Canyon.

A continuous interval of fine-grained sandstone to shale (Mss) overlies TST-5. Much of the Ss wedge of TST-5 is buried under a road that runs parallel to the panel, but Ss can be differentiated reliably from recessive Mss utilizing float characteristics. MFS-5 is placed at the contact between the Ss wedge and the overlying Mss interval, which is assigned to HST-5.

HST-5 is fairly uniform across the stratal panel thickening slightly to the south and can be traced easily on aerial photos due to the distinct olive green color. HST-5 is typically 50-60 meters thick across the panel, reaching a maximum of 67 meters in measured section EI. This may be significant regarding water depth interpretation, as this was also the only location where marine septarian nodules were observed directly weathering from the outcrop. However, significantly smaller marine nodules were found as float in the same interval in Echo Canyon, suggesting this thickness change may simply be due to favorable orientation of the road. The majority of HST-5 is composed of an interval of coarsening-up fossiliferous wacke-packstone parasequences that overlie the Mss interval. The top of HST-5 is marked by an influx of marine and fluvial siliciclastics, which are assigned to the Cox Formation (Underwood, 1962; Budhathoki, 2013). Budhathoki (2013) identified the base of the Cox Formation as a transgressive lag overlying marine carbonates of the Bluff Mesa Formation (Msf) (Figure 5.1D). Despite having similar faunal assemblages, the lag does appear to be distinct from the underlying Msf parasequences and is not simply the coarser-grained top of a parasequence. The lag is unique within the study area as it is positioned above the highstand systems tract, suggesting it might be associated with a lower order transgressive surface. Regardless of the classification of the lag, it is immediately overlain by marine and fluvial siliciclastics representing a non-waltherian shift and a sequence boundary.

6. DISCUSSION

6.1 GEOCHEMISTRY OF SEPTARIAN NODULES

Sulfur, carbon, and oxygen isotopes were extracted from six septarian concretions in the study area (Table 4.6). Four concretions were sampled from the Upper Yucca (UY-1), one from the suspected lacustrine interval of LST-2 (BM-2), and another from the marine shale of HST-5 (BM-5). Samples were taken from locations within 50 meters of the fault dense zone at Echo Canyon. Faults near Echo Canyon acted as conduits for fluid migration, as evidenced by the distribution of radial calcite fans in the Upper Yucca (Li, 2014). Ideally, samples would have been taken from lower density faulted zones near Squaw Canyon, but the only exposure of marine septarian concretions in LST-5 is near Echo Canyon. Results and implications regarding the formational/depositional environment of these septarian nodules are discussed in the following sections.

6.1.1 Carbonate Associated Sulfate (CAS)

During precipitation of carbonate, sulfate ions are incorporated within the crystal structure of the formed mineral (Wotte et al., 2012). Sulfur isotope fractionation during this process is minor. Consequently, CAS represents a proxy for the sulfur isotope composition ($\delta^{34}S$) values of paleo-seawater sulfate during the deposition of carbonates (Payton and Gray, 2012). Rift lakes, which are decoupled from the ocean, may carry a substantially different $\delta^{34}S$ signature than marine waters this may allow us to gain insight on the effect of marine waters on lake systems during the early stages of marine transgression.

Confidence in CAS as an environmental proxy hinges on two assumptions: 1) that the carbonates under examination were formed syndepositionally and 2) did not undergo significant

diagenetic alterations post-burial. Li (2014) analyzed the mineralogy and stratigraphic facies distributions of the Upper Yucca Formation, and concluded that septarian concretions found in this formation likely formed near the sediment-water interface. For the lacustrine or marine septarian concretions of the Bluff Mesa Formation, this study found no contradicting evidence to the genesis model proposed by Li (2014), thus satisfying the first assumption.

Proving that significant diagenetic alteration did not occur is more difficult, but perhaps not entirely necessary. Although the carbon and oxygen isotope composition of carbonates may undergo significant alterations, it is expected that sulfate composition is less affected by migrating fluids during diagenesis, as typically very little sulfate is added to the carbonate associated sulfate pool (Bergersen, 2016). This is because most sulfate is removed through biogenic processes near the sediment-water interface and because, as a tetrahedral molecule, the sulfate ion is a poor fit for the carbonate lattice structure. Extensive meteoric diagenesis is known to decrease the concentration of CAS but $\delta^{34}S$ values typically remain consistent, even after alteration of the primary mineralogy or fabric (Gill et al., 2008). Gill et al. (2008) state the following regarding the use of CAS concentration as a proxy, "we suggest that trends may be preserved, but absolute magnitudes are probably not". These findings suggest that despite diagenetic alteration of septarian concretions, isotopic values recorded within the CAS are likely accurate representations of paleo-water chemistry during deposition. Additionally, due to similar burial histories and exposure to meteoric waters between samples, we can assume that the original CAS concentrations may have changed, but trends may still be preserved.

Due to the high level of confidence in signal preservation for the isotopic composition of CAS, the $\delta^{34}S$ values are considered the most reliable information for the geochemical interpretation of the environmental conditions during the formation of septarian concretions.

CAS extracted from BM-5 is isotopically lighter than the world oceanic average for the Aptian-Albian time (13.6 ‰ vs 16 ‰; Claypool et al., 1980). It should be noted that the Aptian-Albian segment of the global curve was determined from biogenic barite and evaporitic gypsum, rather than CAS, however the difference should be minimal (Claypool et al., 1980). The $\delta^{34}S$ values obtained from BM-2 (18.7 ‰) and UY-1 (17.1 ‰) are fairly similar and notably heavier than those obtained from BM-5. This suggests that ambient water chemistry during deposition of LST-2 was more similar to deposition during Upper Yucca time than deposition during LST-5. These results, along with nodule morphology and stratigraphic distribution, further support the interpretation that fine-grained nodule-bearing sandstones of LST-2 were deposited in a lacustrine environment.

As previously discussed, CAS concentrations should be used to compare trends rather than absolute values. Of the four septarian concretions sampled from the Upper Yucca Formation, only a single sample had a sufficient CAS concentration to yield any results (11 ppm). The samples from the Bluff Mesa Formation, BM-2 (241 ppm) and BM-5 (172 ppm) were significantly more sulfate-rich. Operating under the assumption that BM-2 was deposited in a lacustrine environment we should expect to find lower sulfate concentrations similar to samples taken from the Upper Yucca Formation. These seemingly contradictory results can be explained by three non-exclusive reasons: 1) sulfate concentration decreased variably between samples and the results are meaningless, 2) the lacustrine interval of LST-2 is in close stratigraphic proximity to marine carbonates of HST-1 and HST-2, which means that sulfate-rich marine waters may have diffused into lacustrine nodules of LST-2 during burial diagenesis, or 3) marine waters mixed with lake water during LST-2 without an environmental change from marine to lacustrine

deposition. Drastically different concentrations for only the four Upper Yucca samples seems unlikely, so the first scenario is ignored.

The second scenario is intriguing but there is the constraint that additional sulfur is rarely added to the CAS pool (Bergersen, 2016), making diagenetic enrichment unlikely. The most likely scenario is that of minor marine influence on an alkaline rift lake during marine transgression. This interpretation is supported by the presence of some lacustrine nodules of LST-2 near Echo Canyon that share superficial characteristics with marine nodules of LST-5. It is unclear whether the mechanism for marine sulfate input was due to minor transgressions and regressions, fluid migration along syndepositional faults or through a sediment barrier between the ocean and the lake, or even due to sea spray.

Additional information regarding depositional conditions may be revealed by examining the relationships between formation depth, oxygenation, and isotope fractionation (Figure 6.1). Fresh water is typically a low sulfate environment (Bowen, 1979), so it is not surprising that Upper Yucca samples were extremely sulfate-poor. Facies characteristics and stratigraphic distribution suggest that BM-5 formed in a marine environment. Figure 6.1 illustrates the removal of sulfate in oxygen-free sediments, showing that sulfate is consumed by sulfate-reducing bacteria with increasing depth, leaving sulfate that is enriched in the heavier isotopes available for inclusion in the carbonate crystal lattice. Following this concept, $\delta^{34}S$ of BM-5 should be heavier than the isotope composition of seawater sulfate from Albian oceans, which is approximately 16‰. The isotopically much lighter value of 13.6‰ of BM-5 does not meet this expectation. This, and the absence of pyrite – the prime indicator for bacterial sulfate reduction and the production of sulfide (Canfield, 2001) – indicates that the nodule may not have formed in the sulfate reduction zone. Alternatively, the nodule may have formed deeper in the sediment

where all sulfate is consumed and degradation of organic matter is taken over by methane producers, or at very shallow depth near the surface where organic matter is oxidized by oxygen. For those cases, the isotopically light signature of BM-5 would then have to be explained by a mixing of sulfate from seawater combined with sulfate that is derived from the oxidation of isotopically light sulfide. The green color of the sample, likely caused by the presence of ferrous (reduced) iron indicates that the nodule formed in an oxygen-free environment.

6.1.2 Carbon and Oxygen Isotope Composition

Examination of carbon and oxygen isotopes collected from the same carbonate nodules as discussed above, reveals somewhat surprising results (Table 4.6). The relatively light oxygen isotope composition of BM-5 is indicative of nodule formation in a lacustrine environment, as the isotope composition of Aptian/Albian marine environments should be near zero (Veizer et al., 2000). In fact, the carbon and oxygen isotopic compositions of both BM-5 and BM-2 are similar to those of a multitude of nodules from the Upper Yucca (Llanos, 2017). This is an interesting revelation warranting future investigation.

The simplest explanation is that the carbon and oxygen isotope values from BM-5 are similar to Upper Yucca samples due to shared diagenetic fluids that overprinted the original isotope signatures. However, this interpretation is problematic for two reasons. Firstly, BM-5 nodules are encased in shales, which have notoriously low permeability, preventing significant diagenetic alteration (Magara, 1978). Secondly, although large crystals associated with

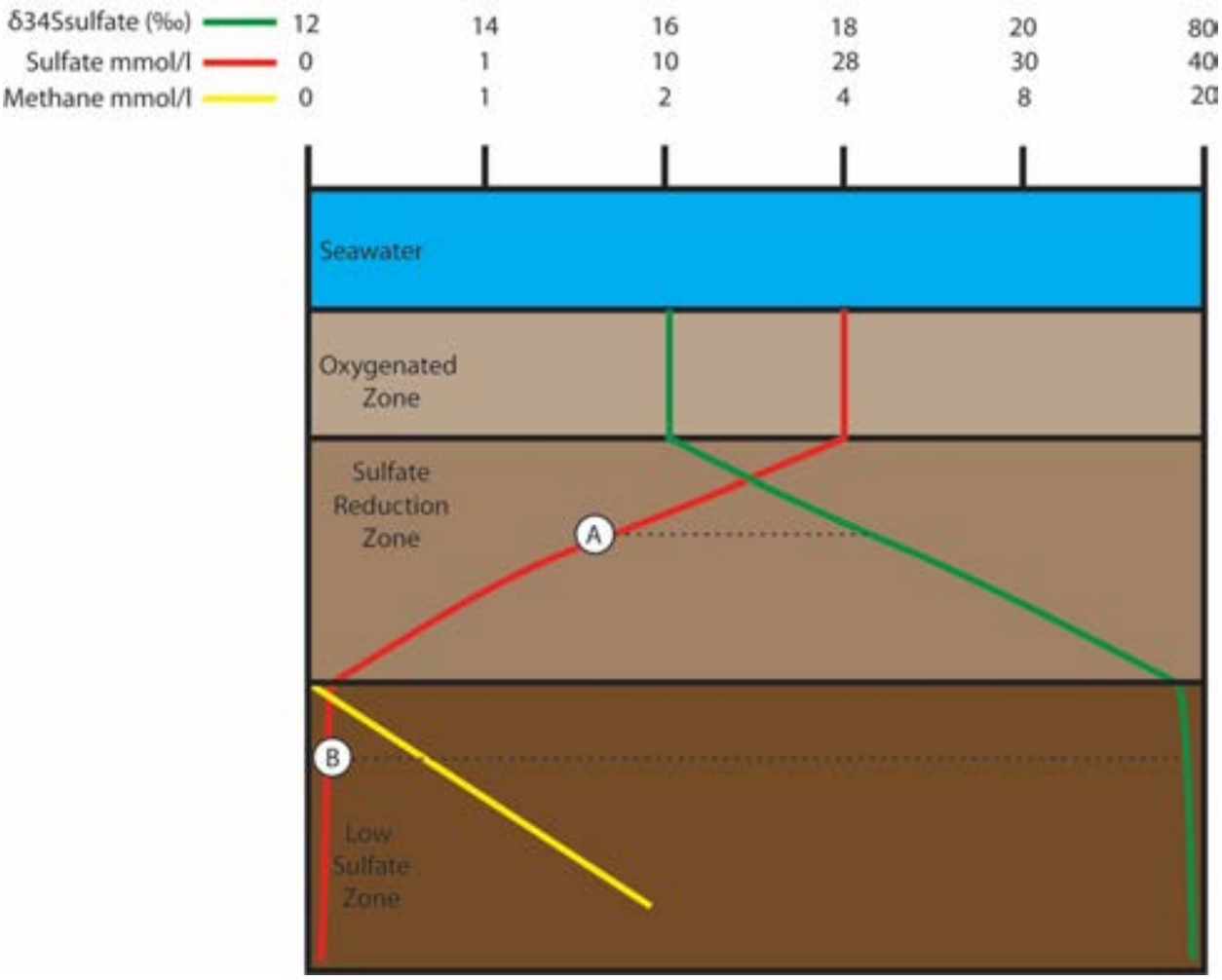

Figure 6.1: Sulfate concentration and fractionation trends (not to scale).
(A) Nodule formation in the sulfate reduction zone results in heavier $\delta^{34}S$ of carbonate associated sulfate. Well-oxygenated bottom waters result in expanded oxygenated and sulfate reduction zones. (B) Nodule formation below the low sulfate zone at the sulfate-methane transition typically result in very heavy $\delta^{34}S$ values as nearly all sulfate has been consumed in the sulfate reduction zone, but little sulfate is incorporated into carbonate due to the low sulfate concentration. Consequently, at a later diagenetic stage, this heavy signal can be easily overprinted by isotopically light sulfate produced from sulfide oxidation.

diagenetic alteration are present within septarian cracks, they are absent in the micritic groundmass, indicating that no pervasive alteration by migrating fluids took place (Figure 4.18E

and F). If sharing of similar diagenetic fluids is invoked to explain the carbon and oxygen isotope results, then both of these issues must be addressed.

Alternatively, the similarity in isotope signatures can be explained by depositional environment, suggesting that BM-5 was formed in a lacustrine environment, similar to the setting of BM-2 (Table 4.6). This possibility is intriguing, but is currently not supported by stratigraphic or fossil evidence. A return to terrestrial deposition would indicate that base level had fallen after TST-5, necessitating the delineation of another depositional sequence. Measured sections that correlate with the Bluff Mesa Formation in the study area show pronounced deepening within Sequence #5, and are discussed in detail within section 6.3. The nodule-producing Mss interval of HST-5 suspiciously thickens southward, similar to lacustrine intervals of the Upper Yucca and lower Bluff Mesa. This study places the Mss interval in a mid-shelf marine environment due to the preponderance of fossil evidence and the lack of stratigraphic proximity to fluvial facies, but the isotope analysis indicates that the depositional history may be more complicated.

6.2 STRATIGRAPHIC ARCHITECTURE AND THE PALEOENVIRONMENT

Analysis of the stratigraphic architecture established in chapter 5 provides insight into the nature of accommodation generation (eustatic vs tectonic), sediment dispersal patterns, and the antecedent topography of the former rift basin during multiple transgressions. This task is aided by facies distribution analysis and attention to the sometimes subtle interactions between sediments and syn-depositional faults.

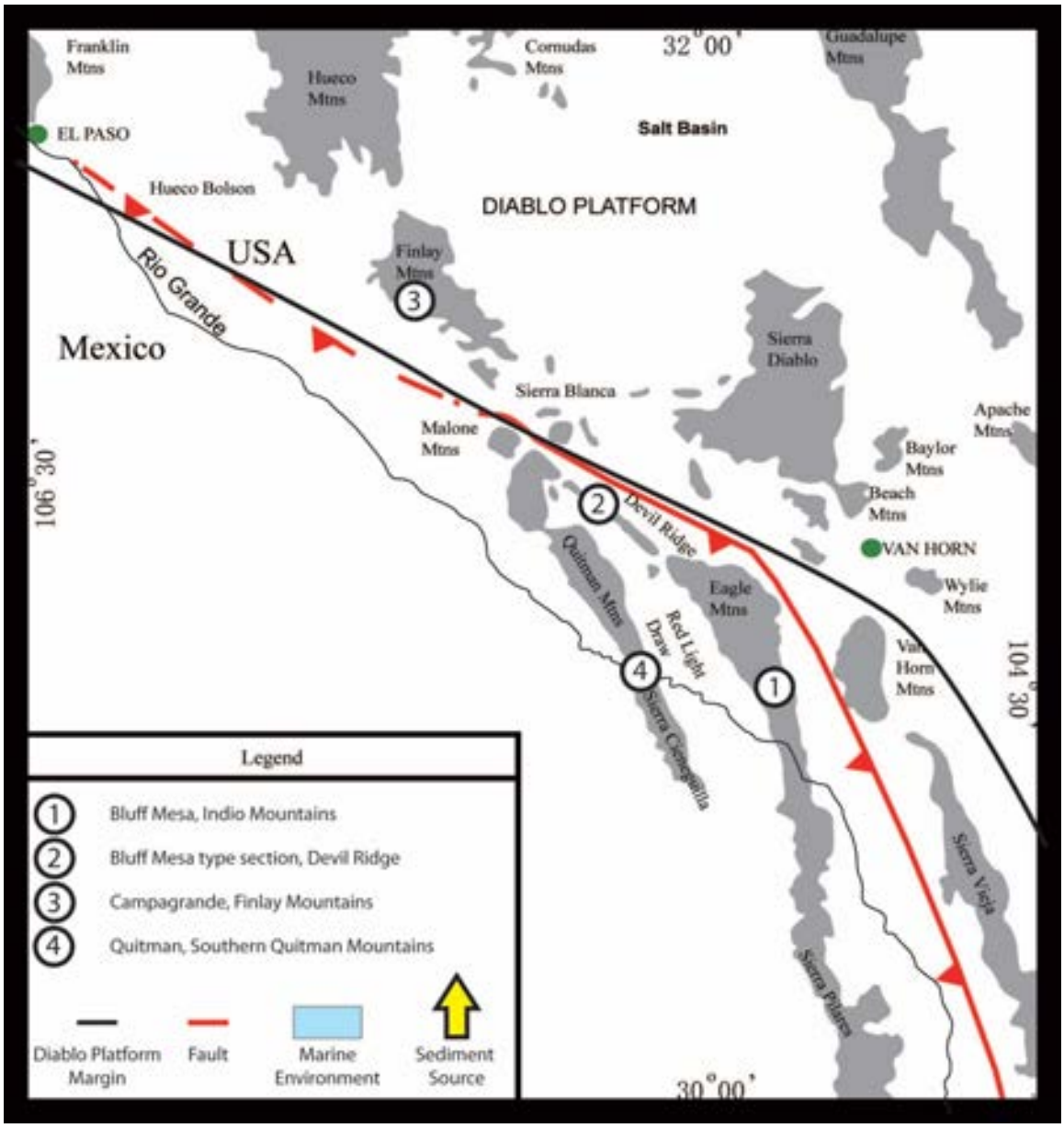

Figure 6.2: Map of regional mountain belts with type section locations.
Regional mountain belts of the northeastern Chihuahua Trough and locations of formational type sections correlated to the Bluff Mesa of the Indio Mountains (1) Locations of the Bluff Mesa type section at Devils Ridge (2) and the Campagrande type section in the Finlay Mountains (3) are taken from Albritton and Smith (1965), while the Quitman Formation of the Southern Quitman Mountains/Sierra Cieneguilla (4) is taken from Reaser (1974). Diablo Platform margin is inferred from (Dickinson and Lawton 2001B) Haenggi (2002) and Mauel et al. (2011). Map and structural elements are adapted from Rohrbaugh (2001), Page (2011), and Li (2014).

6.2.1 Syn-Depositional Faulting and Paleotopography

Li (2014) documented significant evidence for syn-depositional faulting during deposition of the Upper Yucca Formation within the study area. This study finds evidence for syn-depositional faulting and the presence of a local paleotopographic high in the overlying Bluff Mesa Formation centered on the Echo Canyon horst block identified by Li (2014) (Figure 4.1). Li (2014) cited the presence of a stromatolitic boundstone on the Echo Canyon horst block and its absence in adjacent grabens as evidence for a paleotopographic high. Evidence for syn-depositional faulting and the presence of a paleotopographic high during deposition of the Bluff Mesa Formation is documented in the form of thickness changes in siliciclastic intervals and differing facies distributions, which are primarily confined to Sequences #1 and #2 (Figure 5.4; Figure 5.6B and C).

The fluvial interval of LST-1 on the horst block (measured section EH) is significantly thicker than in measured sections EI and EC, which supposedly record deposition in adjacent grabens (Figure 5.4). This thickness change is contradictory to the idea of deposition on a horst block where siliciclastic deposits are expected to thin. Fluvial channel density on the horst block decreases upward until a well-defined channel belt is exposed 6.5 meters below the transition to lacustrine deposition. This belt is 2.5-3 meters thick and contains scattered conglomeratic lags (Fc), possibly representing the true base of Sequence #1 on the horst block. In this scenario, the lacustrine facies that typically underlie Sequence #1 were either not deposited on the horst due to low lake levels or were extremely thin and consequently eroded during the following drop in base level. If the base of this channel belt is treated as a sequence boundary then the fluvial interval decreases to 6.5 meters. This would match the expected trend of thinning fluvial facies over the topographic high associated with the horst block.

The presence of a fluvial tongue that thins over the Echo Canyon horst block and thickens in the adjacent grabens, indicates faults bounding the Echo Canyon horst block were also active during LST-2. The fluvial tongue pinches out to the north separating two distinct lacustrine intervals, which remain distinguishable across the entire stratal panel. This suggests that deposition of the tongue likely coincided with a change in lake depth or chemistry controlled by higher order climate-driven cycles documented by Li (2014). LST-2 thickens onto the horst block but this is primarily attributed to thickening of the basal fluvial belt (Figure 5.4). The bounding faults may have been inactive during this time, resulting in a lack of topography, allowing for deposition of the thick fluvial interval. However, the fluvial tongue within the overlying lacustrine interval thins over the horst block before thickening again in the adjacent graben to the north, indicating reactivation of syn-depositional faults bounding the horst block.

Faults bounding the Echo Canyon horst block remained active at least until base-level rise associated with TST-2, which is recorded as a wedge across most of the stratal panel (Figure 4.2). TST-2 is absent on the horst block but is recorded in the adjacent graben to the south (measured section EC) as a thin sandy marine wackestone between the upper fluvial interval of LST-2 and thick ooid grainstones of HST-2 (Figure 5.4; Figure 5.6B and C). This is important as the graben to the south is interpreted to have been located in a marginward position in relation to the horst block. This indicates that for a brief period of time the Echo Canyon horst block may have been a subaerially exposed island while the adjacent grabens were submerged.

Changes between facies on the Echo Canyon horst block and in adjacent grabens are minimal in the upper Bluff Mesa Formation. An excellent exposure of HST-4 appears identical in facies distribution and thickness across one the horst block bounding faults, indicating any differential paleotopography had been filled by this time. The lack of evidence for syn-

depositional faulting in the upper Bluff Mesa suggests that tectonism was waning through time with eustasy becoming an increasingly important control on depositional patterns. This trend is supported by the strong evidence for syn-depositional faulting in the Upper Yucca Formation (Li, 2014) with major facies differences between horsts and grabens, followed by comparatively less extreme differences documented in the lower Bluff Mesa Formation.

6.2.2 Paleoshoreline and Sediment Dispersal

Four lines of evidence indicate that the Cretaceous paleoshoreline lay to the southeast of the study area are found in the lower marine intervals of the Bluff Mesa Formation (Figure 4.2): 1) northward progradation of shallow marine Cg and Cf barforms in HST-1 and HST-2; 2) northward thickening of both HST-2 and the TST-2 into the basin; 3) presence of continuous Ss intervals confined to the southern half of the panel in HST-2, and 4) increased prevalence of Cg to Cf near Echo Canyon in HST-2.

The northward thickening trend observed in TST-2 and HST-2 is interrupted during deposition of TST-3, which thickens at the stratal panel center (Figure 4.2). Thickening of the package in the stratal panel center in close proximity to the uniquely large erosive basal channels of SB-3 suggest that although the primary siliciclastic point source was located south or east of the study area, the nature of available accommodation had changed. Previous evidence for the panel being oriented close to perpendicular to the paleoshoreline is strong (TST wedge orientation, northward prograding barforms, Cg to Cf ratios, and southern prevalence of continuous Ss deposits in HST-2). However, deposition of those facies may have been overprinted by rapid accommodation generation to the northwest during transgression and the antecedent topography of the basin (i.e. lower available accommodation in the south due to southward thickening of fluvio-lacustrine cycles). Under this scenario, the thick interval of

carbonates deposited during HST-2 filled in most of this antecedent topography, allowing for a straightforward expression of the siliciclastic fairway during TST-3. This preferential siliciclastic fairway was likely still present during TST-4 where another set of prominent channels with decreasing erosive power are confined to the same lateral zone. Utilizing lateral facies changes from fluvial to tidally influenced coastal deposits, Budhathoki (2013) interpreted a siliciclastic point source in the overlying Cox Sandstone approximately 1 kilometer southeast of the channelized zone in the Bluff Mesa Formation. This supports the idea of a siliciclastic point source near Echo Canyon during Bluff Mesa deposition.

The northward thickening trend is partially restored during TST-4 before being fully restored during deposition of TST-5. HST-3 and HST-4 are uniformly thin across the stratal panel but HST-5 thickens slightly to the south. This could be of interest regarding water depth interpretation as the only marine nodules exposed in outcrop were found at measured section EI, which also coincides with the thickest section of HST-5. This may indicate that the comparatively large increase in base-level associated with Sequence #5 resulted in siliciclastic sediment starvation during the early stages of HST-5, which waned as shallower carbonates prograded over the study area. This is supported by the southward thickening of Mss interval of HST-5, which contrasts with the relatively uniform thickness of the overlying Cf parasequences. Interestingly, transgressive systems tracts of the overlying Cox Sandstone consistently thicken southward (Budhathoki, 2013). Budhathoki (2013) interpreted this trend of southward thickening to be indicative of tectonism, which preferentially generated more accommodation space to the south through fault block rotation. This suggests that because southward thickening of marine facies is only observed in the Mss interval, the large rise in base level preceding its deposition

might have been caused by tectonism rather than eustasy. However, this is fairly speculative, as the underlying TST thickens drastically to the north.

6.3 REGIONAL CORRELATIONS

In order to improve our current understanding of Lower Cretaceous transgression of the Chihuahua Trough northeast margin, the Bluff Mesa Formation in the Indio Mountains is correlated to three time-equivalent formations of West Texas (Figure 6.2). Measured section M was selected for correlation in figures 6.3-6.5, as it is located in the stratal panel center and is expected to be more representative of the study area than measured sections near Squaw (over represents basinward deposition) and Echo (over represents landward deposition) canyons. Measured section M is correlated to the Bluff Mesa type section at Devils Ridge (Albritton and Smith, 1965), the Campagrande Formation in the Finlay Mountains (Albritton and Smith, 1965), and the Quitman Formation in Mayfield Canyon of the Southern Quitman Mountains/Sierra Cieneguilla (Reaser, 1974).

6.3.1 Correlations with the Bluff Mesa Type Section, Devil's Ridge

The Bluff Mesa type section measured by Albritton and Smith (1965) is located on Bluff Mesa in the northwest Devil's Ridge area (Figure 6.2). Located approximately 55 kilometers northwest of the Indio Mountains, one might expect more drastic changes between facies distributions and cycle thickness than are observed locally within the study area. The Bluff Mesa at Devil's Ridge is 440 meters of predominantly sandy limestone. This fits the previously observed pattern of northwest thickening in marine strata as the thickest Bluff Mesa interval measured in the Indio Mountains is 343.2 meters. As previously established in chapter five, the shoreline is located to the southeast of the study area. This suggests the Bluff Mesa at Devil's Ridge should contain facies indicative of a more basinward environment. At first glance this

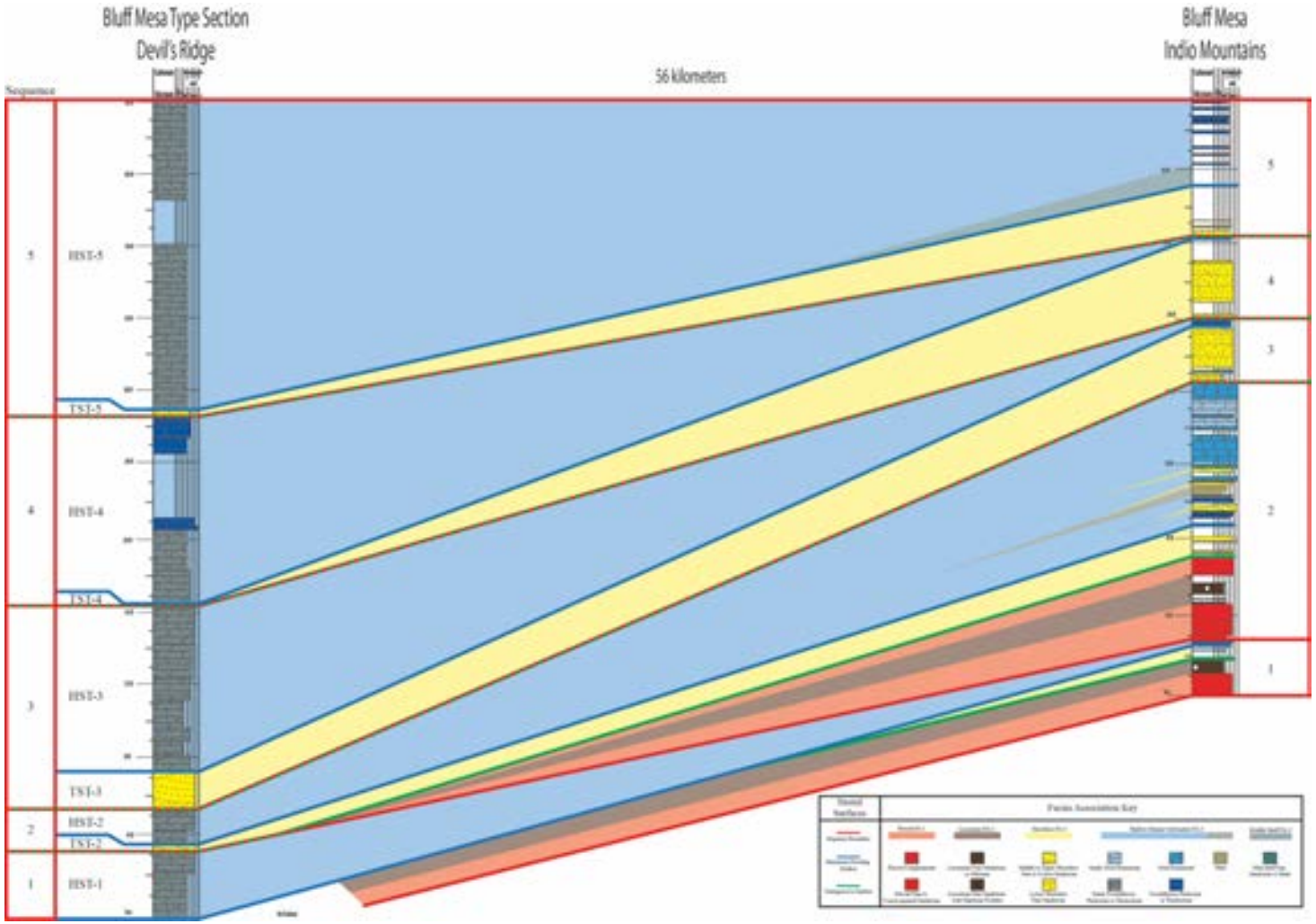

Figure 6.3: Correlation with the Bluff Mesa type section.
Stratigraphic correlation between the Bluff Mesa Formation type section in the Finlay Mountains and the Bluff Mesa Formation in the Indio Mountains. Type section recreated from Albritton and Smith (1965).

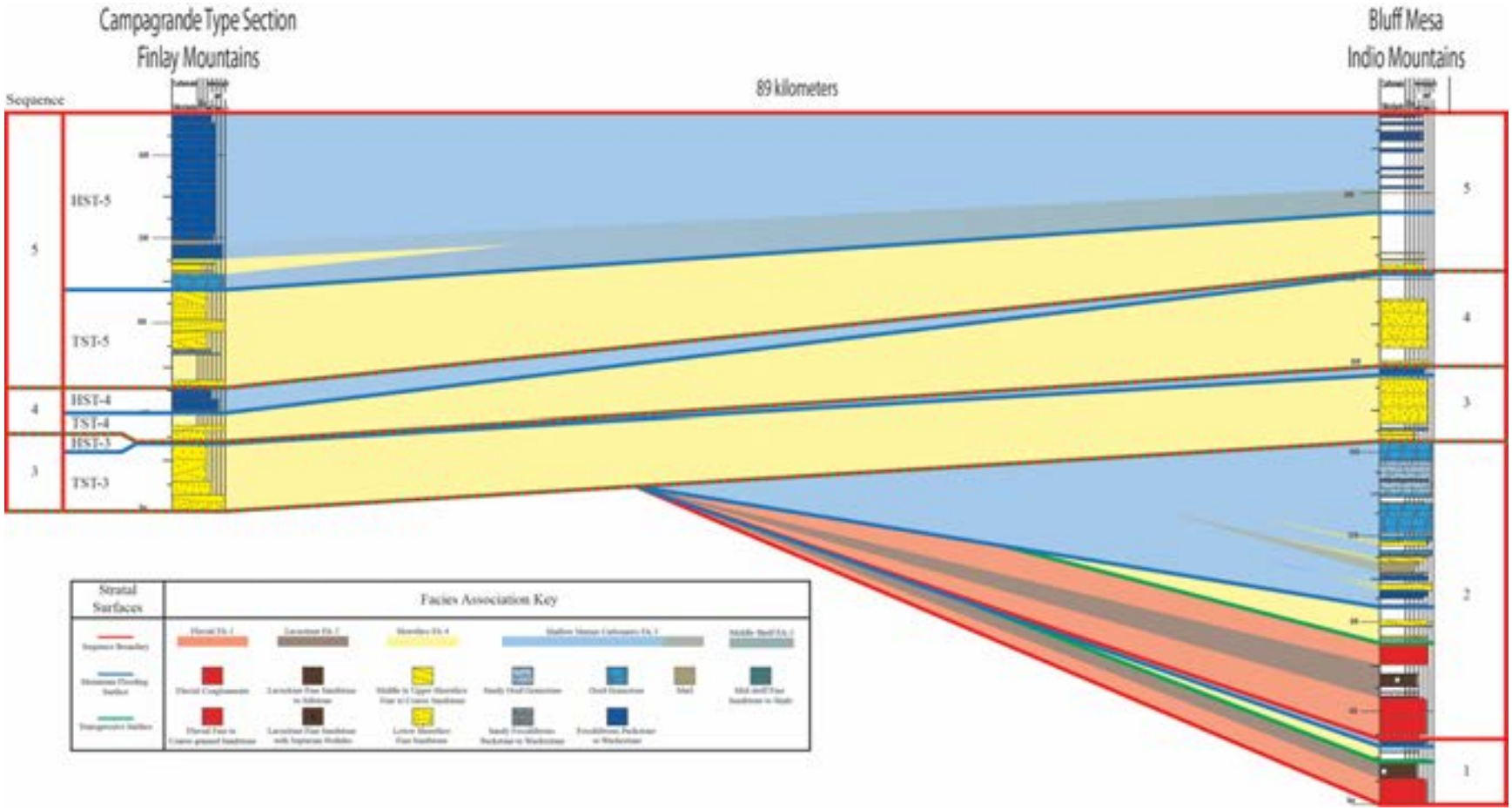

Figure 6.4: Correlation with the Campagrande Formation.
Stratigraphic correlation between the Campagrande Formation type section in the Finlay Mountains and the Bluff Mesa Formation in the Indio Mountains. Type section recreated from Albritton and Smith (1965).

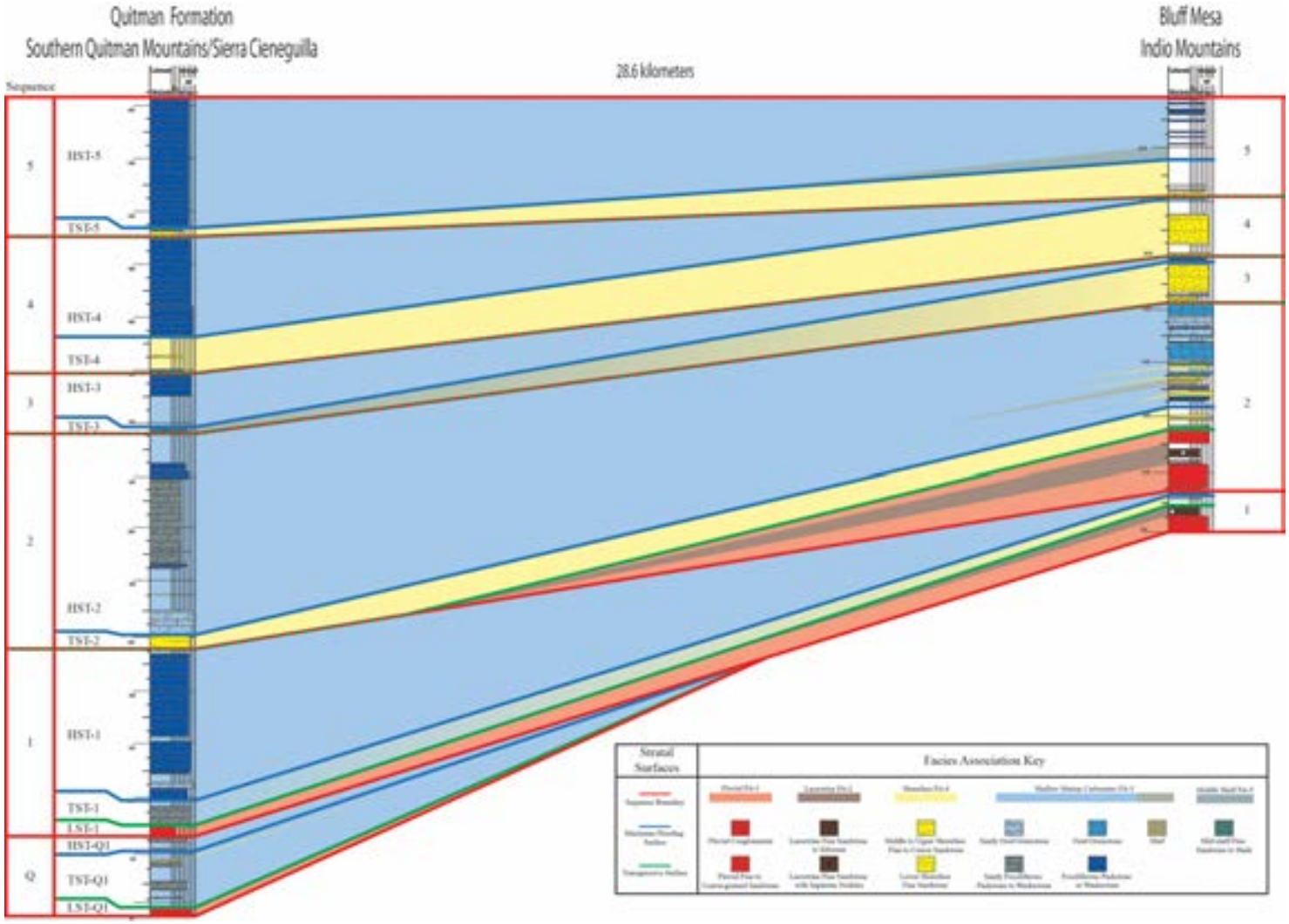

Figure 6.5: Correlation with the Quitman Formation.
Stratigraphic correlation between the Quitman Formation type section in the Southern Quitman Mountains and the Bluff Mesa Formation in Indio Mountains. Type section recreated from Reaser (1974).

appears to be true as clastic intervals are significantly thinner in the type section compared to those observed in the Indio Mountains. However, nearly all of the limestones in the type section are notably sandy, whereas less than 50% of limestones in the Indio Mountains were described as sandy. This is puzzling as sandy limestones (Cs) in this study were interpreted as deposition in either a proximal or lateral position with regards to cleaner limestones. This may be explained by 1) different classification criteria resulting in Albritton and Smith (1965) using a lower siliciclastic percentage cutoff in terming limestones as sandy, or 2) the Bluff Mesa at Devil's Ridge was not deposited in a purely basinward position. Devil's Ridge is located near a slight bend in the paleomargin of the Diablo Platform (Figure 6.2). Although sediment was likely being delivered from the southeast in the Indio Mountains, the Devil's Ridge area was likely receiving siliciclastic sediment from the Diablo Platform to the northeast. If siliciclastic sediment was being delivered from a different source, then the southeast-northwest margin to basin facies patterns between the Indio Mountains and Devil's Ridge would be overprinted.

Albritton and Smith (1965) did not provide any documentation of strata below the base of the Bluff Mesa Formation at the type section, but they did state that the Bluff Mesa conformably overlies the Yucca Formation there. As LST-1 is technically assigned to the Upper Yucca Formation it cannot be accounted for at the type section. Sequence #1 at Devils Ridge is composed of 32 meters of sandy limestone with abundant oysters in the upper 11 meters (Figure 6.3). These limestones are assigned here to HST-1, which is significantly thicker than HST-1 in the Indio Mountains (0.5-3.7 meters). Albritton and Smith (1965) do not use Folk (1959) or Dunham (1962) classifications and therefore it is extremely difficult to utilize grain percentages to differentiate between limestone facies. Fossiliferous vs non-fossiliferous intervals allow for some speculation but due to the lack of data this study rarely differentiates between grainstones

and wackestones in the type section. This makes it fairly difficult to notice subtle changes in lithology that often helped parse transgressive systems tracts from highstand systems tracts at the maximum flooding surface in the Indio Mountains, resulting in most limestone intervals being placed in highstand systems tracts.

The base of sequence #2 is marked by a 3.3m thick coarse-grained sandstone that constitutes the TST-2. LST-2 and TST-2 are both significantly thicker in the Indio Mountains as the drop in base-level isolated the basin, resulting in fluvio-lacustrine deposition. Although it is difficult to say that TST-2 at the type section was deposited in a marine setting, the overlying lacustrine shales that typically follow fluvial deposition in the Indio Mountains are notably absent. Therefore, it is likely that the paleoshoreline did not retreat beyond Devil's Ridge during LST-2 and deposition occurred in the shoreface environment at the type section. HST-2 only measures 18.9 meters thick, this is suspiciously thin when compared to the 79.5 meter average in the Indio Mountains. This could be explained by antecedent topography and siliciclastic sediment input rate in the Devil's Ridge area that that prevented the establishment of a prolific carbonate factory following a relatively quick transgression. Ooid grainstones (Cg) indicative of shallow water deposition are abundant in HST-2 of the Indio Mountains but apparently absent in HST-2 at the type section. This would support the idea that Devils Ridge was in a more basinward position than the Indio Mountains but all the limestones at the type section are considered sandy, possibly suggesting delivery of siliciclastic sediment from the Diablo Platform.

Sequence #3 represents the most significant drop in base-level during purely marine deposition of the Bluff Mesa. This is reflected in the relatively thick (19.5 meters) TST-3 at the type section. Sequence #3 at Devil's Ridge is extremely different than in the Indio Mountains

and is characterized by 90.5 meters of sandy limestone assigned to HST-3. This contrasts starkly with HST-3 that averages only 5 meters in the Indio Mountains. This difference may be explained by a relatively slow transgression that resulted in longer periods of carbonate production in more basinal areas such as Devil's Ridge with transgression occurring slightly later in the Indio Mountains.

Sequence #4 is composed of a mix of sandy and clean limestones in the Devil's Ridge Area. The base of Sequence #4 in the type section is marked by a 0.7 m thick sandstone containing abundant shell fragments assigned to TST-4. The relative smaller thickness of TST-4 compared to LST-3 supports the idea that base-level fall during TST-3 was more extreme. This idea is also supported by the level of erosion recorded in the Indio Mountains where SB-3 cuts over 5 meters down into the underlying highstand but erosion associated with SB-4 does not exceed 1 meter. Sequence #4 is unique at Devil's Ridge in that it is the only sequence where clean limestones are found. A very interesting "black limestone" is located near the top of HST-4. Not much information is given but it may be related to the excellent marker beds that constitute HST-4 in the Indio Mountains as they are also unique and easily traceable across the stratal panel. Changes in the thickness of HST-4 between Devil's Ridge and the Indio Mountains mirror those in HST-3 and suggests that transgression during Sequence #4 in the Devil's Ridge area predates transgression in the Indio Mountains.

The base of Sequence #5 at the type section is marked by 4.3 meters of fine-grained quartz arenite assigned to TST-5. Sequence #5 is associated with overall deepening in the Indio Mountains with deposition of more basinal facies (FA-5) and a relatively non-erosive change to siliciclastic deposition marking SB-5. The relatively "gentle" SB-5 is also expressed at the type section where TST-5 is the only transgressive systems tract composed of fine-grained sandstone

rather than coarse-grained sandstone or conglomerate. HST-5 is composed of 171 meters of thin-bedded sandy limestone that appears to be fairly unfossiliferous. There is no mention of interbedded marls or coarsening up parasequences but the relative thickness increase compared to HST-3 and 4 is mirrored in the Indio Mountains.

The Bluff Mesa type section at Devil's Ridge is correlative to the Bluff Mesa documented in the Indio Mountains (Figure 6.3). Large differences in thicknesses of transgressive systems tracts indicate trapping of siliciclastic sediment in more proximal areas (Indio Mountains) and siliciclastic starvation in more basinal areas (Devil's Ridge). Clear differences in facies distributions help identify the magnitude of base-level changes (i.e. lack of fluvio-lacustrine strata in LST-2 indicates sea-level drop at SB-2 isolated the Indio Mountains area, which returned to a terrestrial environment, but the Devil's Ridge area remained under marine conditions (Figure 6.6B). Other differences in facies distributions, such as the abundance of sandy limestones in the Devils Ridge area, may represent measurable differences in sediment sources or may simply be an artifact of different classification parameters.

6.3.2 Correlations with the Campagrande Formation, Finlay Mountains

The Campagrande Formation was first formally described by Richardson (1904) as a 114m thick succession in the Finlay Mountains near Campo Grande Arroyo (Figure 6.2). The Campagrande Formation is defined as lithologically heterogeneous and includes all Cretaceous deposits older than the Cox Sandstone on the Diablo Platform. The base of the Campagrande is represented by an unconformity and sequence boundary that cuts into the underlying Permian shelf carbonates of the Diablo Platform. The Bluff Mesa Formation sits conformably on fluvio-lacustrine strata of the Upper Yucca Formation, making differentiation from the Campagrande Formation fairly simple where the base is exposed. The Campagrande Formation is equivalent to

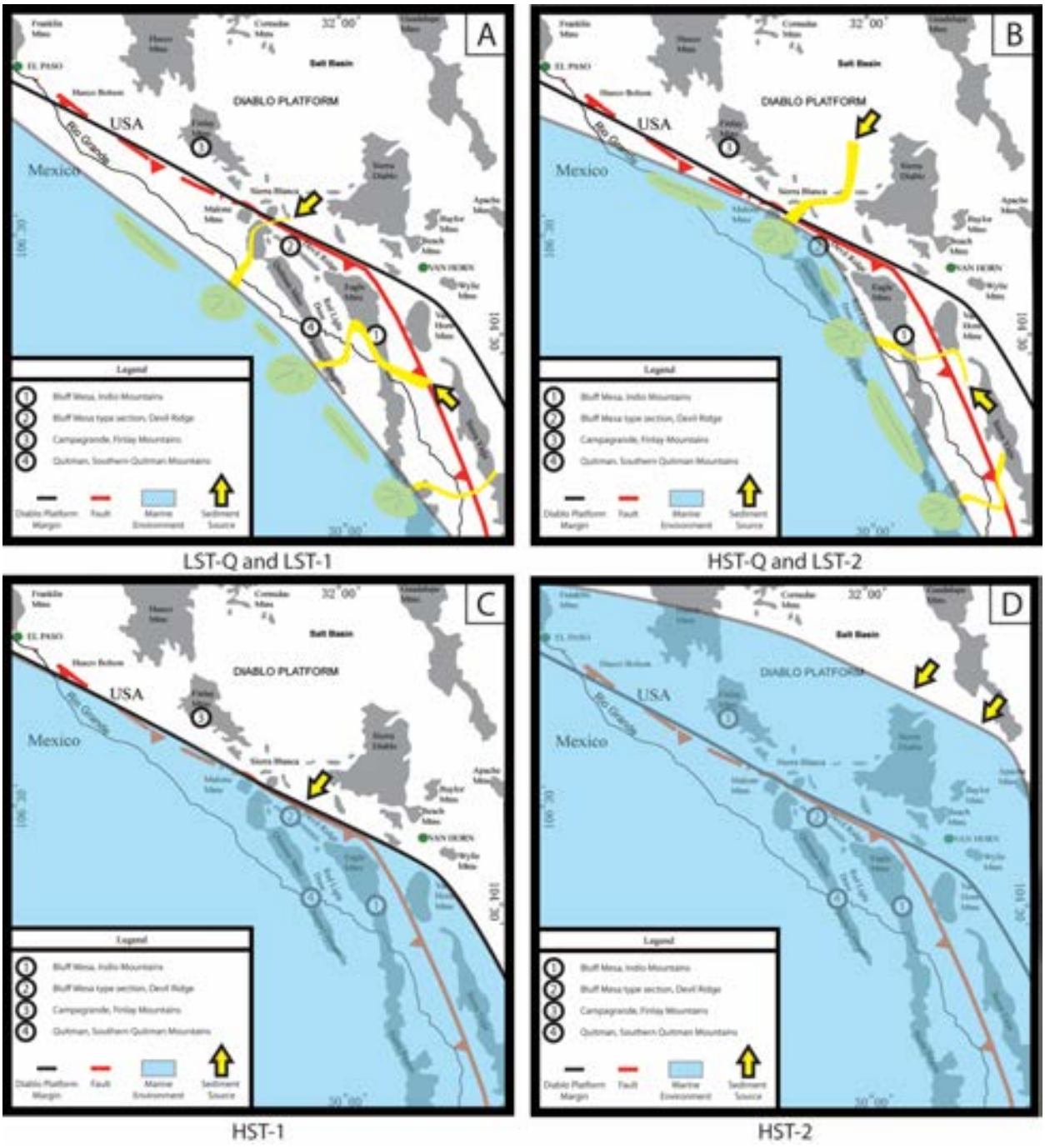

Figure 6.6: Inferred shoreline trends and paleogeographic setting during deposition of various sequence tracts.

(A) LST-Q and LST-1 reconstruction; (B) HST-Q and LST-2 reconstruction; HST-1 reconstruction; (D) HST-2 reconstruction. Diablo Platform margin is inferred from Dickinson and Lawton (2001B), Haenggi (2002), and Mauel et al. (2011). Map and structural elements adapted from Rohrbaugh (2001), Page (2011), and Li (2014).

part of the Bluff Mesa Formation, however there have been no published attempts to correlate distinct surfaces. The type section was recorded in the Finlay Mountains by Albritton and Smith (1965) and is reconstructed in Figure 6.4. Albritton and Smith (1965) noted that the nature of the Campagrande is variable and is more siliciclastic-rich in the Finlay Mountains than in other measured sections to the east near Sierra Prieta. They include a section that is more carbonate-rich but it is incomplete and for this study only the type section is used for correlating surfaces.

If the Campagrande Formation represents Bluff Mesa equivalent deposits on the Diablo Platform one might expect major differences in thickness (total and individual cycles) and facies. The type section recorded by Albritton and Smith (1965) is 180.1 meters thick (Figure 6.4). This is thinner than all complete sections of the Bluff Mesa Formation including Underwood's (1962) original measurement in the Indio Mountains (242 meters), the thinnest section measured in this study (219 meters), and Albritton and Smith's (1965) type section (440 meters). Therefore, the Campagrande Formation must contain either condensed cycles or eroded section. The unconformity at the base of the Campagrande Formation suggests that loss of strata due to erosion on the Diablo Platform likely accounts for the difference in thickness to the Bluff Mesa Formation.

Interpretation of sequence boundaries from the descriptions provided by Albritton and Smith (1965) allows for delineation of distinct cycles, which can be compared to those in the Bluff Mesa Formation (Figure 6.4). The best match for the sequence boundary at the base of the Campagrande Formation within the Indio Mountains is SB-3. Conglomerates within channel fills are observed near measured section EI and the drop in base level is recorded across the entire study area. Conglomerates at the base of the Campagrande are much thicker but this is to be expected as the sediment source is more proximal on the Diablo Platform. If the base of the

Campagrande is interpreted as SB-3, the measured thickness of 180.1 meters is similar to sequences 3-5 of the Bluff Mesa in the Indio Mountains (114.5-174.9 meters). The fact that the Campagrande Formation is slightly thicker than sequences 3-5 of the Bluff Mesa Formation can be explained by shoreface sand sediment trapping that occurred on the shallow platform. Sequence #3 in The Campagrande Formation is 28 meters thick with approximately 27 meters assigned to TST-3. This is similar in thickness to measured sections M and EI, which are located closest to the erosional channel network at SB-3. The most likely scenario is that a minor transgression of the Diablo Platform occurred during TST-2, resulting in thinner deposits than were recorded in the Indio Mountains. Consequently, base-level fall associated with SB-3 exposed these deposits to more intense erosion than their counterparts in the Indio Mountains, resulting in complete loss of any HST-2 deposits and a sequence boundary that cut down into the underlying Permian carbonates on the Diablo Platform.

Sequence #4 in the Campagrande Formation is 22.9 meters with 11.3 meters assigned to the siliciclastic TST-4. This is thinner than Sequence #4 in the Indio Mountains, which ranges from 33.1 to 68.6 meters. Sequence #4 in the Campagrande also differs from Sequence #4 in the Indio Mountains in that TST-4 and HST-4 are of similar thicknesses, whereas TST-4 is an order of magnitude thicker than HST-4 in the Indio Mountains. Two thin limestones are observed higher in the Campagrande section and could represent the true HST-4. However, this interpretation would only make Campagrande Sequence #4 more similar to Sequence #4 in the Indio Mountains in overall thickness but would cause HST-4 to balloon to 29.8 meters thick, more than twice as thick as TST-4. Additionally, this would assign a notable clastic flux including a conglomerate deposit to HST-4, which violates the previously discussed stratigraphic rules in this study. In order to maintain consistency, this clastic flux is instead assigned to TST-5.

The carbonate succession of HST-4 appears nearly identical across the study area when exposed and represents an excellent marker. It is difficult to tell how similar the carbonates of Campagrande HST-4 are to these beds from the descriptions given by Albritton and Smith (1965). They describe three well-exposed nodular limestones that match the HST-4 carbonates of the Indio Mountains more closely than any other facies described in the Campagrande type section. Although Campagrande HST-4 is thicker (11.6 meters) than in the Indio Mountains (6.4 meters) this can easily be explained by shallower water on the Diablo Platform that allowed for increased carbonate production in the photic zone.

Sequence #5 in the Campagrande is 129.2 meters thick with 48.2 meters assigned to TST-5 and 92.7 meters to HST-5. Sequence #5 in the Campagrande is slightly thicker than Sequence #5 in the Indio Mountains but shares many of same characteristics. TST-5 in the Indio Mountains is marked by a change from shoreface sandstones (FA-3) to mid-shelf shales (FA-5). This exact succession of facies is not observed in the Campagrande, however the change from siliciclastic deposition to ooid grainstone clearly signifies marine transgression. A thick succession of interbedded limestone and marl parasequences overly the ooid grainstone. Although a distinct olive color is not mentioned, these parasequences are occasionally fossiliferous and seem extremely similar to the lower Mss interval of HST-5 in the Indio Mountains. The fossiliferous description and relationship with interbedded marls suggest they were deposited basinward from the ooid grainstone, justifying the placement of mfs-5 at the base of the first parasequence. Albritton and Smith (1965) describe the top of the Campagrande as a 3.6 meter, moderately fossiliferous limestone with hematite cubes. Although little iron-staining was observed in the uppermost Bluff Mesa bed on the southern thrust panel, Budhathoki (2013) reported the presence

of iron nodules. This suggests that the top bed of the Campagrande is stratigraphically related to the top bed of the Bluff Mesa in the Indio Mountains.

The Campagrande Formation likely represents the equivalent of Bluff Mesa sequences 3-5 deposited in a shallower environment on the Diablo Platform. Missing sequences 1-2 on the platform can be explained through two different scenarios; 1) transgressions associated with Sequence #1 and #2 were smaller-scale than Sequence #3 and the Diablo Platform was not flooded until TST-3 (Figure 6.6C) or 2) transgression occurred during Sequence #1 and/or #2 but all deposits were eroded during the base-level drop associated with SB-3. Evidence for scenario #2 could be generated if any incomplete Campagrande sections appeared similar to the thick ooid grainstones of HST-2, suggesting some areas escaped erosion. Unfortunately, descriptions of these measured sections are predominantly carbonate but appear similar to HST-5 in both thicknesses and facies types.

6.3.3 Correlations with the Quitman Formation, Southern Quitman Mountains

The Quitman Formation was first described in depth by Adkins (1932) on the eastern side of Quitman Gap. Some authors, such as Huffington (1943) and Albritton and Smith (1965) suggested that the term Bluff or Bluff Mesa should be used to describe carbonate sequences in the Quitman Mountains of Aptian/Albian age. Jones (1968) instead favored the term Quitman Formation for strata exposed in the southern Quitman Mountains and gave a detailed description that divided it into three informal members. This terminology was followed by Reaser (1974), who also applied it to correlative strata in the Sierra Cieneguilla (southern extension of the Quitman Mountains into Mexico). A nearly complete measured section of approximately 600 meters of Quitman Formation is exposed in Mayfield Canyon, where it overlies the Mountain Formation, which is lithologically similar to the Yucca Formation (Reaser, 1974; Monreal and

Longoria, 1999) (Figure 6.5). The Quitman Formation is up to 150 meters thicker than the Bluff Mesa in the Indio Mountains and appears to contain less siliciclastics by volume.

The lower member of the Quitman Formation shares broad characteristics with sequences #1 and #2 of the Bluff Mesa Formation in the Indio Mountains. The base appears somewhat gradational with the underlying Mountain Formation, which may contain early transgressive deposits similar to the Upper Yucca Formation. Approximately 55 meters of sandy marine limestones and poorly exposed sandstones sit above the first sandy limestone assigned to the Quitman Formation. None of these deposits were assigned to fluvio-lacustrine environments by Reaser (1974) but the succession does contain a 7.6 meter covered interval with abundant black silicified wood, which may have been deposited in the fluvial overbank environment similar to Fsl of FA-1. This interval is overlain by 111.9 meters of much cleaner weathering-resistant limestones with interbedded sandstones. This succession of initial marine transgression, followed by a decrease in base-level that returned the basin to a terrestrial environment, and finally marine inundation marked by a thick interval of clean marine carbonates appears strikingly similar to exposures in the Indio Mountains (sequences 1-2). Unlike the Bluff Mesa Formation, the Quitman Formation is interpreted to contain an extra sequence (Figure 6.5, sequence Q) that was deposited during an initial marine transgression that did not inundate the Indio Mountains area. Therefore, the base cycle in the Quitman Mountains is termed Sequence #Q and is time equivalent with Upper Yucca strata in the Indio Mountains. This study reinterprets the aforementioned silicified wood interval as a fluvial deposit, indicating the presence of a LST and sequence boundary. This fluvial succession and the overlying marine carbonates appear superficially similar to Sequence#2 of the Bluff Mesa, but are actually equivalent to Sequence #1. Rising base-level inundated both the Quitman and Indio mountains areas, but higher levels of

accommodation in the Quitman Mountains allowed for deposition of a significantly thicker carbonate sequence. The following decrease in base-level isolated the Indio Mountains area, which returned to a fluvio-lacustrine environment, but sea-level did not migrate southwest of the Quitman Mountains area (Figure 6.6B). This resulted in deposition of the thickest marine siliciclastic interval in the Quitman Formation, which is assigned to TST-2. The superficial similarity between the nature of early transgression in the Quitman Mountains and the Indio Mountains further supports the idea that the basins had similar tectonic regimes and sediment source areas.

The bulk of the Middle Quitman Member is assigned to HST-2 with SB-3 placed below a 3.7m thick siltstone. Reaser (1974) notes that the siltstone weathers light olive gray, possibly resembling fine-grained sandstones of the mid-shelf (FA-5). SB-3 is associated with the largest magnitude drop in base-level after marine inundation in the Bluff Mesa Formation. Assuming that the Quitman Formation records deposition in a basinward position of the Indio Mountains, transgressive systems tracts and lowstands should be thinner and contain more basinal facies. Both of these conditions are satisfied as fine-grained, olive-colored siliciclastics (FA-5) of TST-3 (3.7 meters) in the Quitman Mountains are interpreted to have been deposited basinward of channelized marine siliciclastics (FA-3) of TST-3 (6-30.6m) in the Indio Mountains. Sediment trapping in the shallower water environment near the Indio Mountains likely controlled the drastic change in thinning of TST-3 towards the Quitman Mountains.

The upper 27.4 meters of the Middle Quitman Member are composed of two thin sandstone outcrops overlain by a poorly exposed sandy limestone assigned to TST-4. These deposits are overlain by the 73.2 meters of interbedded fossiliferous limestones and ooid grainstones of HST-4 that represent the well-exposed based of the Upper Quitman Member.

Similar to Sequence #3, Sequence #4 in the Quitman Formation differs from the corresponding sequence in the Indio Mountains in that TST-4 is thinner (27.4 vs 29.8-62 meters) while HST-4 is much thicker (73.2 vs 1.4-6.6 meters). This is to be expected as deposition in the Quitman Mountains occurred in a more basinward position resulting in thinner siliciclastic intervals and thicker carbonate deposits.

TST-5 is marked by 5.8 meters of shale and fine-grained sandstone that conformably overly limestones of HST-4. The designation of SB-5 in the Bluff Mesa of the Indio Mountains is based on the continuous nature of the siliciclastic interval across the southern thrust panel, rather than an erosive siliciclastic-carbonate contact. No mention is made of the lateral continuity of this interval in Reaser's (1974) measured section other than referring to it as a "marker-bed". If SB-5 was not erosive in the more landward location (Indio Mountains), then it is not surprising that it is conformable in the Quitman Mountains as well. Additionally, the sandstone is described as "light olive gray" in color, similar to the mid-shelf sandstones (FA-5) that are assigned to the base of HST-5 in the Indio Mountains. This siliciclastic interval is overlain by 99.1 meters of *Orbitolina* limestone assigned to HST-5. The overlying contact with the Cox Sandstone is not exposed due to complicated faulting, but the missing section is estimated to be less than 20 meters (Reaser, 1974).

The Quitman Formation is largely correlative to the Bluff Mesa Formation with some notable differences in facies distributions and sequence thicknesses. Lowstand and transgressive systems tract siliciclastics are thinner and finer than their Bluff Mesa counterparts in the Indio Mountains, while highstands are generally thicker. Sequences recorded in the Quitman Formation are typically thicker than those in the Bluff Mesa Formation with the entire section measuring slightly over 600 meters in thickness. The Quitman Formation contains an additional

sequence, which is absent in the Upper Yucca and Bluff Mesa formations, indicating the presence of an early transgression that did not inundate the Upper Yucca rift lake in the Indio Mountains area. Despite the presence of an additional sequence, facies descriptions and vertical distributions of the Bluff Mesa Formation in the Indio Mountains more closely resemble those of the Quitman Formation than those of the Bluff Mesa type section. This could be a function of evolved descriptors used by Reaser in 1974 vs the language used by Albritton and Smith (1965). However, these similarities could also be attributed to differing siliciclastic source areas. Proximity of the Bluff Mesa type section to the Diablo Platform suggests sediment delivery from the northeast may have overprinted facies distributions observed in the Indio Mountains. Although the Quitman Formation was certainly located in a basinward position from the Bluff Mesa of the Indio Mountains, it seems likely that sediment input was from a similar southeastern source.

6.4 APPLICATIONS AS AN ANALOG

The primary goal of this study is to provide insight into the nature of transgression over rift lake geomorphologies that can be applied to understanding trap seal characteristics of pre-salt reservoirs of the South Atlantic. Utilization of the Bluff Mesa Formation as an analog despite the lack of evaporites is discussed in sections 6.4.1 and 6.4.2. Regardless of the lack of evaporite deposits, distribution patterns of shallow marine carbonate facies of the Bluff Mesa Formation may help exploration geologists with facies prediction away from existing wells in pre-salt reservoirs (6.4.3). Finally, section 6.4.4 examines the implications of the observed stratigraphic architecture on the Martins-Neto and Catuneanu's rift model (2010) and conditions for estuary development in transgression of rift systems.

6.4.1 The Evaporite Problem

As previously discussed, the syn-post rift stratigraphy exposed in the Indio Mountains does not contain evaporites, somewhat limiting its value as an outcrop analog for the pre-salt petroleum systems of the south Atlantic. The study area was likely located too far from the keel of the Chihuahua Trough for evaporite deposition to have occurred, as these deposits are primarily confined to the trough center (Figure 2.3; Haenggi, 2002). Had the basin physiography been conducive to post-transgression isolation, evaporite precipitation likely would have occurred during LST-2, when the basin was hypothetically isolated following base-level fall recorded by SB-2. If the basin had been isolated and charged with marine water post-transgression, we would expect deposition of evaporites, possibly interbedded with lacustrine or marine sandstone, directly above SB-2. The presence of a thick fluvial channel belt at the base of LST-2 suggests that the basin was not isolated as rivers transported sediment to downdip topographic lows. Fox (2016) documented deltaic complexes that prograded northward into a rift lake of the Upper Yucca Formation just north of Squaw Canyon. This suggests that lake level likely retreated northward following the base-level drop associated with SB-2, while deposition in the study area was the product of an axial fluvial system that was delivering siliciclastic sediment northward towards a topographic low. It is difficult to discern from outcrops in the study area whether the rift lake completely evaporated or the shoreline simply retreated north. If the base-level of the rift lake was lowered and its areal coverage decreased, the lower fluvial interval of LST-2 might be replaced with layered evaporites to the north of the study area. However, no such occurrences have been documented in the Indio Mountains. Sulfate isotopes extracted from septarian nodules indicate that the lacustrine interval of LST-2 was influenced by marine waters, albeit not in the necessary capacity to trigger evaporite deposition.

Despite the lack of evaporites in the study area, the observed stratigraphic architecture can still be a useful analog for pre-salt reservoirs. Following marine transgression and establishment of a functional marine carbonate factory during HST-1, the basin returned to a rift lake environment during LST-2, indicating that the basin structure largely remained intact with favorable conditions for rift lake formation. These findings demonstrate that distinctly marine carbonates may be interbedded with fluvio-lacustrine deposits in the upper reservoir zone or with evaporites in the lower seal, specifically when transgressions were eustatic-driven so that the structures conducive to rift lake formation and basin isolation were preserved. This may also be true for cases where marine transgression was driven by tectonic subsidence, but fault block rotation associated with rift tectonism typically increases basin connectivity with the open ocean through subsidence (Ravnas and Steel, 1998).

6.4.2 South Atlantic Basins Lacking Evaporites

Documented stratigraphic architecture of the Bluff Mesa Formation may also prove useful as an outcrop analog for petroleum plays in the south Atlantic rift system that lack an evaporite seal. Early marine transgressive deposits over rift-generated structures may act as a seal for underlying syn-rift siliciclastic reservoirs, or as a source for younger reservoirs. An analysis of giant oil field discoveries in rift basins showed that 37-53% of seal components were marine carbonates or shale, while evaporites accounted for 40% (Mann et al., 2007; Schwarz, 2016). Staying within the south Atlantic domain, the Pelotas Basin of offshore Brazil and Uruguay represents an interesting frontier basin that is structurally related to extensional basins of Brazil and West Africa but lacks an evaporite seal (Beglinger et al., 2010; Conti et al., 2017). Conti, et al. (2017) identify six speculative petroleum systems within the Pelotas Basin fill ranging from Lower Permian pre-rift source rocks through Miocene post-rift turbidite

complexes. The Atlantida-Imbituba and the Atlantide-Imbe speculative petroleum systems contain Aptian-Albian transgressive marine source rocks that were likely deposited under anoxic conditions, suggesting they are analogous to shales of FA-5 in the upper Bluff Mesa Formation. The Atlantide-Imbe petroleum system is fairly straightforward with the reservoir and seal elements composed of overlying sandstones and shales. However, the Atlantida-Imbituba petroleum system invokes hydrocarbon migration to syn-rift reservoirs composed of eolian sandstones interbedded with volcaniclastics. This syn-rift stratigraphy differs greatly from the fluivo-lacustrine syn-rift deposits observed on much of the Chihuahua Trough margin, making the Indio Mountains a poor outcrop analog for the Atlantida-Imbituba speculative petroleum play.

One might expect that the Indio Mountains are likely a better analog match for basins that also lack evaporites due to increased distances from spreading centers, like the onshore Reconcavo, Tucano, and Jatoba basins of Brazil. Although some of these marginal rift basins have working petroleum systems, all components of the petroleum system are typically of syn-rift fluvio-lacustrine origins (Mello et al., 1994; Magnavita et al., 2012).

6.4.3 Marine vs Lacustrine Carbonates

Pre-salt carbonate reservoir facies in the south Atlantic typically fall under two categories; 1) microbialite (stromatolitic and/or thrombolitic boundstones) (Bahniuk et al., 2015; Wright and Tosca, 2016) or 2) shell-rich coquinas (Thompson et al., 2015). Most studies classify pre-salt carbonate reservoirs as purely lacustrine, but few entertain the possibility of non-marginal marine carbonates. Thompson (2013) showed that molluscan dominated faunas were deposited in an open marine environment in the Sergipe-Alagoas Basin. Moreira et al. (2007) classify the Barra Velha and the Gargau formations as pre-salt reservoir intervals that were

deposited in marginal marine environments in the Santos and Campos basins, respectively. Conversely, Wright and Tosca (2016) contend that the Barra Velha Formation likely formed in a restricted lacustrine environment where biogenic calcite precipitation would likely have been suppressed. Although significant evidence suggests that most pre-salt carbonate reservoir facies of the south Atlantic were deposited in lacustrine environments, the presence of marine carbonates should not be discounted (Thompson et al., 2015).

Recognition of marine carbonates in pre-salt reservoirs may aid with predicting facies distributions away from structural features. This study shows that marine carbonates deposited over rift geometries were essentially unaffected by local paleotopographic highs created by syn-depositional faulting, as carbonates of HST-1 and HST-2 maintained uniform thicknesses across syn-depositional faults bounding the Echo Canyon horst block. These uniform distributions over local topographic highs contrast depositional patterns in lacustrine stromatolite facies, which are strongly controlled by paleobathymetry and are confined to horst blocks in the Upper Yucca Formation (Li, 2014). This suggests marine carbonate facies in pre-salt reservoirs may have larger areal distributions than lacustrine microbialites that were more strongly controlled by local structures and that recognition of marine carbonates would allow for higher confidence in extrapolation of reservoir quality away from the wellbore. It is unclear whether this assumption would hold for lacustrine coquinas, as they are not confined to the photic zone and should therefore exhibit depositional patterns similar to fossiliferous packstones (Cf) of the Indio Mountains. It should be noted that depositional patterns observed in marine carbonates of the Indio Mountains are related to significantly smaller scale paleotopography than footwall highs of half grabens.

6.4.4 Stratigraphic Models

The utility of different surfaces in construction of a sequence stratigraphic model were discussed in Chapter one. It is readily apparent that the Bluff Mesa Formation in the study area cannot be described sufficiently using the rift model proposed by Martins-Neto and Catuneanu (2010). The rift model merges both the transgressive surface and sequence boundary with the flooding surface, which represents accommodation created by mechanical subsidence. The rift model predicts that the TST should be thin or absent, however transgressive systems tracts are present in every sequence across the southern thrust panel. Another integral key to the rift basin model is that fluvial deposits are interpreted as progradational infill and are placed at the top of the highstand systems tract instead of at the base of the lowstand systems tract. The erosional nature of fluvial facies of FA-1 suggests that they represent a decrease in base level, and therefore a sequence boundary, rather than progradational infilling of the basin.

An original goal of this study was to test the application of the sequence stratigraphic rift model proposed by Martins-Neto and Catuneanu (2010) in a mixed carbonate-siliciclastic system due to well-documented differences between carbonate and siliciclastic reactions to accommodation space generation. Application of this test requires the presence of carbonates and tectonically generated accommodation. Tectonism certainly played an important role in facies distributions as syn-depositional faults created relatively minor paleotopographic highs but because transgression was primarily eustatic-driven, expression of Martins-Neto and Catuneanu's (2010) model in a mixed carbonate-siliciclastic rift system cannot be described with this data set.

As previously discussed in chapter one, transgressive deposits on passive margins are broadly typified by backstepping estuarine facies deposited within an incised valley when

accommodation is generated through eustatic sea-level fluctuations (Catuneanu, 2006). As this study finds that most accommodation generation was eustatic-driven, one might expect that transgressive systems tracts of the Bluff Mesa Formation would resemble those on passive margins. On the contrary, this study found little evidence for transgressive deposition in an estuarine environment. Li (2014) assigned a sandy oyster-rich packstone to an estuarine or other marginal marine environment based on the low faunal diversity and the strong association between oysters and brackish salinity. Although this study still places Li's (2014) oyster-rich packstone in the transgressive systems tract (TST-1), the bed was found to contain marine fauna along strike and is interpreted as open marine (Cs). TST-2 is primarily composed of thin-bedded marine sandstone (Ss) with subordinate amounts of marine carbonates (Cf and Cs) with high faunal diversity not normally associated with brackish estuarine environments. The apparent absence of estuarine deposits that typically accompany eustatic-driven accommodation may be due to the antecedent topography of the rift lake basin. Facies distributions in the Bluff Mesa and Upper Yucca formations suggest the basin was becoming lower relief with waning tectonism and erosion of footwall highs, resulting in progressively less input from transverse drainage systems and more from an axial drainage system (Ravnas and Steel, 1998; Li, 2014; Fox, 2016). This trend away from transverse drainage systems, which create deeper incised valleys than axial systems due higher slope gradients (Ravnas and Steel, 1998), likely resulted in a broader basin with fewer deeply incised valleys conducive to estuary development.

7. SUMMARY AND CONCLUSIONS

Facies distributions in the Bluff Mesa Formation were controlled by a suite of interrelated factors superimposed on the antecedent topography that was a product of rift lake deposition in an active rift basin. Detailed petrographic analysis lead to identification of twelve lithofacies (Tables 4.1-5); matrix-supported pebble conglomerate (Fc), trough cross-bedded quartz arenite (Fs), horizontal laminated quartz arenite (Fsl), burrowed fine-grained quartz arenite (Ls), massive nodule-bearing mudstone (Lm), ooid grainstone (Cg), fossiliferous wackestone-packstone (Cf), sandy packstone-grainstone (Cs), marl (Cm), hummocky/swaley cross-stratified quartz arenite (Ss), matrix-supported carbonate clast conglomerate (Sc), and olive green shale, siltstone, and fine-grained quartz arenite (Mss). These thirteen lithofacies were then partitioned into five depositional facies associations; fluvial (FA-1), lacustrine (FA-2), shallow open marine carbonate shoal (FA-3), siliciclastic lower-upper shoreface (FA-4), and siliciclastic mid-shelf (FA-5). The facies associations encompass a wide range of terrestrial and marine environments that demonstrate the evolution of the trough margin during a 3rd-order transgression. The Bluff Mesa Formation in the Indio Mountains is composed of five 4^{th}-order sequences that typically consist of fluvial and lacustrine lowstand systems tracts, shoreface siliciclastic transgressive systems tracts with scattered thin-bedded carbonates, and robust shallow marine carbonate highstand systems tracts with subordinate marine siliciclastics.

The Bluff Mesa Formation exhibits an overall northward thickening trend from 219 meters thick in Echo Canyon to 343 meters in Squaw Canyon (Figure 4.1; Figure 4.2). Individual sequences and systems tracts exhibit a wider range of thickness variations across the stratal panel. Fluvial and lacustrine lowstands thicken slightly to the south and are confined to sequences #1 and #2. Transgressive systems tracts form prominent northward thickening wedges

in sequences #1 and #2, but are fairly uniform in thickness across the stratal panel in sequences #3-#5. Highstands are usually uniform in thickness across the stratal panel but thicken northwards in Sequence #2 and slightly southward in Sequence #5.

Transgression and accommodation generation were primarily eustatic-driven in the study area based on the asymmetrical nature and robust thicknesses of transgressive systems tracts. Tectonism was an important controlling factor in the nature of accommodation generated during fluvio-lacustrine deposition of the Upper Yucca Formation (Li, 2014). However, its impact waned through time as facies changes across horst-bounding faults are subtle in the lower Bluff Mesa Formation (i.e. fluvial belts thinning over horsts and thickening into grabens in sequences #1 and #2) before essentially vanishing in the upper Bluff Mesa. Stratigraphic sequences and surfaces are easily correlated between the Bluff Mesa Formation in the study area and the Bluff Mesa type section at Devil's Ridge (Figure 6.3), lending further credence to the idea that major base-level changes were a product of global eustatic fluctuations.

Correlations between the Bluff Mesa Formation of the Indio Mountains with the Quitman Formation (southern Quitman Mountains) and the Campagrande Formation (Finlay Mountains) shed light on the history of Aptian-Albian transgression of the Chihuahuan Trough's northeastern margin. Results allow for shoreline placement at several key stratigraphic intervals (Figure 6.4). Although some general speculation has been made regarding the stratigraphic relationship between the Bluff Mesa Formation and the Quitman Formation (Monreal and Longoria, 1999), this study is the first to tie specific stratigraphic surfaces outside of formation bases (i.e. base Quitman correlates with base Bluff Mesa). Correlation between the Bluff Mesa Formation and the Campagrande Formation is the first of its kind, with results indicating the Campagrande is the Diablo Platform equivalent to sequences #3-#5 of the Bluff Mesa.

Had rift lake basin physiography in the study area been conducive to evaporite deposition, it would have likely occurred during LST-2 following the initial marine transgression. Despite lacking evaporites, the Bluff Mesa Formation of the Indio Mountains is a useful analog for certain South Atlantic extensional basins. Abundant organic material and isotope geochemistry suggest that the Mss interval of HST-5 represents a good analog for transgressive marine shales acting as source rocks (Atlantide-Imbe play, Pelotas Basin). Different underlying stratigraphy (eolian and volcanoclastics vs fluvio-lacustrine) indicate the Mss interval may represent a seal analog for Aptian/Albian marine shales in the Atlantide-Imbetuba play, but this is significantly more speculative than the source rock analog for the Atlantide-Imbe play.

The stratigraphic architecture and facies distributions of the Bluff Mesa Formation in the Indio Mountains suggest that multiple pulses of base-level rise and transgression occurred before eventual drowning of the basin following TS-2. This suggests that the transition from the upper reservoir to the overlying evaporite seal may be multiphased and more complex than most published pre-salt reservoir models indicate. This study envisions two non-exclusive types of "transitional zone": 1) a zone of marine carbonates and/or shale interbedded with evaporites and 2) a zone of marine carbonates interbedded with lacustrine carbonates overlain by a competent evaporite seal. Shales are expected to replace evaporites in both scenarios in extensional basins lacking evaporites.

A transitional zone composed of interbedded marine carbonates and evaporites might result in multiple isolated lenses of reservoir-quality rock that may not be charged because of stratigraphically bounding seal facies. Accurate imaging of base salt and sub-salt reservoir geometries are notoriously difficult (Beasley et al., 2010). If this zone lies below the base-salt

pick, net pay and net-to-gross will be overestimated. Alternatively, a transitional zone located above the base-salt pick may compromise seal integrity in prospects where the evaporite seal is sufficiently thin. The existence of this transitional zone is also expected to carry important implications from an engineering standpoint regarding drilling and casing plans, as evaporites and carbonates have very different physical properties.

Unlike the first transitional zone, implications regarding a zone of interbedded marine carbonates and lacustrine carbonates assume that base salt is correctly picked. The presence of marine carbonates in upper pre-salt reservoirs would be of interest to reservoir engineers as pore types and permeability can vary drastically between stromatolitic lacustrine carbonates and typical marine packstones and grainstones (Ahr, 2009). Differences between marine carbonates and lacustrine coquinas may be less pronounced due to the similar bioclastic fabricsf. This study shows that the presence of marine carbonates in pre-salt reservoirs would also have implications for the distribution of reservoir facies. Highstand systems tracts following transgressions in the study area are composed of northward thickening shallow marine carbonates that are essentially unaffected by paleotopography, even when the basin returned to fluvio-lacustrine deposition following the next drop in base-level. This contrasts with fluvio-lacustrine facies that sporadically exhibit moderate thinning over local topographic highs within southward thickening lowstand systems tracts. Lacustrine stromatolite facies distributions are strongly controlled by syn-depositional faulting (Li. 2014). This indicates that if/when marine carbonates are identified in pre-salt reservoirs, they may have greater areal distributions and can be mapped over syn-depositional structural features with higher confidence than lacustrine carbonates.

8. REFERENCES

Adkins, W.S., 1932, the Mesozoic Systems in Texas, *in* Sellards, E.H., Adkins, W.S., and Plummer, F.B. *eds*., The Geology of Texas: Texas University Bulletin, v. 1, p. 239-518.

Ahr, W.M., Mancini, E.A., and Parcell, W.C., 2011, Pore characteristics in microbial carbonate reservoirs: AAPG Search and Discovery Article #30167.

Albritton, C.C., and Smith, J.F.Jr., 1965, Geology of the Sierra Blanca area, Hudspeth County, Texas: United States Geological Survey, Professional Paper 479, 131 p.

Anderson, T.H., and Nourse, J.A., 2005, Pull-apart basins at releasing bends of the sinistral Late Jurassic Mojave-Sonora fault system, *in* Anderson, T.H., Nourse, J.A., McKee, J.W., and Steiner, M.B., *eds*., The Mojave-Sonora megashear hypothesis: Development, assessment, and alternatives: Geological Society of America Special Paper 393, p. 97–122.

Anderson, T.H., and Silver, L.T., 2005, The Mojave-Sonora megashear—Field and analytical studies leading to the conception and evolution of the hypothesis, *in* Anderson, T.H., Nourse, J.A., McKee, J.W., and Steiner, M.B., *eds*., The Mojave-Sonora megashear hypothesis: Development, assessment, and alternatives: Geological Society of America Special Paper 393, p. 1–50.

Arai, M., 2014, Aptian/Albian (Early Cretaceous) Paleogeography of the South Atlantic: A Paleontological Perspective: Brazilian Journal of Geology, 44 (2), p. 339-350.

Araujo-Mendieta, J., and Casar-González, R., 1987, Estratigrafía y sedimentología del Jurasico Superior en la Cuenca de Chihuahua, norte de Mexico: Revista del Instituto Mexicano del Petroleo, 19, (1), p. 6-29.

Ashley, G.M., 1990, Classification of Large-Scale Subaqueous Bedforms: A New Look at an Old Problem: Journal of Sedimentary Petrology, 60, p. 160-172.

Bahniuk A.M., Anjos, S., França, A.B., Matsuda, N., Eller, J., Mckenzie, J.A., and Vasconcelos, C., 2015, Development of Microbial Carbonates in the Lower Cretaceous Codó Formation (North-East Brazil): Implications for Interpretation of Microbialite Facies Associations and Paleoenvironmental Conditions: Sedimentology, 62, p. 155-181.

Barton, L.L., and Tomei, F.A., 1995, Characteristics and Activities of Sulfate- Reducing Bacteria, *in* Barton, L.L., *ed*., Biotechnology Handbooks: Plenum Press, New York, v. 8, p. 1-23.

Bathurst, R.G.C., 1975, Carbonate Sediments and their Diagenesis, Developments in Sedimentology 12: Elsevier/Amsterdam, 658 p.

Beasley, C.J., Fiduk, J.C., Bize, E., Boyd, A., Frydman, M., Zerilli, A., Dribus, J.R., Moreira, J.L.P., and Capaleiro Pinto, A.C., 2010, Brazil's Presalt Play: Oil Field Review, Autumn 22 (3), p. 28-37.

Beglinger, S.E., Doust, H., and Cloetingh, S., 2010, Relating Petroleum System and Play Development to Basin Evolution: Brazilian South Atlantic Margin: AAPG Search and Discovery Article #40520.

Beglinger, S.E., Doust, H., and Cloetingh, S., 2012, Relating Petroleum System and Play Development to Basin Evolution: West African South Atlantic Basins: Marine and Petroleum Geology, 30, p. 1-25.

Bergersen, E., 2016, Geochemical signatures as a chemostratigraphic tool to correlate stacked carbonates of the Glorieta, Victorio Peak, Cutoff, and Upper San Andres Formations West Dog Canyon, Guadalupe Mountains, New Mexico: University of Texas at El Paso, M.S. Thesis, 103 p.

Blakey, R.C., 2003, Detailed Paleogeography Maps: online resources available at the University of Northern Arizona Department of Geology, URL:https://www2.nau.edu/rcb7/globaltext2.html.

Bosence, D.W.J., 1998, Stratigraphic and Sedimentological Models of Rift Basins, *in* Purser, B.H., and Bosence, D.W.J., *eds*., Sedimentation and Tectonics in Rift Basins: Red Sea Gulf of Aden: Springer Geology, p. 9-25.

Bowen, H.J.M., 1979, Environmental Chemistry of the Elements: Academic Press, London, 333 p.

Brown, M.L., and Dyer, R., 1987, Mesozoic geology of northwestern Chihuahua, Mexico, *in* Dickinson, W.R., and Klute, M.A., *eds*., Mesozoic Rocks of Southern Arizona and Adjacent Areas: Arizona Geological Society Digest, 18, p. 381- 394.

Bryant, I., Herbst, N., Daily, P., Dribus, J.R., Fainstein, R., Harvey, N., McCoss, A., Montaron, B., Quirk, D., and Tapponnier, P., 2012, Basin to Basin: Plate Tectonics in Exploration: Oil Field Review, Autumn 24 (3), p. 38-57

Budhathoki, P., Langford, R.P., Pavlis, T.L., and Page, S.J., 2010, Sequence Stratigraphic Framework of the Cretaceous Cox Sandstone, Indio Mountain, West Texas: GSA Abstract, paper 269-7.

Budhathoki, P., 2013, Integrated Geological and Geophysical Studies of the Indio Mountains and Hueco Bolson, West Texas: M.S. Thesis, The University of Texas at El Paso, 111 p.

Canfield, D.E., 2001, Biogeochemistry of Sulfur Isotopes: Reviews of Mineralogy and Geochemistry 43, p. 607-636.

Cantu-Chapa C.M., Sandoval-Silva, R., and Arenas-Partida, R., 1985, Evolucion sedimentaria del Cretacico Inferior en el norte de Mexico: Revista Instituto Mexicano del Petroleo, 17(2), p. 14-37.

Carciumaru, D., 2005, Structural Geology and tectonics on the northern Chihuahua trough: Master's thesis, The University of Texas at El Paso, p.

Carciumaru, D., and Ortega, R., 2008, Geologic Structure of the Northern Margin of the Chihuahua Trough: Evidence for Controlled Deformation During Laramide Orogeny: Boletin de la Sociedad Geologica Mexicana, v. 60, num. 1, p. 43-69.

Carminatti, M., Wolff, B., and Gamboa, L., 2008, New Exploratory Frontiers in Brazil: 19th World Petroleum Congress, Madrid, Spain.

Catuneanu, O., 2006, Principles of Sequence Stratigraphy: Elsevier, Amsterdam. 375 p.

Claypool, G.E., Holser, W.T., Kaplan, I.R., Sakai, H. and Zak, I., 1980, the age curves for sulfur and oxygen isotopes in marine sulfate and their mutual interpretation: Chemical Geology, v. 28, p. 199–260.

Collinson, J.D., 1996, Alluvial Sediments, *in* Reading, H.G., *ed*., Sedimentary Environments: Processes, Facies and Stratigraphy: Blackwell publishing, p. 37-82.

Coney, P.J., 1976, Plate tectonics and the Laramide orogeny: New Mexico Geological Society, Special Publication 6, p. 5-10.

Conti, B., de Jesus Perinotto, J.A., Veroslavsky, G., Castillo, M.G., de Santa Ana, H., Soto, M., and Morales, E., 2017, Speculative Petroleum Systems of the Southern Pelotas Basin, Offshore Uruguay: Marine and Petroleum Geology, v. 83, p. 1-25.

Cordoba, D.A., 1969, Mesozoic Stratigraphy of Northeastern Chihuahua, Mexico, *in* Cordoba, D.A., Wengerd, S.A., and Shomaker, J.W., *eds*., The Border Region (Chihuahua, Mexico, & USA): New Mexico Geological Society 20th Annual Fall Field Conference Guidebook, p. 91-96.

Davison, I., and Underhill, J.R., 2012, Tectonics and Sedimentation in extensional rifts: Implications for Petroleum Systems, *in* Gao, D., *ed*., Tectonics and Sedimentation: Implications for Petroleum Systems: AAPG Memoir 100, p. 15-42.

DeFord, R.K., 1958a, Cretaceous platform and geosyncline, Culbertson and Hudspeth counties, Texas: Van Horn, Texas: Society of Economic Paleontologists and Mineralogists, Permian Section, Guidebook 1958 Field Trip, 90 p.

DeFord, R.K., and Haenggi, W.T., 1970, Stratigraphic Nomenclature of Cretaceous Rocks in Northeastern Chihuahua, *in* The Geologic Framework of the Chihuahua Tectonic Belt; in Honor of Professor Ronald K. DeFord: West Texas Geological Society and The University of Texas at Austin, p. 175-196.

Dickinson, W.R., and Lawton, T.F., 2001a, Carboniferous to Cretaceous assembly and fragmentation of Mexico: Geological Society of America Bulletin, v. 113, p. 1142–1160.

Dickinson, W.R., and Lawton, T.F., 2001b, Tectonic setting and sandstone petrofacies of the Bisbee basin (USA-Mexico): Journal of South American Earth Sciences, v. 14, p. 475–504.

Dietrich, R.V., 1997, Carbonate concretions: a bibliography: http://condor.cmich.edu/cdm/ref/collection/p1610-01coll1/id/3165

Dietzel, P.T., 2013, Physical and Sequence Stratigraphy of the Late Cretaceous Chispa Summit Formation, Jeff Davis County, Texas: University of Texas at El Paso, M.S. Thesis, 107 p.

Dumas, S., and Arnott, R.W.C., 2006, Origin of Hummocky and Swaley Cross-Stratification – the Controlling Influence of Unidirectional Current Strength and Aggradation Rate: Geology, v. 34, p. 1073-1076.

Dunham, R. J., 1962, Classification of Carbonate Rocks According to Depositional Texture, *in* Ham, W. E. *ed*., Classification of Carbonate Rocks: American Association of Petroleum Geologists Memoir, p. 108-121.

Duque-Botero, F., 2006, Paleoenvironmental Implications of the Indidura Formation (Cenomanian/Turonian), Northeastern Mexico: a High Resolution Stratigraphic Study: Florida International University, Ph.D. Dissertation, 172 p.

Eardley, A.L., 1938, Sediments of Great Salt Lake, Utah: AAPG Bulletin, v. 22, p. 1305-1411.

Flügel, E., 2010, Microfacies of Carbonate Rocks: Analysis, Interpretation and Application: Springer-Verlag, Berlin, p. 984.

Folk, R.L., 1959, Practical Petrographic Classification of Limestones: American Association of Petroleum Geologists Bulletin, v. 43, p. 1-38.

Fox, M.R., 2016, Sedimentologic and stratigraphic analysis of synrift siliciclastic fluvial and lacustrine strata in the Lower Cretaceous upper Yucca Formation, Indio Mountains, West Texas: University of Texas at El Paso, M.S. Thesis, 138 p.

Gill, B.C., Lyons, T.W., and Frank, T.D., 2008, Behavior of carbonate-associated sulfate during meteoric diagenesis and implications for the sulfur isotope paleoproxy: Geochimica et Cosmochimica Acta, v. 72, i. 19, p. 4699-4711.

Gomes, P.O., Kilsdonk, B., Grow, T., Minken, J., and Barragan, R., 2012, Tectonic Evolution of the Outer High of Santos Basin, Southern Sao Paulo Plateau, Brazil, and Implications for Hydrocarbon Exploration, *in* Gao, D., *ed*., Tectonics and Sedimentation: Implications for Petroleum Systems: AAPG Memoir 100, p. 125-142.

Gonzalez-Leon, C.M., Scott, R.W., Loser, H., Lawton, T.F., Robert, E., and Valencia, V.A., 2008, Upper Aptian-Lower Albian Mural Formation: Stratigraphy, biostratigraphy and depositional cycles on the Sonoran shelf, northern Mexico: Cretaceous Research, v. 29, p. 249– 266.

Gunnarsson, I., and Arnórsson, S., 2000, Amorphous Silica Solubility and the Thermodynamic Properties of H_4SiO_4 in the Range of 0 to 350 C at Psat: Geochemica et Cosmochemica Acta, 64, p. 2295-2307.

Heller, P.L., Komar, P.D., and Pevear, D.R., 1980, Transport Processes in Ooid Genesis: Journal of Sedimentary Petrology, v. 50, no. 3, p. 943-951.

Haenggi, W.T., 2001, Tectonic history of the Chihuahua Trough, Mexico and adjacent USA; Part I, the pre-Mesozoic setting: Boletin de la Sociedad Geologica Mexicana, Tomo LIV, p. 28-66.

Haenggi, W.T., 2002, Tectonic History of the Chihuahua Trough, Mexico and Adjacent USA, Part II: Mesozoic and Cenozoic: Boletin de la Sociedad Geologia Mexicana, 54, p. 38-94.

Haenggi, W.T. and Muehlberger, W.T., 2005, Chihuahua Trough – A Jurassic pull-apart basin, *in* Anderson, T.H., Nourse, J.A., McKee, J.W., and Steiner, M.B., *eds*., The Mojave-Sonora megashear hypothesis: Development, assessment, and alternatives: Geological Society of America Special Paper 393, p. 619-629.

Huffington, R.M., 1943, Geology of the Northern Quitman Mountains, Trans-Pecos Texas: Geological Society of America Bulletin, v. 54, no. 7, p. 987-1047.

Jones, B.R., 1968, the Geology of the Southern Quitman Mountains and Vicinity, Hudspeth County, Texas: Texas A&M University, Ph.D. Dissertation, 179 p.

Jones, B.R., and Reaser, D.F., 1970, Geology of Southern Quitman Mountains, Hudspeth County, Texas: Texas Bureau of Economic Geology, Geologic Quadrangle Map No. 39.

King, R.E., and Adkins, W.S., 1946, Geology of a Part of the Lower Conchos Valley, Chihuahua, Mexico: GSA Bulletin, v. 57, p. 275-294.

Lambiase, J.J., and Bosworth, W., 1995, Structural Controls on Sedimentation in Continental Rifts", *in* Lambiase, J.J., *ed*., Hydrocarbon Habitat in Rift Basins: Geological Society Of London, Special Publications 80, p. 117-144.

Lambiase, J. J., and Morley, C.K., 1999, Hydrocarbons in rift basins: The role of stratigraphy: Philosophical Transactions—Royal Society Mathematical, Physical and Engineering Sciences, vol. 357, no. 1753, p. 877–900. doi:10.1098/rsta.1999.0356.

Lehman, T.M., 1991, Sedimentation and tectonism in the Laramide Tornillo Basin of west Texas: Sedimentary Geology, 75, p. 9-28.

Leng, M.J., Lamb, A.L., Heaton, T.H.E., Marshall, J.D., Wolfe, B.B., Jones, M.D., Holmes, J.A., and Arrowsmith, C., 2006, Isotopes in Lake Sediments, *in* Leng, M.J., *ed*., Isotopes in Paleoenvironmental Research: Springer, Netherlands, p. 147-184.

Li, X.W., 2014, Sedimentologic, Stratigraphic, and Diagenetic Analysis of Microbialite-Bearing Lacustrine Rift Sequence within the Lower Cretaceous Yucca Formation, Indio Mountains, West Texas: University of Texas at El Paso, M.S. Thesis, 151 p.

Llanos, A., 2017, "Genesis of Unique Carbonate Fans in a Pre-salt Reservoir Analog, Indio Mountains, West Texas" University of Texas at El Paso, MS Thesis, 94 p.

Magara, K., 1978, Compaction and Fluid Migration: Elsevier, Amsterdam, 329 p.

Magnavita, L.P., Szatmari, P., Cupertino, J.A., Destro, N., and Roberts, D., 2012, The Reconcavo Basin, *in* Roberts, D.G. and Bally, A.W., *eds*., Regional Geology and Tectonics: Phanerozoic Rift Systems and Sedimentary Basins: Elsevier, Amsterdam, p. 383-419.

Mann, P., Gahagan, L., and Gordon, M.B., 2003, Tectonic Setting of the World's Giant Oil and Gas Fields: AAPG Memoir 78, p. 15–105.

Mann, P., Horn, M., and Cross, I., 2007, Emerging Trends from 69 Giant Oil and Gas Fields Discovered from 2000-2006: AAPG Search and Discovery #110045.

Markello, J.R., Koepnick, R.B., Waite, L.E., and Collins, J.F., 2008, The Carbonate Analogs Through Time (CATT) Hypothesis and the Global Atlas of Carbonate Fields: A Systematic and Predictive Look at the Phanerozoic Carbonate Systems, *in* Lukasik, J., and Simo, J.A., *eds*., Controls on Carbonate Platform and Reef Development: SEPM Special Publication 89, p. 15–54.

Martin, L., and Dominguez, J.M., 1994, Geological History of Coastal Lagoons, *in* Kjerfve, B., *ed*., Coastal Lagoon Processes: Elsevier Oceanography, s. 60, p. 41-67.

Martins-Neto, M.A., and Catuneanu, O., 2010, Rift Sequence Stratigraphy: Marine and Petroleum Geology, 27, p. 247-253.

Mauel, D.J., Lawton, T.F., González-León, C.M., Iriondo, A., and Amato, J.M., 2011, Stratigraphy and age of Upper Jurassic strata in north-central Sonora, Mexico: Southwestern Laurentian record of crustal extension and tectonic transition: Geosphere, v. 7, p. 390–414.

Mello, M.R., Koutsoukos, E., Mohriak, W., and Bacoccoli, G., 1994, Selected Petroleum Systems in Brazil, *in* Magoon, L.B. and Dow, W.G., *eds*., The Petroleum System – from Source to Trap: AAPG Memoir 60, p. 499-512.

Miall, A.D., 1978, Lithofacies Types and Vertical Profile Models in Braided River Deposits: A Summary, *in* Miall, A.D., *ed*., Fluvial Sedimentology: Canadian Society of Petroleum Geologists Memoir, 5, p. 597-604.

Miall, A.D., 1985, Architectural Element Analysis: A New Method of Facies Analysis Applied to Fluvial Deposits: Earth Science Reviews, 22, p. 261-308.

Miall, A.D, 2010, Alluvial Deposits, *in* James, N.P., and Dalrymple, R.W., *eds*., Facies models 4: Geological Association of Canada, Toronto (Canada), p. 105-137.

Mohriak, W.U., Mello, M.R., Dewey, J.F., and Maxwell, J.R., 1990, Petroleum Geology of the Campos Basin, Offshore Brazil, in Brooks, J., *eds*., Classic Petroleum Provinces: Geological Society of London, Special Publications, v. 50, p. 119-141.

Molina-Garza, R.S. and Iriondo, A., 2007, the Mojave-Sonora megashear: The hypothesis, the controversy and the current state of knowledge, *in* Alaniz-Alvarez, S.A. and Nieto-Samaniego, A.F., *eds*., Geology of Mexico: Celebrating the Centenary of the Geological Society of Mexico: Geological Society of America, Special Paper 422, p. 233–259.

Monreal, R., and Longoria, J., 1999, A revision of the Upper Jurassic and Lower Cretaceous stratigraphic nomenclature for the Chihuahua trough, north-central Mexico: Implications for lithocorrelations, *in* Bartolini, C., Wilson, J.L., and Lawton, T.F. *eds*., Mesozoic Sedimentary and Tectonoic History of North-Central Mexico: Geological Society of America, Special Paper 340, p. 69-92.

Moreira, J.L.P., Madeira, C.V., and Gil, J.A., 2007, Bacia de Santos: Boletim de Geociêcias da Petrobrás, Rio de Janeiro 15, p. 511-529.

Muehlberger, W.R., 1992, Tectonic Map of North America, Southeast Sheet: American Association of Petroleum Geologists, 1: 5,000,000.

Olmstead, G.A., and Young, K., 2000, Late Jurassic Ammonites from the Northeastern Chiricahua Mountains, Southeast Arizona: New Mexico Geology, 22, p. 1-7.

Page S.J., 2011, Fold-Thrust System Overprinting Syn-Rift Structures on the Margin of an Inverted Rift Basin: Indio Mountains, West Texas: M.S. Thesis, The University of Texas at El Paso, 60 p.

Paytan, A., and Gray, E.T., 2012, Sulfur Isotope Stratigraphy, *in* Gradstein, F.M., Ogg, J.G., Schmitz, M., and Ogg, G. *eds*., The Geologic Time Scale: Elsevier, p. 167-179.

Pettijohn, F.J., 1957, Sedimentary Rocks: Harper and Row, 2nd edition, 718 p.

Peryam, T.C., Lawton, T.F., Amato, J.M., González-León, C.M., and Mauel, J. D., 2012, Lower Cretaceous strata of the Sonora Bisbee Basin: A record of the tectonomagmatic evolution of northwestern Mexico: Geological Society of America Bulletin, 124, p. 532–548.

Peterson, J.A., 1985, Petroleum Geology and Resources of Northwestern Mexico: U.S. Geological Survey Circular 943, p. 1-30.

Plint, A.G., 2010, Wave- and Storm-Dominated Shoreline and Shallow-Marine Systems, *in* James, N.P., and Dalrymple, R.W., *eds*., Facies models 4: Geological Association of Canada, Toronto (Canada), p. 167-199.

Popp, B.N., and Wilkinson, B.H., 1983, Holocene lacustrine ooids from Pyramid Lake, Nevada, *in* Peryt, T.M., *ed*., Coated Grains: Springer-Verlag, Berlin, p. 142–153.

Quirk, D.G., Schødt, N., Lassen, L., Ings, S.J., Hsu, D., Hirsch, K.K., and Von Nicolai, C., 2012, Salt Tectonics on Passive Margins: Examples from Santos, Campos and Kwanza Basins, *in* Alsop, G.I., Archer, S.G., Hartley, A.J., Grant, N.T., and Hodgkinson, R., *eds*., Salt Tectonics, Sediments and Prospectivity: Geological Society, London, Special Publications 363, p. 207-244.

Ramirez-M., J.C., Acevedo-C., F., 1957, Notas sobre la geología de Chihuahua: Asociacion Mexicana de Geologos Petroleros, Boletín, IX, p. 583-772.

Ravnås, R., Steel, R.J., 1998, Architecture of marine rift-basin successions: American Association of Petroleum Geologist Bulletin, v. 82, p. 110-146.

Reading, H.G., and Collinson, J.D., 1996, Clastic Coasts, *in* Reading, H.G. *ed*., Sedimentary Environments: Process, Facies and Stratigraphy: Blackwells, Cornwall, 154-231.

Reaser, D.F., 1974, Geology of Cieneguilla Area, Chihuahua and Texas: University of Texas at Austin, Ph.D. Dissertation, 340 p.

Renaut, R.W., and Gierlowski-Kordesch, E.H., 2010. Lakes, *in* Dalrymple, R.W., James, N.P., *eds*., Facies Models: Geological Association of Canada, Toronto (Canada), pp. 541-575.

Richardson, G. B., 1904, Report of a Reconnaissance in Trans-Pecos Texas North of the Texas and Pacific Railway: Texas University Mineral Survey Bulletin, v. 9, 119 p.

Rigby, J.K., and Scott, R.W., 1981, Sponges from the Lower Cretaceous Mural Limestone in Arizona and Northern Mexico: Journal of Paleontology, v. 55, no. 3, pp. 552-562.

Rimstidt, J.D., 1997, Quartz Solubility at Low Temperatures: Geochemica et Cosmochemica Acta, 61, p. 2553-2558.

Rodriguez-Torres, R.R., 1969, Mesozoic Stratigraphy of Sierra de la Alcaparra, Northeastern Chihuahua, *in* Cordoba, D.A., Wengard, S.A., and Shomaker, J.W., *eds*., The Border Region (Chihuahua, Mexico & USA): New Mexico Geological Society 20th Annual Fall Field Conference Guidebook, p. 173-175.

Rohrbaugh, R.T., 2001, Contractional and Extensional Deformation Kinematics of the Southern Indio Mountains, Trans-Pecos Texas: M.S. Thesis, The University of Texas at El Paso, 83 p.

Schwarz, S., 2016, Syn-rift drainages and sedimentary fill architecture: a case study in the Jurassic of the Dampier Sub-basin: M.S. Thesis, Colorado School of Mines, 115 p.

Scott, R.W., 1981, Biotic relations in Early Cretaceous coral-algal-rudist reefs, Arizona: Journal of Palaeontology, v. 55, no. 2, pp. 463-478

Silver, L.T., and Anderson, T.H., 1974, Possible left-lateral early to middle Mesozoic disruption of the southwestern North American craton margin: Geological Society of America Abstracts with Programs, v. 6, no. 7, p. 955–956.

Spencer, J.E., Richard, S.M., Gehrels, G., Gleason, J., and Dickinson, W.R., 2011, Age and tectonic setting of the Mesozoic McCoy Mountains Formation in western Arizona, USA: Geological Society of America Bulletin v. 123; no. 7/8; p. 1258–1274.

Stern, R.J., and Dickinson, W.R., 2010, The Gulf of Mexico is a Jurassic backarc basin: Geosphere, v. 6, p. 739– 754.

Stevens, J.B., and Stevens, M.S., 1990, Stratigraphy and major structural tectonic events along and near the Rio Grande, Trans-Pecos Texas and adjacent Chihuahua and Coahuila, Mexico, in Geology of the Big Bend and Trans-Pecos Texas: South Texas Geological Society, Guidebook, p. 56-94.

Sumner, D.Y., and Grotzinger, J.P., 1993, Numerical Modeling of Ooid Size and the Problem of Neoproterozoic Giant Ooids: Journal of Sedimentary Petrology, v. 63, pp. 974-982.

Thompson, D.L., 2013, the stratigraphic architecture and depositional environments of non-marine carbonates from Barremian-Aptian Pre-Salt strata of the Brazilian continental margin: Ph.D. Dissertation, Monash University, 277 p.

Thompson, D.L., Stilwell, J.D., and Hall, M., 2015, Lacustrine Carbonate Reservoirs from Early Cretaceous Rift Lakes of Western Gondwana: Pre-Salt Coquinas of Brazil and West Africa: Gondwana Research, 28, p. 26-51.

Tucholke, B.E., and Schouten, H., 1988, Kane Fracture Zone: Marine Geophysical Researches, 10, p. 1-39.

Underwood, J.R., 1962, Geology of Eagle Mountains and vicinity, Trans-Pecos Texas: University of Texas at Austin, Ph.D. dissertation 559 p.

Underwood, J.R., 1980, Geology of the Eagle Mountains, Hudspeth County, Texas: New Mexico Geological Society Guidebook, 31st Field Conference, Trans-Pecos Region, p. 183-193

Veizer, J., Godderis, Y., and Francois, L.M., 2000, Evidence for decoupling of atmospheric CO2 and global climate during the Phanerozoic eon: Nature, v. 408, p. 698-701.

Villasenor, A.B., Gonzalez-Leon, C.M., Lawton, T.F., and Aberhan, M., 2005, Upper Jurassic Ammonites and Bivalves from the Cucurpe Formation, Sonora, Mexico: Revista Mexicana de Ciencias Geologicas, 22, p. 65-87.

Wang, Y., Huang, C., Sun, B., Quan, C., Wu, J., and Lin, Z., 2014, Paleo-CO Variation Trends and the Cretaceous Greenhouse Climate: Earth-Science Reviews, v. 129, p. 136-147.

Wotte, T., Shields-Zhou, G.A., and Strauss, H., 2012, Carbonate-associated sulfate: Experimental comparisons of common extraction methods and recommendations toward a standard analytical protocol: Chemical Geology, v. 326-327, p. 132-144.

Wright, V.P., and N.J. Tosca, 2016, Geochemical Model for the Formation of the Pre-Salt Reservoirs, Santos Basin, Brazil: Implications for Understanding Reservoir Distribution: AAPG Search and Discovery Article #51304.

Zeller, R.A.Jr., 1970, Geology of Little Hatchet Mountains, Hidalgo and Grant Counties, New Mexico: New Mexico Bureau of Mines and Mineral Resources, Bulletin 96, 23 p.

9. APPENDIX

Depositional Facies

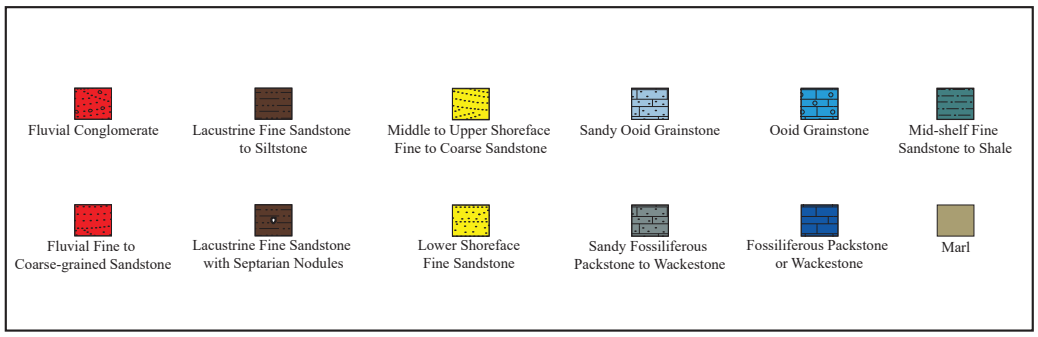

Grain Types

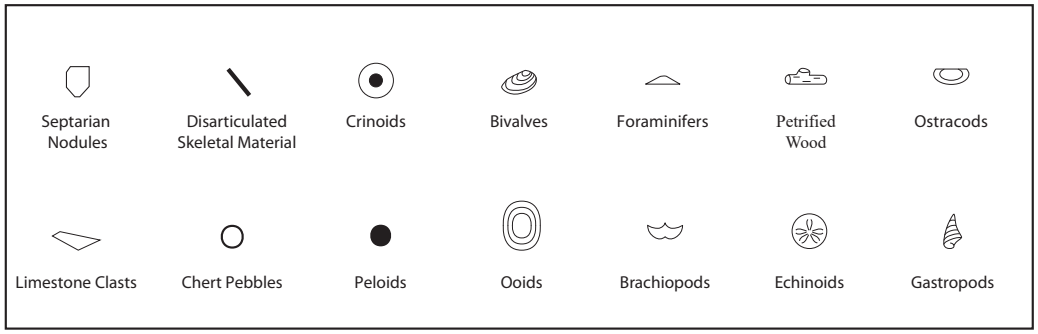

Sedimentary Structures

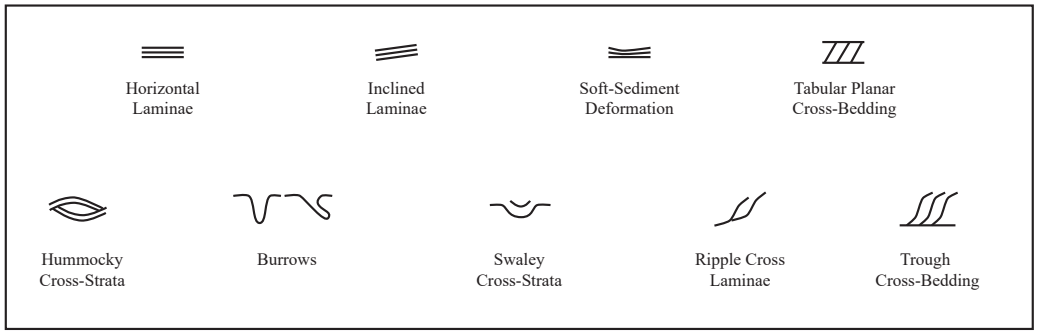

Echo Canyon Measured Section (EC)

Top	30°46'52.82"N	104°59'45.71"W	Interval	Kuy - Kbm pg 1/6
Base	30°46'34.98"N	104°59'58.83"W	Strike and Dip	322° 28°

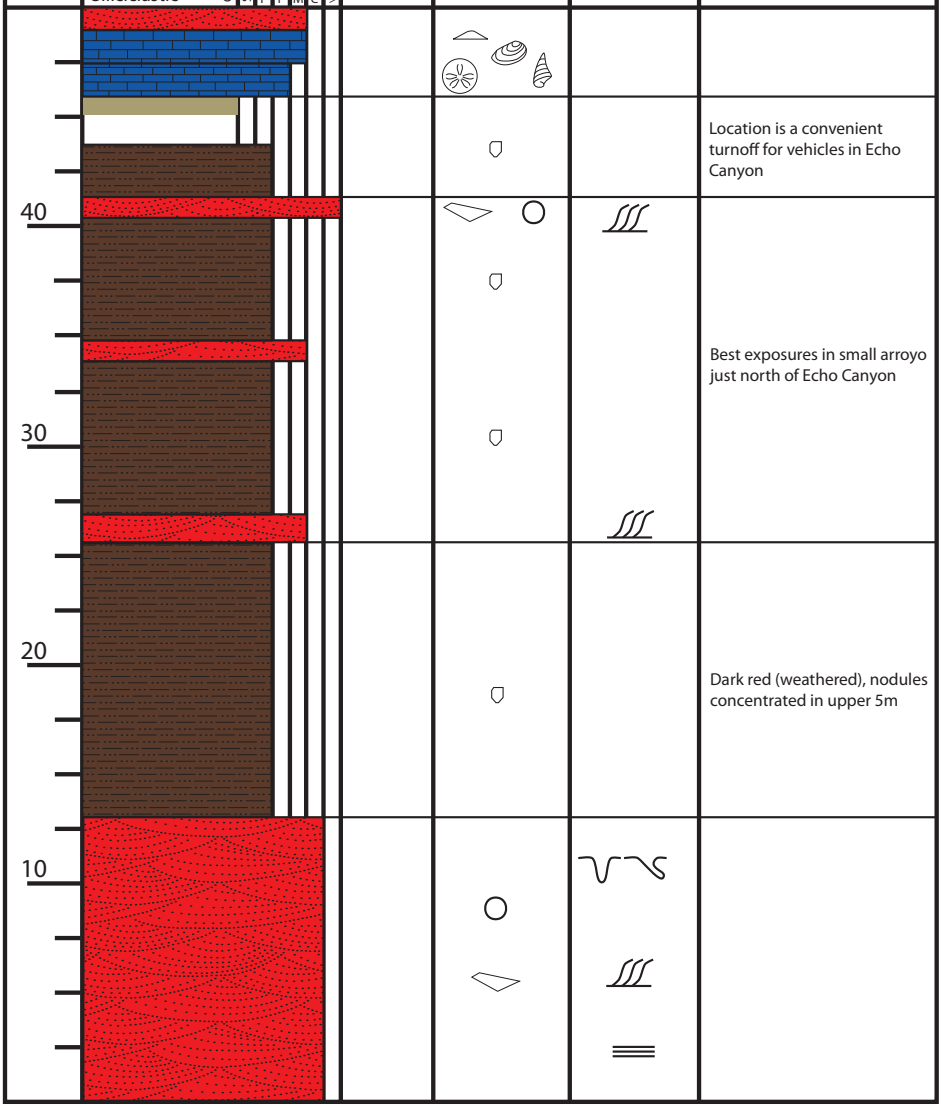

Thickness (M)	Sample or Outcrop Photo	Clast or Grain Type	Sedimentary Structures	Comments
				Location is a convenient turnoff for vehicles in Echo Canyon
				Best exposures in small arroyo just north of Echo Canyon
				Dark red (weathered), nodules concentrated in upper 5m

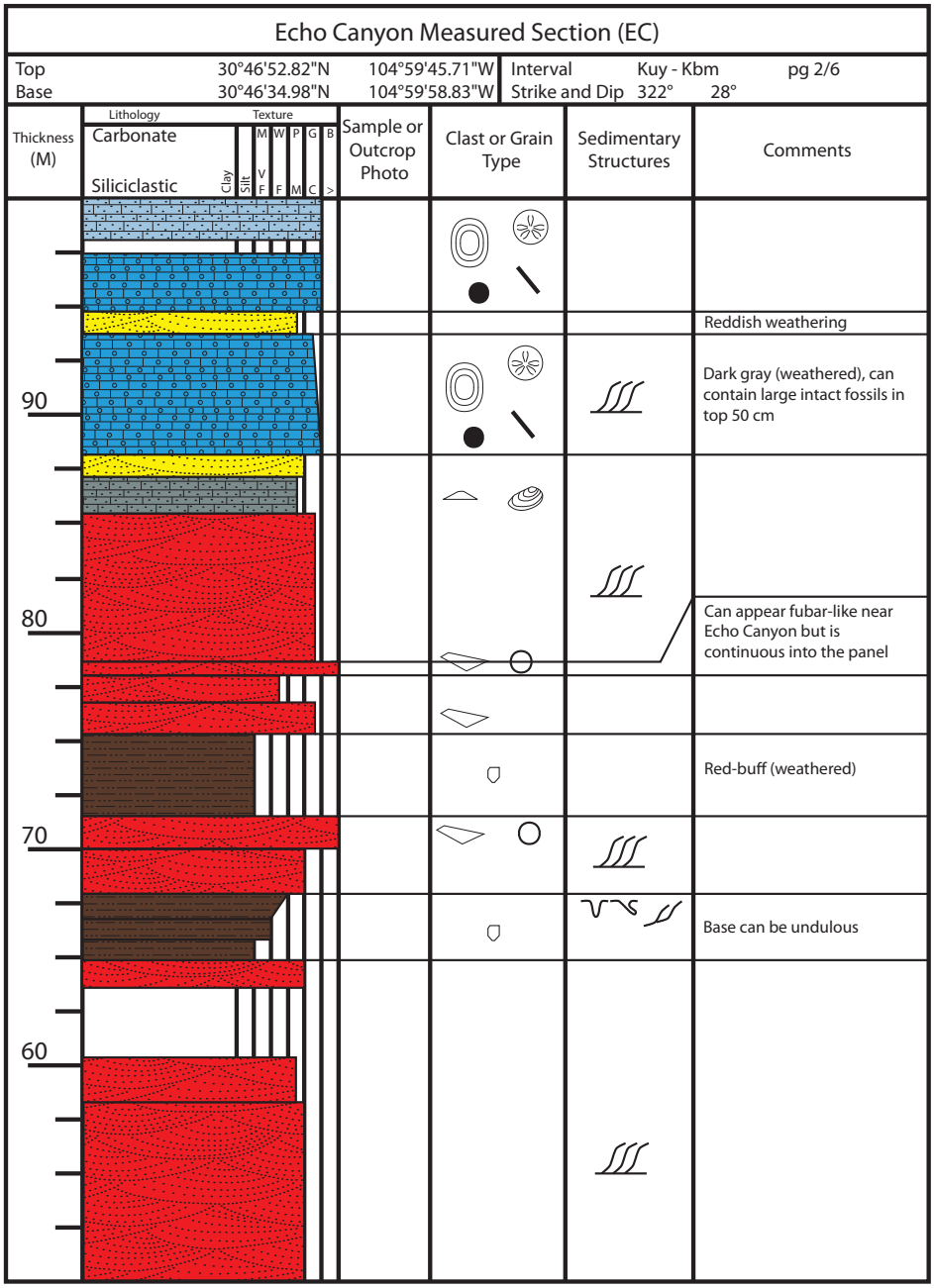
Echo Canyon Measured Section (EC)
Top 30°46'52.82"N 104°59'45.71"W
Base 30°46'34.98"N 104°59'58.83"W
Interval Kuy - Kbm pg 2/6
Strike and Dip 322° 28°
Thickness (M)
Lithology
Carbonate
Siliciclastic
Clay
Silt
Texture
M W P G B
V F F M C >
Sample or Outcrop Photo
Clast or Grain Type
Sedimentary Structures
Comments
90
80
70
60
Reddish weathering
Dark gray (weathered), can contain large intact fossils in top 50 cm
Can appear fubar-like near Echo Canyon but is continuous into the panel
Red-buff (weathered)
Base can be undulous

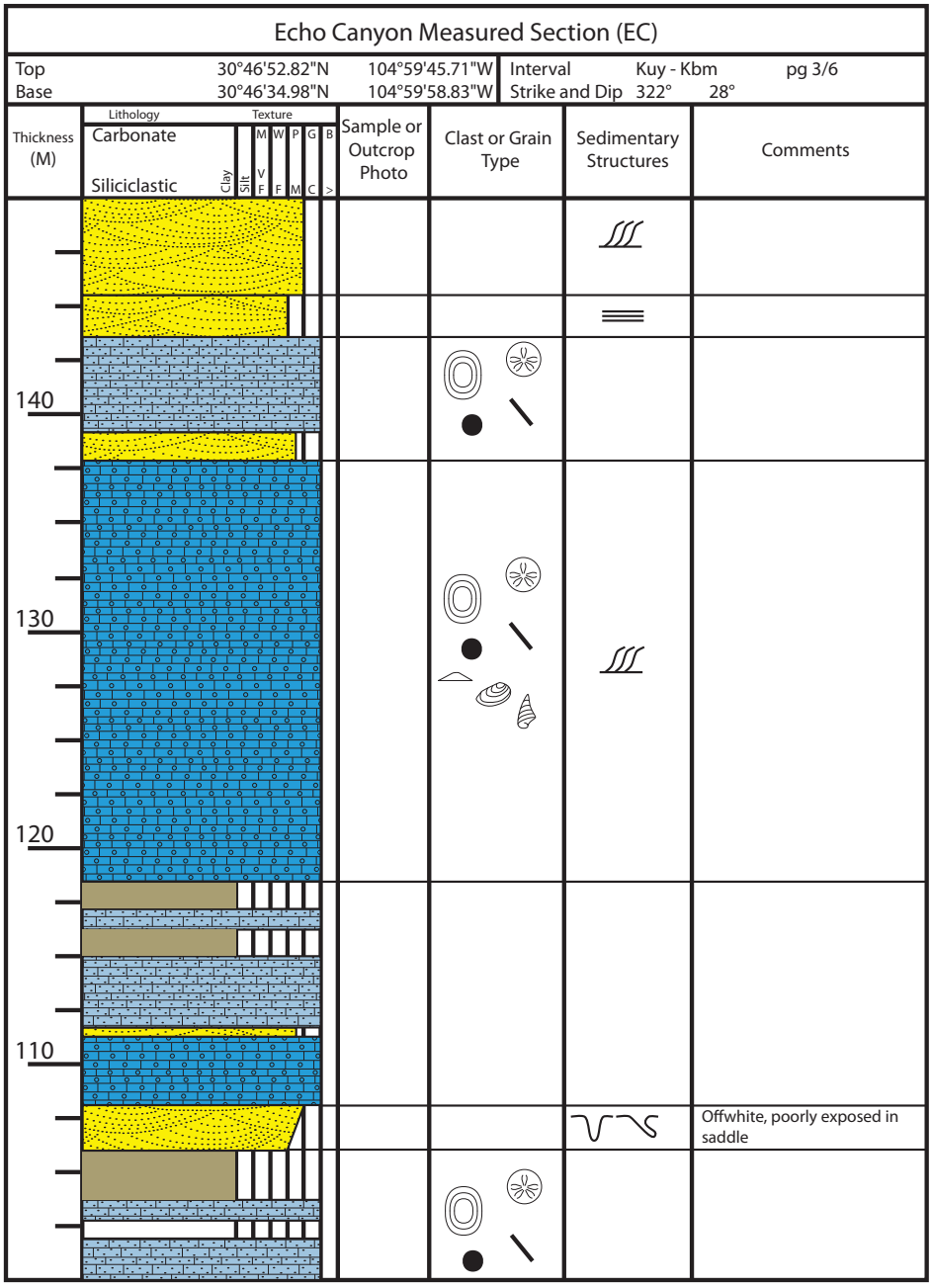
Echo Canyon Measured Section (EC)
Top 30°46'52.82"N 104°59'45.71"W
Base 30°46'34.98"N 104°59'58.83"W
Interval Kuy - Kbm pg 3/6
Strike and Dip 322° 28°
Thickness (M)
Lithology
Carbonate
Siliciclastic
Clay
Silt
Texture
M W P G B
V F F M C >
Sample or Outcrop Photo
Clast or Grain Type
Sedimentary Structures
Comments
140
130
120
110
Offwhite, poorly exposed in saddle

Echo Canyon Measured Section (EC)

Top	30°46'52.82"N	104°59'45.71"W	Interval	Kuy - Kbm	pg 4/6
Base	30°46'34.98"N	104°59'58.83"W	Strike and Dip	322°	28°

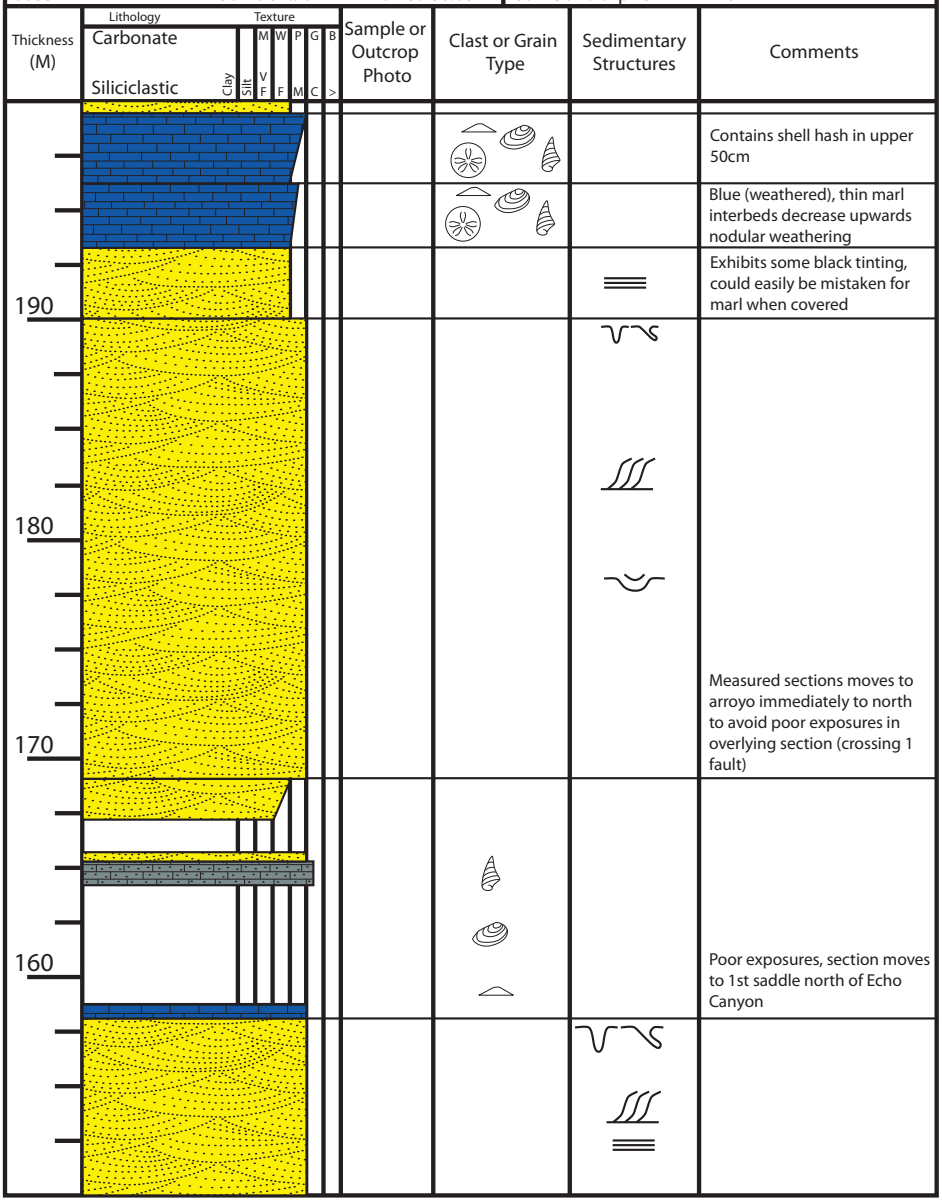

Echo Canyon Measured Section (EC)

Top	30°46'52.82"N	104°59'45.71"W	Interval	Kuy - Kbm	pg 5/6
Base	30°46'34.98"N	104°59'58.83"W	Strike and Dip	322°	28°

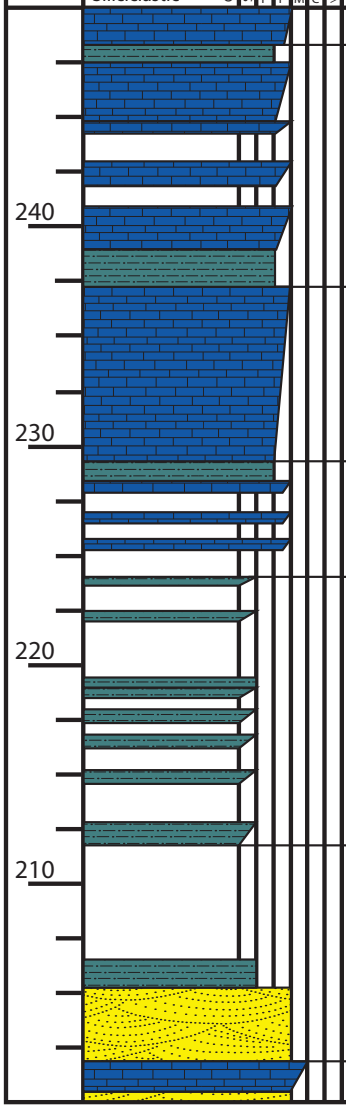

Thickness (M)	Sample or Outcrop Photo	Clast or Grain Type	Sedimentary Structures	Comments
				Dip changes to 25° north of arroyo but cannot be traced into hillside due to poor exposures
				Poorly exposed, multiple parasequences
				Poorly exposed, parasequence tops are documented in arroyo, cubic weathering pattern, scattered offwhite ss intervals can be mistaken for poorly exposed outcrops but are only float
				Poorly exposed due to road
				Greenish gray with rose tinting, weathering pattern very distinct with prominent vertical fractures

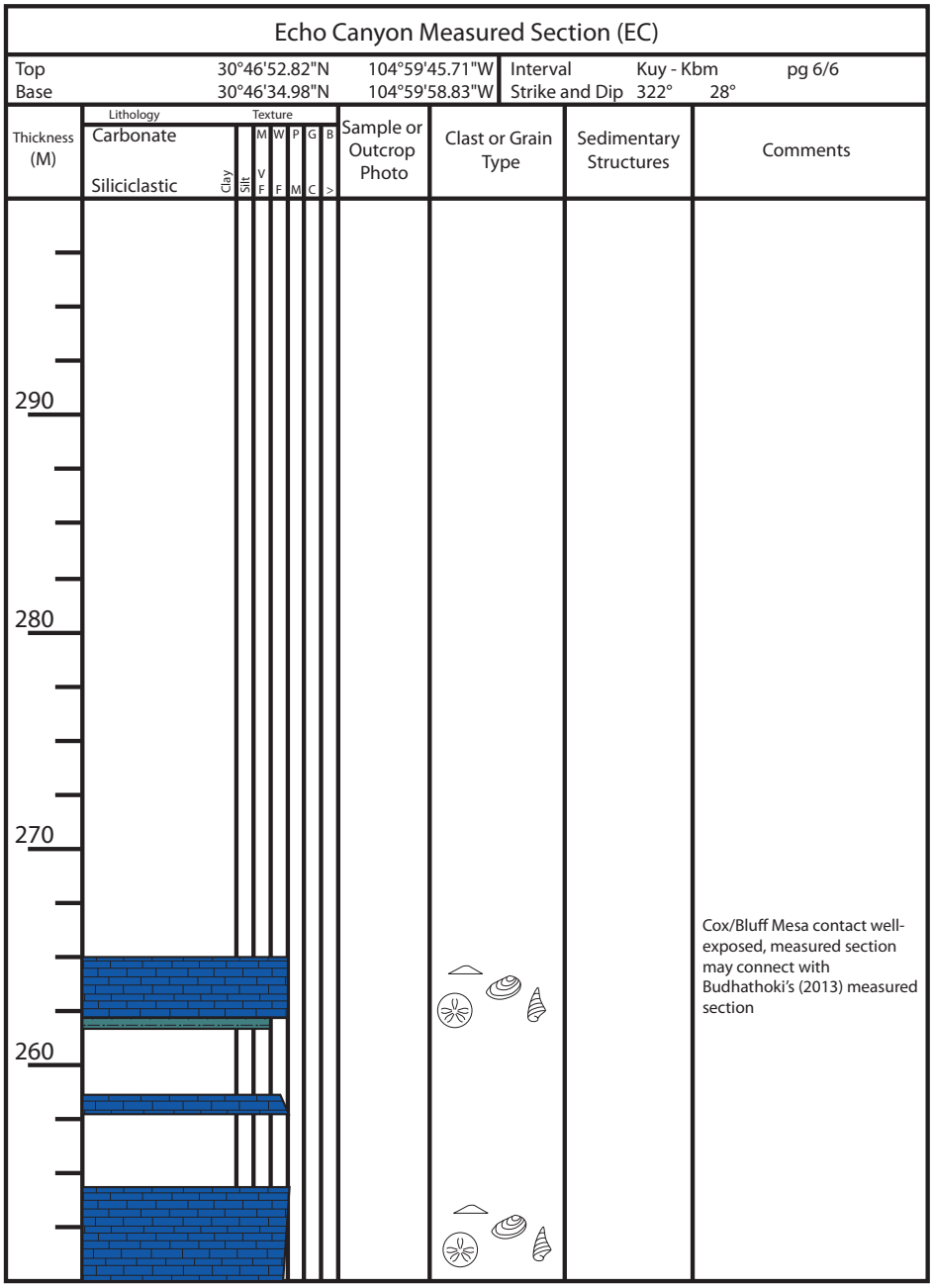
Echo Canyon Measured Section (EC)
Top 30°46'52.82"N 104°59'45.71"W
Base 30°46'34.98"N 104°59'58.83"W
Interval Kuy - Kbm pg 6/6
Strike and Dip 322° 28°
Thickness (M)
Lithology
Carbonate
Siliciclastic
Texture
Clay
Silt
M
V F
F
M
C
W
P
G
B
>
Sample or Outcrop Photo
Clast or Grain Type
Sedimentary Structures
Comments
290
280
270
260
Cox/Bluff Mesa contact well-exposed, measured section may connect with Budhathoki's (2013) measured section

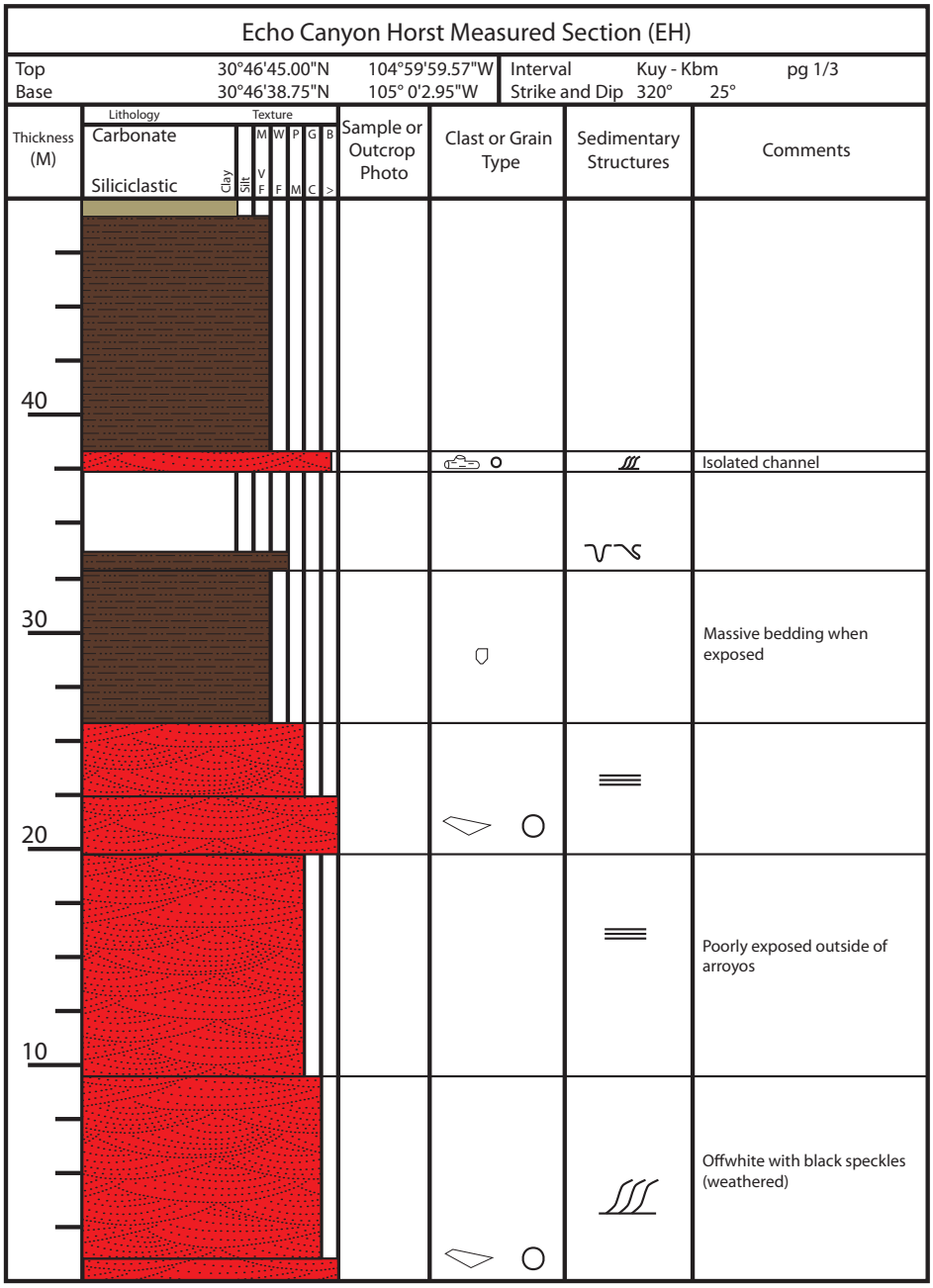
Echo Canyon Horst Measured Section (EH)
Top 30°46'45.00"N 104°59'59.57"W
Base 30°46'38.75"N 105° 0'2.95"W
Interval Kuy - Kbm pg 1/3
Strike and Dip 320° 25°
Thickness (M)
Lithology
Carbonate
Siliciclastic
Clay
Silt
Texture
M W P G B
V F F M C >
Sample or Outcrop Photo
Clast or Grain Type
Sedimentary Structures
Comments
40
30
20
10
Isolated channel
Massive bedding when exposed
Poorly exposed outside of arroyos
Offwhite with black speckles (weathered)

Echo Canyon Horst Measured Section (EH)

Top	30°46'45.00"N	104°59'59.57"W	Interval	Kuy - Kbm	pg 2/3
Base	30°46'38.75"N	105° 0'2.95"W	Strike and Dip	320°	25°

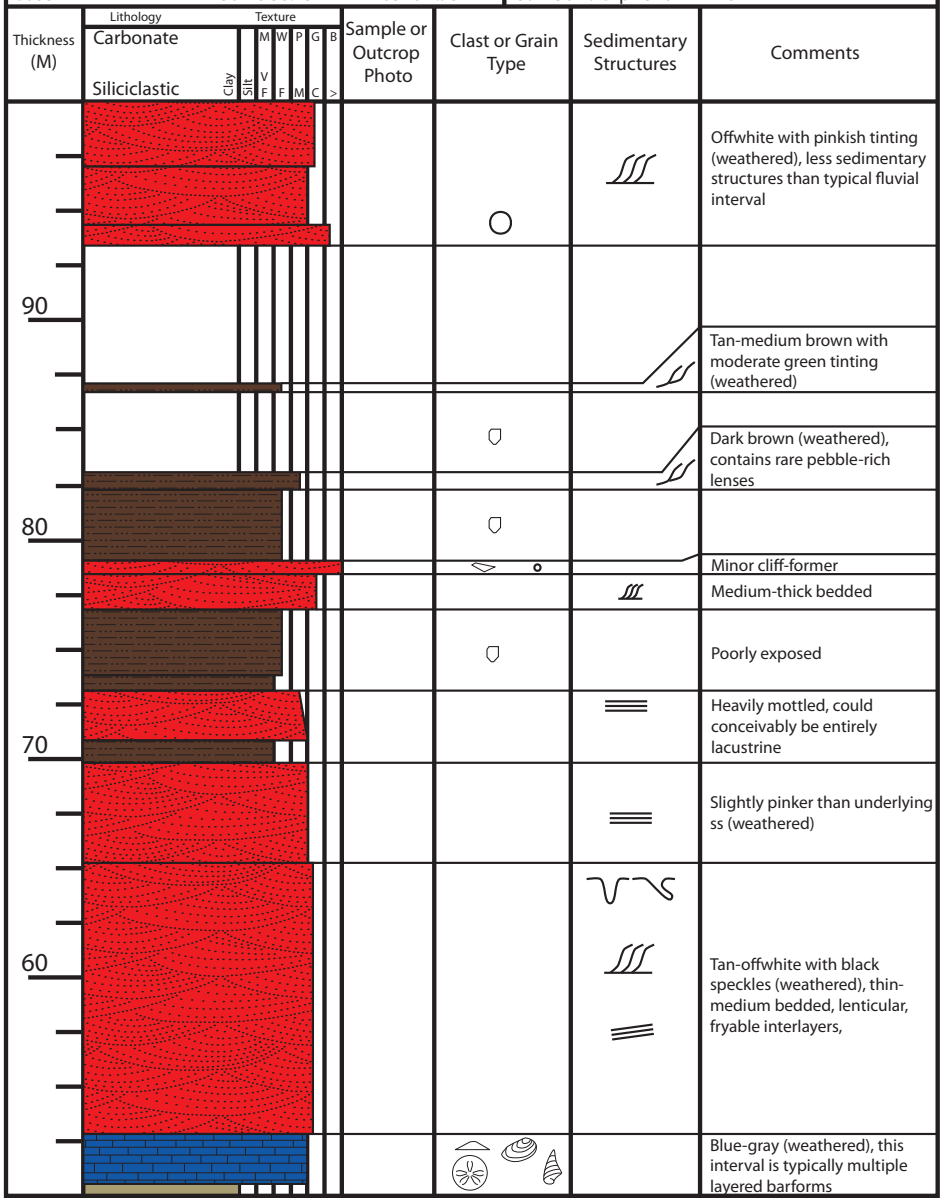

Sample or Outcrop Photo	Clast or Grain Type	Sedimentary Structures	Comments
			Offwhite with pinkish tinting (weathered), less sedimentary structures than typical fluvial interval
			Tan-medium brown with moderate green tinting (weathered)
			Dark brown (weathered), contains rare pebble-rich lenses
			Minor cliff-former
			Medium-thick bedded
			Poorly exposed
			Heavily mottled, could conceivably be entirely lacustrine
			Slightly pinker than underlying ss (weathered)
			Tan-offwhite with black speckles (weathered), thin-medium bedded, lenticular, fryable interlayers,
			Blue-gray (weathered), this interval is typically multiple layered barforms

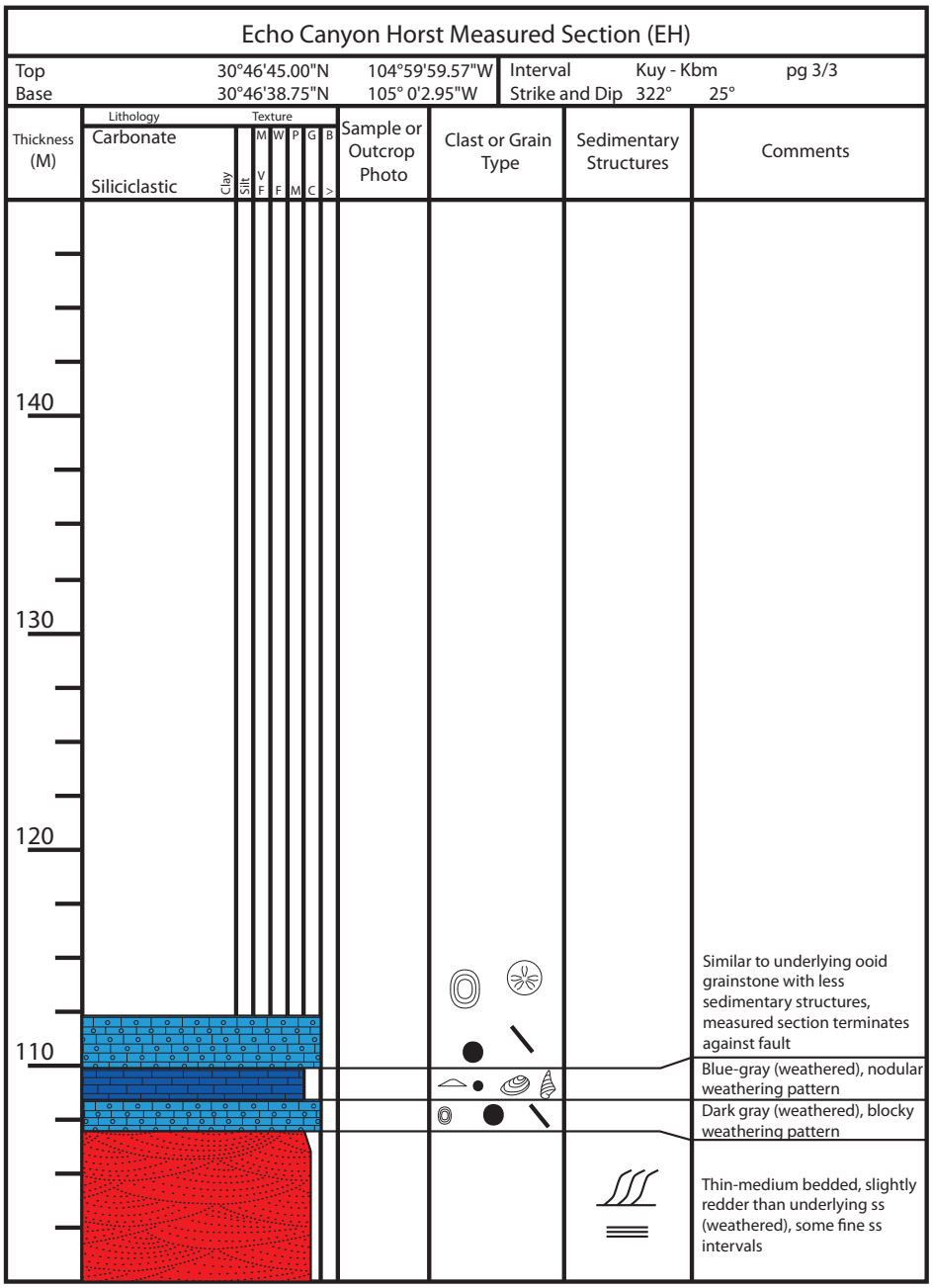
Echo Canyon Horst Measured Section (EH)
Top 30°46'45.00"N 104°59'59.57"W
Base 30°46'38.75"N 105° 0'2.95"W
Interval Kuy - Kbm pg 3/3
Strike and Dip 322° 25°
Thickness (M)
Lithology
Carbonate
Siliciclastic
Clay
Silt
Texture
M
W
P
G
B
V F
F
M
C
>
Sample or Outcrop Photo
Clast or Grain Type
Sedimentary Structures
Comments
140
130
120
110
Similar to underlying ooid grainstone with less sedimentary structures, measured section terminates against fault
Blue-gray (weathered), nodular weathering pattern
Dark gray (weathered), blocky weathering pattern
Thin-medium bedded, slightly redder than underlying ss (weathered), some fine ss intervals

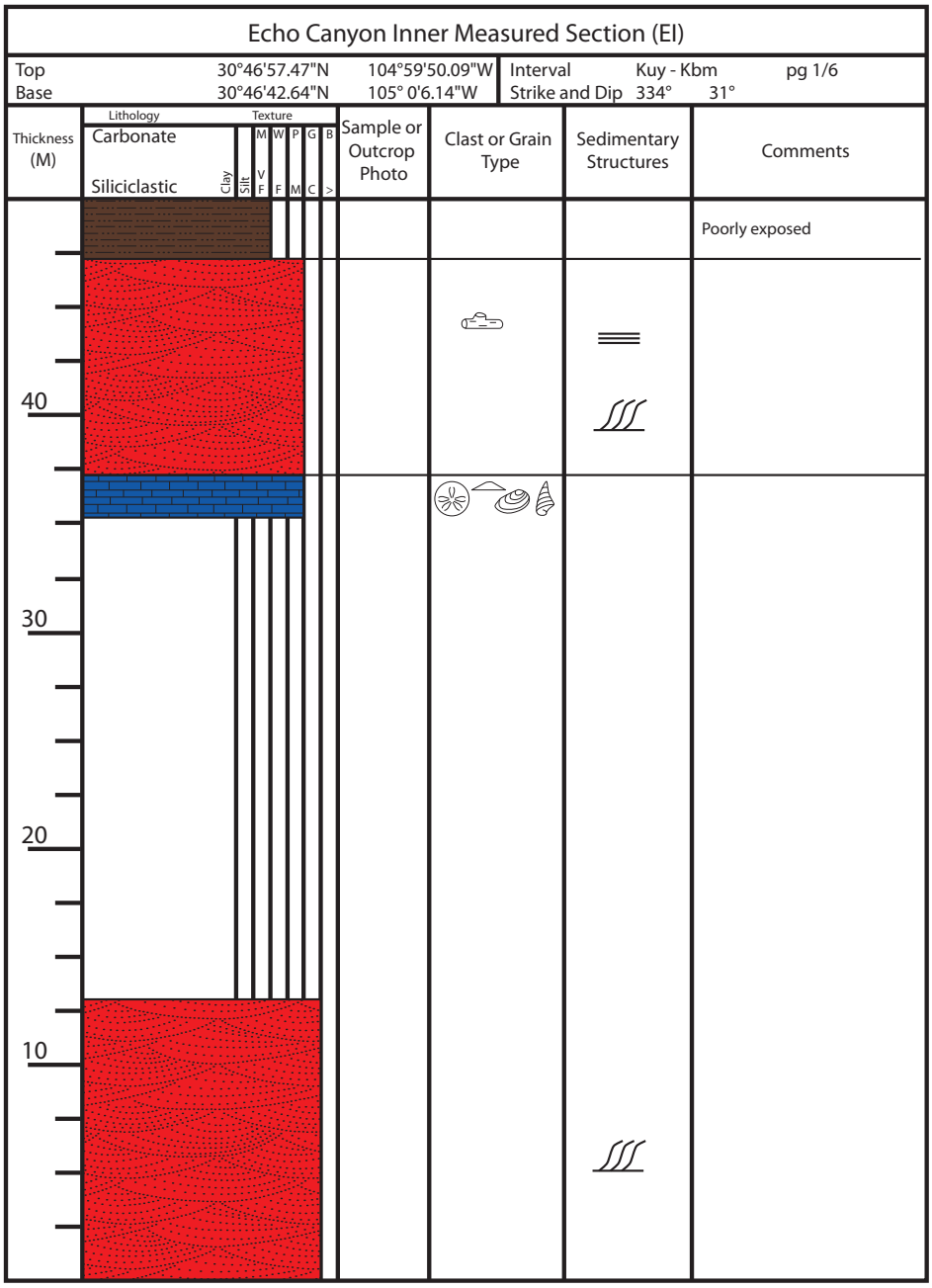
Echo Canyon Inner Measured Section (EI)
Top 30°46'57.47"N 104°59'50.09"W
Base 30°46'42.64"N 105° 0'6.14"W
Interval Kuy - Kbm pg 1/6
Strike and Dip 334° 31°
Thickness (M)
Lithology
Carbonate
Siliciclastic
Clay
Silt
Texture
M
V F
F
M
C
G
>
B
Sample or Outcrop Photo
Clast or Grain Type
Sedimentary Structures
Comments
Poorly exposed
40
30
20
10

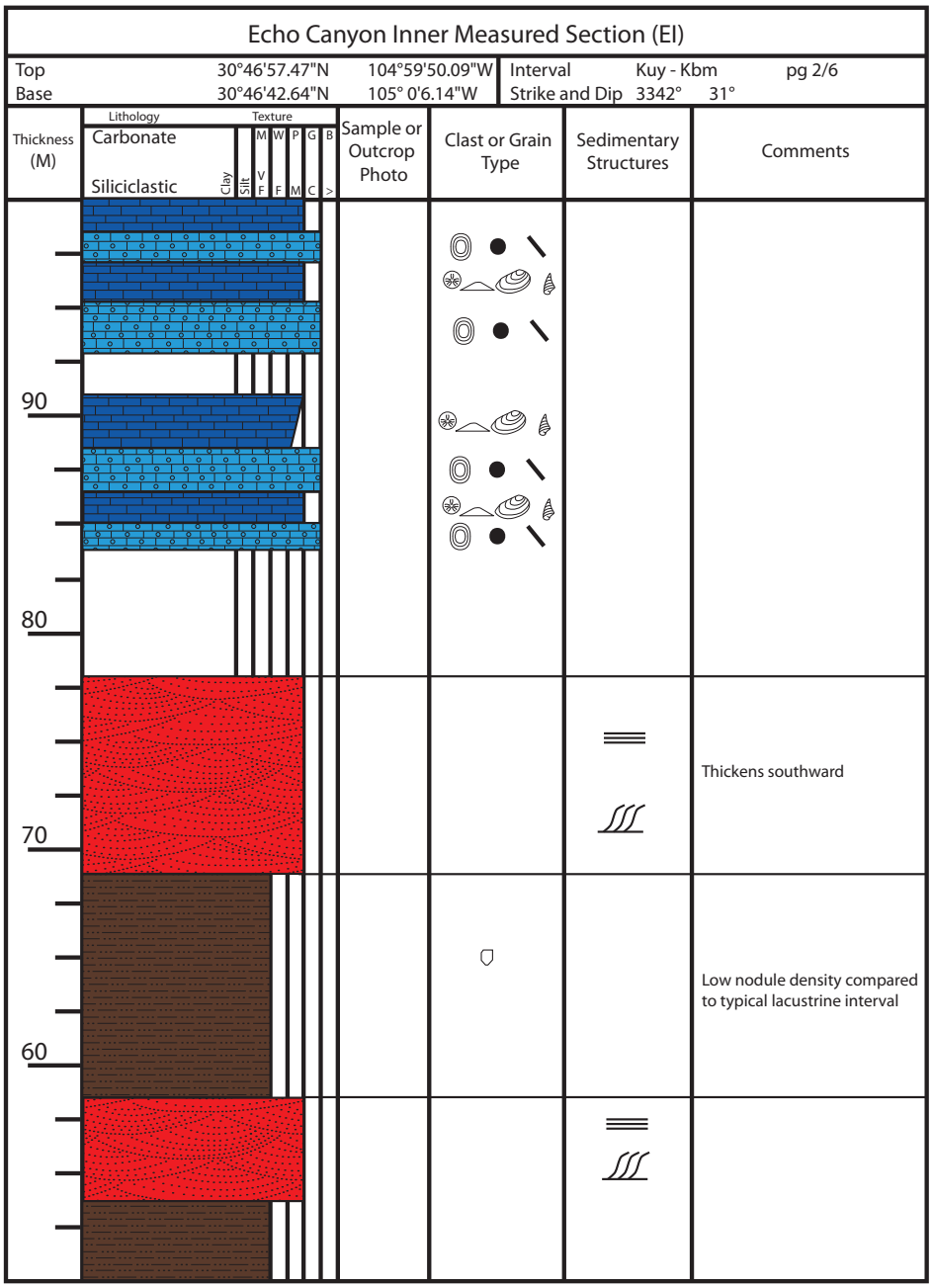
Echo Canyon Inner Measured Section (EI)
Top 30°46'57.47"N 104°59'50.09"W
Base 30°46'42.64"N 105° 0'6.14"W
Interval Kuy - Kbm pg 2/6
Strike and Dip 3342° 31°
Thickness (M)
Lithology
Carbonate
Siliciclastic
Clay
Silt
Texture
M W P G B
V F F M C >
Sample or Outcrop Photo
Clast or Grain Type
Sedimentary Structures
Comments
90
80
70
60
Thickens southward
Low nodule density compared to typical lacustrine interval

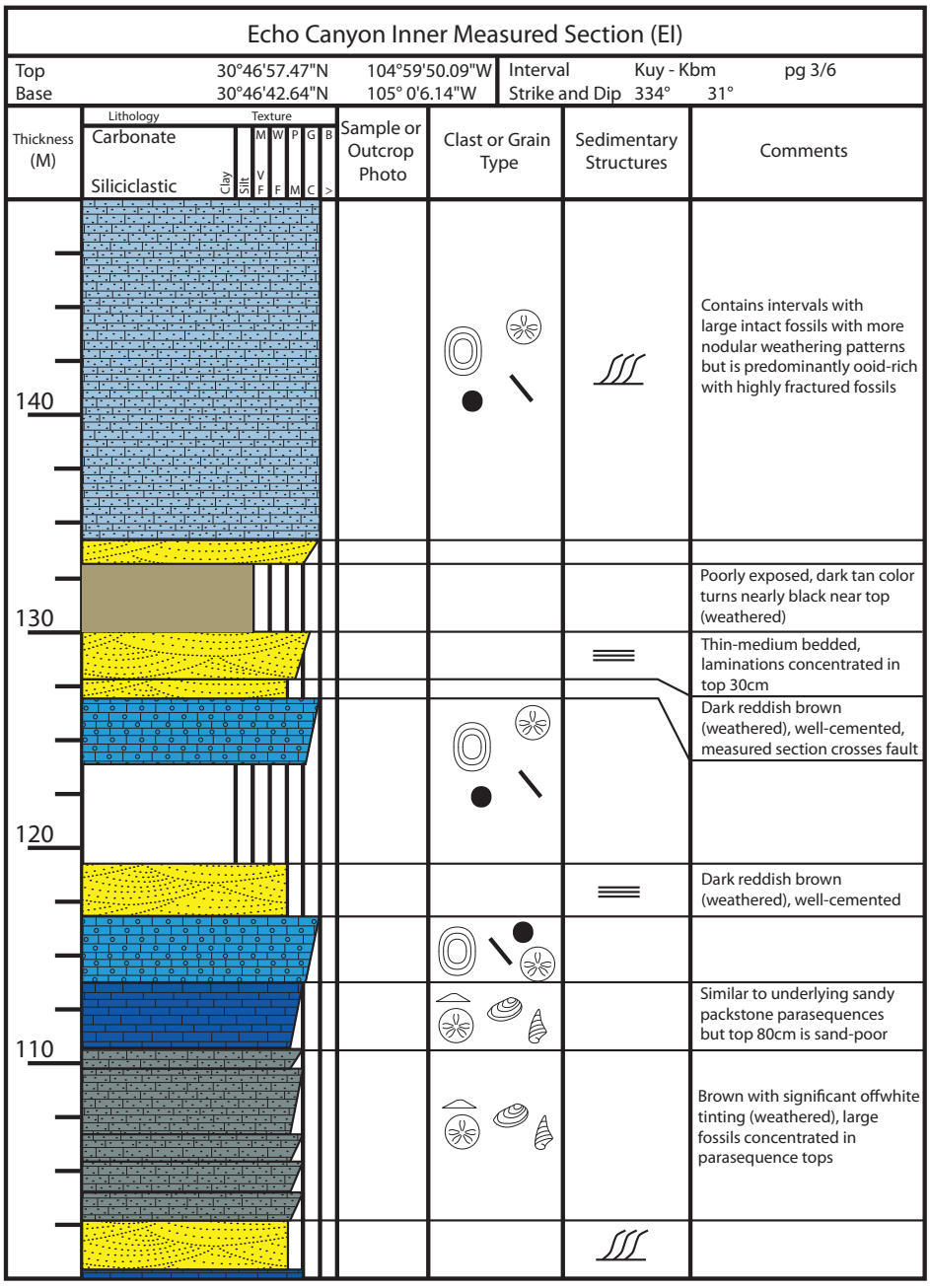
Echo Canyon Inner Measured Section (EI)
Top 30°46'57.47"N 104°59'50.09"W
Base 30°46'42.64"N 105° 0'6.14"W
Interval Kuy - Kbm pg 3/6
Strike and Dip 334° 31°
Thickness (M)
Lithology
Carbonate
Siliciclastic
Clay
Silt
Texture
M
W
P
G
B
V F
F
M
C
>
Sample or Outcrop Photo
Clast or Grain Type
Sedimentary Structures
Comments
140
130
120
110
Contains intervals with large intact fossils with more nodular weathering patterns but is predominantly ooid-rich with highly fractured fossils
Poorly exposed, dark tan color turns nearly black near top (weathered)
Thin-medium bedded, laminations concentrated in top 30cm
Dark reddish brown (weathered), well-cemented, measured section crosses fault
Dark reddish brown (weathered), well-cemented
Similar to underlying sandy packstone parasequences but top 80cm is sand-poor
Brown with significant offwhite tinting (weathered), large fossils concentrated in parasequence tops

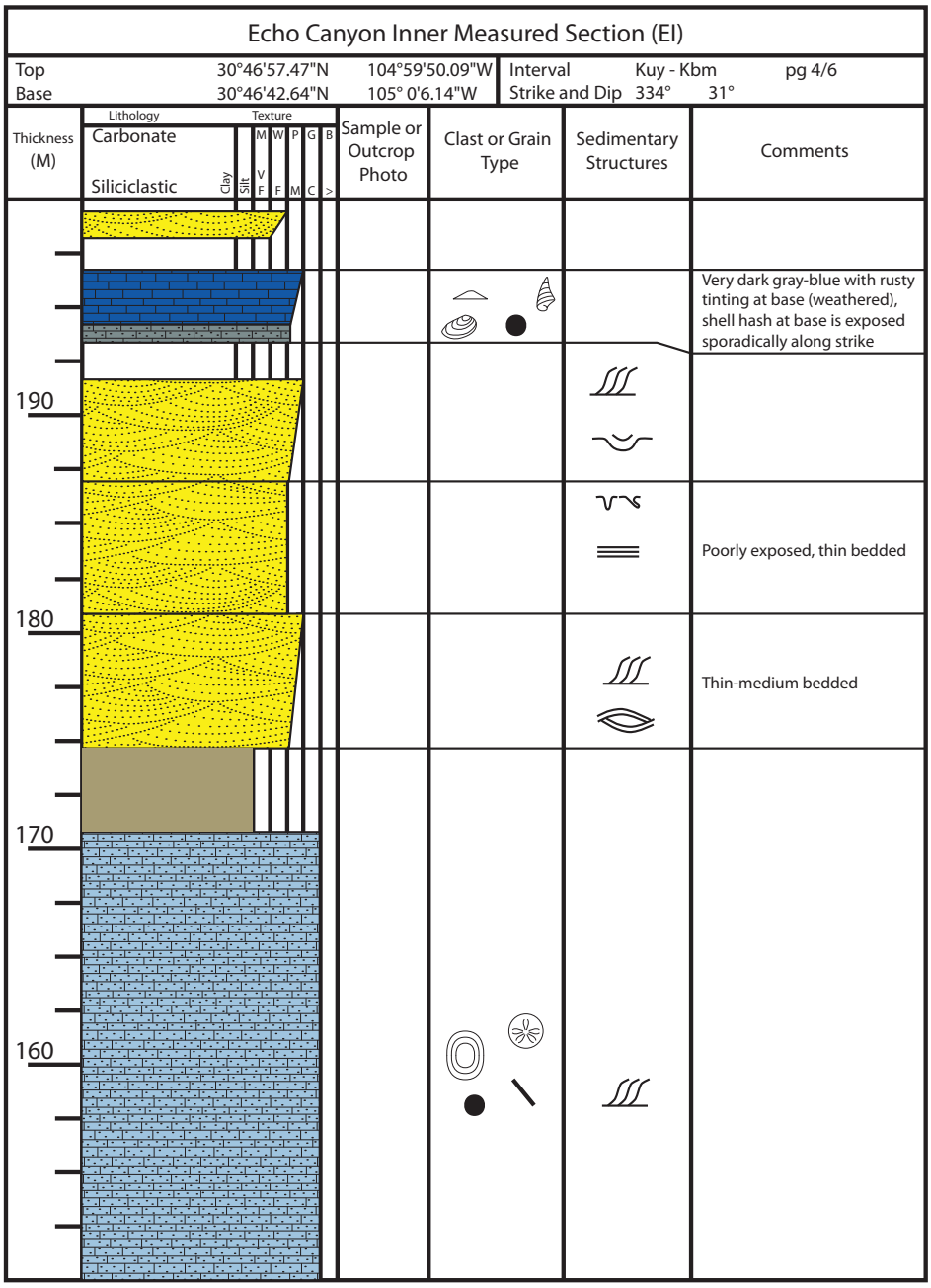
Echo Canyon Inner Measured Section (EI)
Top 30°46'57.47"N 104°59'50.09"W
Base 30°46'42.64"N 105° 0'6.14"W
Interval Kuy - Kbm pg 4/6
Strike and Dip 334° 31°
Thickness (M)
Lithology
Carbonate
Siliciclastic
Texture
Clay
Silt
M
V F
F
M
C
>
W
P
G
B
Sample or Outcrop Photo
Clast or Grain Type
Sedimentary Structures
Comments
190
180
170
160
Very dark gray-blue with rusty tinting at base (weathered), shell hash at base is exposed sporadically along strike
Poorly exposed, thin bedded
Thin-medium bedded

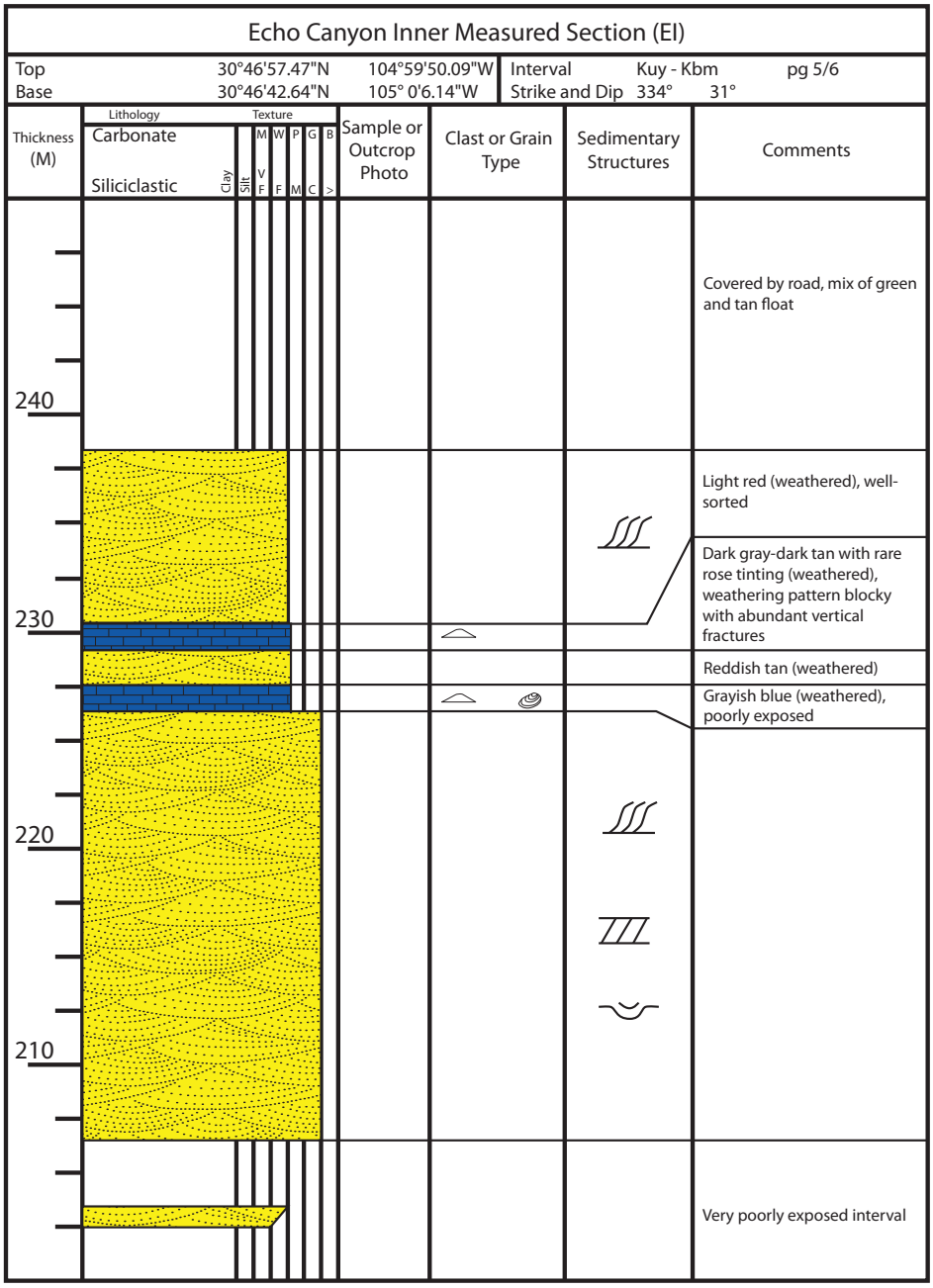
Echo Canyon Inner Measured Section (EI)
Top 30°46'57.47"N 104°59'50.09"W
Base 30°46'42.64"N 105° 0'6.14"W
Interval Kuy - Kbm pg 5/6
Strike and Dip 334° 31°
Thickness (M)
Lithology
Carbonate
Siliciclastic
Texture
Clay
Silt
M
V F
F
M
C
W
P
G
B
>
Sample or Outcrop Photo
Clast or Grain Type
Sedimentary Structures
Comments
240
230
220
210
Covered by road, mix of green and tan float
Light red (weathered), well-sorted
Dark gray-dark tan with rare rose tinting (weathered), weathering pattern blocky with abundant vertical fractures
Reddish tan (weathered)
Grayish blue (weathered), poorly exposed
Very poorly exposed interval

Echo Canyon Inner Measured Section (EI)

Top	30°46'57.47"N	104°59'50.09"W	Interval	Kuy - Kbm
Base	30°46'42.64"N	105° 0'6.14"W	Strike and Dip	334° 31°

pg 6/6

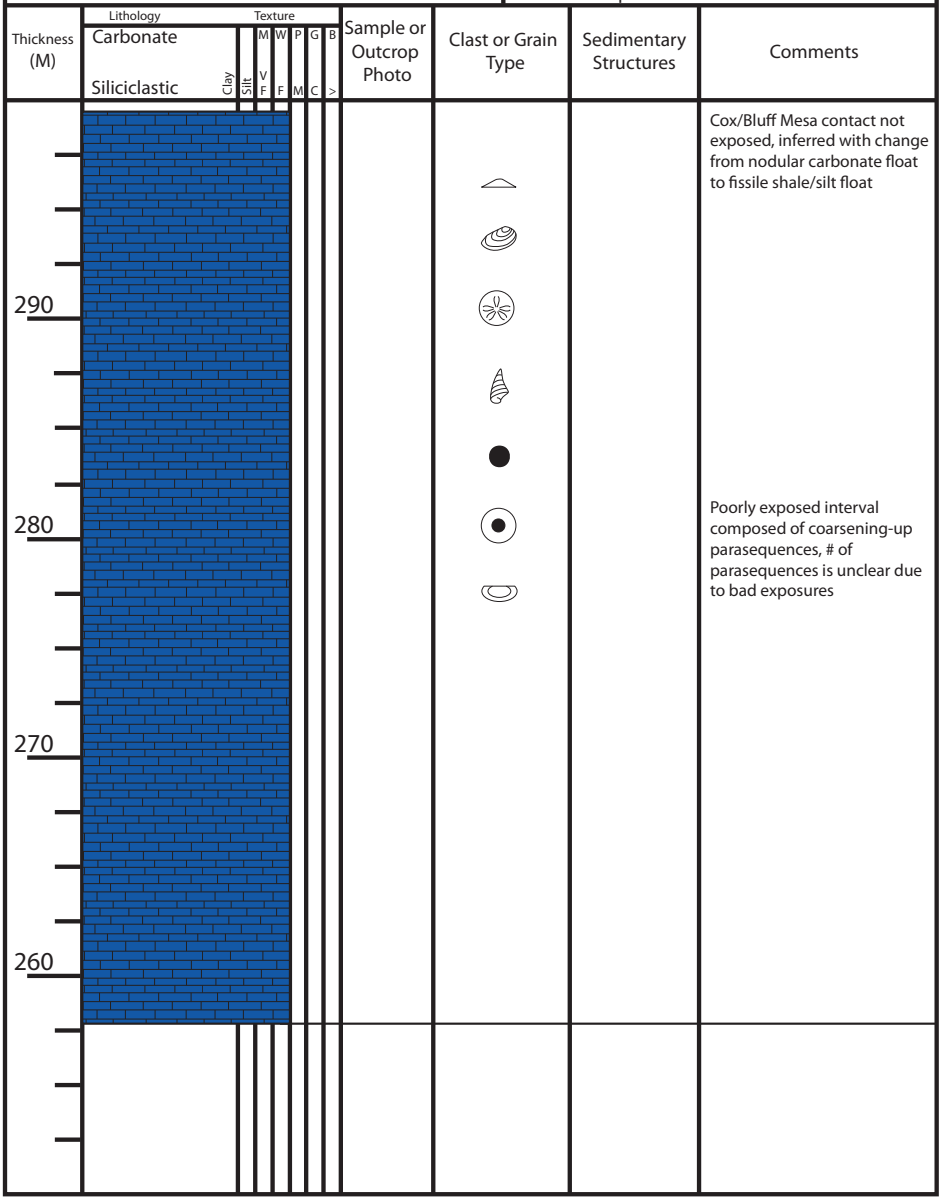

Sample or Outcrop Photo	Clast or Grain Type	Sedimentary Structures	Comments
			Cox/Bluff Mesa contact not exposed, inferred with change from nodular carbonate float to fissile shale/silt float
			Poorly exposed interval composed of coarsening-up parasequences, # of parasequences is unclear due to bad exposures

Middle Measured Section (M)

Top	30°47'14.05"N	105° 0'4.58"W	Interval	Kuy - Kbm	pg 1/7
Base	30°46'59.11"N	105° 0'24.32"W	Strike and Dip	335°	31°

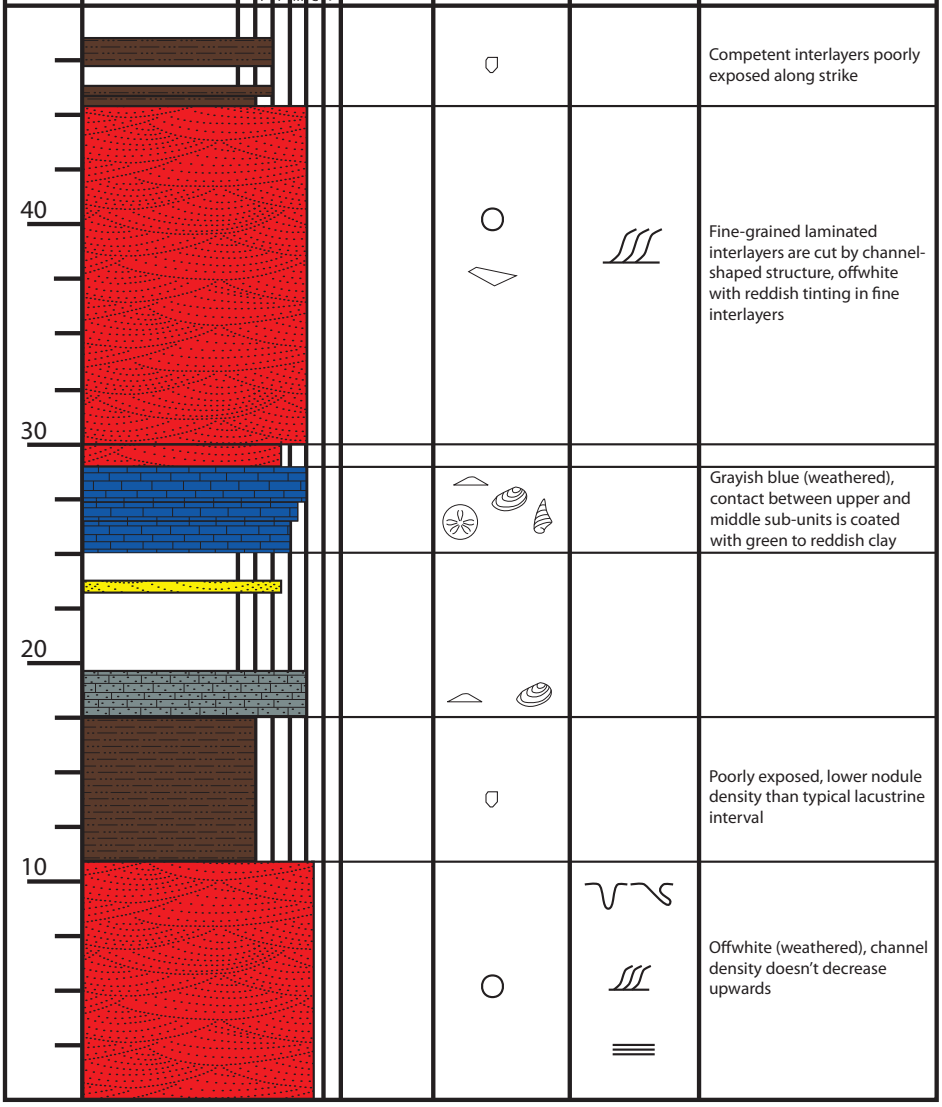

Sample or Outcrop Photo	Clast or Grain Type	Sedimentary Structures	Comments
			Competent interlayers poorly exposed along strike
			Fine-grained laminated interlayers are cut by channel-shaped structure, offwhite with reddish tinting in fine interlayers
			Grayish blue (weathered), contact between upper and middle sub-units is coated with green to reddish clay
			Poorly exposed, lower nodule density than typical lacustrine interval
			Offwhite (weathered), channel density doesn't decrease upwards

Middle Measured Section (M)

Top	30°47'14.05"N	105° 0'4.58"W	Interval	Kuy - Kbm	pg 2/7
Base	30°46'59.11"N	105° 0'24.32"W	Strike and Dip	335°	31°

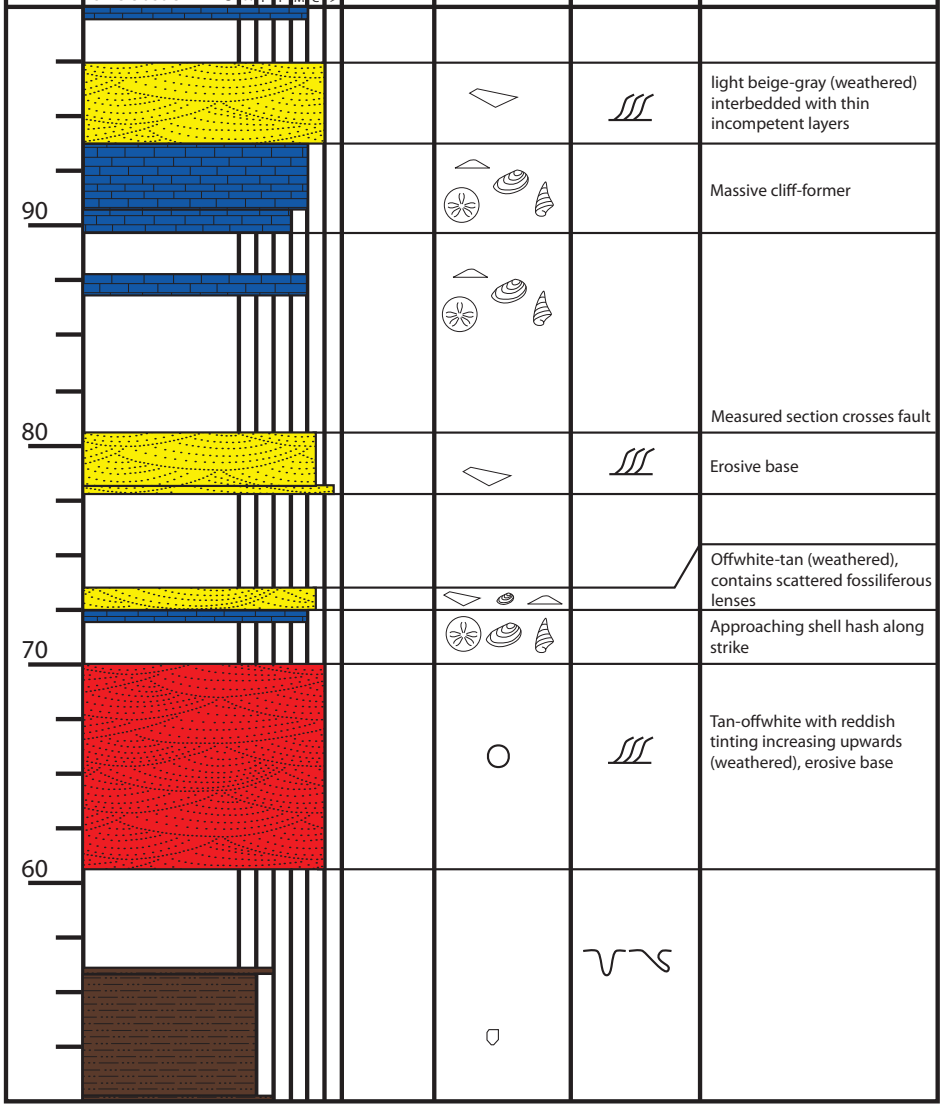

Middle Measured Section (M)

Top	30°47'14.05"N	105° 0'4.58"W	Interval	Kuy - Kbm	pg 3/7
Base	30°46'59.11"N	105° 0'24.32"W	Strike and Dip	335°	31°

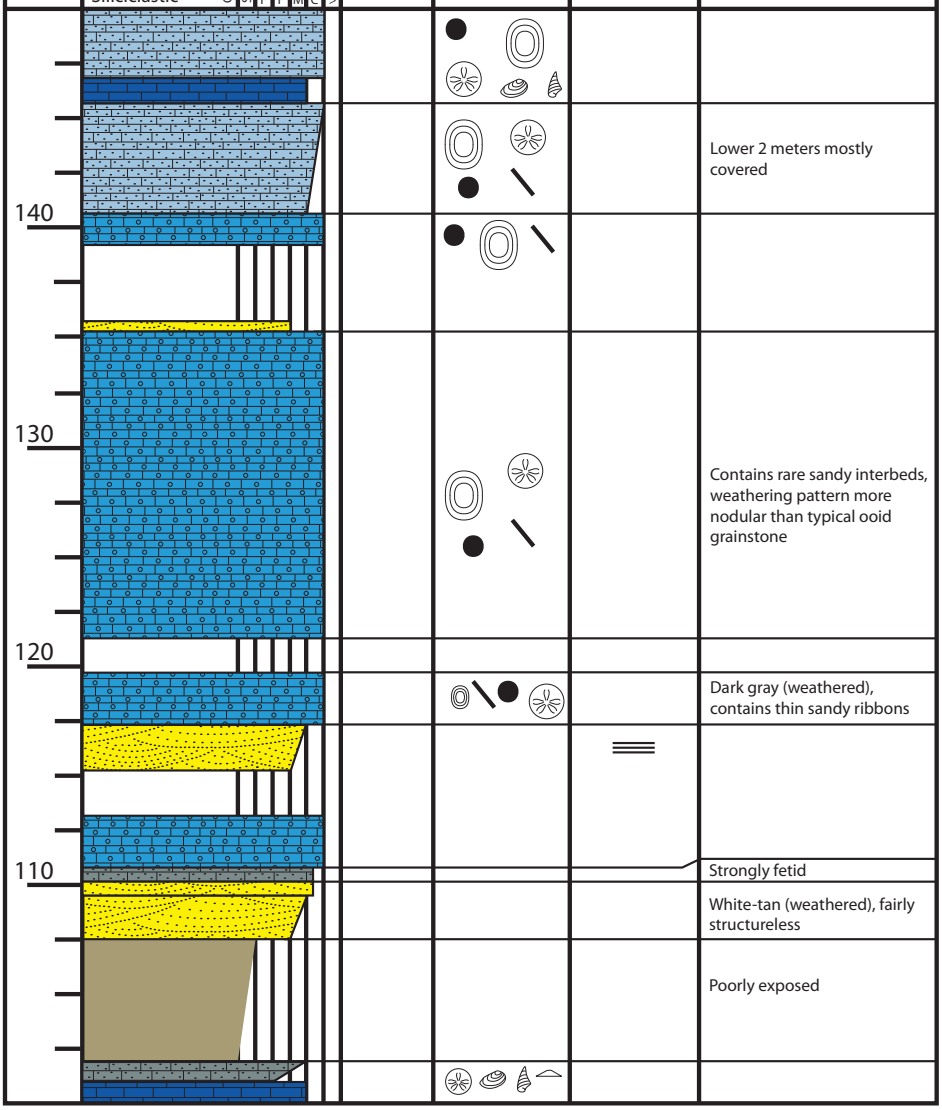

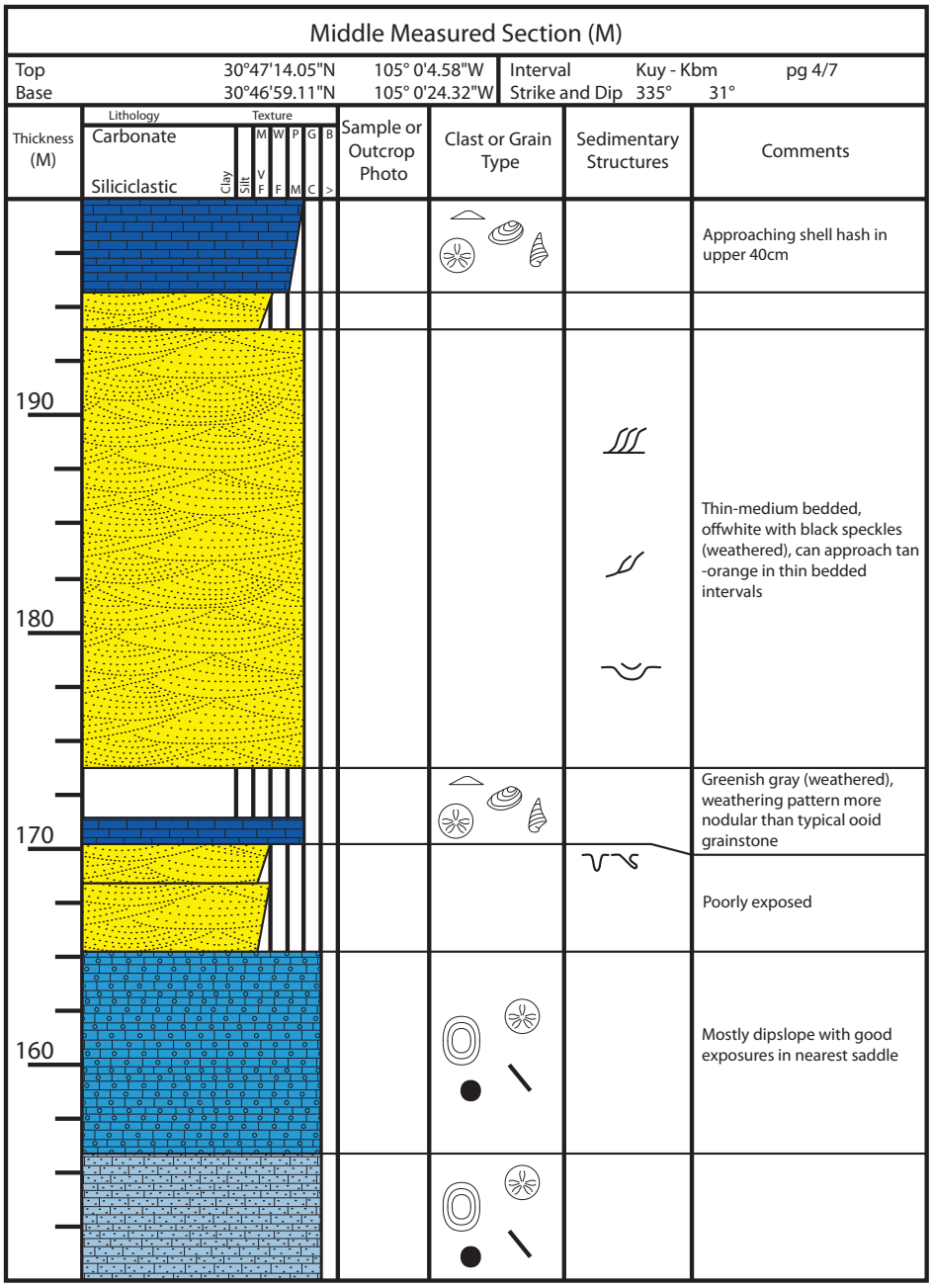
Middle Measured Section (M)
Top 30°47'14.05"N 105° 0'4.58"W
Base 30°46'59.11"N 105° 0'24.32"W
Interval Kuy - Kbm pg 4/7
Strike and Dip 335° 31°
Thickness (M)
Lithology
Carbonate
Siliciclastic
Texture
Clay
Silt
M
W
P
G
B
V F
F
M
C
>
Sample or Outcrop Photo
Clast or Grain Type
Sedimentary Structures
Comments
190
180
170
160
Approaching shell hash in upper 40cm
Thin-medium bedded, offwhite with black speckles (weathered), can approach tan -orange in thin bedded intervals
Greenish gray (weathered), weathering pattern more nodular than typical ooid grainstone
Poorly exposed
Mostly dipslope with good exposures in nearest saddle

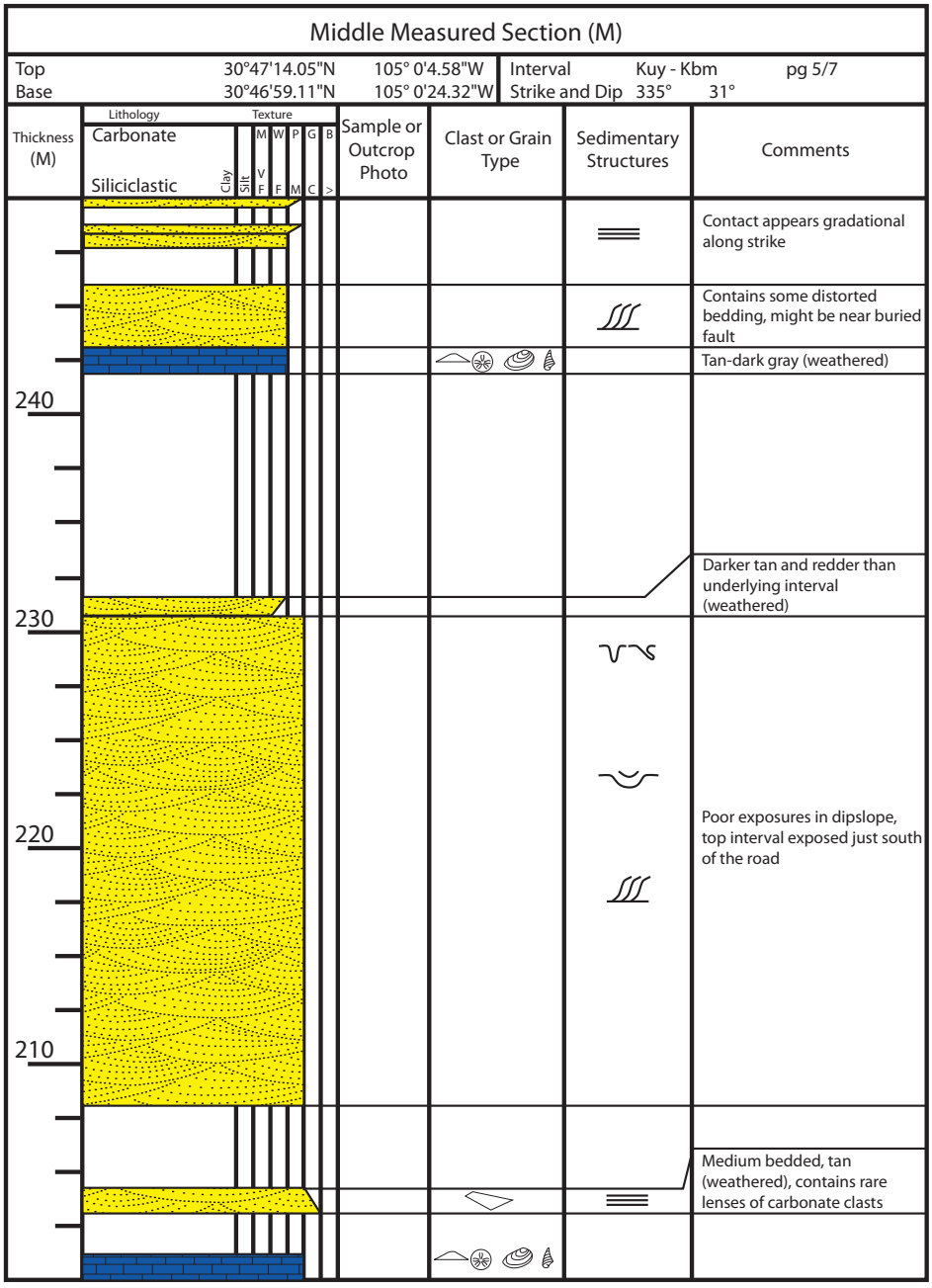
Middle Measured Section (M)
Top 30°47'14.05"N 105° 0'4.58"W
Base 30°46'59.11"N 105° 0'24.32"W
Interval Kuy - Kbm pg 5/7
Strike and Dip 335° 31°
Thickness (M)
Lithology
Carbonate
Siliciclastic
Clay
Silt
Texture
M W P G B
V F F M C >
Sample or Outcrop Photo
Clast or Grain Type
Sedimentary Structures
Comments
240
230
220
210
Contact appears gradational along strike
Contains some distorted bedding, might be near buried fault
Tan-dark gray (weathered)
Darker tan and redder than underlying interval (weathered)
Poor exposures in dipslope, top interval exposed just south of the road
Medium bedded, tan (weathered), contains rare lenses of carbonate clasts

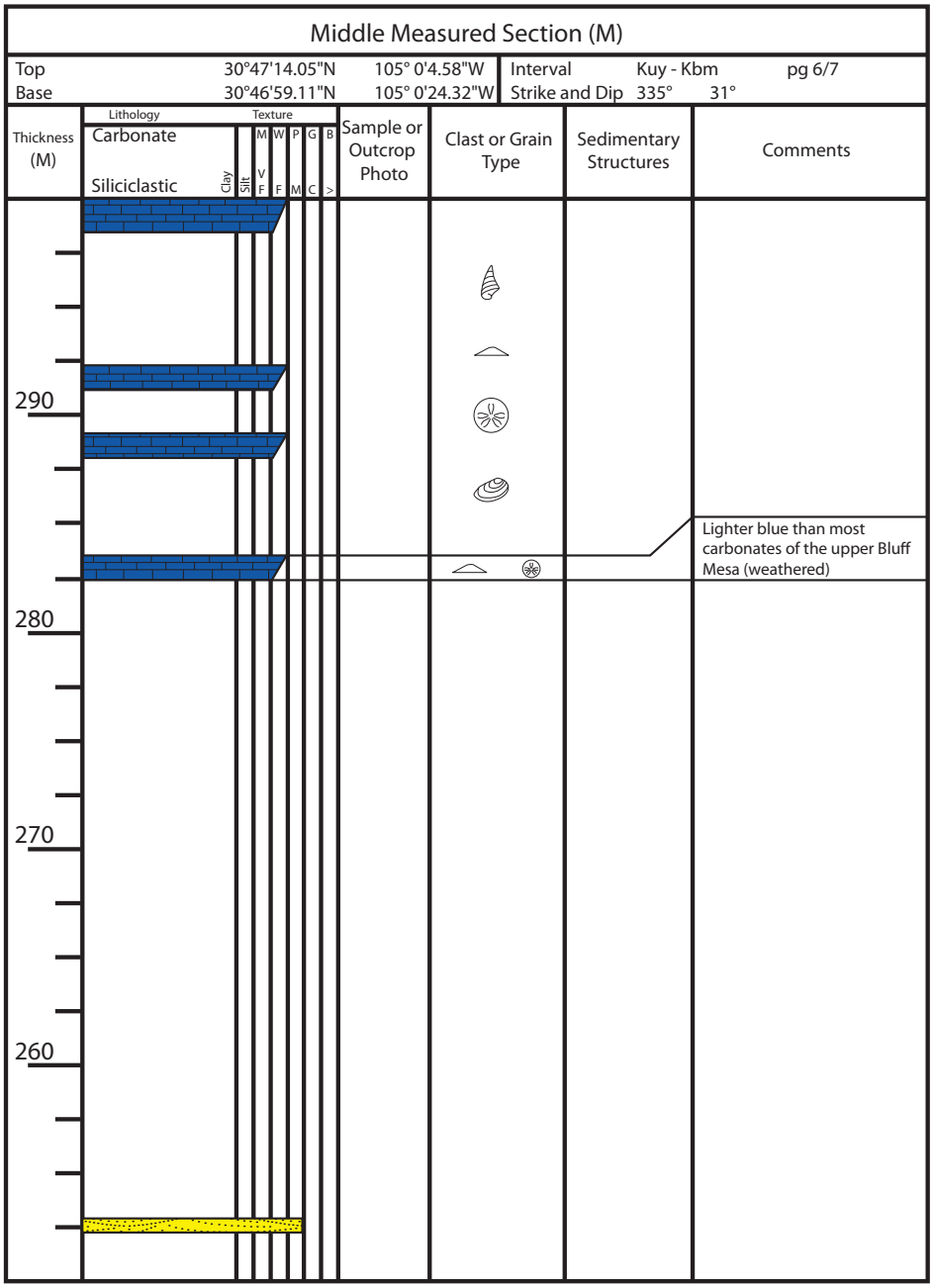
Middle Measured Section (M)
Top 30°47'14.05"N 105° 0'4.58"W
Base 30°46'59.11"N 105° 0'24.32"W
Interval Kuy - Kbm pg 6/7
Strike and Dip 335° 31°
Thickness (M)
Lithology
Carbonate
Siliciclastic
Clay
Silt
Texture
M W P G B
V F F M C >
Sample or Outcrop Photo
Clast or Grain Type
Sedimentary Structures
Comments
290
280
270
260
Lighter blue than most carbonates of the upper Bluff Mesa (weathered)

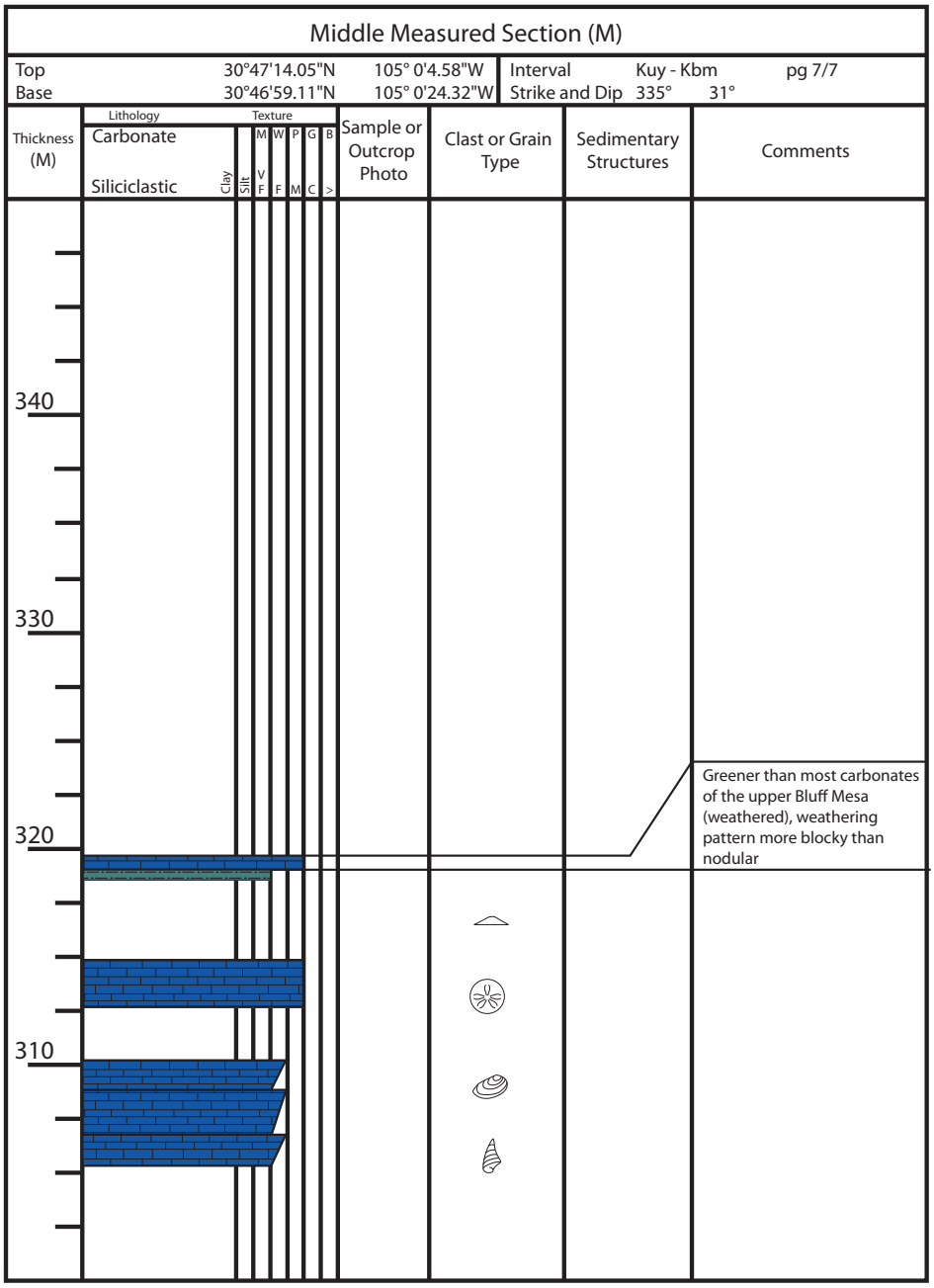
Middle Measured Section (M)
Top 30°47'14.05"N 105° 0'4.58"W
Base 30°46'59.11"N 105° 0'24.32"W
Interval Kuy - Kbm pg 7/7
Strike and Dip 335° 31°
Thickness (M)
Lithology
Carbonate
Siliciclastic
Clay
Silt
Texture
M
W
P
G
B
V F
F
M
C
>
Sample or Outcrop Photo
Clast or Grain Type
Sedimentary Structures
Comments
340
330
320
310
Greener than most carbonates of the upper Bluff Mesa (weathered), weathering pattern more blocky than nodular

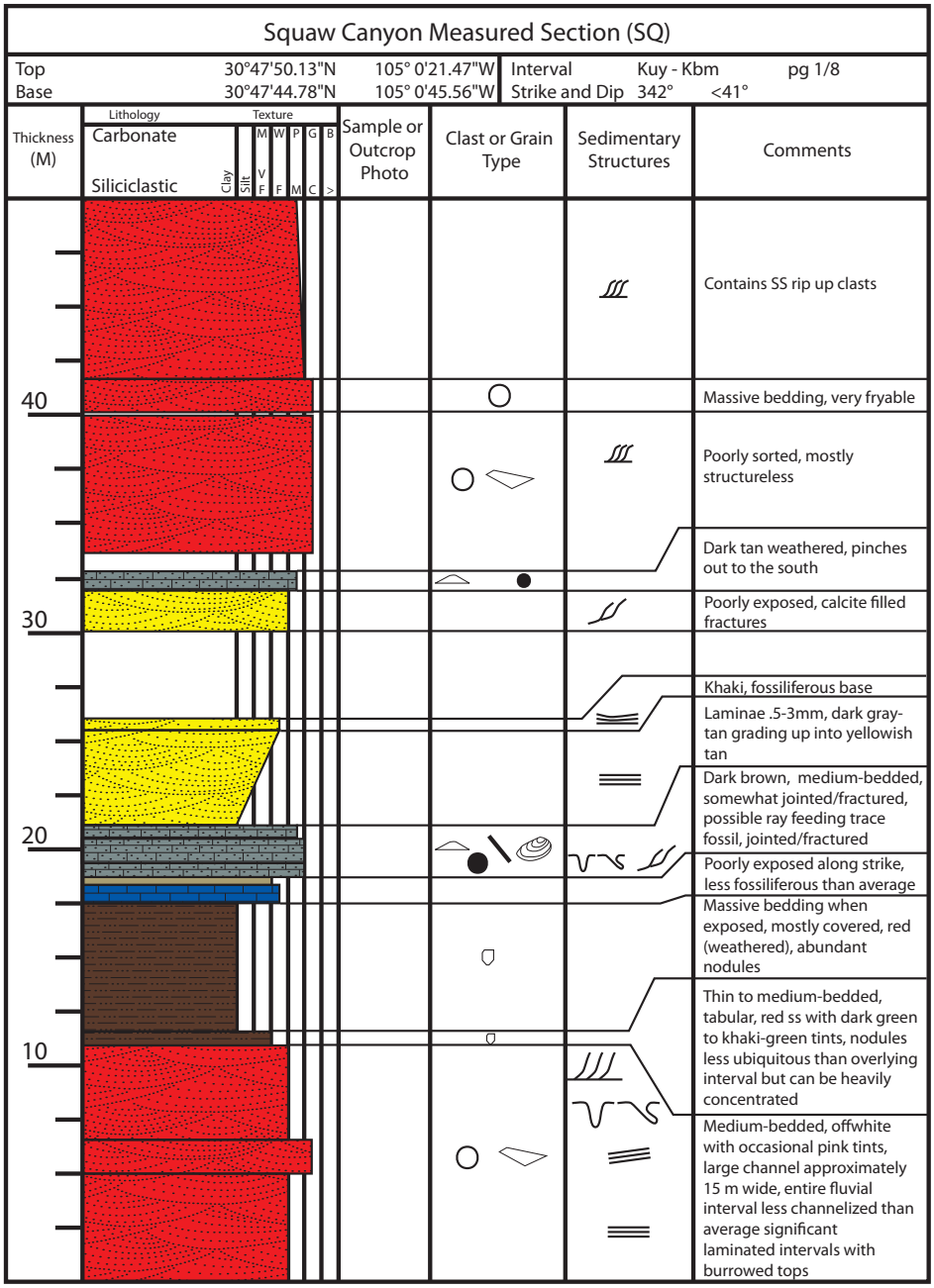
Squaw Canyon Measured Section (SQ)
Top 30°47'50.13"N 105° 0'21.47"W
Base 30°47'44.78"N 105° 0'45.56"W
Interval Kuy - Kbm pg 1/8
Strike and Dip 342° <41°
Thickness (M)
Lithology
Carbonate
Siliciclastic
Clay
Silt
Texture
M W P G B
V F F M C >
Sample or Outcrop Photo
Clast or Grain Type
Sedimentary Structures
Comments
40
30
20
10
Contains SS rip up clasts
Massive bedding, very fryable
Poorly sorted, mostly structureless
Dark tan weathered, pinches out to the south
Poorly exposed, calcite filled fractures
Khaki, fossiliferous base
Laminae .5-3mm, dark gray-tan grading up into yellowish tan
Dark brown, medium-bedded, somewhat jointed/fractured, possible ray feeding trace fossil, jointed/fractured
Poorly exposed along strike, less fossiliferous than average
Massive bedding when exposed, mostly covered, red (weathered), abundant nodules
Thin to medium-bedded, tabular, red ss with dark green to khaki-green tints, nodules less ubiquitous than overlying interval but can be heavily concentrated
Medium-bedded, offwhite with occasional pink tints, large channel approximately 15 m wide, entire fluvial interval less channelized than average significant laminated intervals with burrowed tops

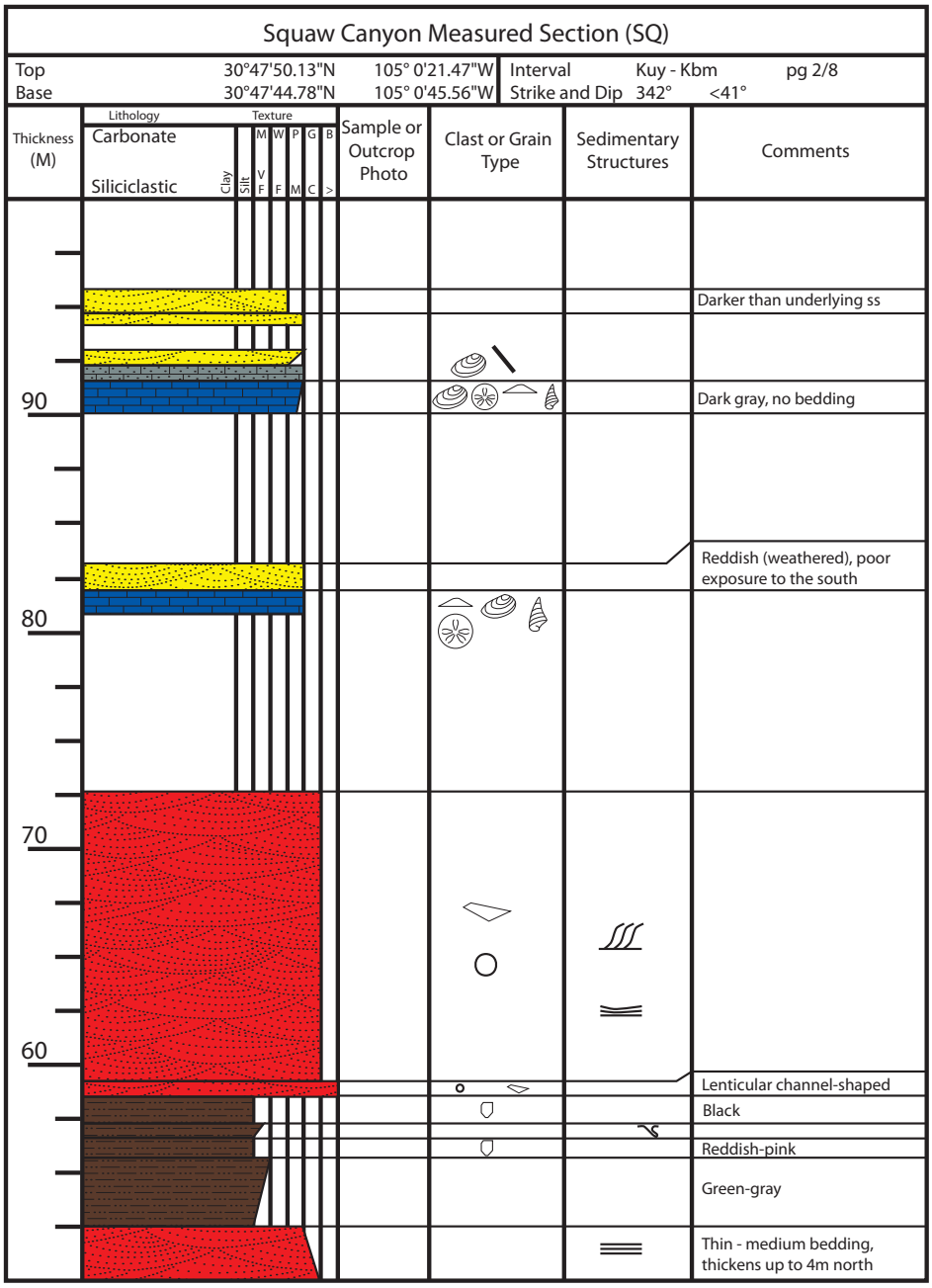
Squaw Canyon Measured Section (SQ)
Top 30°47'50.13"N 105° 0'21.47"W
Base 30°47'44.78"N 105° 0'45.56"W
Interval Kuy - Kbm pg 2/8
Strike and Dip 342° <41°
Thickness (M)
Lithology
Carbonate
Siliciclastic
Clay
Silt
Texture
M W P G B
V F F M C >
Sample or Outcrop Photo
Clast or Grain Type
Sedimentary Structures
Comments
90
80
70
60
Darker than underlying ss
Dark gray, no bedding
Reddish (weathered), poor exposure to the south
Lenticular channel-shaped
Black
Reddish-pink
Green-gray
Thin - medium bedding, thickens up to 4m north

Squaw Canyon Measured Section (SQ)

Top	30°47'50.13"N	105° 0'21.47"W	Interval	Kuy - Kbm	pg 3/8
Base	30°47'44.78"N	105° 0'45.56"W	Strike and Dip	342°	<41°

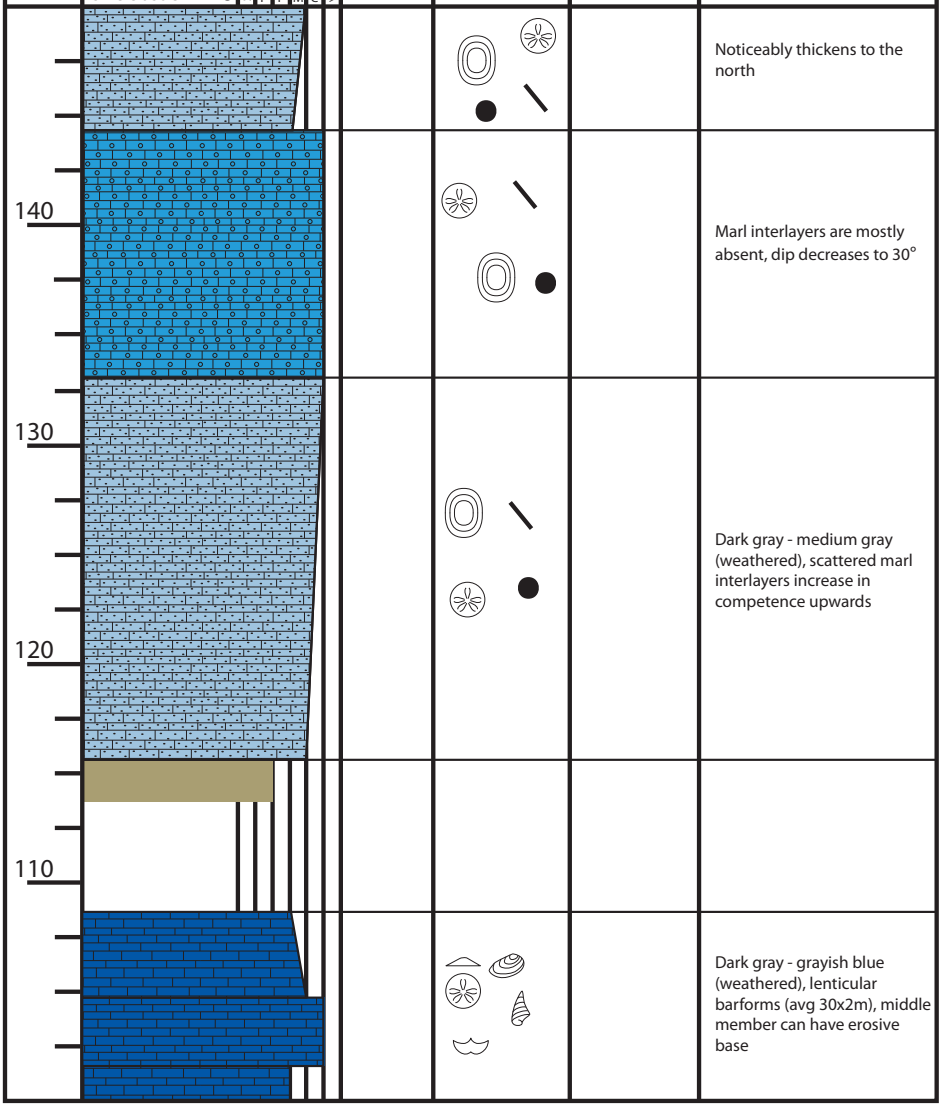

Squaw Canyon Measured Section (SQ)

Top	30°47'50.13"N	105° 0'21.47"W	Interval	Kuy - Kbm pg 4/8
Base	30°47'44.78"N	105° 0'45.56"W	Strike and Dip	342° <41°

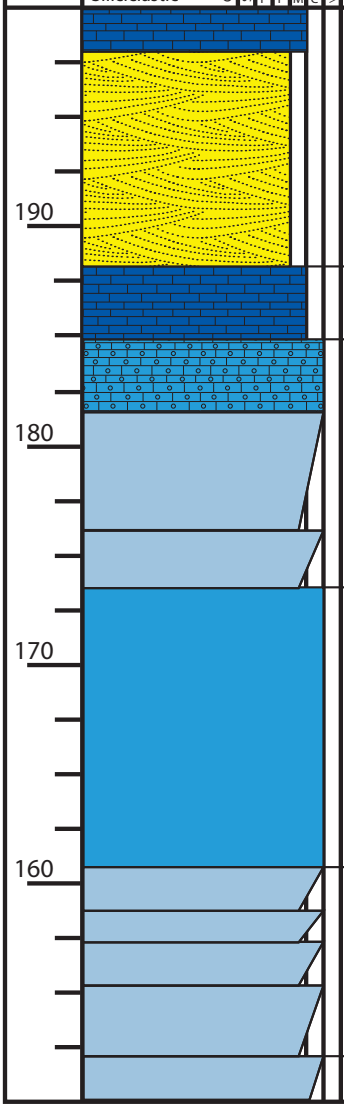

Thickness (M)	Sample or Outcrop Photo	Clast or Grain Type	Sedimentary Structures	Comments
				Top 10cm approaching shell hash
				Cross-stratification on 5-10cm and 1m scales
				Siliciclastic content decreases upwards in individual parasequences
				Noticeably thickens to the north

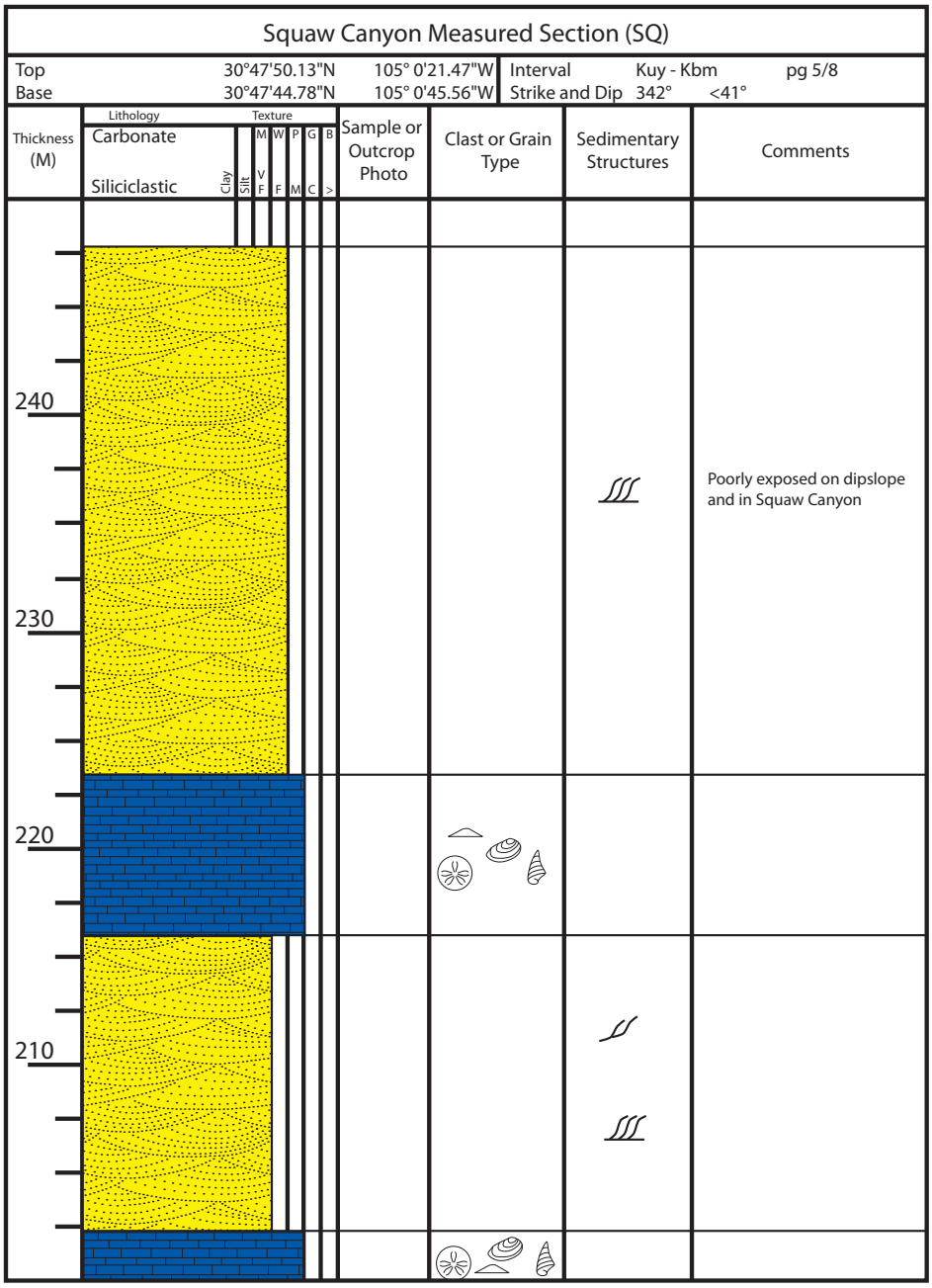
Squaw Canyon Measured Section (SQ)
Top 30°47'50.13"N 105° 0'21.47"W
Base 30°47'44.78"N 105° 0'45.56"W
Interval Kuy - Kbm pg 5/8
Strike and Dip 342° <41°
Thickness (M)
Lithology
Carbonate
Siliciclastic
Texture
Clay
Silt
M
V F
F
M
C
W
P
G
B
>
Sample or Outcrop Photo
Clast or Grain Type
Sedimentary Structures
Comments
240
230
220
210
Poorly exposed on dipslope and in Squaw Canyon

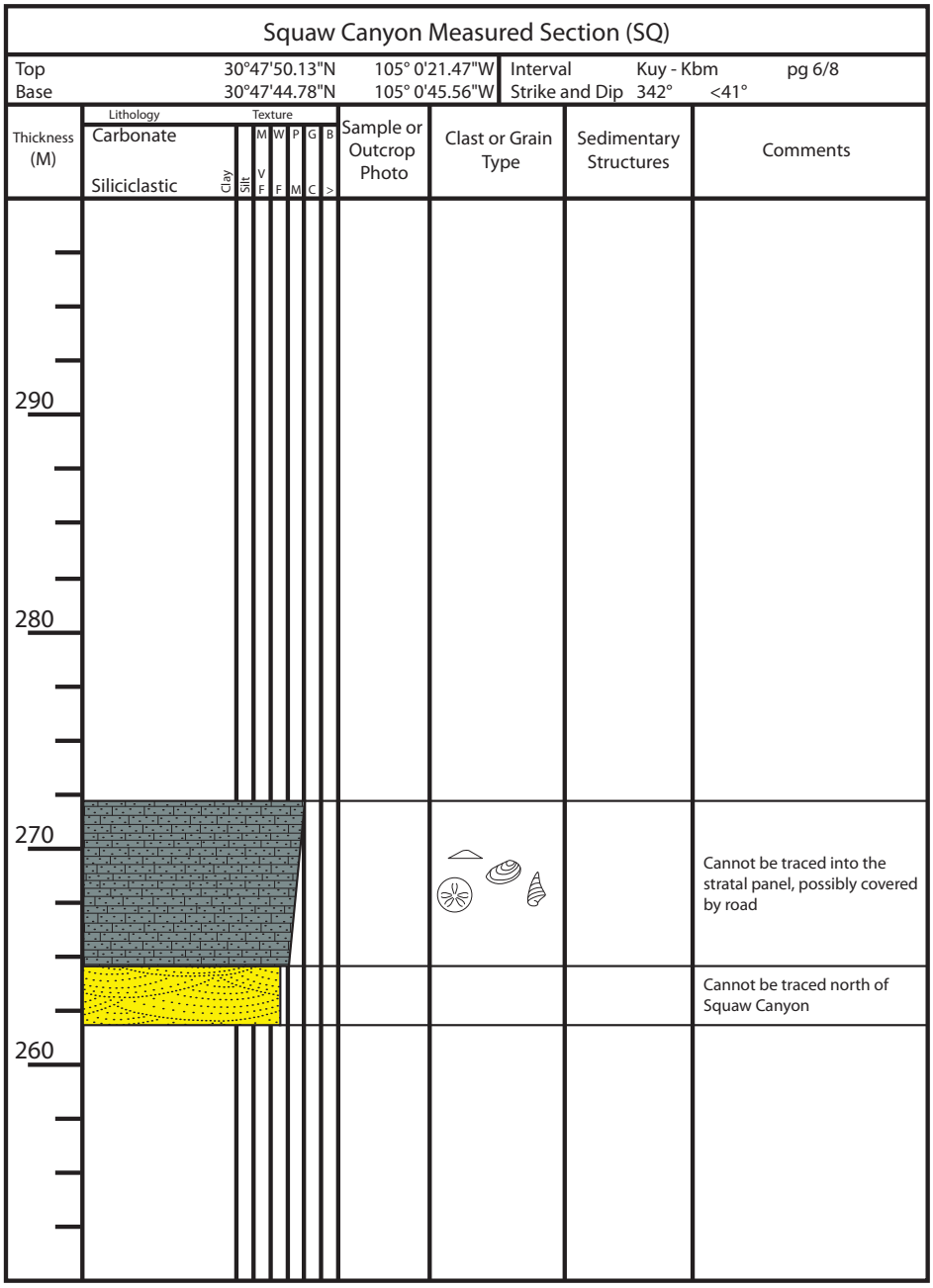
Squaw Canyon Measured Section (SQ)
Top 30°47'50.13"N 105° 0'21.47"W
Base 30°47'44.78"N 105° 0'45.56"W
Interval Kuy - Kbm pg 6/8
Strike and Dip 342° <41°
Thickness (M)
Lithology
Carbonate
Siliciclastic
Clay
Silt
Texture
M
W
P
G
B
V F
F
M
C
>
Sample or Outcrop Photo
Clast or Grain Type
Sedimentary Structures
Comments
290
280
270
260
Cannot be traced into the stratal panel, possibly covered by road
Cannot be traced north of Squaw Canyon

Squaw Canyon Measured Section (SQ)

Top	30°47'50.13"N	105° 0'21.47"W	Interval	Kuy - Kbm	pg 7/8
Base	30°47'44.78"N	105° 0'45.56"W	Strike and Dip	342°	<41°

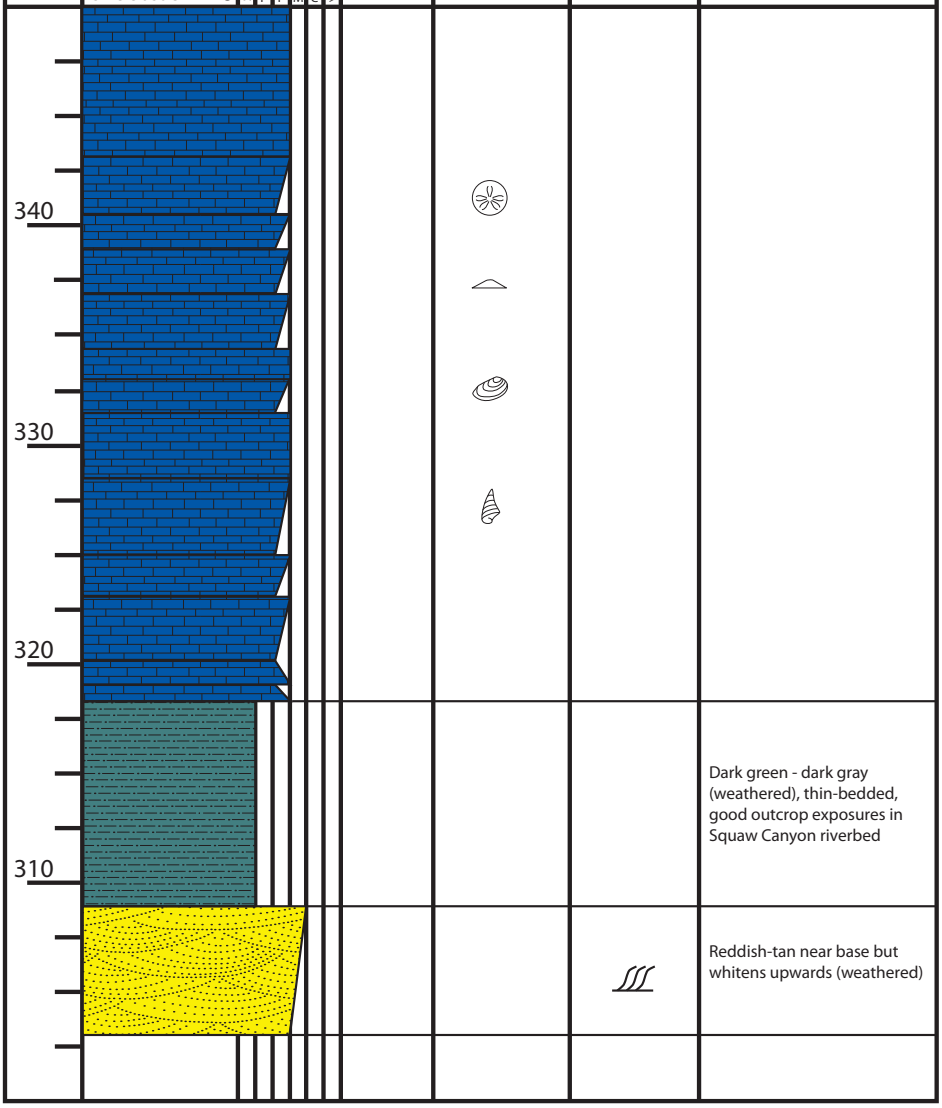

Sample or Outcrop Photo	Clast or Grain Type	Sedimentary Structures	Comments
			Dark green - dark gray (weathered), thin-bedded, good outcrop exposures in Squaw Canyon riverbed
			Reddish-tan near base but whitens upwards (weathered)

Squaw Canyon Measured Section (SQ)

Top	30°47'50.13"N	105° 0'21.47"W	Interval	Kuy - Kbm pg 8/8
Base	30°47'44.78"N	105° 0'45.56"W	Strike and Dip	342° <41°

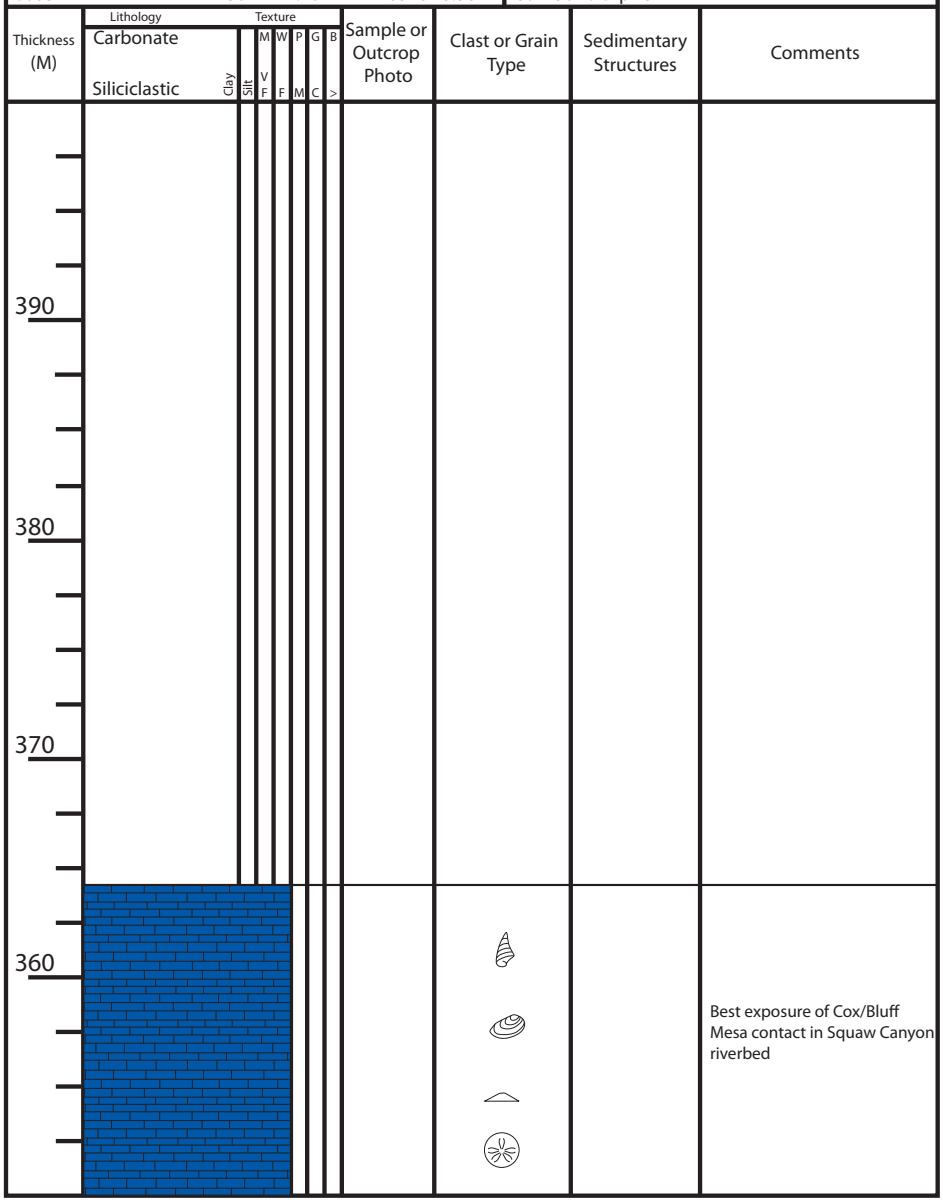

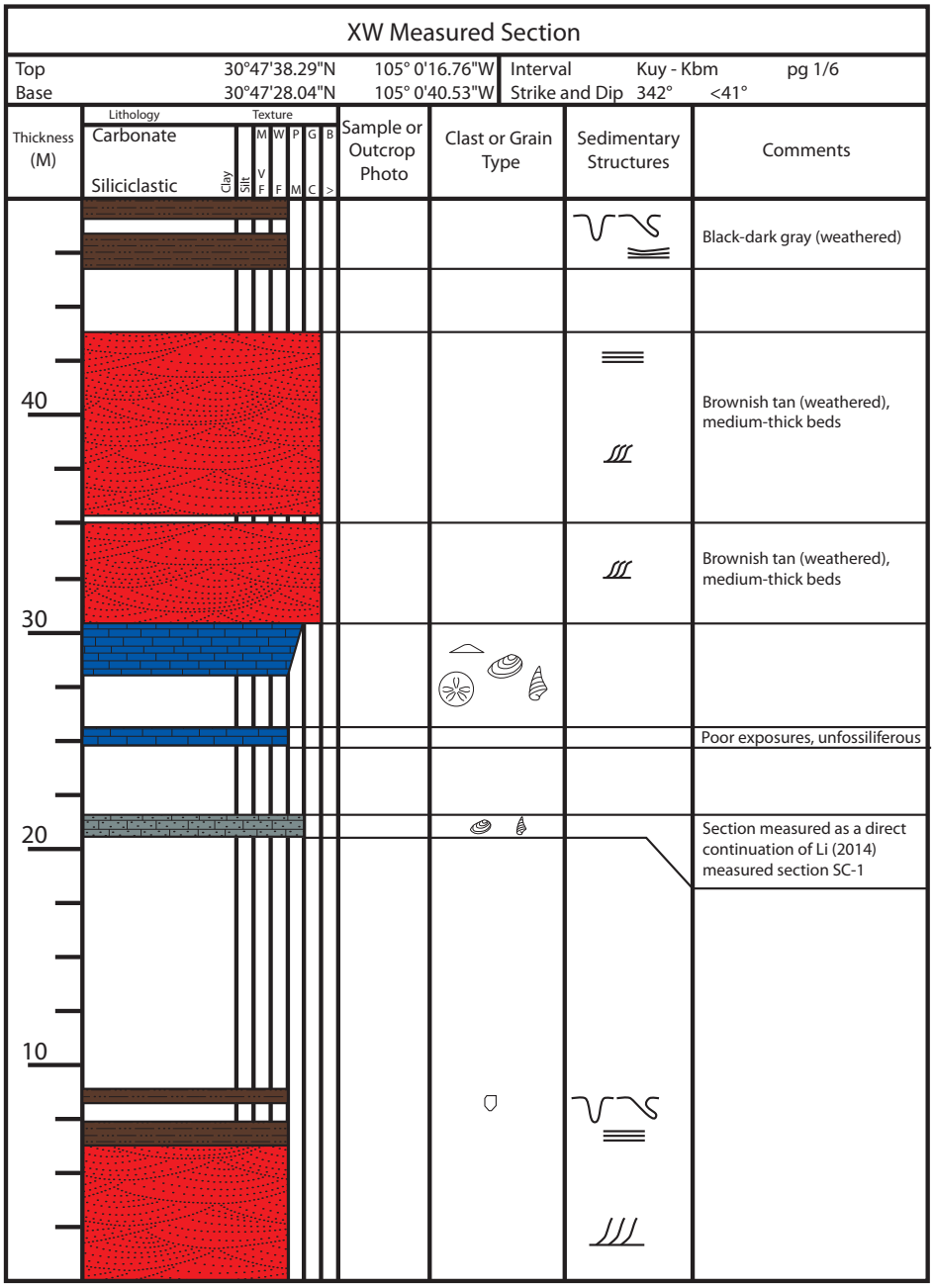
XW Measured Section
Top 30°47'38.29"N 105° 0'16.76"W
Base 30°47'28.04"N 105° 0'40.53"W
Interval Kuy - Kbm pg 1/6
Strike and Dip 342° <41°
Thickness (M)
Lithology
Carbonate
Siliciclastic
Texture
Clay
Silt
V F
F
M
C
M W P G B
>
Sample or Outcrop Photo
Clast or Grain Type
Sedimentary Structures
Comments
40
30
20
10
Black-dark gray (weathered)
Brownish tan (weathered), medium-thick beds
Brownish tan (weathered), medium-thick beds
Poor exposures, unfossiliferous
Section measured as a direct continuation of Li (2014) measured section SC-1

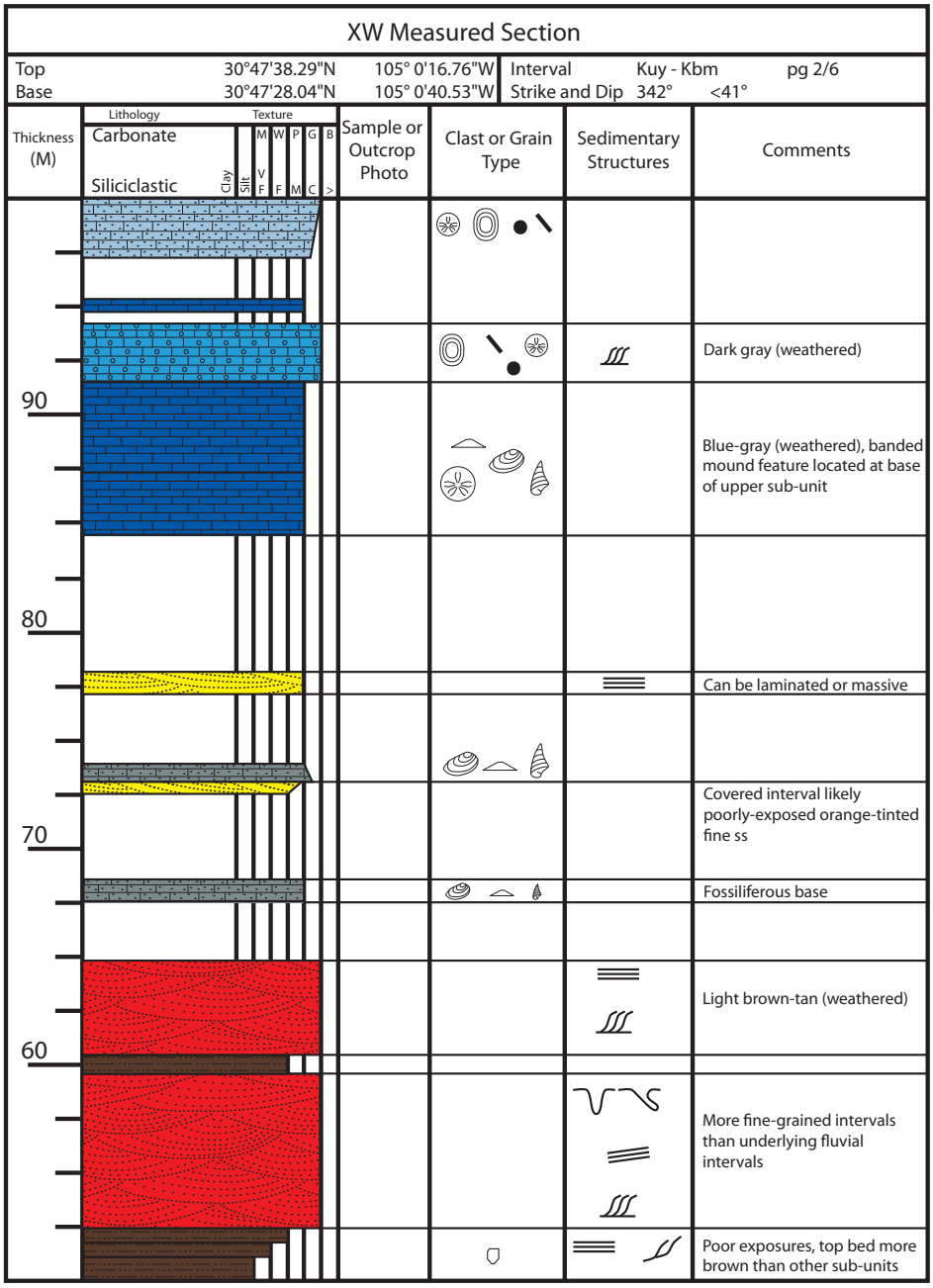
XW Measured Section
Top 30°47'38.29"N 105° 0'16.76"W
Base 30°47'28.04"N 105° 0'40.53"W
Interval Kuy - Kbm pg 2/6
Strike and Dip 342° <41°
Thickness (M)
Lithology
Carbonate
Siliciclastic
Clay
Silt
Texture
M W P G B
V F F M C >
Sample or Outcrop Photo
Clast or Grain Type
Sedimentary Structures
Comments
90
80
70
60
Dark gray (weathered)
Blue-gray (weathered), banded mound feature located at base of upper sub-unit
Can be laminated or massive
Covered interval likely poorly-exposed orange-tinted fine ss
Fossiliferous base
Light brown-tan (weathered)
More fine-grained intervals than underlying fluvial intervals
Poor exposures, top bed more brown than other sub-units

XW Measured Section

Top	30°47'38.29"N	105° 0'16.76"W	Interval	Kuy - Kbm	pg 3/8
Base	30°47'28.04"N	105° 0'40.53"W	Strike and Dip	342°	<41°

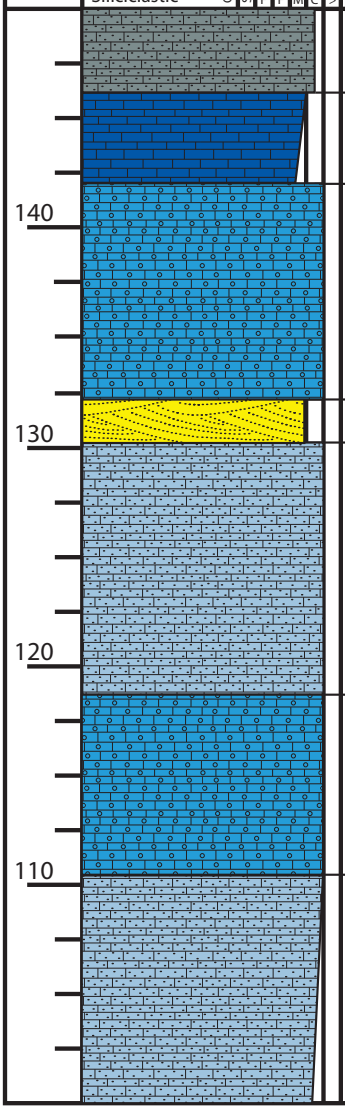

Thickness (M)	Sample or Outcrop Photo	Clast or Grain Type	Sedimentary Structures	Comments
				Poor exposures, rusty tan (weathered)
				Blue-gray (weathered), nodular weathering pattern
				Subordinate silty packstone interbeds
				Offwhite-pinkish tan, medium-bedded
				Interlayered with thin-bedded less sandy intervals
				Massive cliff-former, dark gray (weathered)

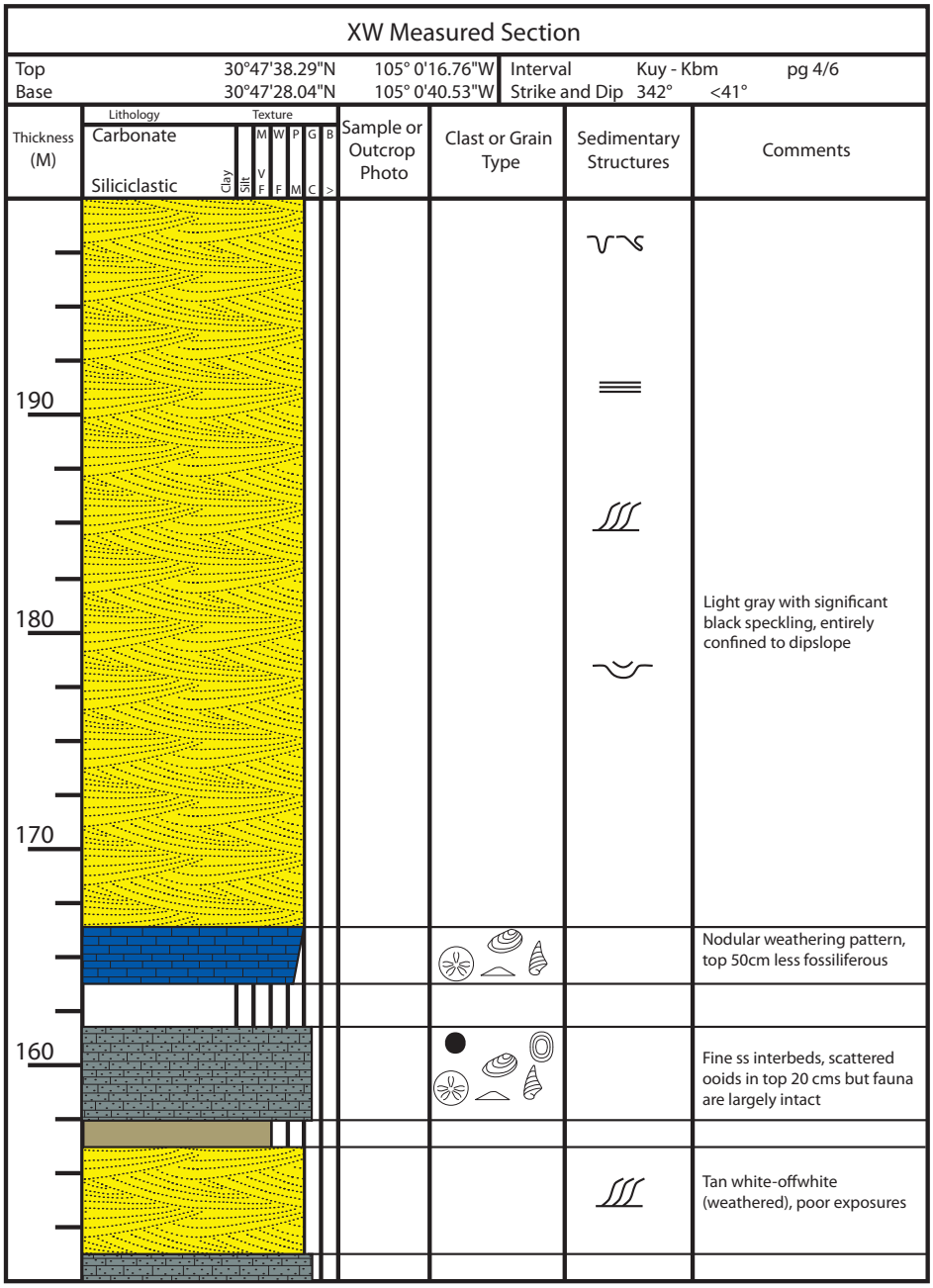
XW Measured Section
Top 30°47'38.29"N 105° 0'16.76"W
Base 30°47'28.04"N 105° 0'40.53"W
Interval Kuy - Kbm pg 4/6
Strike and Dip 342° <41°
Thickness (M)
Lithology
Carbonate
Siliciclastic
Texture
Clay
Silt
M
W
V F
F
M
C
P
G
>
B
Sample or Outcrop Photo
Clast or Grain Type
Sedimentary Structures
Comments
190
180
170
160
Light gray with significant black speckling, entirely confined to dipslope
Nodular weathering pattern, top 50cm less fossiliferous
Fine ss interbeds, scattered ooids in top 20 cms but fauna are largely intact
Tan white-offwhite (weathered), poor exposures

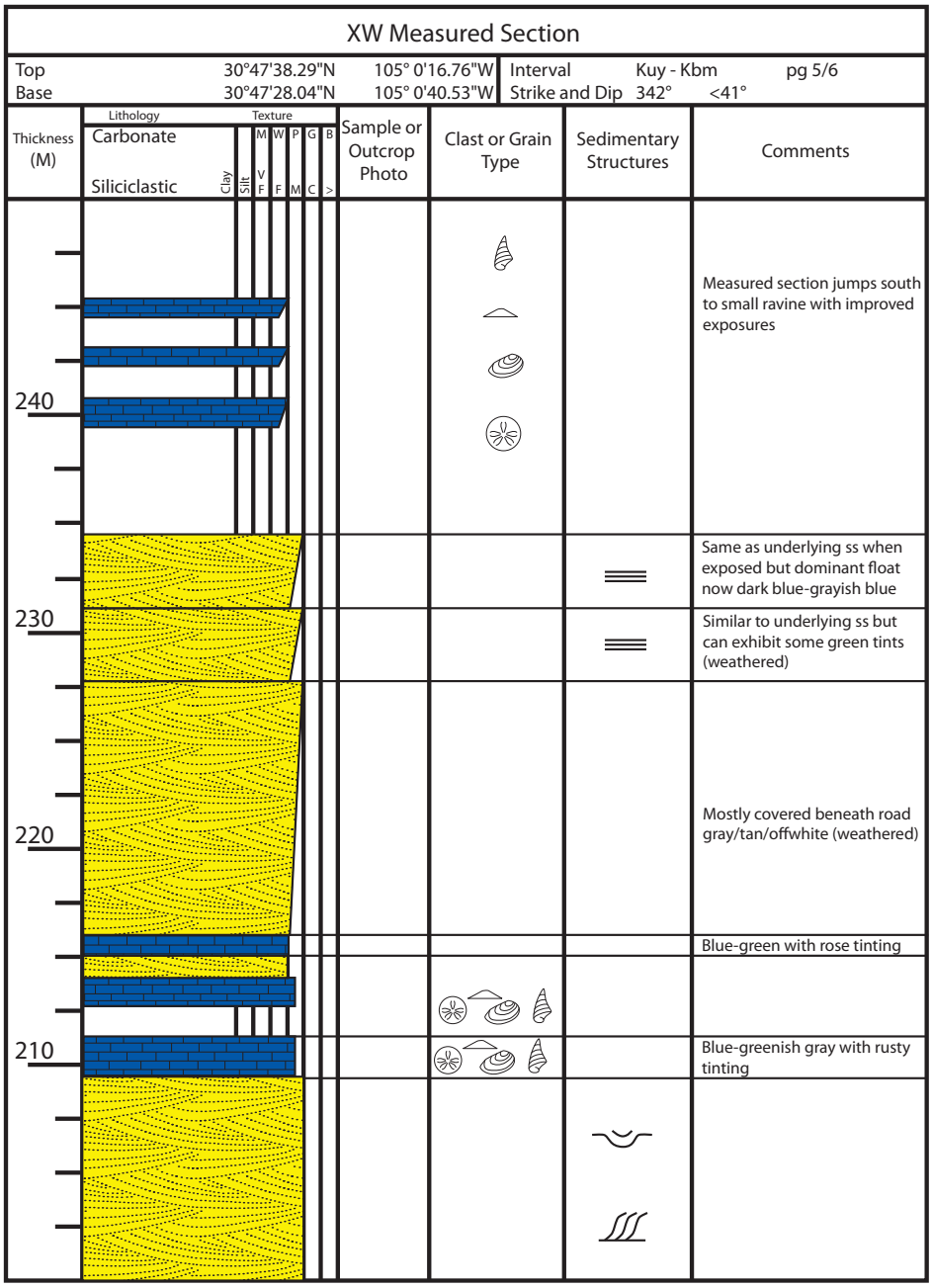
XW Measured Section
Top 30°47'38.29"N 105° 0'16.76"W
Base 30°47'28.04"N 105° 0'40.53"W
Interval Kuy - Kbm pg 5/6
Strike and Dip 342° <41°
Thickness (M)
Lithology
Carbonate
Siliciclastic
Clay
Silt
Texture
M
W
P
G
B
V F
F
M
C
>
Sample or Outcrop Photo
Clast or Grain Type
Sedimentary Structures
Comments
240
230
220
210
Measured section jumps south to small ravine with improved exposures
Same as underlying ss when exposed but dominant float now dark blue-grayish blue
Similar to underlying ss but can exhibit some green tints (weathered)
Mostly covered beneath road gray/tan/offwhite (weathered)
Blue-green with rose tinting
Blue-greenish gray with rusty tinting

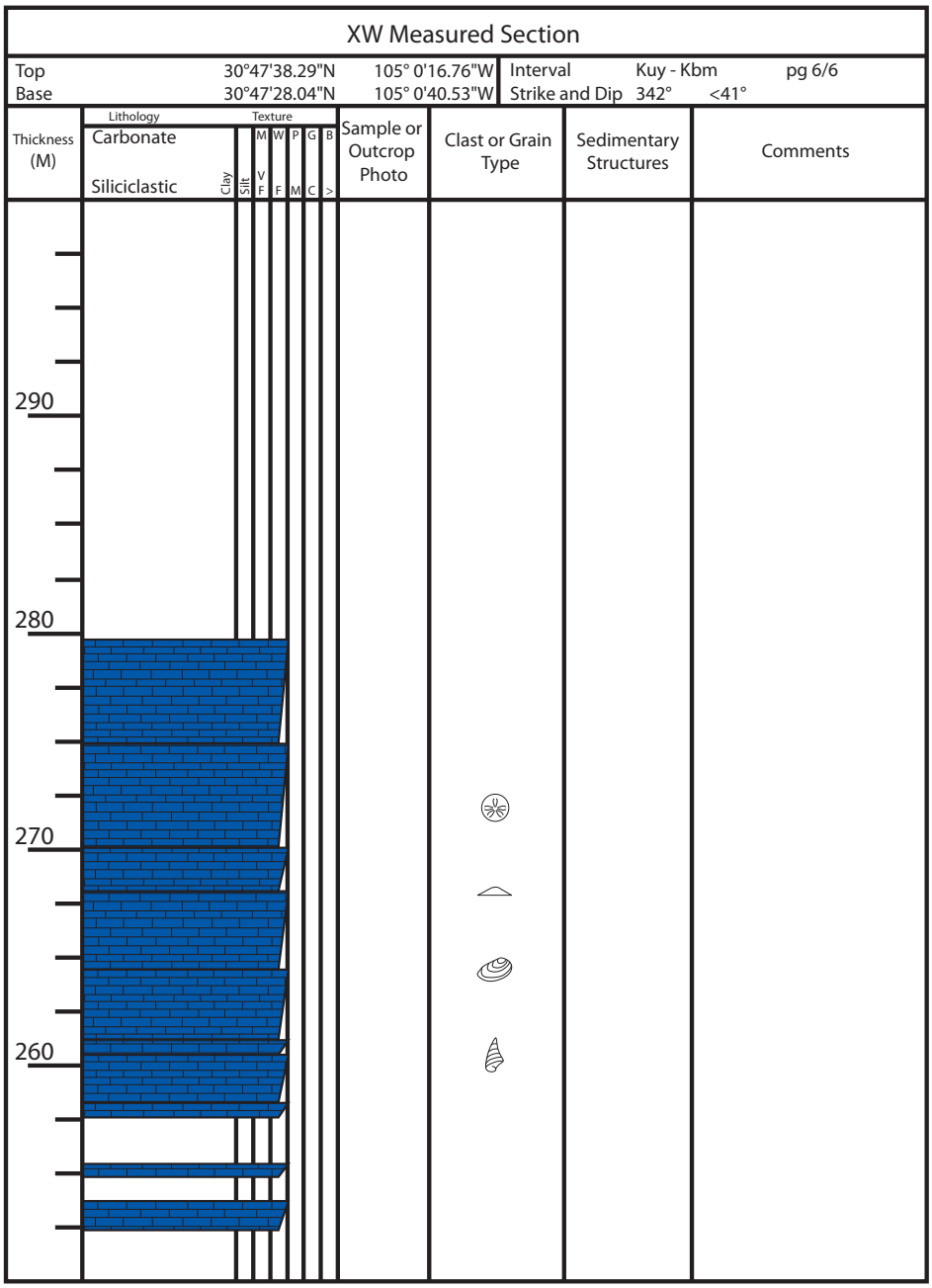
XW Measured Section
Top 30°47'38.29"N 105° 0'16.76"W
Base 30°47'28.04"N 105° 0'40.53"W
Interval Kuy - Kbm pg 6/6
Strike and Dip 342° <41°
Thickness (M)
Lithology
Carbonate
Siliciclastic
Clay
Silt
Texture
M
V F
F
M
C
G
B
Sample or Outcrop Photo
Clast or Grain Type
Sedimentary Structures
Comments
290
280
270
260

VITA

Andrew Thomas Anderson was born in Minneapolis, Minnesota and was raised in Chicago, Illinois. He received his Associate of Science in May of 2010 from Triton College before pursuing his Bachelor's of Science in chemistry at the University of Illinois at Chicago. In May of 2013, he graduated with a Bachelor's of Science in Earth and Environmental Science from the University of Illinois at Chicago after a single introductory geology course persuaded him to switch majors.

In August of 2014 he moved to El Paso to pursue his Master's of Science in Geology at University of Texas at El Paso (UTEP). While at UTEP he competed on the 2016 American Association of Petroleum Geologists (AAPG) Imperial Barrel Award team, where they took first place internationally out of 176 schools from 42 countries. In the summer of 2017 he worked as a geoscience intern at Hess Corporation in their Guyana exploration group.

After completing his Master's thesis, Andrew plans to pursue a position as an exploration geologist with an oil and gas firm.

Email: atand22son@gmail.com

This thesis was typed by the author, Andrew Anderson.